Zeitschrift: IABSE reports = Rapports AIPC = IVBH Berichte
Band: 59 (1990)

Rubrik: Theme C: Assessment of remaining fatigue life

THEME C

Assessment of Remaining Fatigue Life

Estimation de la durée de vie restante

Abschätzung der Restlebensdauer

Leere Seite
Blank page
Page vide

Measurement of Service Stress and Fatigue Life Evaluation of Bridges

Mesure des contraintes à l'état de service et évaluation de la durée de vie des ponts

Betriebsspannungsmessungen und Lebensdauerberechnungen von Brücken

Kentaro YAMADA
Professor
Nagoya University
Nagoya, Japan

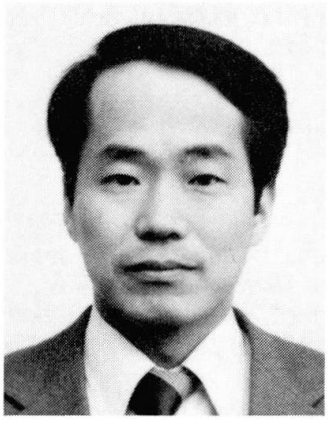

Kentaro Yamada, born 1946, received his civil engineering degree at Nagoya University, and PhD at University of Maryland, MD, USA. Since then, he has been involved in fatigue tests of welded structures, application of fracture mechanics, and field measurement of service stresses of highway bridges.

SUMMARY

Service stresses have been measured by using a histogram recorder. Fatigue life is evaluated using the Miner's cumulative damage rule and the ECCS fatigue-strength diagrams. Calculated fatigue lives of main members are longer than a hundred years whereas for secondary members, relatively short. These results are consistent with the observation of major fatigue cracks in secondary members.

RÉSUMÉ

Les contraintes à l'état de service ont été mesurées à l'aide d'un enregistreur d'histogramme. La durée de vie est évaluée en utilisant la loi de cumul du dommage de Miner et les courbes de résistance à la fatigue du CECM. Les durées de vie calculées pour les éléments principaux sont supérieures à cent ans, alors que celles des éléments secondaires sont relativement courtes. Ces résultats sont en accord avec les observations des principales fissures de fatigue recensées dans les éléments secondaires.

ZUSAMMENFASSUNG

Mit einem Histogramm-Registriergerät wurden Betriebsspannungen gemessen. Für die Berechnung der Lebensdauer werden das Gesetz von Miner über die Schadensakkumulation und die EKS-Ermüdungsfestigkeitskurven verwendet. Die so berechnete Lebenserwartung beträgt für die Haupttragelemente mehr als hundert Jahre, während sie für die untergeordneten Elemente relativ gering ausfällt. Diese Resultate stimmen mit der Beobachtung überein, dass die grössten Ermüdungsrisse in untergeordneten Elementen auftreten.

1. INTRODUCTION

Both stresses and their frequency of in the structural members of highway bridges have increased due to an increasing weight and number of trucks in the past two decades in Japan. It has led to some fatigue cracks in structural members in highway bridges [2,3]. Although the cracks were mainly found in the secondary members and caused no immediate danger to the bridge, they may grow in size with stress cycles and cause serious maintenance problems to the bridges. In order to investigate the cause of cracks, stress measurements were often carried out.

This study was to evaluate the fatigue life of structural members in five steel bridges based on the measured stress range histograms. The bridges include a riveted truss bridge, a composite plate girder bridge, a non-composite plate girder bridge, a box girder bridge with orthotropic steel deck and an arch bridge subjected to different traffic conditions.

2. SERVICE STRESS MEASUREMENT OF BRIDGES

2.1 Description of Bridges

1) Bridge A: It is a 60-year old riveted Warren truss bridge, as shown in Fig. 1, with a span of 73 m and a 16 m wide roadway. The bridge is daily subjected to about 250 trains at a speed of about 10 km/h and about 10,000 vehicles, in which 11 percent are trucks. The traffic is considered rather light in Japan.

2) Bridge B: It is a welded plate girder bridge built in 1967, with a span of 27.9 m and a 7.0 m wide roadway for two lanes, as shown in Fig.2. The spacings of main girders are 2.0 m and the sway bracings are placed at 5.58 m intervals. The reinforced concrete deck was originally 23 cm thick, and was later added by a 12 cm thick steel-fiber reinforced concrete in 1979. It is a private bridge in a steel works. Although about twenty special trucks of more than 785 kN (80 tons) pass on it daily, the number of daily truck traffic is very small.

3) Bridge C: It is a two-span continuous plate girder bridge built in 1964, with eight main girders spaced at 3.2 m intervals, as shown in Fig.3. The total length is 40 m with two spans of 20 m each. The roadway is for six lanes, threc lanes for each direction. The deck is made of 19 cm thick reinforced concrete slab. The bridge situates in an industrial area and carries about 100,000 vehicles daily. About half of the passing vehicles are trucks and it is considered to be under severe traffic condition. The bridge was repaired and retrofitted in 1982, when cracks were found in the fillet weld at the upper end of vertical stiffener. The stress measurement was carried out in 1984 [4].

4) Bridge D: It is a three-span box girder bridge with orthotropic steel decks, built in 1964. It has a 96 m center span and two 77 m side spans, as shown in Fig.4. It is situated on the same route as Bridge C, and is also subjected to severe traffic condition. Several fatigue cracks were found in the corner of diaphragms, and rehabilitation works were carried out in 1989.

5) Bridge E: It is a two-hinge deck type arch bridge built in 1964. The arch has 54 m span and the width of roadway is 9.9 m, as shown in Fig.5. The bridge is subjected to about 80,000 vehicles every day, and 26 percent of them are trucks. The bridge is also subjected to severe traffic condition. Fatigue cracks were found in stringers of floor system and vertical members of arch. The cracks of the stringers were repaired and the cracked parts were stiffened. Further repair and strengthening of the arch and replacement of concrete slab into orthotropic steel deck are underway.

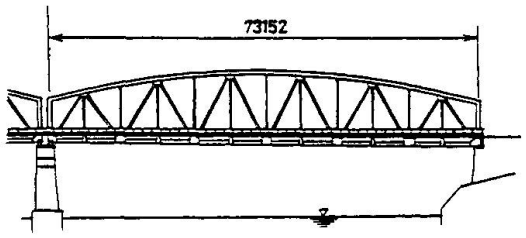

Fig.1 Bridge A: Riveted truss bridge

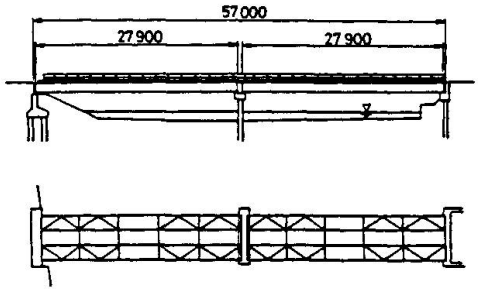

Fig.2 Bridge B: Composite plate girder bridge

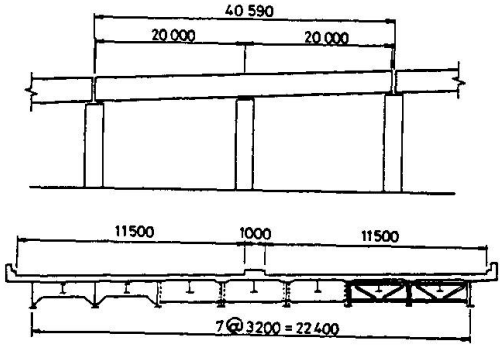

Fig.3 Bridge C: Non-composite plate girder bridge

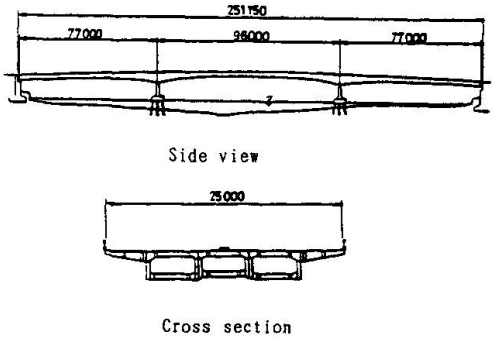

Fig.4 Bridge D: Three span continuous box girder bridge

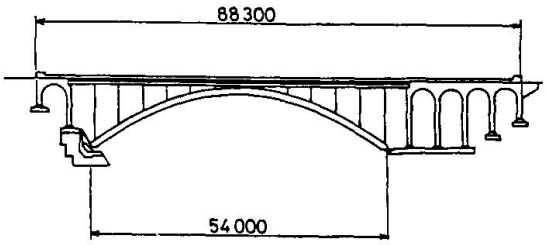

Fig.5 Bridge E: Deck type arch bridge

2.2 Measurement under Model Vehicle of Controlled Weight

Trucks of controlled weight of 196 kN (20 tons) are often chosen to be model vehicles in order to represent the design truck T-20. The model vehicles are placed at several points on the bridge or driven at a certain speed through the bridge. Static and dynamic strains are measured by using strain gages. The dynamic strains are recorded in magnetic tape data recorder, and then monitored by a synchroscope or a pen-recorder. The test results are often compared with the analytical results. This type of measurements causes some difficulties as to stop the normal traffics, which are often very heavy in Japan.

2.3 Measurement of Service Stress Range Histogram

Stresses under service condition are important to evaluate the durability of structures. Service stresses can be measured by using a Histogram Recorder, as

shown in Fig.6 [9]. It analyzes the strain waves in real time and records the stress ranges and the number of their occurrence. The analysis may be based on rainflow counting method, peak counting method, level crossing counting method, and so on. The rainflow counting method was used in this study to obtain stress range histogram. The Histogram Recorder has some advantages as that it requires no traffic control, and the disadvantage is that it distinguishes neither the type of trucks nor their axle weight. Therefore, stresses under model vehicle with controlled weight are often measured and used as reference values.

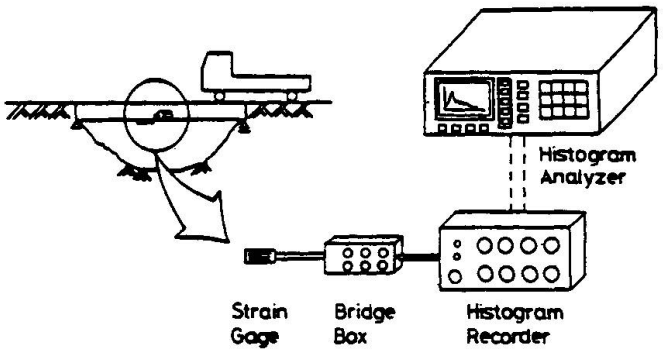

Fig.6 Measurement of stress histogram

Examples of the stress range histogram measured for 24 hours are shown in Fig. 7, where the ordinate indicates stress range and the abscissa shows the number of half stress cycles in logarithmic scale. The stress ranges corresponding to the model vehicles are also shown as reference values.

The stress histogram of a diagonal member of the Bridge A is shown in Fig.7a. The model vehicles are a 22.5-ton dump truck with 3 axles and a train with 6 cars. It seems that the upper peak of stress cycles is caused by the trains. The stress cycles below the reference value by the model truck may be caused by lighter trucks and the other vehicles and that above the reference value by the train is considered to be caused when the trucks and the train passed on the bridge simultaneously.

Figs.7b and 7c show stress range histograms measured at a lower flange and the upper end of a vertical stiffener of Bridge B, respectively. The measured maximum stress range in the lower flange is close to reference stress range by the 1140 kN (116 tons) trailer truck. And that in the lower flange of Bridge B is about 80 MPa, about twice of that in the diagonal members of Bridge A.

Fig.7d shows stress range histogram measured at bottom of longitudinal rib in the orthotropic steel deck of Bridge D. The model vehicle was a crane truck of 364 kN (37.1 tons). The maximum stress range was about 105 MPa, about twice of stresses due to the model vehicle. It is either because the trucks weigh more than the model vehicle, or because heavy trucks crossed the bridge simultaneously. There was extremely large number of low stress ranges. This may be explained by the frequent passage of small trucks or vibration in the orthotropic steel deck due to the passing traffics.

Fig.7e shows stress range histogram measured at the arch rib of passing lane side of Bridge E. The reference stress ranges due to a truck of 206 kN (21 tons) passing on the slow lane or on the passing lane, or three same trucks are also shown in the figure. The measured stress range were larger than the stresses by the three trucks. It implies that vehicles weighed more than the model trucks frequently passed on the bridge.

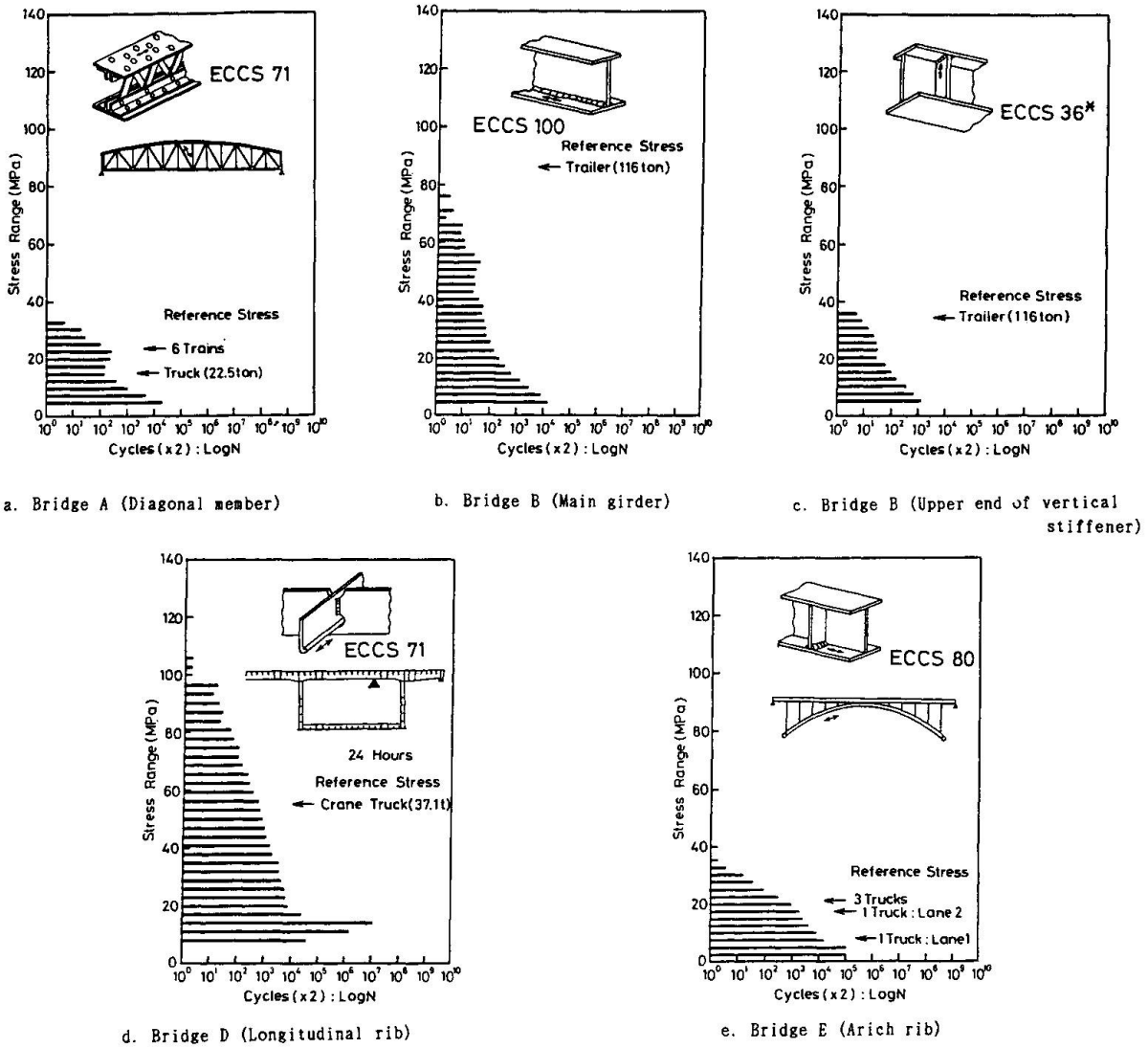

Fig.7 Example of stress range histogram records

The stress range histograms of Bridges D and E were different from that of Bridges A and B. This is because the volume of traffics is much greater in Bridges D and E than in Bridges A and B. For example, about 250 trains and 10,000 vehicles passed on Bridge A, while over 100,000 vehicles passed on Bridge D and about 80,000 vehicles passed on Bridge E for 24 hours.

3. EVALUATION OF FATIGUE LIFE BASED ON MEASURED STRESS RANGE HISTOGRAM

3.1 Detail Categories

In this study the design S-N diagrams specified in the ECCS Recommendation for the Fatigue Design of Steel Structures [8] were used to evaluate the fatigue strength of weld details. Since the design S-N diagrams correspond to the mean-2xs (s:standard deviation) S-N diagrams, the computed fatigue life is the lower bound fatigue life. The design S-N diagrams are given for classified structural detail. The detail categories evaluated for fatigue life in this study are also shown in Fig.7.

1) Bridge A: Riveted joints are classified as ECCS 71.

2) Bridge B and C: The lower flange of the plate girder is fillet-welded to the web, and this detail is classified as ECCS 100. The upper end of the vertical stiffener (connection plate) with a cross beam or a lateral bracing can be considered as load-carrying fillet weld, and it is ECCS 36 if root-cracking is assumed.

3) Bridge D: The stress range of longitudinal ribs welded to lateral ribs in the orthotropic steel deck is used from that measured at the bottom of the longitudinal rib. The welds are assumed as load-carrying fillet weld and it is classified as ECCS 71 for toe crack.

4) Bridge E: The upper and the lower ends of the vertical members are fillet-welded to splice plates, which are then riveted to the arch rib and the floor system. The weld detail is classified as ECCS 71. The arch rib has stiffeners that are fillet-welded to the arch rib web. The detail is non-load-carrying fillet weld, and is classified as ECCS 80.

3.2 Evaluation of Fatigue Life Based on Service Loading

Two types of design S-N diagrams specified in the ECCS Recommendation are used to evaluate the fatigue damage based on the stress range histogram, as shown in Fig.8.

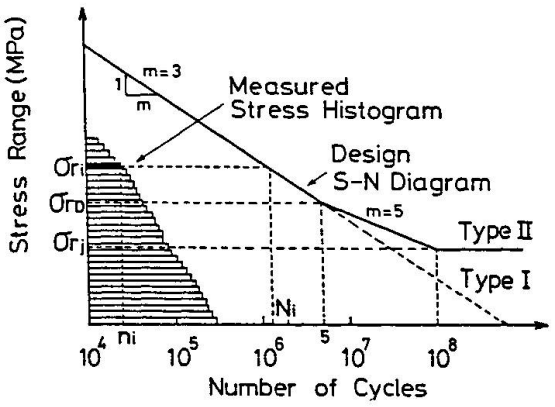

Fig.8 ECCS design S-N diagram

1) Type I (Modified miner's rule): The S-N diagram of slope of m=3 is extended linearly.
2) Type II (Three line method): The slope of the S-N diagram m is equal to 3 for N less than 5 million cycles, and 5 for N between 5 million and 100 million cycles. Stress ranges below the cut-off limit are neglected.

To carry out the damage calculation, the actual number of stress cycles n_i corresponding to each stress range σ_{ri} is obtained first from the histogram. Then the number of cycles to failure N_i corresponding to each σ_{ri} is obtained from the S-N diagram. The fatigue damage D is the sum of n_i/N_i for all stress range in the histogram, i.e.,

$$D = \Sigma\ (n_i/N_i) \qquad (1)$$

where it is assumed that the detail fails due to fatigue, when D becomes unity. Since all the measured stress range histograms in this study are for 24 hours, the

evaluated D according to Eq.1 indicates the fatigue damage in one day. Assuming that the data is obtained in a typical day and that the traffic condition will remain unchanged, the expected fatigue life L is given by the following equation.

$$L(\text{year}) = 1/(365 \times D) \qquad (2)$$

The fatigue life may also be evaluated by using the equivalent stress range concept. The equivalent stress range $\sigma_{r,eq}$ is obtained from the S-N diagrams by assuming that the sum of n_i/N_i becomes unity at the time of fatigue failure. When one wants to use the type II S-N diagram (three line method), those stress range below the fatigue limit are considered by using slope m = 5 and those below the cut-off limit are neglected in the calculation of $\sigma_{r,eq}$ [8].

4. FATIGUE EVALUATION AND DISCUSSION

4.1 Influence of Traffic

Fatigue lives of the above-mentioned structural details in the Bridges A and B computed from the measured stress histograms are plotted in Fig.9. The two bridges were subjected to relatively light traffics, and their fatigue life are shown by the solid symbols in Fig.9. The fatigue life of the main members of Bridge A yields to more than 220 years, and that of the tension flanges of Bridge B are between 120 and 140 years. Even the upper end of vertical stiffeners of Bridge B showed the life longer than 90 years. Considering that the evaluated fatigue life is the lower bound because of the use of the lower bound S-N diagrams, it may be safe to concluded that fatigue cracks would hardly occur in these details, provided that traffic condition will remain unchanged and structural deterioration such as corrosion will not take place.

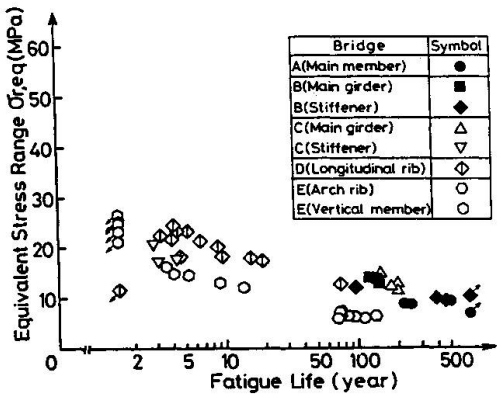

Fig.9 Equivalent stress range and fatigue life for Bridges A and B

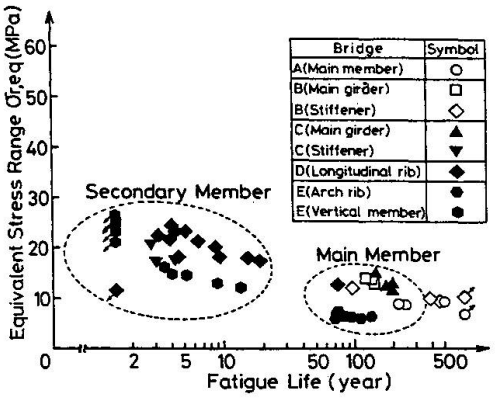

Fig.10 Equivalent stress range and fatigue life for Bridges C, D and E

Bridges C, D and E were subjected to severe traffic condition, and their fatigue lives are plotted by the solid symbols in Fig.10. If the structural details are grouped into main members and secondary members, the computed fatigue lives can be also grouped accordingly. For example, the fatigue lives of the tension flange of Bridge C are more than 100 years, and that of the arch ribs of Bridge E is between 70 and 130 years. On the contrary, the fatigue lives of the vertical members of the arch are less than 4 years, that of the longitudinal ribs in Bridge D are less than 20 years, and that of the upper and lower ends of the vertical members of Bridge E are below 15 years. Actually, the welded details in these secondary members were found susceptible to fatigue cracking previously [2,3,4]. Therefore, the fatigue lives obtained from the measured stress range histogram are a good

indicator of the severeness of structural detail against fatigue, even though the fatigue lives computed here are still inaccurate due to many uncertainties involved in the analysis.

Bridges B and C are both plate girder bridges with similar structural details, and their fatigue lives are plotted by the solid symbols in Fig. 11. It is noted that the main girder of Bridge B showed shorter fatigue life than Bridge C, although Bridge C are subjected to about 100,000 vehicles daily. This may be because Bridge B carries special vehicles of of over 785 kN (80 tons). However, the upper ends of the vertical stiffeners in Bridge B showed long fatigue lives. This may be due to the 35 cm thick concrete slab and the 2.0 m girder spacing in Bridge B. They reduced the stresses and hence increased the fatigue life. On the contrary the Bridge C has a 19 cm thick concrete slab and 3.2 m girder spacings.

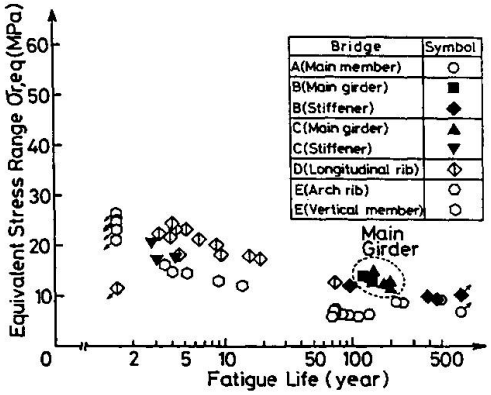

Fig.11 Equivalent stress range and fatigue life for Bridges B and C

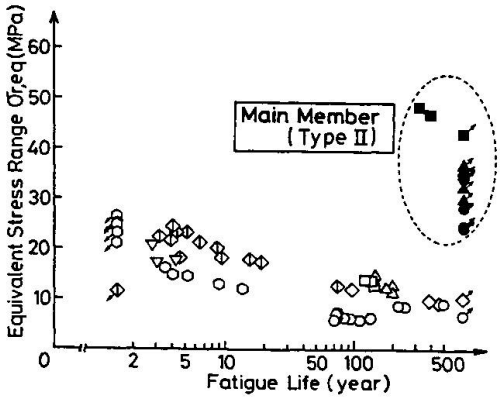

Fig.12 Equivalent stress range and fatigue damage for main members

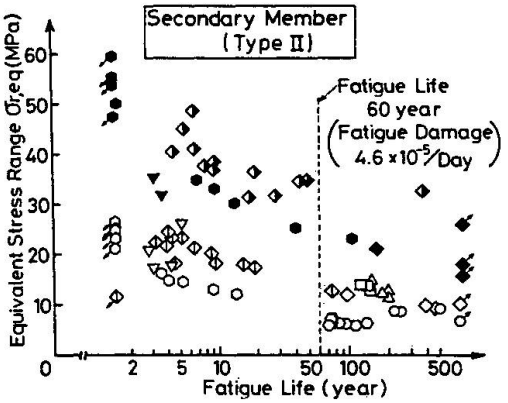

Fig.13 Equivalent stress range and fatigue damage for secondary members

4.2 Influence of S-N Diagrams

The type II S-N diagram (Three line method) was also used to evaluate the fatigue life of each detail, and the results are plotted in Figs. 12 and 13. In Fig. 12, computed fatigue life of the main members (the tension flanges and the arch ribs) using the type II S-N diagram are shown by the solid symbols. They are over 300 years, longer than that evaluated by using the type I S-N diagram. This is because most of the stress ranges in the histograms are below the cut-off limit and they are neglected in the type II S-N diagram. In the case of the arch ribs of the

bridge E, the fatigue life becomes infinite because all stress ranges are below the cut-off limit.

The fatigue lives of the secondary members are shown by the solid symbols in Fig.13. Although the equivalent stress ranges increase, the computed fatigue lives are similar to the lives computed based on the type I S-N diagram. A good part of the stress ranges in the histogram were above cut-off limit and contributed to the fatigue damages of the secondary members. Some secondary members actually experienced fatigue crackings, and therefore this trend can also be used to evaluate the severeness of stresses against fatigue.

The fatigue lives computed here should still be considered as relative values. This is because the fatigue strength in the long life region in the S-N diagrams has not yet been clarified due to the lack of experimental data. The fatigue behavior of structural details in long life region, especially under variable amplitude stress cycles, should be further investigated.

4.3 Fatigue Damage Threshold

We may be able to define fatigue damage threshold for bridge members. The fatigue damage threshold is the damage D_{th}, above which the fatigue cracking may occur in a certain period of time. As mentioned above, the fatigue prone details, known from the past experiences, showed relatively large fatigue damage, and hence yielded to short fatigue lives. The dotted line in Fig.13 clearly separate the fatigue-prone secondary members from the main members. It corresponds to fatigue life of 60 years, or daily fatigue damage of 4.6×10^{-6}.

5. SUMMARY

The measurement of the service stress ranges is important to evaluate the durability of bridges or similar steel structures against fatigue. In this study, stress histograms were collected for five bridges and evaluated. Then the fatigue damages and fatigue lives of the details were computed according to evaluated the design S-N diagrams recommended by the ECCS. The following summarizes the results.

1) The histogram of service stress ranges may be conveniently measured by a Histogram Recorder.

2) The service stress ranges often showed larger stress ranges than the stresses caused by design trucks, such as T-20 and TT-43.

3) Little possibility of fatigue cracking of the main members of highway bridges exists during service period, because the evaluated fatigue lives were in the order of a hundred years or over.

4) The fatigue lives of the secondary members, which experienced fatigue cracking previously, were much shorter than that of the main members.

5) The selection of design S-N diagrams may yield to large discrepancy in the computed fatigue life based on the service stress range histogram. Thus, it is necessary to establish better design S-N diagram in the long life region based on experimental data.

6) The evaluated fatigue life may not be as accurate as expected, but it has relative meaning in expressing the severeness of stresses in the details against fatigue.

7) The daily fatigue damage of $D = 4.6 \times 10^{-6}$ may be used as a fatigue damage threshold value to identify whether the detail is fatigue-prone or not in highway

bridges.

ACKNOWLEDGEMENT

This study was partly supported by the Grant-in Aid for Scientific Research from the Japanese Ministry of Education, Science and Culture. Much help from Dr. M. Kato, Mr. Y. Ishiguro and Mr. Ma Zhiliang of Nagoya University is highly appreciated.

REFERENCE

1) Japan Road Association, Standard Specification for Highway Bridges, 1980. (in Japanese)
2) NISHIKAWA, K., The Fatigue Problem and Repair and Rehabilitation of Highway Bridges, Bridge and Foundation, Vol.17, No.8, 1983. (in Japanese)
3) IWASAKI, M. et al., Fatigue Cracking in Steel Bridge members and Recommendation of Retrofitting Method, Yokogawa Bridge Works Technical Report, No.18, 1989. (in Japanese)
4) Public Works Research Institute, Ministry of Construction, Loading Test on Kyowa Viaduct, PWRI Report No.2123, 1984. (in Japanese)
5) Public Works Research Institute, Ministry of Construction, Measurement of Stress Histogram on Composite Bridge with Fatigue Damage, PWRI Report No.2344, 1986. (in Japanese)
6) Public Works Research Institute, Ministry of Construction, Investigation on Durability and Rehabilitation of Existing Bridges, PWRI Report No.2420, 1986. (in Japanese)
7)British Standard Institution: Steel, Concrete and Composite Bridges, Part 10, Code of practice for Fatigue, 1980.
8) European Convention for Constructional Steelwork: ECCS Recommendations for the Fatigue Design of Steel Structures, 1985.
9) YAMADA, K. and MIKI, C.; Recent Research on Fatigue of Bridge Structure in Japan, Journal of Constructional Steel Research, Vol.13, 1989.

Theoretical Evaluation of Remaining Fatigue Life of Steel Bridges

Evaluation théorique de la durée de vie restante de ponts en acier

Theoretische Abschätzung der Restlebensdauer von Stahlbrücken

Annibale Luigi MATERAZZI
Civil Engineer
University of Rome
Rome, Italy

Annibale Luigi Materazzi received his civil engineering degree at the University of Rome in 1977. In 1986 he earned the degree of «Dottore di Ricerca». His research interests are in the fields of fatigue of bridges and offshore structures and fracture mechanics of concrete.

Emanuele F. RADOGNE
Professor
University of Rome
Rome, Italy

Emanuele Radogne, born 1930, directs research work into the dynamic response of structures in service, probabilistic analyses, problems of fracture mechanics of concrete, and redesign of concrete structures.

SUMMARY
An operative methodology for the assessment of remaining fatigue life of existing railway bridges is presented. Either the Miner rule or the Paris crack propagation law can be used. Examples are provided in order to show the method's sensitivity to variation of input data. A critical examination of the results leads to justification for field measurements of structural response.

RÉSUMÉ
L'article présente une méthode d'évaluation de la durée de vie restante de ponts de chemin de fer existants en acier. Cette méthode permet aussi bien l'application de la loi de Miner que celle de la loi de Paris pour la propagation de fissures. Quelques applications numériques sont présentées ensuite afin de montrer la sensibilité de la méthode par rapport à la variation des données. Un examen critique des résultats justifie les mesures sur la structure.

ZUSAMMENFASSUNG
Vorgestellt wird eine operationelle Methode zur Abschätzung der Restlebensdauer bestehender Eisenbahnbrücken aus Stahl. Hierfür eignen sich sowohl das Verfahren von Miner als auch die Gleichung von Paris für das Risswachstum. Anhand von Beispielen wird die Empfindlichkeit der Methode für Änderungen der Eingabe-Parameter gezeigt. Eine kritische Prüfung der Resultate rechtfertigt die Durchführung von Messungen im Feld.

1. INTRODUCTION

In the recent years the attention toward durability has considerably increased, as many structures are approaching the end of their service lives and damages due to materials' deterioration are reported [1]. In this frame the problem of the evaluation of the fatigue damage and of the corresponding ramaining life begins to set up concretely, especially in the case of the bridges.
The analytical procedure for the evaluation of remaining fatigue life has been well known for a long time [2,3] but its practical application demands for reliable data and probabilistic methods.
In the present paper the attention is paid to the case of steel railway bridges because in these structures it is often possible to detect the fatigue cracking and to known with better approximation the magnitude and the cycles' number of past loads.

2. STATEMENT OF THE PROBLEM

In the present paper the problem of the evaluation of residual life is dealt with at Level 2, for an assigned value of the safety index ß, with reference to a steel railway bridge. The structure is supposed to have been designed for fatigue with the criteria of Eurocode 3 [4].
It is in general possible to get additional information on the time history of the stress cycles in service, by means of strain measurements. The measures must be carried out during time intervals long enough to make possible the delicate process of extrapolation of measured data to the whole future life of the bridge.
In this phase it is also necessary to set the correspondence between number of cycles and duration of time. It is often possible to examine in situ the hot spots of steel structure, in order to detect the presence and the length of eventual fatigue cracks by means of suited instruments .
The evaluation of the residual life is performed at an assigned time T, which corresponds to a known fraction of the duration of the design life. The stress collective, on the basis of field measurements, is assumed to be different from the one used at the time of the design. The corresponding damage is computed applying the Miner rule.
Then the influence of the load sequence is investigated applying the Paris law.
The comparison of the numerical results encourages in carrying out in situ strain measurements, in order to improve the knowledge of the stress collective.

3. THE EVALUATION OF RESIDUAL LIFE

In the frame of the Level 2 methods for the assessment of safety, the residual fatigue life may be expressed as:

$$T_{res} = T_{res}(\mathbf{X}, ß_0) \tag{1}$$

where T_{res} is the duration of the residual life, $\mathbf{X}$ is the m-component vector of the design variables and $ß_0$ is the prescribed value of the safety index.
If the problem parameters are:

$$\mathbf{X} = \{T_{past}, \Delta\sigma_{past}(t), \Delta\sigma_{fut}(t), R(N)\}^T \tag{2}$$

where T_{past} is the duration of the past life, $\Delta\sigma_{past}(t)$ is the time history stress cycles applyed in the past, $\Delta\sigma_{fut}(t)$ is the time history of future stress cycles, $R(N)$ is the law of fatigue behaviour of material, then the (1) reduces to:

$$T_{res} = T_{res}(T_{past}, \Delta\sigma_{past}(t), \Delta\sigma_{fut}(t), R(N), ß_0) \tag{3}$$

Everyone of these parameters, except β_0, is in general a random variable. The safety index β depends on the same parameters and on T_{res}:

$$\beta = \beta(T_{res}, T_{past}, \Delta\sigma_{past}(t), \Delta\sigma_{fut}(t), R(N)) \tag{4}$$

The solution of the eq. (1) may be found by iteration solving the (4) in the form $\beta = \beta_0$. The (4) expresses a conventional Level 2 safety problem. Its solution requires to write down the limit state condition in the case of fatigue failure $Z(\underline{X})=0$. If the fatigue damage is computed using the Miner rule, then it is particularly simple:

$$Z = \Delta - \sum_{i=1}^{k} \frac{n_i}{N_i} = 0 \tag{5}$$

where n_i is the number of the stress cycles having amplitude $\Delta\sigma_i$, N_i is the number of the stress cycles of the same amplitude which would lead to failure and Δ is the ultimate value of the damage.
If the Paris law is used to evaluate the propagation of a critical fatigue crack, the eq. (5) modifies into the:

$$Z = a_f - a \tag{6}$$

where a is the current length of the crack and a_f is the corresponding ultimate value.
Then in both cases the basic variables $\underline{X}$ are transformed in a corresponding set of uncorrelated normal standard variables $\underline{x}$. Also the limit state condition is projected in the space of the variables $\underline{x}$ and becomes $z(\underline{x})=0$.
The limit state condition is approximated by means of an hyper-plane tangent to it in the point nearest to the origin:

$$z(\underline{x}) \approx \sum_{i=1}^{m} \alpha_i x_i + \beta = 0 \tag{7}$$

where $\underline{\alpha}$ is the vector of direction cosines of the normal to that hyper-plane. Then it follows:

$$\beta = -\sum_{i=1}^{m} \alpha_i x_i \tag{8}$$

and β is computed by iteration.
The value of Tres corresponding to $\beta = \beta_0$ is the solution of the eq. (2).

4. SOME REMARKS ON INPUT PARAMETERS

4.1 The stress collective

The time history of the loads applied to a structural component of a steel bridge is a random process, as it is the response to a random load, the traffic. In general it is a wide-banded process, whose power spectral density exhibits several maxima, corresponding to the structural natural modes and to the maxima of input process. In the study of the fatigue phenomena it is useful to know the statistic properties of the stress cycles of the response process.

It is well known that in the case of narrow-banded response the amplitudes of the stress cycles are Rayleigh distributed:

$$p(\Delta\sigma) = (\Delta\sigma)/\mathrm{var}(\Delta\sigma))\exp(-\Delta\sigma 2/2\mathrm{var}(\Delta\sigma)) \quad (9)$$

In the opposite case when the response process is infinitely wide-banded the distribution of the amplitudes is approximately normal.
By means of integration it is possible to find the corresponding stress collective. In the case of narrow band the integration of eq. (9) leads to:

$$N = N_{max}\exp(-\Delta\sigma 2/2\mathrm{var}(\Delta\sigma)) \quad (10)$$

with $N_{max} = vT$, where v is the frequency of the process and T is its duration.
It is easy to see that eq. (10) is a parabola in semilogarithmic scale (Fig.1a).
In the case of wide band the stress collective is computed by numerical integration and shows the trend of Fig.1b.
Also when the distribution of the cycles amplitudes is neither Normal, nor Rayleigh it is necessary to resort to numerical integration.

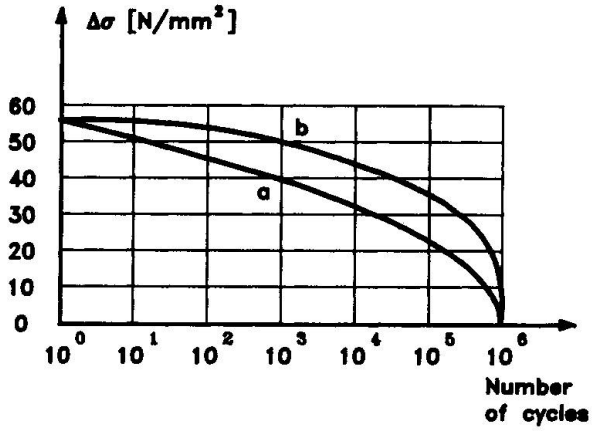

Fig.1 Stress collective: a) narrow band and b) wide band structural response

4.2 The damage criterion

The simplest and most widely used damage criterion for the evaluation of the fatigue life under variable amplitude loading is due to Palmgren e Miner. It expresses the fatigue damage D as:

$$D = \sum_{i=1}^{k} \frac{n_i}{N_i} \quad (11)$$

On the basis of laboratory tests Miner [5] reports that the range of values for D was from 0.61 to 1.49, with an average value close to unity.
In 1954 Marco e Starkey [6] report that in the case of sequences of ascending stress amplitudes the average value for D was 1.49 and in the case of descending loading the average value for D was found to be 0.78. To simulate this behaviour they propose the following non-linear damage criterion:

$$D = \sum_{i=1}^{k} \left(\frac{n_i}{N_i}\right)^{\delta} \quad (12)$$

with δ depending on the order of application of loading blocks.
In the '60 the methods of assessment of damage based on fracture mechanics assert themselves, especially in the field of mechanical engineering. Among the others we remember the Paris - Erdogan law [7]:

$$da/dN = C(\Delta K_I)^n \quad (13)$$

where da/dN is the rate of crack propagation and ΔK_I is the opening mode stress intensity factor. The crack does not grow if ΔK_I is lower than a threshold value K_{IC}. The fatigue failure occurs when the crack length a reaches the critical value a_f. Further improvements to this criterion are due to Klesnil e Lukas [8], who consider the threshold value as a function of the stress history and to Forman, Kearney , Engle [9], who take into account the ratio between the minimum stress and the maximum one in every cycle $R=\sigma min/\sigma max$.
In 1978 Hashin e Rotem [10] propose a non-linear damage criterion which remembers the sequence of stress cycles. It is expressed by the recurrent relation:

$$D = \mu_i \quad (14)$$

$$\mu_i = \mu_{(i-1)}^{A} + n_i/N_i$$

with $A = (\Delta\sigma_i - \Delta\sigma_e)/(\Delta\sigma_{i-1} - \Delta\sigma_e)$
where $\Delta\sigma_e$ is the material endurance limit.

5. NUMERICAL APPLICATIONS

The proposed method of analysis was applied to an actual case, to test its validity and the sensitivity to input parameters.
A steel railway bridge was considered. The evaluation of the remaining fatigue life was performed at a welded joint of a secondary beam of the deck.
As far as the material is concerned, the SN law is assumed to be a straight line in logarithmic scale, without endurance limit, following the equation:

$$N\Delta\sigma^l = B \quad (15)$$

with $l = 5$ and $B = 10^{16}$.
the ordinate at 10^6 cycles is therefore 100 N/mm^2. It corresponds to the mean value minus two standard deviations.
The crack propagation law is the Paris-Erdogan one with $n = 3.3$, $C = 2.43\times10^{-12}$ and $\Delta K_{IC} = 5.8$ MN/$m^{3/2}$. These figures correspond to the mean value of variables.
The stresses applied to the structural member during its past life were extimated to fit into a collective of parabolic shape having a total duration of 100×10^6 cycles and maximum ordinate $\Delta\sigma_{max}$ of 50 N/mm^2. The collective of future stresses was supposed to have the same shape with the same values of duration and maximum ordinate.
The evaluation of fatigue damage was performed using the Miner rule, adopting as its critical value 0.8, as suggested by Augusti [11]. The residual life was computed at Level 2 applying the procedure presented in the chapter 3., for the value $\beta_o=3$ of the safety index. Also the values $\beta_o=2$ and $\beta_o=4$ were considered as a reference. Input data are presented in Table 1.
The analysis led to the following extimates of the residual life T_{res}, expressed as number cycles: for $\beta_o=2$ $T_{res} = 3.30\times10^{10}$, for $\beta_o=3$ $T_{res} = 6.53\times10^{9}$, per $\beta_o=4$ $T_{res} = 1.17\times10^{9}$.
Then a sensitivity analysis was stated, varying some of the most important parameters.
First of all the influence of the mean value of the

random variable	distribution	expected value	c.o.v.
$\Delta\sigma_{max}$	log-normal	50 N/mm^2	0.20
T_{past}	log-normal	10^8 cycles	0.10
$\Delta\sigma_{SN}$	log-normal	167 N/mm^2	0.20
Δ	log-normal	0.8	0.20

Table 1 Input data of the basic case (Miner rule)

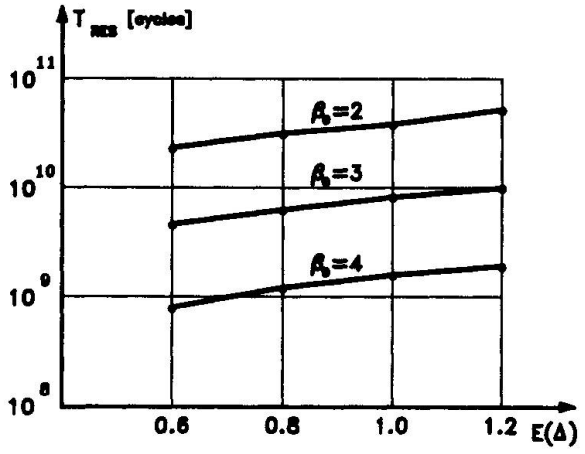

Fig.2 Remaining life as a function of the mean value of the limiting figure of the Miner sum

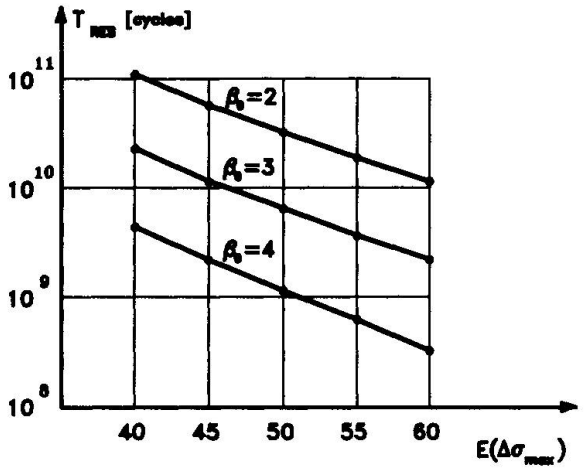

Fig.3 Remaining life as a function of the mean value of $\Delta\sigma_{max}$ expressed in N/mm^2

limiting value of the Miner sum was examined, varying it in the range between 0.6 and 1.2.

The corresponding results are reported in Fig.2. In all the three cases considered for β_0 a nearly twofold variation of the residual life was found between the most favorable case and the least one.

Then the influence of the parameters relating to the stress collective of the past was investigated. In the Figs. 3 and 4 the results of the sensitivity tests toward the variation of the expected value of $\Delta\sigma_{max}$ and of its coefficient of variation $V(\Delta\sigma_{max})$ are reported. For the mean value a range between 40 e 60 N/mm^2 was assumed. It lead to variations of about ten times on the evaluation of the residual life for all the three cases of β_0. As far as the coefficient of variation is concerned, value ranging between 0.10 and 0.25 were considered. The corresponding variation on the residual life was 3.4 times for β_0=2, 5.2 times for β_0=3 and 11 times for β_0=4.

Then the sensitivity to the duration of the past life was investigated, separately considering the effect of its mean value variation (Fig.5) and of the c.o.v variation (Fig.6). The mean value varyed between 10^6 and 10^9 cycles. For β_0=2 and β_0=3 a reduced sensitivity was found and for β_0=4 a sensitivity was found only for very high number of cycles, near 10^9.

As far as the coefficient of variation is concerned (investigated range: 0.1 to 0.25), very little sensitivity was found for all the figures of β_0 considered.

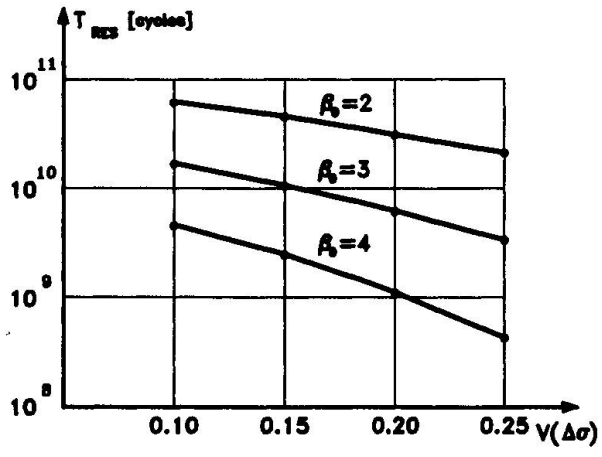

Fig.4 Remaining life as a function of the c.o.v. of $\Delta\sigma_{max}$

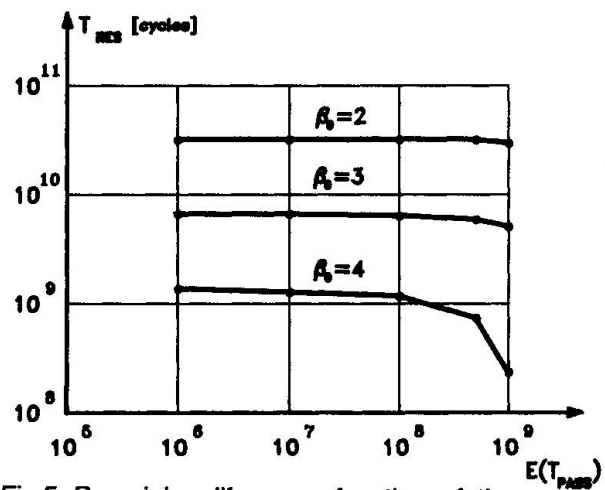

Fig.5 Remaining life as a function of the mean value of the past life

At the end of this part of the investigation the case of simultaneous variation of all input data was considered: first in the most favorable direction, then in the least favorable. The results are reported in Table 2.
Then an analysis of residual life was carried out applying the Paris-Erdogan law Input data are presented in Table 3 and the results are reported in Fig.7.
The numerical computations were performed under two different hypotheses of load application: ascending loading and descending loading. Four values of the initial crack length were also considered: 2,3,4,5 mm.

Case	$\beta = 2$	$\beta = 3$	$\beta = 4$
the most favorable	3.44×10^{11}	9.77×10^{10}	2.76×10^{10}
the basic case	3.30×10^{10}	6.53×10^{9}	1.17×10^{9}
the least favorable	4.36×10^{9}	0.0	0.0

Table 2 Duration of the remaining life expressed as number of cycles

random variable	distribution	expected value	c.o.v.
$\Delta\sigma_{max}$	normal	50 N/mm^2	0.20
C	normal	1.43×10^{-12}	0.10
a_f	normal	40 mm	0.10

Table 3 Input data of the basic case (Paris law)

6. COMMENTS ON THE NUMERICAL RESULTS

Examining the results of numerical computations we can observe that the selected figure for β_0 has a great influence. In fact changing from the value 3.0, which is suggested by the Joint Committee on Structural Safety [12] and is the basic value of our analyses, to 2 the residual life increases an average 5 times and changing to 4 the life reduces an average 5 times.
During the numerical analysis the influence of the parameters describing the stress collective and of the limiting value of the Miner sum was investigated. The major sources of uncertainty are the mean value of the maximum stress range, its coefficient of variation and the damage criterion.
The idea rises from this to reduce the sources of uncertainties with experimental in situ observations oriented toward two directions. The first one is to detect

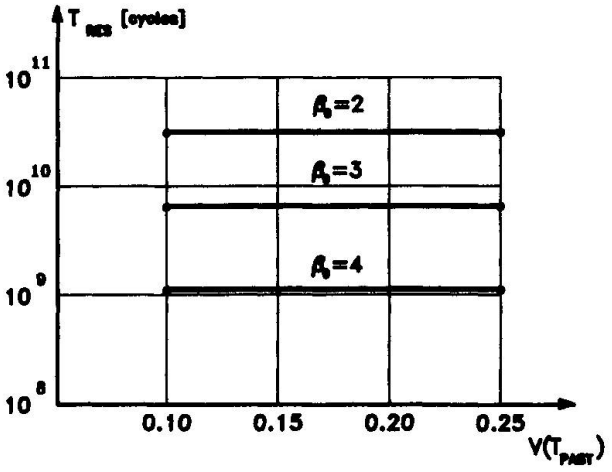

Fig.6 Remaining life as a function of the c.o.v. of the past life

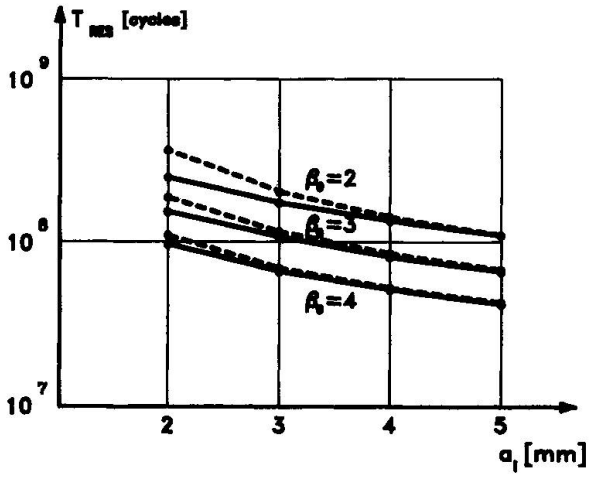

Fig.7 Remaining life computed with the Paris law: continuous line decreasing load, dashed line increasing load. ai is the initial value of the fatigue crack

the fatigue damage of the material by means of the measurement of the length of fatigue cracks. The second one is to improve the extimate of future stress history by means of sampling observations of bridge vibrations, extended to time intervals sufficient to warrant measure stationarity.
The application of the Miner rule with the improved data leads to better results. An alternative way is to use the Paris law, which allows to directly use load data without statistical reordering and the results of damage measurements.
The presented methodology is well suited to be a consistent procedure for the calibration of partial safety factors employed by the Level 1 methods.

7. CONCLUSIONS

The previous examination showed the differences between the procedures for the safety analysis of brand new structures and the existing ones. The first are methods connected to conventional probabilistic models and are intended to be support for the design process, the second ones can take advantage of experimental in situ tests that give improved information on the structural behaviour. Also in the case of fatigue problems it is often possible to gain better information whether using the Miner rule or applying the Paris law.
The theoretical fundamentals of the estimate of the residual fatigue life at Level 2 were reviewed.
The numerical experiments, which were carried out with reference to the case of a steel railway bridge, showed that the application of the method based on the Miner rule leads to estimates highly dependent on the uncertainties enbedded into the parameters that describe the past stress collective. This result encourages to undertake field tests to ascertain the damage accumulated in the past.
The use of the method based on fracture mechanics allow to improve the estimate quality and to take advantage of the information from field control of structural behaviour.
Than it seems reasonable the suggestion to subject the steel railway bridges to periodic control in order to detect incipient fatigue damage and to progressively update the evaluation of residual life. So it is possible to plan eventual strengthening works.

REFERENCES

1. MACCHI G., RADOGNA E.F., MATERAZZI A.L., Synergetic effects of environments actions and fatigue. IABSE Symposium "Durability of structures", Lisbon, 1989, pp. 493-8.

2. HIRT M. A., Remaining fatigue life of bridges. IABSE Symposium "Mainteinance, Repair and Rehabilitation of Bridges", Washington, D.C., 1982, pp. 113-29.

3. STIER W., STEINHARDT O., VALTINAT G., KOSTEAS D., Residual fatigue life of railway bridges. IABSE Colloquium "Fatigue of steel and concrete structures", Lausanne, 1982, pp. 823-31.

4. COMMISSION OF THE EUROPEAN COMMUNITIES, Eurocode No.3: Common unified rules for steel structures, 1984.

5. MINER M. A., Cumulative damage in fatigue. ASME Journal of Applied Mechanics, Vol.12, 1945,pp. A159-A164.

6. MARCO S. M., STARKEY W. L., A concept of fatigue damage. Transactions of the ASME, Vol 76, 1954, pp. 627-32.

7. PARIS P., ERDOGAN F., A critical analysis of crack propagation laws. ASME Journal of Basic Engineering, dec. 1963, pp. 528-34.

8. KLESNIL M., LUKAS P., Influence of strength and stress history on growth and stabilisation of fatigue cracks. Engineering fracture mechanics, Vol. 4, 1972, pp. 77-92.

9. FORMAN R.G., KEARNEY V.E., ENGLE R.M., Numerical analysis of crack propagation in cyclic-loaded structures. Journal of Basic Engineering, Trans. ASME, Sept. 1967, pp. 459-64.

10.HASHIN Z., ROTEM A., A cumulative damage theory of fatigue failure. Materials science and engineering, Vol. 34, 1978, pp. 147-60.

11.AUGUSTI G., BARATTA A., CASCIATI F., Probabilistic methods in structural engineering. Chapman and Hall, London, 1984.

12.DITLEVSEN O., MADSEN H.O., Proposal for a code for the direct use of reliability methods in structural design. Joint Committee on Structural Safety, Working Document, Nov. 1989.

Leere Seite
Blank page
Page vide

Safe Life Evaluation of Existing Bridges

Evaluation conservatrice de la durée de vie des ponts existants

Bestimmung der sicheren Lebensdauer bestehender Brücken

Fred MOSES
Prof. of Civil Eng.
Case Western Reserve Univ.
Cleveland, OH, USA

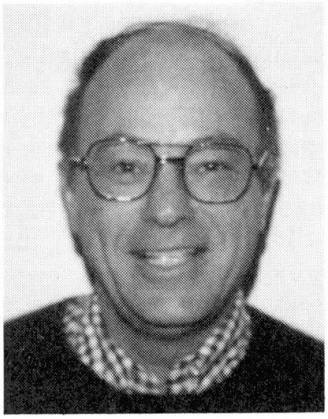

Fred Moses received a civil engineering degree from CUNY in 1960 and a PhD from Cornell in 1963. Since joining Case Institute, Professor Moses has been active in structural optimization and reliability with special applications to bridge and offshore structures including loading, safety analysis and system reliability studies.

SUMMARY

Estimates of the safe remaining life of existing steel bridges affect decisions on inspection, maintenance, replacement, truck weight, permit posting limits and even changes in new weight regulations. A reliability model has been developed and calibrated to produce uniform and consistent fatigue checking procedures for different spans, geometrics, bridge types, and traffic. These methods have been adopted in recent AASHTO Guide Specifications for fatigue design of new bridges and safe-life evaluation of existing steel bridges. The same model has been extended to compute costs associated with proposed truck-weight regulations. These costs affect new designs and particularly, existing estimates of bridge repair and damage.

RÉSUMÉ

L'évaluation de la sécurité des ponts en acier existants influence les décisions relatives à l'inspection, la maintenance, le remplacement, le poids des camions, les limites de charge à imposer, et peut même engendrer des modifications dans les lois réglant le poids des camions. Un modèle de charge a été développé et calibré afin de conduire à des vérifications à la fatigue uniformes et cohérentes pour différentes portées, géométries, types de ponts et trafics. Ces méthodes ont été adoptées dans les nouvelles recommandations AASHTO pour la conception à la fatigue des nouveaux ponts et l'évaluation de la sécurité des ponts en acier existants. Ce même modèle a été étendu afin d'estimer les coûts liés aux propositions de règlements pour le poids des camions. Ces coûts influencent la conception actuelle et, plus particulièrement, les estimations des réparations et du dommage de ponts existants.

ZUSAMMENFASSUNG

Die Abschätzung der sicheren Restlebensdauer bestehender Stahlbrücken beeinflusst Entscheidungen betreffend Inspektion, Unterhaltung oder Ersatz einer Brücke, betreffend signalisierte Gewichtslimiten oder Änderungen der gesetzlichen Gewichtsbeschränkungen. Ein Modell zur Bestimmung der Ermüdungssicherheit von Stahlbrücken wurde entwickelt. Es wurde so angepasst, dass es in einheitlicher Art und Weise für verschiedene Brückentypen, Spannweiten, Geometrien und Verkehrsmischungen anwendbar bleibt. Die Methode wurde in den kürzlich erschienenen AASHTO-Empfehlungen für die Ermüdungsbemessung neuer Brücken und die Bestimmung der sicheren Lebensdauer bestehender Stahlbrücken übernommen. Dasselbe Modell wurde mit dem Ziel erweitert, die Kosten zu berechnen, welche durch Änderungen der Gewichtsbeschränkungen verursacht werden. Betroffen durch solche Änderungen sind die Kosten neuer Konstruktionen und, in vermehrtem Masse, die Reparaturkosten bestehender Brücken.

1. INTRODUCTION

A companion paper describes a reliability-oriented load prediction model for the random fatigue damage accumulation per year [1]. This damage was expressed in terms of traffic, material and analysis random variables. The data base was expressed in terms of nominal values and bias and respective coefficients of variation. The study described in this paper utilizes the probabilistic damage accumulation and data base to determine safety indices for fatigue failure modes. These safety indices are used to calibrate fatigue procedures for evaluation. These procedures contain nominal checking procedures and factors of safety for both redundant and nonredundant load path structures. The aim is to have uniform and consistent safety indices over the full range of traffic spectra, bridge types and spans. These methods have been incorporated into two recently adopted AASHTO Guide Specifications for design of new steel bridges and safe life evaluation of existing steel bridges [2,3]. Assessment of safe remaining fatigue life is useful for developing inspection intervals, scheduling repair and replacement and making permit decisions. A second application of the fatigue risk model is the extension to a cost allocation study of new truck weight regulations. Projected increases in truck weight and volume changes affect the cost of fatigue damages. Projections were made using the reliability model to the remaining life and costs for over 70,000 steel bridges in the United States over the coming 50-year period [4].

2. FATIGUE RELIABILITY MODEL

This section formulates a reliability approach to predict that the fatigue life of steel beam attachments will be less than the estimated life. Several points to note are: (1) the assumptions of the model, (2) the random variables in the true fatigue life, and (3) the sensitivity of the risk to the statistical parameters of these random variables. The safety margin is expressed in terms of a failure function, g, as in usual structural reliability practice.

$$g = Y_F - Y_S \tag{1}$$

Failure does not occur if $g < 0$. Y_F is life at which failure occurs (a random variable), and Y_S is specified life (deterministic). The expression for Y_F is given in the other paper.

2.1 Safety Index

The safety index (or beta) is the number of standard deviations between the mean of g and the boundary of the safe value of g. If g is normal, the risks corresponding to β are found from a normal probability table, e.g. $\beta = 3$ gives a risk of 0.001. Beta typically falls in the 1 to 4 range in most structural applications. If the variables are not normal, computer programs are available to compute β for general distributions of random variables and failure functions g. The programs output the safety index, β, and the most likely failure values. The latter helps assess in the failure event each random variable. The accuracy in characterizing the statistics of any single variable will decrease as the total number of variables increase as, say, in the fatigue model which has ten random variables. Thus, if we seek a risk of 10^{-4}, the design point value for each variable may fall in only the 10^{-2} range. Thus, realistic and accurate assessments of reliability can be made without requiring an unrealistic amount of data.

2.2 Calibration

Code writers have a responsibility in selecting a consistent target safety index, or β, for a code check. One approach is to base the decision on economics, i.e., an optimum failure rate occurs when the cost trade-off of increasing the safety factor balances the risk reduction of future failures. A problem here is expressing the cost of failure. Another approach is to compile historical failure rates. If the rate is deemed acceptable, this can be considered the societal target

risk. A difficulty is to isolate failures truly related to code checks. Most structural failures occur because of blunders or gross errors in design concept, detailing or fabrication and are *not* related to the code checking. The approach usually adopted for establishing the target beta is to assess the present design provisions and perform safety index calculations over a wide range of representative practice (e.g., for different bridge spans, geometries, attachments). In general, there will be a wide range observed in computed β's because uncertainties were not consistently considered in the original development of the specifications. The aim in any new code provisions should be uniform or consistent target reliabilities. Thus, an average beta based on present standards is selected and this becomes the target for future code provisions.

2.3 Selection of Safety Factors

Figure 1 shows the beta vs. safety factor, γ, for a 100' span bridge and category C detail. The figure was obtained by substituting value a of γ in the expression for fatigue damage (Eq. 22 of Ref. 1) and computing the corresponding safety index, β using Eq. 1 herein. Plots similar to Figure 1 were made for different spans, and different fatigue detail attachments [5]. It was shown that the plot of β vs. γ is not sensitive to such changes so a single representative curve such as Figure 1 could be used. In the calibration, the target beta is selected as an average of the betas implicit in present design practice.

Fourteen AASHTO design cases (A-N) with different truck volumes, detail categories, spans impact factors, lateral distribution factors, and support conditions (simply supported or continuous) are shown in Table 1 to evaluate an average beta implicit in the present AASHTO design practice. This is done by taking sections which just satisfy the present AASHTO fatigue criteria and computing the implicit safety factor, γ. The designs selected were intended to be both representative of typical cases and also to represent possible extreme occurrences. For example, case H has a mean impact of 1.20 and a mean girder distribution of 0.50. The corresponding β's found from the γ versus β graph for each case are shown in Table 1. For example, for redundant or multiple load path members, Table 1 shows, that most of the design points fall around a beta of 2.0. This is midway in the range of the betas (0.7-3.6) corresponding to all the design points. The average β of 2.0 corresponds in Figure 1 to a reliability factor γ of 1.35. The same analysis was repeated for nonredundant details. The mean of the range of betas (1.5-5.3) for nonredundant details appears to be about 3.0. This corresponds to a reliability factor, γ, of 1.75. From this analysis of the average betas for existing design the target safety index for redundant and nonredundant members was fixed as 2.0 and 3.0, respectively, in the proposed evaluation procedure.

These examples demonstrate quite strongly the advantages of the proposed format. For redundant spans, we try and achieve our target β of 2 for all the design cases while AASHTO produced betas ranging from 0.7 to 3.6. Design with high betas is uneconomical, while the low betas will have relatively low probabilities that the actual fatigue life will exceed the predicted life. Similarly, for the non-redundant cases, the proposed evaluation methods try to achieve a target β of 3.0 for all cases compared to AASHTO betas that range from 1.5 to 5.3. The target betas will not be achieved exactly even for the proposed procedures. More factors would be needed to make this possible. The scatter in beta, however, will be smaller. The corresponding betas for these sections are shown in columns (5) and (7) of Table 1 for redundant and nonredundant members, respectively. The scatter in beta for redundant members is between 1.85 and 2.17 (as against 0.7 to 3.6 for AASHTO methods) and for nonredundant members it is between 2.85 and 3.10 (as against 1.5 to 5.3 for AASHTO methods). Hence, the proposed procedures achieve the goals of a more uniform safety index.

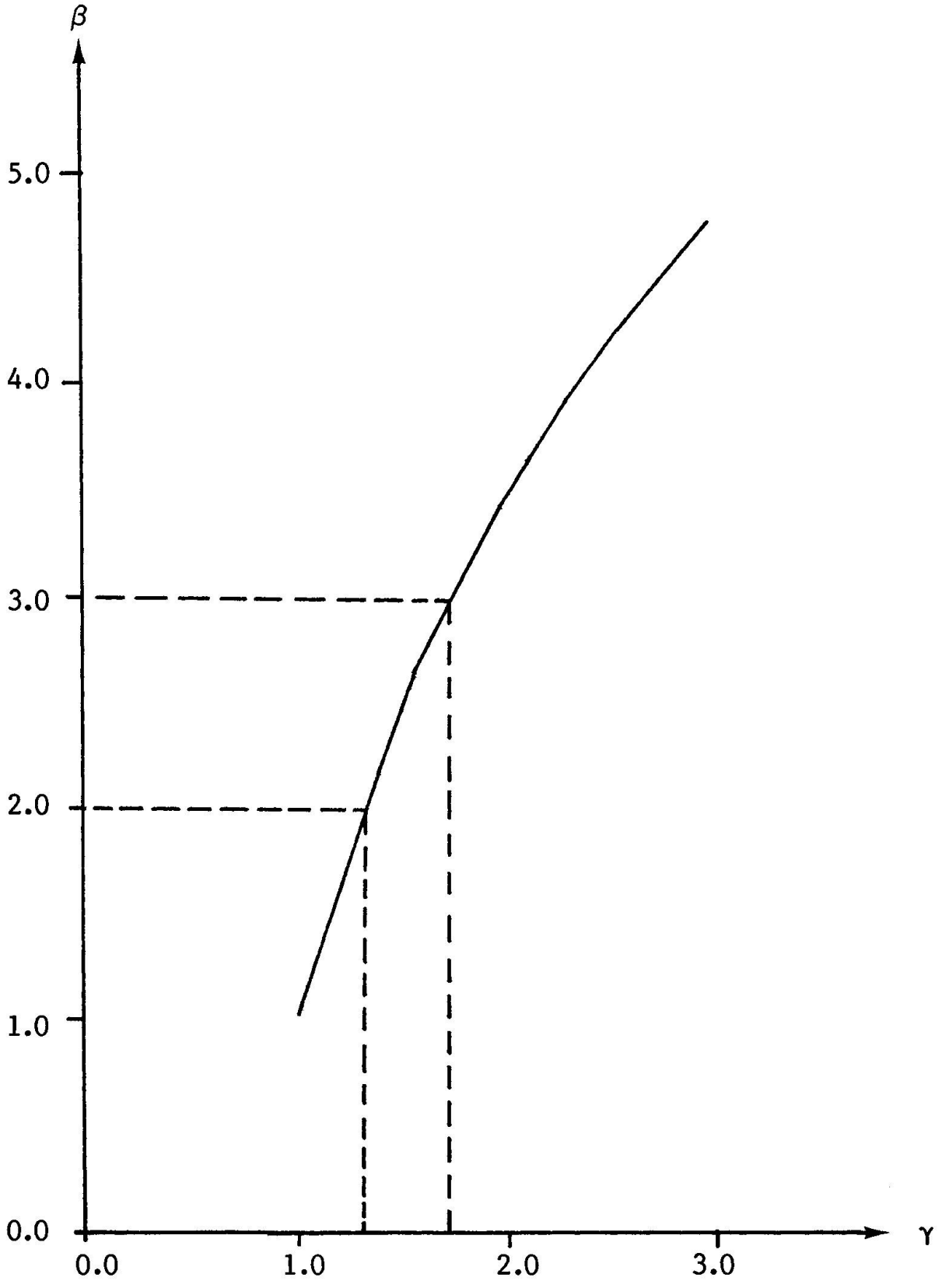

Figure 1. Mean γ vs. β curve.

2.4 Safety Factor Adjustments in Evaluation Procedure

The evaluation procedures have been developed with the following aims: (1) consistent and uniform reliability over the range of application (all spans, categories, lives, volumes); (2) flexible to incorporate site-specific data; (3) flexible to provide the Engineer with a better (usually longer) fatigue life estimate if more effort is applied. The first aim was satisfied by the calibration process. A target safety index has been fixed to achieve consistent and uniform reliability. The other two goals are obtained by incorporating several alternatives to the basic procedure. Some of the alternatives need site-specific data, while some other alternatives require more analysis effort by the Engineer. It should also be noted that in the evaluation, the Engineer can also obtain the mean fatigue life as well as the safe life. This should help explain why a span, which does not satisfy a safe life check, may not show any visual signs of fatigue cracking. Typically, the mean life will be about 5 times the computed safe life for redundant spans and 10 times the safe life for nonredundant spans. For a span not meeting the required safe life, the Engineer can select different options including more frequent inspection or control on vehicles.

Most of the alternatives in the evaluation lead to lower safety factors. The concept here is that risk is influenced by both the safety factor and the uncertainty. The same target safety index can therefore be achieved by reducing uncertainties and using a smaller safety factor. For example, availability of stress measurements for an attachment rather than the computed value permit the reliability factors, γ, to be reduced by 0.85. Use of measured truck weight spectra to provide a site-specific equivalent effective weight for the fatigue design vehicle reduces the γ's by 0.95. Finite element analysis to compute attachment stresses rather than the distribution chart or formulas provided in the specification reduce γ's by a factor 0.96.

2.5 Fatigue Limit

It is generally accepted that a constant amplitude fatigue limit exists for typical bridge details. If all cycles in a variable amplitude spectrum are below this constant amplitude fatigue limit, the fatigue life for the spectrum would be infinite. More research is still required to determine if a fatigue limit exists for a variable amplitude stress spectrum when only several stress cycles exceed the constant amplitude fatigue limit. Long life fatigue tests being conducted at Lehigh, TRRL, Maryland, and elsewhere may help resolve this issue. As one illustration,the reliability program was modified to exclude all the stress cycles below the constant amplitude fatigue limit while computing the fatigue damage. The results show that even after the model has been changed (a fatigue limit is introduced), the average betas from the proposed method and the AASHTO method are still almost the same [5].

3. PROPOSED FATIGUE EVALUATION PROCEDURES

A proposed bridge fatigue evaluation procedure based on the above reliability analysis was approved as a Guide Specification by AASHTO. Although optional as a requirement, it is being developed for a new edition of the commonly used AASHTO Maintenance Inspection Manual. This document is used to evaluate on a two year cycle, each of the nation's 600,000 bridges. The fatigue evaluation specification is primarily intended to determine the remaining safe life for application to inspection, maintenance, repair, replacement strategies, permit review and general truck weight control policies.

3.1 Application

This section summarizes the recently approved AASHTO Guide Specifications for fatigue evaluation of steel bridges [3]. The specifications for assessing remaining safe life apply only to uncracked members subjected to primary stresses that are normally calculated in design. The

stress range is calculated first and used to predict the remaining mean and safe fatigue lives. The remaining mean life is the best possible estimate of the actual remaining life. The remaining safe life is a more conservative estimate which provide a level of reliability comparable to present AASHTO fatigue provisions. Alternatives that may be used at the option of the Engineer are given for several steps in the procedure. Each attachment must be considered individually.

The stress range for fatigue evaluation can be calculated by the following steps or, alternatively, can be determined from field measurements. A fatigue truck is used to represent the variety of trucks of different types and weights in the actual traffic. This truck has three axles with axle spacings of 14 ft and 30 ft and axle weights of 6, 24 and 24 kips respectively. This spacing approximates that for the 4- and 5-axle semitrailers that do most of the fatigue damage to bridges. The gross weight of the fatigue truck is 54 kip; this weight was developed from extensive weigh-in-motion data. Alternatively, the gross weight can be calculated from a truck-weight histogram obtained from weigh station or weigh-in-motion data for the site. Alternative axle spacings and weight distributions based on site data are also permitted.

The effects of more than one truck on the bridge at a time can be neglected unless there are conditions of close spacing of the trucks. The dynamic impact caused by different trucks usually vary considerably. Test data indicate that a factor of 10 percent is appropriate for fatigue evaluations. Poor joint or pavement conditions, however, require higher values.

The stress range is based on the moment or axial load range caused by the passage of the fatigue truck across the bridge. The lateral distribution factors for the fatigue evaluation are based on a single truck at the centerline of a traffic lane rather than on trucks in all lanes. Field tests have shown that the bending stress of actual bridge members is below that calculated by normal procedures, which conservatively neglect such effects as unintended composite action, contributions from nonstructural elements such as parapets, unintended partial end fixity at abutments, and direct transfer of load through the slab to the supports. To account for these effects, the computed section modulus is increased by appropriate percentages for composite and noncomposite sections, respectively.

Reliability factors are provided to assure adequate reliability in calculating the remaining safe life for different cases. Basic factors are recommended for redundant and nonredundant members. The corresponding probabilities that the actual remaining fatigue life will exceed the calculated remaining safe life are about 97.7 percent and 99.9 percent, respectively. The reliability factor is 1.0 for calculating the remaining mean life. If the compressive dead load stress is high enough so that essentially all of the stress cycles caused by normal traffic are completely in compression, the fatigue life is assumed to be infinite. If the maximum stress range in tension falls below the fatigue limit for a particular detail, crack growth will not occur and infinite fatigue life may be assumed. This situation, which applies primarily to higher detail categories (C and above), is checked by comparing the factored stress range with a fatigue limit value calibrated to a β of 2 to provide an adequate reliability that crack initiation will not occur. This fatigue limit value is equal to (1/2.75) times the present AASHTO allowable stress range for the over-two-million cycle category.

Finite remaining life: If a given detail does not satisfy the infinite life check, the remaining safe fatigue life (in years) corresponding to the factored stress range is calculated for a lifetime average truck volume and a selected number of stress cycles per truck passage. Alternatively, more refined procedures that involve growth rates and changes in truck weights with time can be used to calculate the remaining fatigue life. Detail constants are for the detail categories in the present AASHTO specifications. The equivalent number of stress cycles per truck passage is given for various cases.

Options if remaining life is inadequate: The evaluation procedure gives four options that may be pursued if the Engineer considers the calculated remaining safe fatigue life to be inadequate. These include (1) calculating fatigue life more accurately, (2) restricting traffic on the bridge, (3) repairing the bridge, or (4) instituting periodic inspections.

4. EVALUATION OF PROPOSED TRUCK WEIGHT REGULATIONS

In most industrialized countries there is increasing economic and political pressures to allow heavier vehicles and special permit trucks. The productivity gains are impressive from such weight increases and pavement damage can be mitigated or reduced by allowing vehicles with up to nine or more axles. A recent Bridge Impact Study by the writer was conducted for the Transportation Research Board under a congressionally mandated truck weight study [4]. It is only for bridges that increased truck weights may cause damages which offset the expected gains to freight shippers. Most of the bridge cost concerns strength capacity and increasing numbers of structurally deficient bridges. Fatigue costs were also considered. The approach used in the study is a reliability model similar to that given above for fatigue evaluation. This model gives the increasing risk of fatigue cracking as a bridge ages and accounts for different truck spectra. The probability that the actual fatigue life will be less than current life can be obtained from the reliability index.

4.1 Fatigue Damage

Fatigue damage is caused by all trucks passing over the bridge. If present truck weight regulations are changed, a percentage of the trucks in present traffic will be replaced by the new heavier trucks permitted. To calculate the relative fatigue damage caused by traffic before and after the change, it is necessary to know the composition of the truck traffic before and after the change; that is, the percentages of different types and weights of trucks in the traffic. In essence, the proposed fatigue cost model projects present expenditures for fatigue problems in steel bridges and adjusts these costs based on changes in traffic projections and passage of time.

4.2 Present Fatigue Cost

An estimate of the present expenditures on fatigue problems is required so that they can be used as a base case in projecting the expenditures associated with new truck weight scenarios. A limitation in a state survey is that agencies generally have great difficulty in assessing the costs of fatigue damage and relating these to vehicle regulations. In addition to the state survey, an estimate of the current annual cost of fatigue damage on steel structures in the United States was discussed with several experts on fatigue damage and repairs in highway bridges. For example, Dr. John Fisher stated that he has personal knowledge of fatigue problems on several hundred bridges. Based on these discussions an annual figure of $50 million would be an appropriate estimate. These include all costs to (a) repair actual or potential fatigue damage, (b) replace bridges that are unsafe because of fatigue damage and cannot be economically repaired, (c) perform engineering studies to evaluate actual or potential fatigue problems revealed by routine inspections or suggested by experience with similar bridges at other sites, (d) make engineering studies to develop appropriate corrective measures if required, (e) make extra inspections required to monitor fatigue cracking or check certain types of bridges that have had fatigue problems at other sites, and (f) reroute traffic when a bridge is closed because of fatigue problems.

Over the next 50 years, $50 million per year of damage (present value) totals $2.5 billion. There are 75,000 steel bridges on Interstate and primary routes and $2.5 billion in damage represents about 12% of the net value of such structures. This percentage is not unreasonable since present AASHTO fatigue design procedures are based on a 5% exceedance probability for fatigue life

failure and further, many steel bridges were constructed before any fatigue provisions were in place and in recent years there has been significant increases in truck volume and average weight.

4.3 Future Fatigue Costs

The fatigue risk model is used to extrapolate the present fatigue damage costs as they increase in the future due to a) passage of time and accumulation of more cycles of loading, and b) changes in weight regulations which accelerate the damage rate. For different weight changes or scenarios the costs are found by computing fatigue cost vs. a damage ratio, R. The reference or base value for cost is \$50 million per year. The damage ratio, R, is defined as:

$$R = \Sigma_i P_i R_i \tag{2}$$

where i - indicates span interval (including both simple and continuous spans)
P_i - percent of steel bridges in span interval i
R_i - applicable damage ratio for interval i.

$$R_i = \frac{\Sigma_t \Sigma_W V(t,W,S)\, M(i,t,W,S)^3}{\Sigma_t \Sigma_W V(t,W,B)\, M(i,t,W,B)^3} \tag{3}$$

where t - truck vehicle type
W - weight interval for truck type t
$V(t,W,S)$ - volume for truck type t, weight interval W, and proposed truck weight scenario S
$M(i,t,W,S)$ - maximum bending moment for span i, for weight W, and type t, in scenario S
$V(t,W,B)$ - base case (current) volume for type t, weight interval W
$M(i,t,W,B)$ - corresponding moments for base case

4.4 Future Damage

In the bridge evaluation, the reliability model is applied to a single bridge (with known design life and site parameters). The approach now is to extrapolate to the entire system of existing bridges. An average present life of 25 years was used as typical for existing Interstate and major route structures that are affected by fatigue problems. New weight regulations change the rate of "aging". A parameter y is used to express future damage, D_f, in terms of present damage, D_0.

$$D_f = D_0 \frac{25 + (AGE - 25)\, R}{25} = D_0 y \tag{4}$$

Where y = aging parameter
AGE = average bridge age at a future time compared to present 25 year age.
R = ratio of the annual damage after new weight regulations to present annual damage from Eq. (2).
D_0 = damage accumulated at present
D_f = damage accumulated at future date

R is the ratio of damage before and after a change in truck weight regulations and accounts for both truck weight and volume changes. A productivity analysis was part of the truck weight study to project volume changes within each truck type and region in the U.S. Because of the wide range of design loadings and truck volumes for the population of existing bridges, the fatigue risk procedure must be calibrated for the average safety margin of the entire population. Based on the number of fatigue problems to date, a beta of 2.5 seems reasonable. This implies a

probability of 0.006 for a fatigue failure on an existing bridge. A .006 risk would mean 450 fatigue failure. This is plausible in view of Professor John Fisher's comment above.

Using a β = 2.5, y = 1 (present age) and the risk model in Eq. (1) leads to a mean safety margin of 14. This means that the typical bridge has an expected life 14 times the present average life of 25 years. As the structure ages, and further damage is accumulated, beta decreases. For example, when beta falls to 1.5 in the future the risk for an average steel bridge will have increased from .006 (at the present time) to about 0.067. This represents an increased risk ratio of 11.2. Using the 75,000 bridge sample, instead of the cumulative 450 failed bridges at present, there is expected to be a cumulative total of 5,025 damaged bridges at that time. It is assumed that damage costs increase in direct proportion to the number of failed bridges. Thus, the total cost at the future time, when beta is 1.5, will be 11.2 times the present $50,000,000 or $560,000,000 per year. In order to compare with productivity benefits future damage costs are transformed to constant equivalent annual costs over the next 50 years.

4.5 Examples

Fifty years of future life are projected to cover the remaining life of the existing population of steel bridges. New steel bridges will be based on the new truck weight regulations to have adequate fatigue life and are not included in this cost analysis. For example, the equivalent uniform annual cost of fatigue damage with no change in present damage rate is $157M/year using i = 7%. If the new truck regulations double the damage ratio, R, to 2.0, the fatigue damage increased to $320M/year. Sensitivity studies were carried out to find the fatigue costs for different assumed present beta, interest rates and other statistical parameters [4].

4.6 Proposed Truck Weight Regulations

It is shown above that the present equivalent annual cost of bridge fatigue damage with no change in regulation is $157M/year. This is based on the fatigue risk model to extrapolate the present expenditures of $50M/year will increase as bridges "age" increasing the risk. Several different weight change scenarios were studied along with data from productivity projections to estimate the volume of truck changes. As a base case, the present U.S. legal truck weight limit is 80,000 lbs although many jurisdictions permit higher weight under special legal, legislative or administrative actions.

Adoption of a proposed Canadian Interprovincial truck regulation, for example, would increase the gross weight from 80,000 to 131,000 on a 65' wheel base as well as other weight increases for shorter wheel base vehicles. The fatigue damage increase using Eq. 2 was found to be R = 1.41 [4]. This raises fatigue damage costs by an estimated $65M/year. In general, it is found that truck weight regulations have a much greater cost impact due to causing strength deficiencies than shortening of fatigue life. Such conclusions assume that funds will be expended to increase strength capacity levels to requirements for increased truck weights. One possibility is that agencies will restrict heavy vehicles to special routes which do not require strength upgrades. In that case, the fatigue cost may be a significant proportion of the total bridge costs. In all, some 20 truck weight scenarios were studied using the FHWA data file of some 600,000 bridges. With respect to all weight regulations studied, productivity gains far outweighed bridge costs.

5. CONCLUSIONS

1. Reliability models are available to develop nominal fatigue checking formats and safety margins which lead to uniform and consistent reliability indices.
2. Sufficient data is now available to calibrate the model to use performance experience as a guide for computing target indices for singe and redundant load path systems.

3. A Guide Specification has been presented and adopted by AASHTO which is based on the model discussed herein and has been extensively used by several agencies.
4. Extensions of the fatigue risk model estimated future bridge damage costs if truck weight regulations permit heavier loadings and more rapid aging of structures.
5. It is important that increased tax revenue be available to the bridge system to ensure adequate funds for increased inspection, repair and eventually earlier replacement.

6. ACKNOWLEDGMENTS

The author acknowledges the contributions of his coworkers on the project, C.S. Schilling and K.S. Raju. Other assistance from I. Friedland and H. Cohen, TRB Contract Managers and Project Consultants, Professor John Fisher and Dr. Abba Lichtenstein are appreciated.

REFERENCES

1. "Bridge Load Models for Fatigue", IABSE Workshop on Remaining Fatigue Life of Steel Structures, Lausanne, 1990.

2. Guide Specifications for Fatigue Design of Steel Bridges, AASHTO, Washington, D.C., 1989.

3. Guide Specifications for Fatigue Evaluation of Steel Bridges, AASHTO, Washington, D.C., 1990.

4. Moses, F., "Effects on Bridges of Alternative Truck Configurations and Weights", NCHRP Contract HR2-16(b) Report to Transportation Research Board, Washington, D.C., December 1989.

5. Moses, F., Schilling, C.G. and Raju, K.S., "Fatigue Evaluation Procedures for Steel Bridges", NCHRP 299, Transportation Research Board, Washington, D.C., 1987.

Table 1 Comparison of β's in proposed methods and present AASHTO methods

			β		β	
		Detail	Redundant Members		Nonredundant Members	
Designation	Span	Category	AASHTO	Proposed	AASHTO	Proposed
(1)	(2)	(3)	(4)	(5)	(6)	(7)
A	120'SIMPLE	C	1.05	1.99	1.85	2.93
B	100'SIMPLE	C	2.00	2.02	2.90	2.96
C	60'SIMPLE	A	2.05	2.03	2.10	2.85
D	60'SIMPLE	B	2.15	1.97	2.65	2.92
E	60'SIMPLE	C	2.20	2.10	3.20	2.93
F	60'SIMPLE	D	2.75	1.97	3.90	2.91
G	60'SIMPLE	E	3.10	1.85	5.35	2.87
H	30'SIMPLE	C	0.70	2.16	1.50	3.09
I	100'CONT	A	1.45	2.06	1.50	2.89
J	100'CONT	B	1.60	2.01	2.00	2.98
K	100'CONT	C	1.65	2.05	2.80	2.99
L	100'CONT	D	2.05	2.01	3.45	2.97
M	100'CONT	E	2.40	1.90	4.80	2.96
N	60'CONT	C	3.55	2.17	4.10	3.10

Accumulation of Fatigue Damage, Automatically Recorded and Evaluated

Cumul du dommage en fatigue: enregistrement et analyse automatiques

Schadensakkumulation infolge Ermüdung: automatische Aufzeichnung und Auswertung

Tomas NAVRATIL
Cybernetics Engineer
Tesla Elstroj
Prague, Czechoslovakia

Tomas Navratil, born 1960, received his M.S. degree at the Czech Technical University in Prague. For six years, he has been interested in control and data acquisition systems as well as software development. At present he is working on his PhD thesis at the Czech Technical University.

Pavel MAREK
Assoc. Prof.
Sportovni stavby
Prague, Czechoslovakia

Pavel Marek, born 1932, obtained his civil engineering degree and PhD at the Czech Technical University in Prague. Over the past 25 years, he has been involved in structural steel research and teaching at Czech and foreign universities. At present, he is a Visiting Professor at the San Jose State University of California.

Milos VLK
Assoc. Prof.
Technical University
Brno, Czechoslovakia

Pavel Vlk, born 1937, received his mechanical engineering degree at the Technical University in Brno. For 23 years, he studied fatigue and brittle fracture and applications of findings to industrial practice. At present, he is a university teacher.

Ivo HEPNAREK
Dr. Eng.
Vitkovice-Institute of Applied Mechanics
Brno, Czechoslovakia

Ivo Hepnarek, born 1948, received his civil engineering degree at the Technical University in Brno. Fields of professional interest are numerical and experimental analysis of static and dynamic response of full-scale steel structures.

SUMMARY
This paper presents a method of recording and evaluating the accumulation of fatigue damage using an electronic device. User needs and available evaluation algorithms are discussed. The paper also includes a brief description of the hardware and software aspects. Finally, experience from field use, an example and future prospects are presented.

RÉSUMÉ
Cet article présente une méthode d'enregistrement et d'analyse du dommage de fatigue faisant intervenir un dispositif électronique. Les besoins de l'utilisateur ainsi que les algorithmes d'analyse à disposition y sont discutés. L'article contient également une brève présentation de quelques aspects du matériel et du logiciel. Enfin, il présente des expériences d'applications pratiques, un exemple ainsi que des développements futurs.

ZUSAMMENFASSUNG
Der vorliegende Artikel erläutert eine Methode zur Aufzeichnung und Auswertung der Schadensakkumulation infolge Ermüdung mit elektronischen Hilfsmitteln. Bedürfnisse der Benützer sowie zur Verfügung stehende Auswertungs-Algorithmen werden diskutiert. Ebenso ist eine kurze Beschreibung einiger Hard- und Softwareaspekte enthalten. Erfahrungen aus praktischen Anwendungen, ein Beispiel und künftige Entwicklungsmöglichkeiten werden vorgestellt.

1. INTRODUCTION

In using the Limit States Design Method for assessment of reliability, the structure and its components are considered to have adequate reliability if the defined most unfavourable responses, the extreme characteristics, do not exceed the limit value. These values, defined for all the reliability conditions during the life of the structure, can be grouped in carrying capacity limit states and serviceability limit states.

Special attention has to be paid to the evolution of the extreme characteristics of the structure to the loading. Especially in case of fatigue and for the evaluation of the accumulation of fatigue damage during the lifetime lack of input data may cause severe problems.

The subject of this paper is a description of a device which allows recording of the time dependent response of a structure to the loading and easy evaluation of the accumulation of fatigue damage as well as corresponding residual fatigue life.

As electronic components become more reliable and consume less power so that a device can be operated for long periods of time without maintenance, an idea has emerged to build a device which can replace costly and sensitive apparatuses like tape recorders to collect, preprocess and store information on the response history of metallic structures such as bridges, guyed masts etc. It was clear in the very beginning that such a device has to be designed to withstand various climatic and mechanical stresses. For that purpose, one-chip microcontrollers and other integrated circuits are an ideal solution.

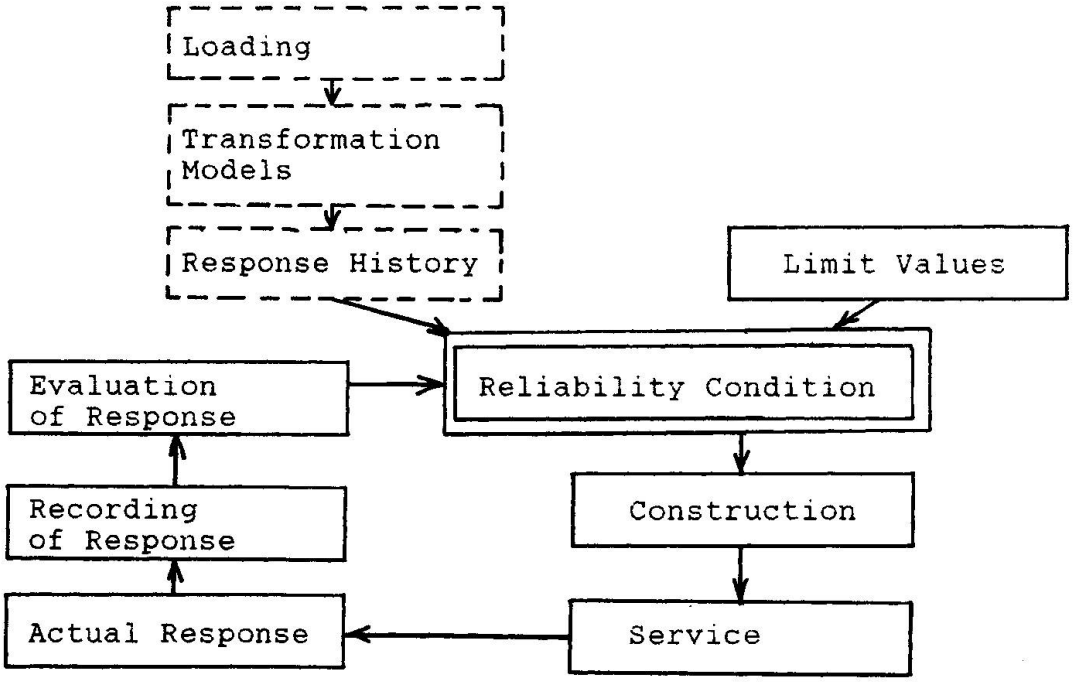

Fig. 1 Feedback Loop

2. USERS' DEMANDS ON THE DEVICE

In order to make the purpose of the device clear, let be mentioned the case when there are substantial uncertainties in the loading and/or the transformation model to establish the response to the loads as discussed in the feedback loop (see Fig. 1).

The structure is built and assessed subsequently based on observations in service. The response history is then evaluated and used as feedback to assess the reliability conditions. This approach is used quite frequently in the assessment of the reliability condition for fatigue [2]. It may lead to a modification of the existing structure or to an increase in the general body of knowledge, improvement of specification, etc.

The purpose of the device is the monitoring of the strain history of the metallic structure and recording the processed information in a non-volatile memory. The operator then connects the communication cable with the device and transfers the stored data into a portable computer where the information is to be evaluated.

This formulation was precised during the developing of the device, in connection with obtaining more information on the recording device currently used by the customer, while the compatibility became the main point of view, for example, analog input within the range of +- 12 V of the measured quantity was required.

There were several demands on the ease of operation and maintenance and flexibility. In the lab sample, six channels of analog input were implemented and active channels are selected by the software. Two methods of the preprocessing of the information and input hystheresis were to be selectable. For verifying the design, switches were used in the device, but in production the options will be firmware-selected so that less reliable components and cables can be eliminated.

The information is to be stored in a non-volatile memory. A CMOS memory device, backed-up by a battery, was used to satisfy the demand. The capacity of the memory can range between 2K and 16K bytes, depending on the method used and the number of channels.

Two methods of transferring the data into some evaluating device have been considered. The first possibility is to use a standard serial communication cable and to transfer the data in the desired format (RS 232) into a computer carried by the operator. An IBM PC compatible or the Sharp portable computer are two examples.

The second method is to replace the whole memory module by a fresh one and to carry the recorded module to the office where its contents can be read by a special adapter connected to a personal computer. This method eliminates the need of the computer to be carried into the field.

3. THE HARDWARE SOLUTION

The hardware has been designed to use Czechoslovak components where possible. An 8048 microcontroller with an external program memory has been chosen for the lab sample in order to achieve a greater debugging ability. For volume production, the 8748 or 80C48 types with a built-in program memory and a low power consumption are to be used.

The controller is clocked by a 6 MHz oscillator from which the timing information is derived to the timer and the baud rate generator. The controller's bus and ports communicate with the program storage, analog multiplexer, A/D converter, serial port, configuration switches and 8255 peripheral circuit to which the memory module is attached.

The analog input circuitry is designed to process up to six input signals within the range from -12V to +12V. The range is divided into 256 levels.

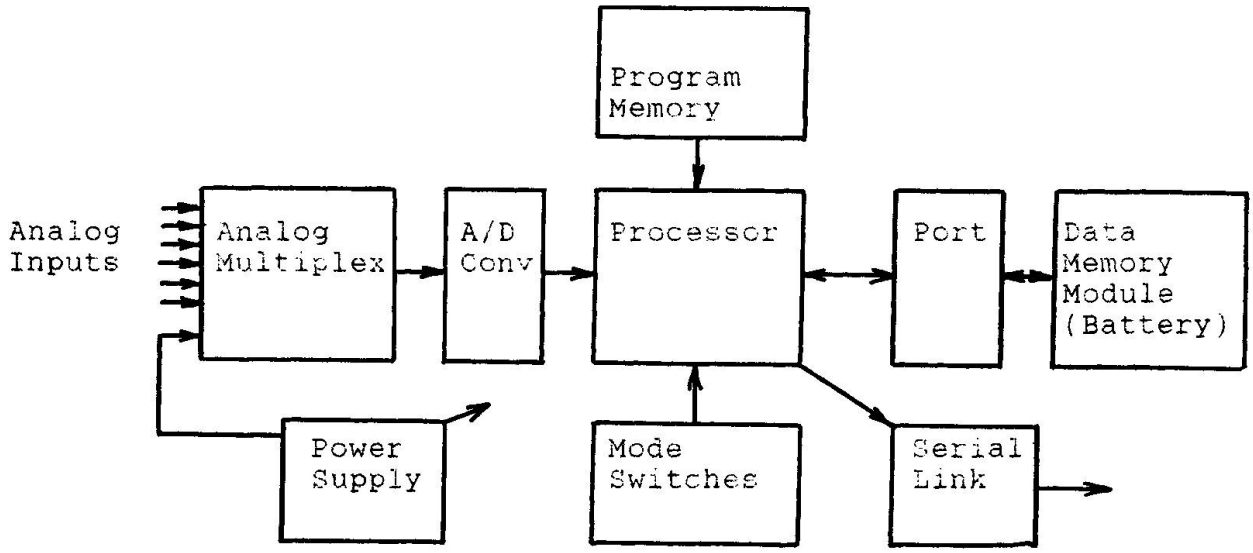

Fig.2 Block diagram of the device

The input analog multiplexer connects one of the six inputs to the A/D converter. Another analog signal can be selected by the multiplexer: the power sense signal which indicates the power failure. In that case the microcontroller disables the access to the memory.

The A/D converter converts the value of the input voltage to an 8-bit number. Though a lower resolution is required by the software, this amount of information is easy to manipulate with and is used for generating the input hystheresis. The binary number is obtained by a software controlled D/A converter and a comparator.

The asynchronous serial port is also software driven by one bit of the microcontroller's port. The TTL level signal is transformed to RS 232 levels. The transfer rate is software selectable; in the lab version 2400 bps are selected.

The configuration switches select the options of operation:

active channels, hystheresis and the preprocessing method.

An 8255 programmable peripheral interface is used to control the non-volatile memory in which the preprocessed information is stored. The memory is not directly connected to the microcontroller so that the memory module can be easily removed from the device and replaced by a fresh one. The 8255 circuit generates the addresses and control signals for the memory, the data are transferred through one of its ports. The memory cycles are controlled by the software. In the beginning of each cycle, supply voltage is checked so that in the case of a power failure the data can not be damaged. After the data are written into the memory, the checksum in the last byte is updated to ensure the data validity. If a power failure occurs, the controller notices it and resets the 8255 circuit whose ports go to the low level. Thus, the content of the memory is kept intact because the memory access is initiated by a high level on the module's control inputs.

The memory module itself consists of one or two CMOS memory circuits and CMOS logic circuits, a battery and other elements. The CMOS devices are permanently powered by a lithium battery on-board. The battery life can be estimated at five years.

During the transportation of the memory module, its inputs are kept low by resistors. In the reading adapter in the office the module is repowered by an external source and its content can be read and written into.

The power source for the device can be selected to be supplied by several voltages. In the lab sample, a simple 220 Vac 50 Hz line was chosen. Under certain conditions, when operated in a mobile structure, a 24 Vac supply may be preferred as well as a dc-dc transducer.

The device, when operated in extreme low temperature conditions like in a mountain area, may contain a thermostatic subsystem that keeps its temperature within the allowed range. The system's tolerance to high temperatures is determined by the quality of the used components and can be estimated at 100 deg C. The heat production of the device itself is very low due to the low-power CMOS technology used.

The lab sample was designed to verify the function and explore the possibilities and the users' real needs; that is the reason why its mechanical construction was not the main imperative point of view. However, the planned volume-production devices should withstand raw mechanical conditions. This aim will be achieved by using the quality printed circuit board technology with as small moving parts as possible, reliable components and a robust metallic case.

4. SOFTWARE

The software has been written in the microcontroller's machine language so that the demands on optimal code are fulfilled. The microcontroller's internal memory is very limited and it cannot be saved during power failure. Thus, the data memory must always keep all information needed.

The software in the program memory has three main parts. The first part is used for interfacing with the 'real world'. It manages the input signal selector, the A/D conversion, the power check and the timer.

The second part is the data preprocessing and storing into the memory. It is dependent on the employed method of analysis; the rain-flow method was used in the lab sample, the options using or omitting the mean value are selectable. This part also manages the memory depending of the number of inputs and the method used.

The third part was incorporated into the program for outputting the data via the serial line. This part gets the data from the memory, converts them to a convenient ASCII format and transmits them through the port using its own baud rate generator.

5. FIELD USE

The experiments verified the device's ability to collect the information from one of several analog sources, preprocess it using the rain-flow algorithm, store the data in the non-volatile memory and output them to the operator. There is a connection of the maximum number of channels, computing the requirements of the method used, the processor's speed and the input bandwidth, and also a connection between the storage demands of method used, the number of channels and the required capacity of the data memory.

The field usage confirmed the need of a reliable operation because one unreliable connector can cause a loss of worthy data.

6. EXAMPLE

As an example, applying the device in evaluating the lifetime of excavator for the brown coal surface mining may be mentioned. The stress in the evaluated location was measured in a selected operating mode in the coarse of approximately one month. The obtained representative spectrum of the response is shown in Fig. 3. This information was further used in estimating the life to initiation of fatigue crack.

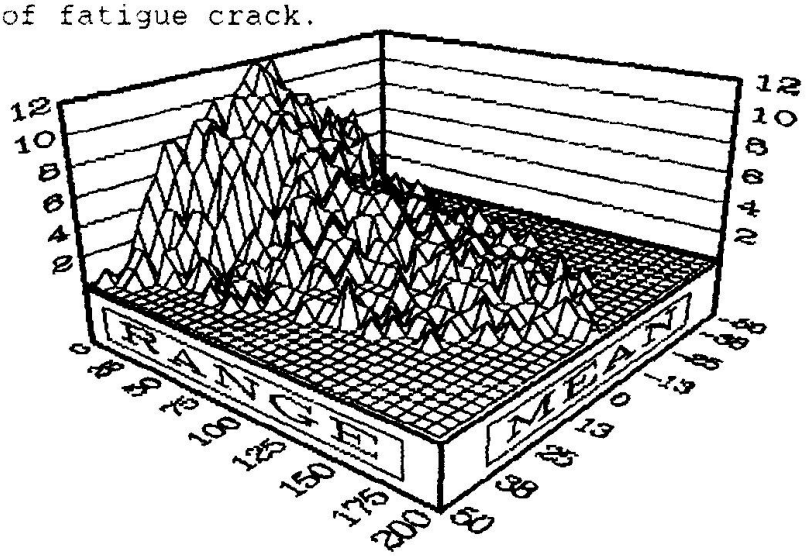

Fig. 3 An example of evaluated data

7. CONCLUSION AND FUTURE PROSPECTS

This paper described a method of measuring, processing and storing the data on fatigue damage of the structure. A microprocessor-based electronic device doing that job was presented. We hope that in mass use, thanks to its low price, it may be mounted permanently on critical parts of the structure and monitor its history so that the residual life may be determined as well as theoretical knowledge may be acquired.

The device should collect and evaluate the data concerning the level of the fatigue damage in real time and accumulate it for long periods of time.

References

[1] Marek, P. - Kennedy, D. J. L.: Development of Structural Steel Design Standards. University of Alberta, Dept. of Civil Eng., Structural Eng. Report 154, October 1987, Edmonton.

[2] Dibley, J.E. - Wilson, A. B. - Bose, B.: Fatigue Monitoring on an Ore Unloader. In: Proceedings of IABSE Colloquium "Fatigue of Steel And Concrete Structures", Lausanne 1982.

Leere Seite
Blank page
Page vide

Vibration Fatigue of Steel Bridges of the Bullet Train System

Fatigue due aux vibrations dans des ponts en acier du réseau de trains à grande vitesse

Schwingungsbedingte Ermüdung von Stahlbrücken des Japanischen Schnellzugnetzes

Kenji SAKAMOTO
Chief Researcher
Track & Structure Laboratory
Tokyo, Japan

Chitoshi MIKI
Associate Professor
Tokyo Inst. of Technology
Tokyo, Japan

Atushi ICHIKAWA
Chief Researcher
Track & Structure Laboratory
Tokyo, Japan

Makoto ABE
Researcher
Track & Structure Laboratory
Tokyo, Japan

SUMMARY
Fatigue cracks caused by out-of-plane vibration were observed in steel bridges of the Tokaido Shinkansen. Crack growth behaviour, measured cyclic stresses, evaluation of fatigue damage, and retrofitting methods are described.

RÉSUMÉ
Des fissures de fatigue causées par des phénomènes de vibration dans les éléments ont été observées sur des ponts en acier du Tokaido Shinkansen. Cet article présente le comportement de la propagation de ces fissures, les mesures des cycles de contraintes, l'évaluation du dommage en fatigue, ainsi que les méthodes de réparation possibles.

ZUSAMMENFASSUNG
In Stahlbrücken der Tokaido Shinkansen-Expresslinien wurden Ermüdungsrisse festgestellt, die vermutlich durch Schwingungen einzelner Elemente aus ihrer Ebene verursacht wurden. In diesem Bericht werden das Ausbreitungsverhalten solcher Risse, Messungen zyklischer Belastungen, die Ermittlung des Ausmasses von Ermüdungsschäden sowie mögliche Instandstellungsverfahren erläutert.

1. INTRODUCTION

One quarter century has passed since the Tokaido Shinkansen was opened for service. Tokaido Shinkansen is one of the bullet train system in Japan operating at the maximum speed of 220km per hour 230 trains daily (Fig.1). Various types of fatigue damages have happened in steel bridges of Tokaido Shinkansen, some of them being comparatively rare with the those in bridges of conventional railway system. Fatigue crackings due to the out-of-plane vibration-induced stresses are typical ones which appeared in the plate girder bridges, box girder bridges and stringers of truss bridges. Vibration-induced stresses under the passage of bullet trains at these bridge details are not of very high amplitude, but of high frequency. No fatal accident due to this type of crack has yet been reported, but retrofitting works are essential to meet the recent demand for an increasing train speed of 270km per hour and a greater transportation capacity. This report describes a behaviors of fatigue cracking, stress measurements, retrofitting works applied and results of remaining life evaluation.

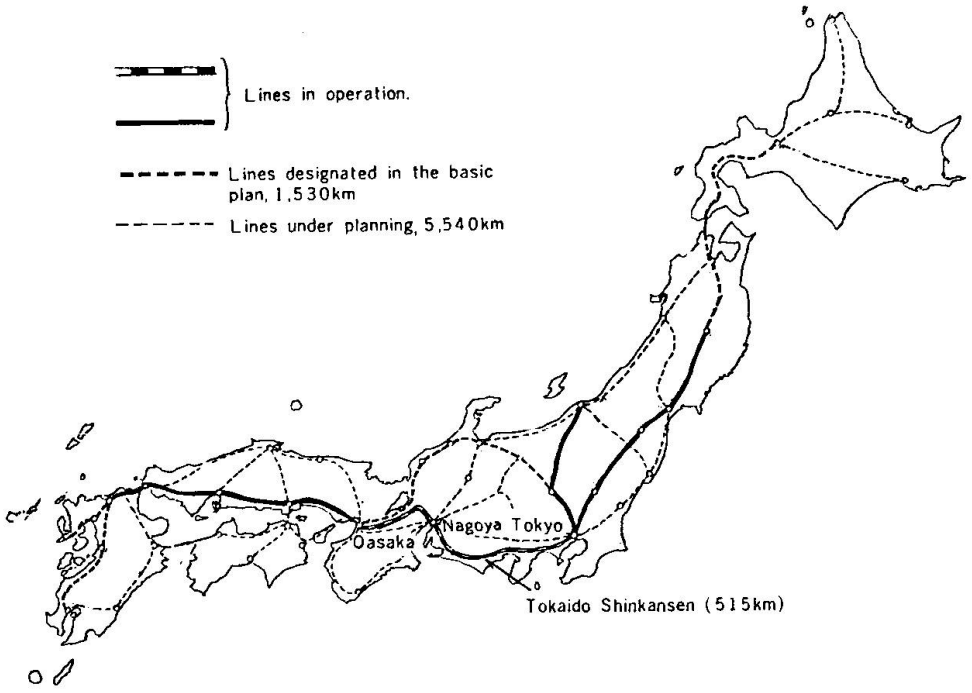

Fig.1 Network of bullet train system

2. OUTLINE OF THE BRIDGE STRUCTURE OF THE TOKAIDO SHINKANSEN

Table 1 shows the quantities of bridges by type of the Tokaido Shinkansen. Steel bridges were designed in accordance with the design specifications established in 1961 and welded structures were adopted for all shop joints. Fig.2 shows the design live load and anticipated use conditions of the Tokaido Shinkansen.

Type	Structure	Number of spans
Steel	Deck plate Girder (I section)	194
	Box Girder	139
	Through plate Girder	155
	Composite Beam	258
	Through Truss	135
Concrete	Reinforce Concrete	3307
	Presstrest Concrete	389
Total		4577

Table 1 Quantities by Bridge Type

Anticipated use conditions

Maximum speed	200 km/h
Number of trains per day	80
Number of cars per train	8 or 12
Design fatigue life	70 years

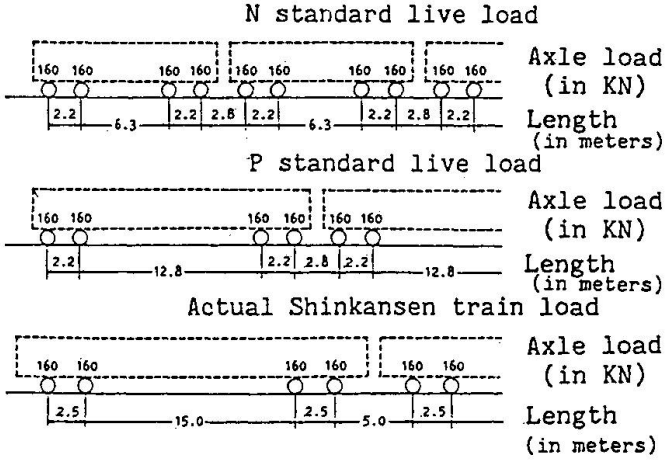

Fig.2 Design live load and anticipated use conditions

Table 2 shows allowable fatigue stresses for various types of joints in the 1961 specifications. These allowable fatigue stresses were based on the fatigue strength at 2 x 10^6 cycles of each structural joints. The designer used the load of 180 kN axle weight which are 20 kN larger than the axial load of the design load as shown in fig.2, taking into consideration a possible increase in traffic in the future. By the end of December 1989, nearly one million trains had passed along the line. The steel bridges in the Tokaido Shinkansen have suffered very severe loading condition caused by high-speed train operation and highly repetitive frequencies. Nevertheless, a fault in the structure has never led to an accident.

In the process of their service, however, some types of fatigue damage have been observed as shown in fig.3. No fatigue damage due to low fatigue strength has not observed in main members where fatigue was assessed in the design stage. However, fatigue cracks which are the result of secondary stresses and displacement induced stresses are often discovered in such various structural elements as girder webs, stringer webs, floor beam webs, side walks, connections of attached facilities and diaphragms. One of these fatigue crackings which occurs relatively frequently and whose cause has not been made much clear is a fatigue crack which occurs on a web plate at the lower end of a siffener (hereinafter referred to as the "lower end of a stiffener"). This fatigue cracks is in parallel with the lower flange.

Category	Types of stress	Fatigue allowable stress (kg/cm²)	Types of joints
A	Tension	$\frac{2000}{1-2/3k}$	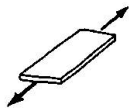
$\bar{A}$	Compression	$\frac{2400}{1-k}$	
B	Tension	$\frac{1500}{1-2/3k}$	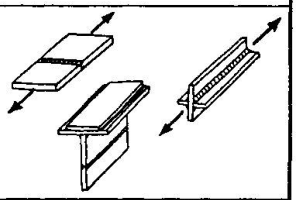
$\bar{B}$	Compression	$\frac{1800}{1-k}$	
C	Tension	$\frac{1260}{1-3/4k}$	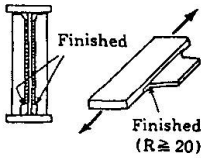
$\bar{C}$	Compression	$\frac{1440}{1-k}$	
D	Tension	$\frac{1000}{1-2/3k}$	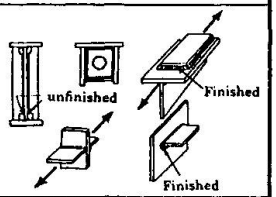
$\bar{D}$	Compression	$\frac{1200}{1-k}$	
E	Tension	$\frac{700}{1-3/4k}$	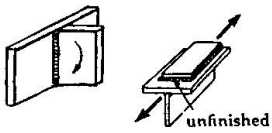
$\bar{E}$	Compression	$\frac{800}{1-k}$	

Note, $k = \frac{|\sigma|_{min}}{|\sigma|_{max}}$

Table 2 Fatigue allowable stress (1961)

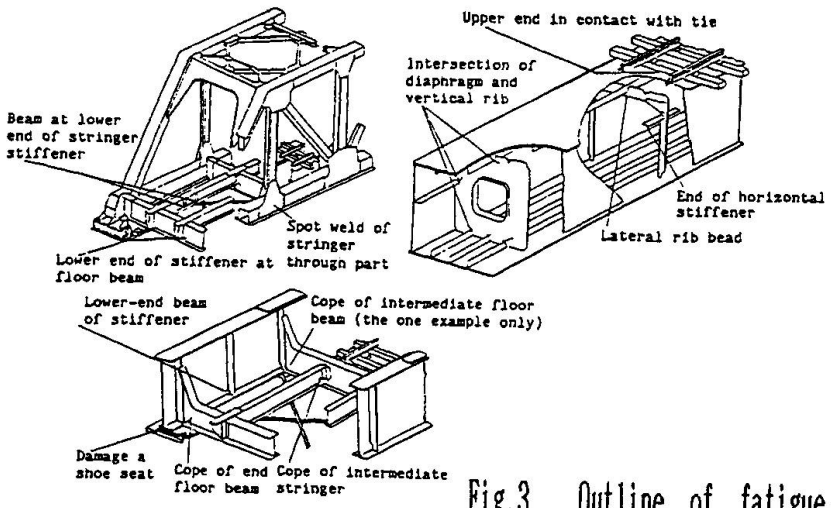

Fig.3 Outline of fatigue damage

3. VIBRATION INDUCED FATIGUE CRACKS IN THE LOWER END OF THE STIFFENER

Fig. 4 shows cracked girder web. This type of fatigue cracks occurred at the lower end of the stiffener on girder webs of box girder bridges and stringer webs of through truss bridges. Characteristically, no crack has occurred at the end of the stiffener to which floor beams or sway bracings are connected. These fatigue cracks began to be observed in 1978. To date, cracks have been observed in about 10,000 details of about 200 box girder bridges and in about 100 details of five through type truss bridges. Countermeasures were taken against all parts of through type truss bridges which were considered to undergo cracking.

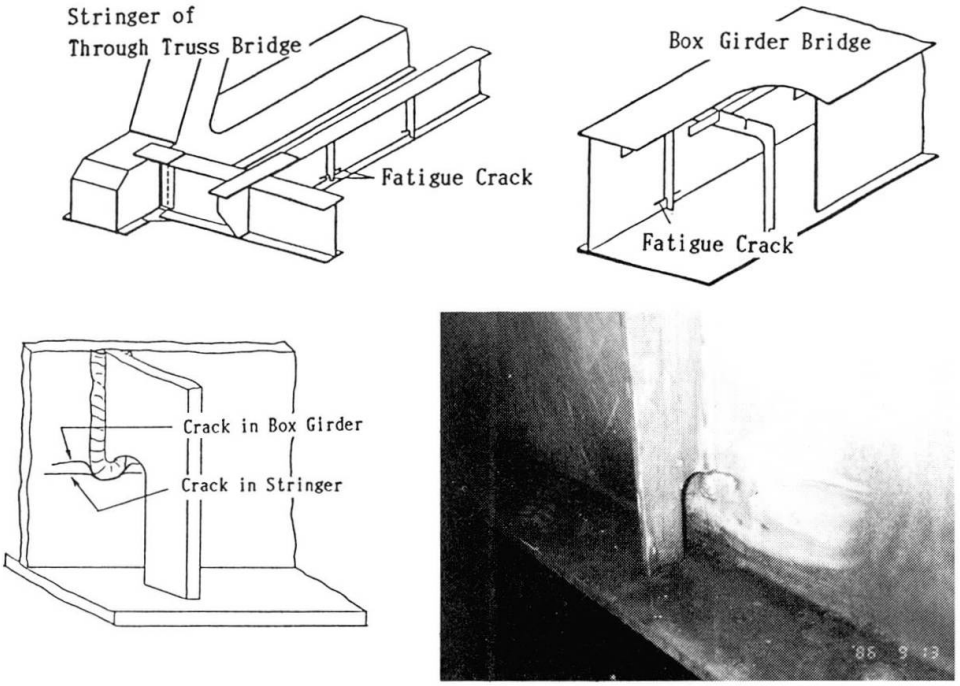

Fig.4 Fatigue crack at stiffener end

4. FAILURE MODE AND ANALYSIS

4.1 Measurement of the Cyclic Stresses

The stringer of a truss bridge was selected for cyclic stress study. This truss bridges has a standard floor system of the Tokaido Shinkansen whose span is 60 m, and the span of stringers is about 10 m. Measurement was made by comparison concerning whether there are sway bracings(Fig.5) and differences in train speeds. Dynamic strain measurement was conducted by placing strain gauges to the back and surface of the web plate at the lower end of the welded portion. The strain gauges were located 5 to 10 mm away from the lower end of weld toes (Fig. 6) stress records were processed as follows.

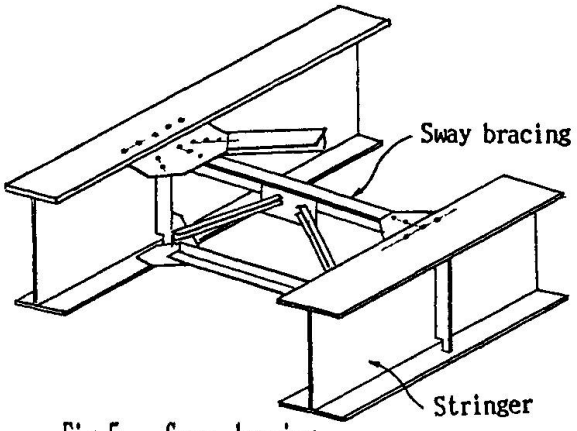

Fig.5 Sway bracing

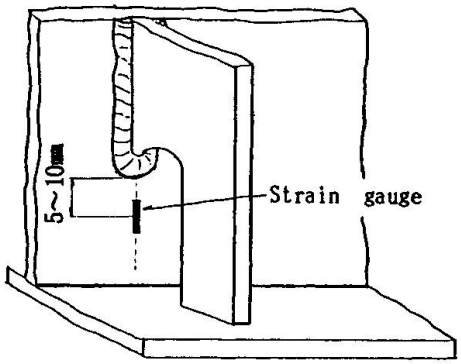

Fig.6 Position of strain gauge

(1) Stress-time analog records were transformed into digital data and the range pair method was applied to obtain stress range histgram.

(2) The linear damage law (modified Miner's law) was applied to evaluate the degree of fatigue damage. The JNR category B design curve was used in the analysis because measured stresses include some influence of stress concentration due to weld beads.

4.2 Results of Measurements and Analysis

Fig.7 shows a typical stress records on the stringer web and the results of frequency analysis. S-1 and S-2 are stress records at same point of stiffener end detail without sway bracing when a train passed away at a speed of 203 km/h and 178 km/h respectively. S-3 is a stress by train passing at a speed of 203 km/h at a position to which sway bracing is connected. Train speeds were obtained, using a strain gauge fitted to the track. Major results of this test can be summarized as follows;
As obviously shown by the comparison between S-1 and S-3, at the detail where sway bracing exists, stress amplitude is smaller than where sway bracing does not exists, and the high-frequency component is also smaller. This is considered to be due to horizontal vibrations of the lower flange.
Stresses in S-1 is the largest measured value in this structure and its stress waveform exhibits a resonating behavior. However, S-2, the stress waveform of a low-speed train (v=178 km/h) does not produce as large stress as S-1 (v=203 km/h). Therefore, horizontal vibration of the lower flange was induced only by the passage of high speed trains. In order to examine this resonating behavior, a stress was separated into the in-plane component and the out-of-plane component as shown in Fig.8. Its results indicate that the stress at the lower end of the stiffener without sway bracing detail is mainly caused by out-of-plane distorsion of the web plate. From this, it seems possible to say that the source of a predominating stress which occurs at the lower end of a stiffener is horizontal vibrations of the lower flange.
Fig.9 shows the stress histgram and the degree of fatigue damage of each stress component. The results suggest that fatigue cracks occurred in several years under S-1 stress history.
However, S-2 shows not so high degree of damage.

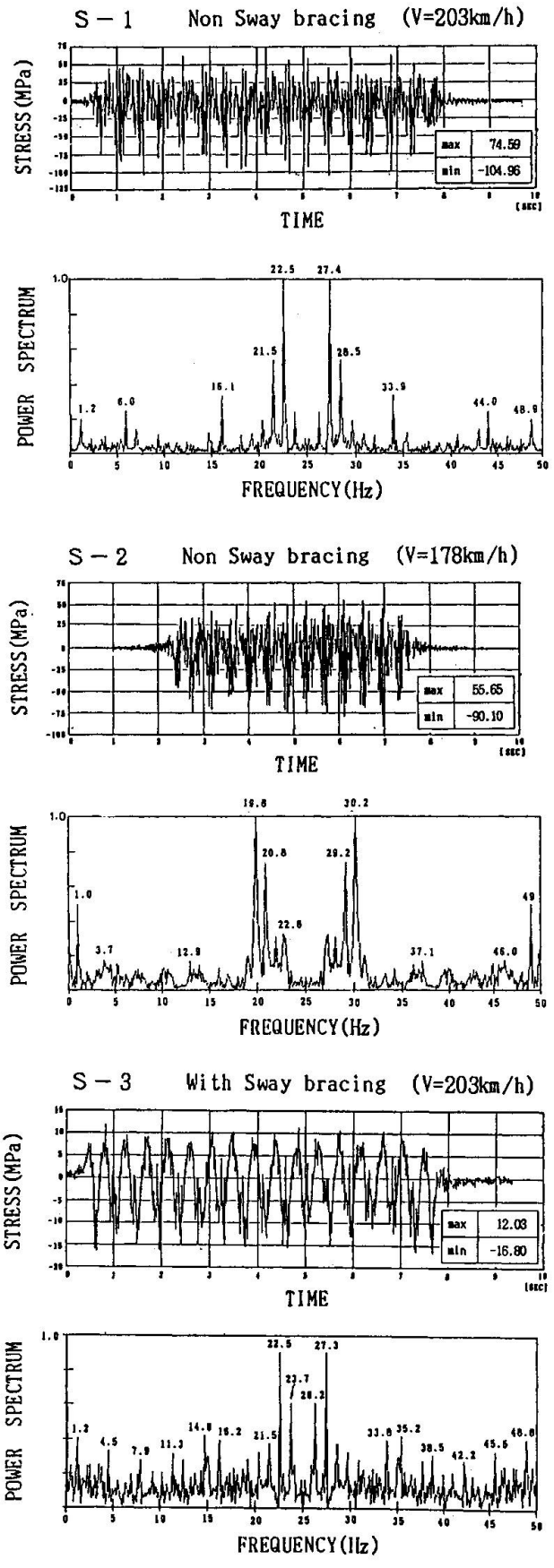

Fig. 7 Representative stress wave in Bridges mesured

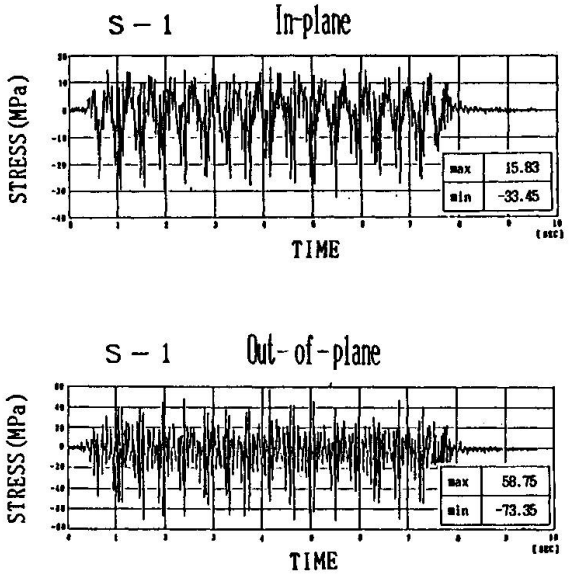

Fig.8 Stress component in In-plane and Out-of-plane of web

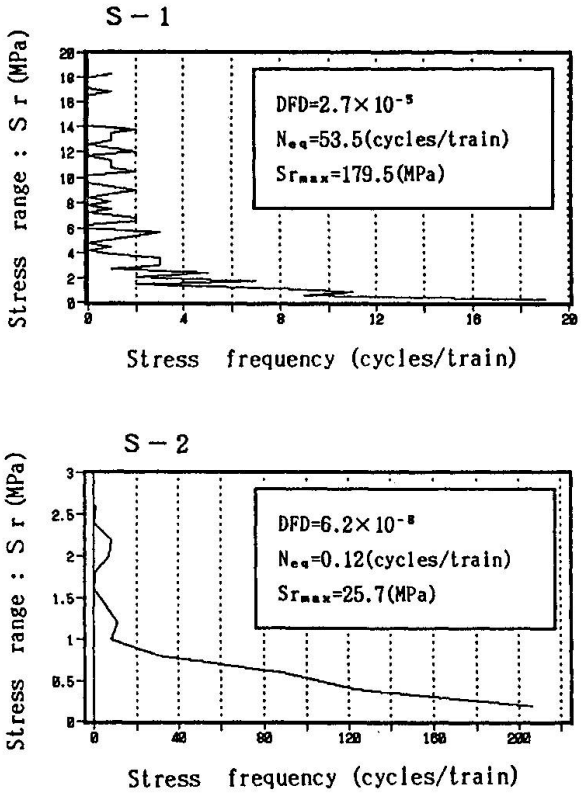

Fig.9 Stress frequency and Degree of Fatigue damage (DFD)

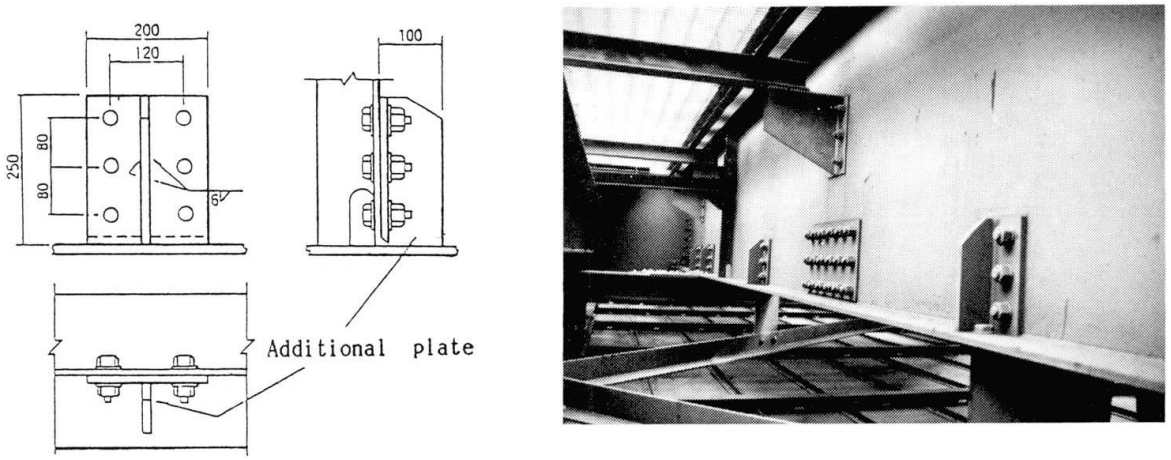

Fig.10 Retrofitting by additional plate

5. RETROFITTING METHODS

As a countermeasure against these fatigue cracks, it is most effective to stop local horizontal vibrations of lower flange which cause fatigue cracks. In some truss bridge stringers, fatigue cracks were removed by applying of arc air gouging and rewelded and then an additional plates were installed by high-strength bolts (Fig. 10). In some cases a sway bracing was also added. Another possible measure is to increase the fatigue strength of the detail. As it is costly to add plates to a slight fatigue crack, it was necessary to consider an economic method for raising fatigue strength. It is advisable to improve the fatigue strength of the toe of a fillet weld and prevent occurrence of additional crack in a part where occurrence of a fatigue crack is not confirmed as a preventive measure. Application of TIG (Tungsten Inert Gas) arc remelting has considered as an effective and economic method for repairing a fatigue crack at the toe of a fillet weld and improving fatigue strength.

5.1 Application Test of TIG Arc Remelting

Repair of the Lower end of a stiffener by TIG arc remelting is required to be conducted, while ensuring that the form of the toe of a fillet weld will be smooth and that penetration will be deep enough to fuse slight fatigue cracks which occur at the toe and is visually undiscoverable. The appearance of the bead under various application conditions and the amount of fusion in the boxing-welded portion were investigated. As a result, it was found that under the conditions as shown in Table 3 fusion was about 2mm in the case of stand-up position and the shape of the bead was in good condition. It was also found that confirmation of the position of a crack is necessary in carrying out the work because there is the possibility of a gap occurring between the position of the maximum fusion by the TIG dressing and the position of a crack.

Electrode diameter	3. 2㎜
Current	240A
Voltage	13～14V (arc length 0～1㎜)
Speed	45～60s/100㎜
Aiming position	0 to 1㎜ from the toe of weld
Torch angle	90°

Table 3 Condition of TIG arc remelting

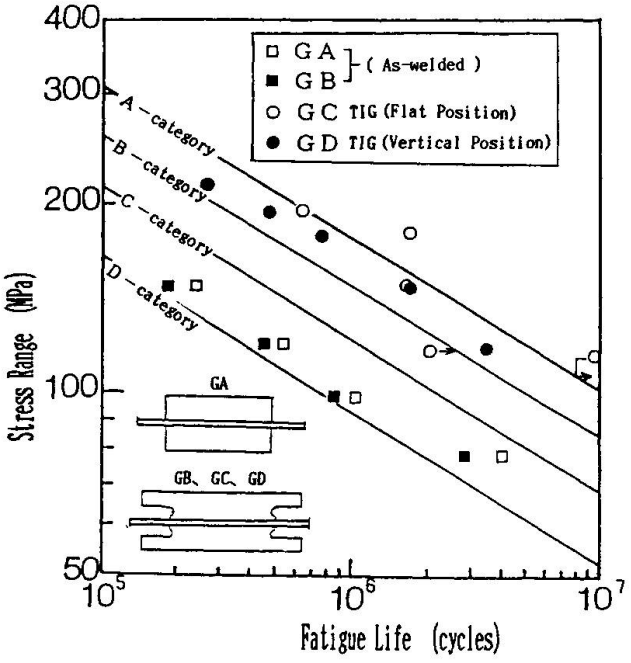

Fig.11 Results of fatigue test

5.2 Improvement of Fatigue Strength by TIG Dressing

In order to confirm the effect of the TIG dressing on this stiffener end detail, fatigue testing was conducted on specimens simulating this detail and applying conditions in actual bridges. Two type of specimens(GC and GD) were TIG dressed under the conditions as given in Table 3. Specimens GC were treated by TIG arc remelting in a face-down position and specimens GD were TIG dressed in a stand-up position, considering actual application conditions.
The result of fatigue testing is shown in Fig. 11. It was found that the fatigue strength of as-welded specimens slightly exceeded the category D of the design curve, while the fatigue strength of TIG dressed specimens exceeded the category B curve. The TIG dressing improved the shape of the toe of weld which affects occurrence of a crack and reduces stress concentration, thus improving fatigue strength.

6. OTHER CONSIDERATION IN FIELD APPLICATIONS OF TIG DRESSING

In executing the work, it was decided that the working procedure would be established as given in Fig.12. All details were observed by qualified inspectors by using eddy current test and magnetic particle test. Before applying the TIG dressing, the shapes of beads were examined. As a result, no special problem was found in the appearance of the beads. However, due to excessive grinding of beads at the time of manufacturing, throat depths of fillet welds were found to be unsatisfactory in some details. In such a weld, in addition to the countermeasures as given in 5, a measure to prevent occurrence of a fatigue crack from the root is necessary. One or two passes of fillet welds were added to such details.

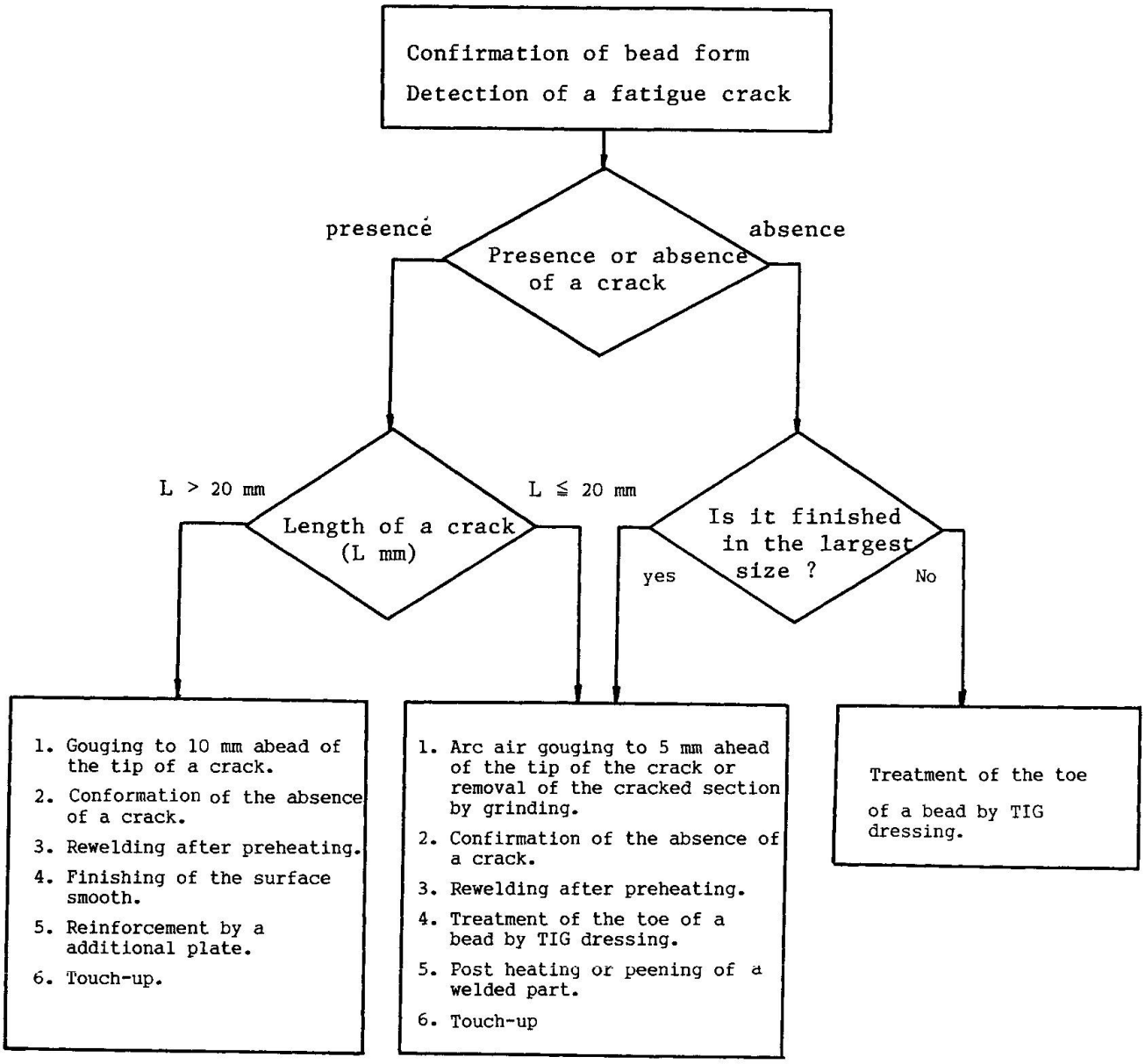

Fig. 12 Retrofitting process

7. CONCLUSION

The retrofitting by the TIG dressing was conducted in 300 box girders. The repaired parts have been inspected specially emphatically but recurrence of a fatigue crack has not been reported.
At present, an evaluation of current soundness is underway for all steel bridges of the Tokaido Shinkansen in preparation for higher speeds and larger transport capacities in the future. As part of this program, several bridges of all types were selected as model bridges and various studies including local stresses, fatigue crack growth behavior in various structural details, and monitoring system of fatigue cracking are being performed.

Fatigue of Cross-Beam Connections in Plate-Girder Highway Bridges

Fatigue dans les attaches des entretoises de ponts-routes à section ouverte

Ermüdung der Querträger-Anschlüsse in Strassenbrücken mit offenen Querschnitten

Ichiro OKURA
Assist. Prof. of Civil Eng.
Osaka University
Osaka, Japan

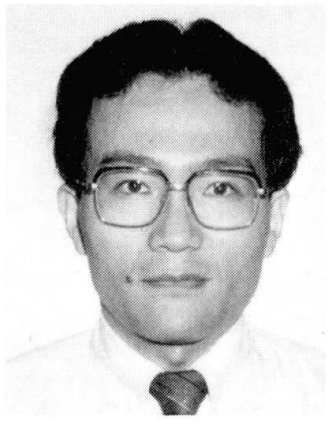

Ichiro Okura, born 1955, received bis BSc, MSc und Dr. Eng. degrees in civil engineering from Osaka University in 1977, 1979 and 1985, respectively. His research field is steel structures.

Yuhshi FUKUMOTO
Prof. of Civil Eng.
Osaka University
Osaka, Japan

Yuhshi Fukumoto, born 1932, received his MSc degree in civil engineering from Kyoto University and PhD degree from Lehigh University. He has held professorship at Nagoya University from 1963 to 1986.

SUMMARY

Fatigue cracks often grow from connections of cross beams to main girders in plate-girder highway bridges. The structural parameters which govern cracking at cross-beam connections are examined based on the overall behaviour of the bridges. Cracking patterns at cross-beam connections are determined from fatigue tests. A recommendation is given for connection details between concrete slabs and main girder flanges.

RÉSUMÉ

Les fissures de fatigue prennent souvent naissance à la liaison entre les entretoises et les poutres maîtresses des ponts-routes à section ouverte. Les paramètres structuraux qui régissent la fissuration aux liaisons avec les entretoises sont examinés en se basant sur le comportement global des ponts. Des modèles de fissuration des liaisons avec les entretoises sont déterminés à partir d'essais de fatigue. Une recommandation est donnée pour des détails de liaison entre la dalle de béton et les ailes des poutres maîtresses.

ZUSAMMENFASSUNG

Ermüdungsrisse in Strassenbrücken mit offenen Querschnitten gehen oft von den Verbindungen zwischen Quer- und Hauptträgern aus. Die Einflussfaktoren, die den Rissverlauf an den Verbindungsstellen bestimmen, werden unter Berücksichtigung des Gesamtverhaltens der Brücke untersucht. Das Rissverhalten an den Verbindungsstellen wird anhand von Ermüdungsversuchen betrachtet. Es werden Empfehlungen gemacht zur Gestaltung der Konstruktionsdetails bei der Verbindung zwischen Betonfahrbahnplatte und Hauptträgerflansch.

1. INTRODUCTION

In many plate girder highway bridges in the urban area of Japan, fatigue cracks are often observed at the connections of main girders with secondary members such as cross beams, sway bracings and lateral bracings. At the connections of cross beams to main girders in the plate girder bridges of the Hanshin Expressway in Osaka, four types of fatigue cracks are detected, as shown in Fig.1.

-Type 1 crack is initiated either on the bead or at the toe at the end of the fillet weld between the connection plate and the top flange of the main girder.
-Type 2 crack is initiated at the upper scallop of the connection plate, and grows diagonally through the connection plate itself.
-Type 3 crack is initiated at the toe at the end of the fillet weld connecting the connection plate to the main girder web, and grows downward along the toe on the connection plate side.
-Type 4 crack is initiated and grows along the toe on the web side of the fillet weld between the top flange and the web of the main girder.

Investigation of the causes of the crack initiation and the development of repair methods have been under way at various research institutions. However satisfactory results are not yet available.

In 1985 the authors carried out the field stress measurement of an existing plate girder bridge of the Hanshin Expressway to make clear the local stresses causing the cracking at the cross-beam connections[1,2]. They then formulated the relationship between the local stresses and the three-dimensional behavior of the bridge under traffic loading[3].

The objectives of this paper are:

-to present the parameters introduced from the structural behavior of a plate girder bridge, which govern the cracking at the cross-beam connections,
-to show the patterns of the cracking at the cross-beam connections from fatigue tests, and
-to give a recommendation to the connection details between concrete slab and main girder flange.

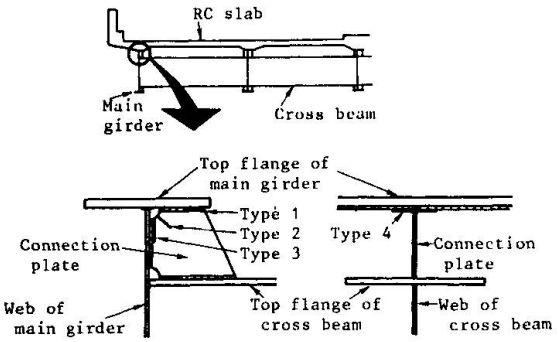

Fig.1 Fatigue cracks at cross-beam connections of plate girder bridge

2. STRUCTURAL PARAMETERS AFFECTING CRACK INITIATION

2.1 Relationship between Local Stresses and Rotations of Concrete Slab and of Cross Beam

As shown in Fig.2, the membrane stress σ_{my} in the vertical direction in the connection plate and the plate-bending stress σ_{by} in the main girder web are main factors to cause Types 1 and 4 fatigue cracks, respectively[1,2]. The relationship between those local stresses and the rotations of concrete slab and of cross beam is given by[3]

$$\begin{bmatrix}\sigma_{my}\\ \sigma_{by}\end{bmatrix} = \begin{bmatrix}k_{m1} & k_{m3}(\gamma-k_{m123})\\ k_{b1} & k_{b3}(\gamma-k_{b123})\end{bmatrix}\begin{bmatrix}\theta_{s0}\\ \theta_{g}\end{bmatrix} \tag{1}$$

where θ_{s0}=rotation of concrete slab due to the slab-deformation caused by wheel loads(see Fig.3), θ_g=rotation of cross beam due to the vertical displacements of main girders(see Fig.3), γ=coefficient depending on the position of a vehicle in the direction of the roadway width, and k_{m1}, k_{m3}, k_{m123}, k_{b1}, k_{b3} and k_{b123}=constants which relate the local stresses to the rotations of concrete slab and of cross beam.

2.2 Structural Parameter for Concrete-Slab Rotation

Referring to Fig.4, the rotation θ_{s0} of concrete slab at the position (a, 0) where a main girder is located, is expressed by[3]

$$\theta_{s0} = (a/D_c)\{P/(2\pi^2)\}\varphi_p(x/a)\,\varphi(x/a)\Big[\sum_{m=1}^{\infty}\{(-1)^m/m^2\}\sin(m\pi x/a)$$
$$(1+m\pi|y|/a)\exp(-m\pi|y|/a)\Big] \tag{2}$$

where a=spacing between main girders, D_c=flexural rigidity of concrete slab, P=a concentrated load, $\varphi_p(x/a)$=correction factor for the wall parapets on both sides of the roadway, and $\varphi(x/a)$=correction factor to treat the concrete slab as a continuous plate.

Equation(2) implies that the concrete-slab rotation θ_{s0} varies with values of a/D_c. The values of a/D_c are determined by the dimensions of concrete slab. Hence the reciprocal of a/D_c, namely, D_c/a is chosen as a structural parameter for θ_{s0}. The bridges with smaller values for D_c/a are more susceptible to cracking, since the decrease of D_c/a increases θ_{s0} and then results in the

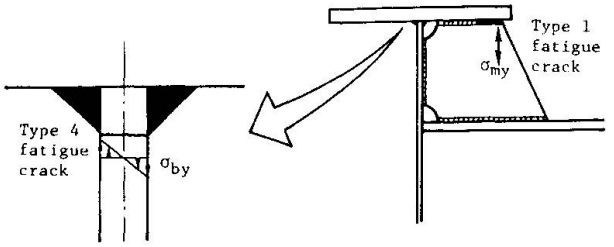

Fig.2 Local stresses σ_{my} and σ_{by}

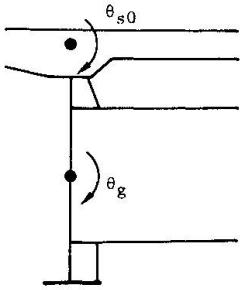

Fig.3 Rotations θ_{s0} and θ_g

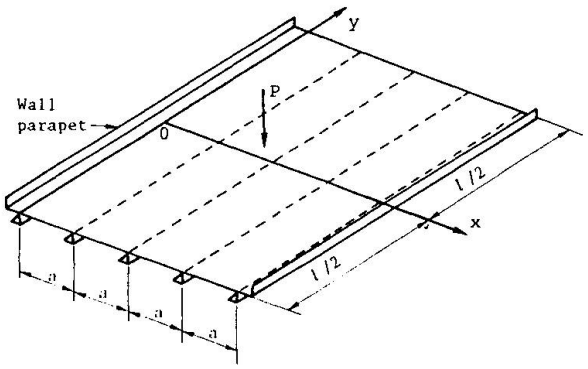

Fig.4 Concrete slab under concentrated load P

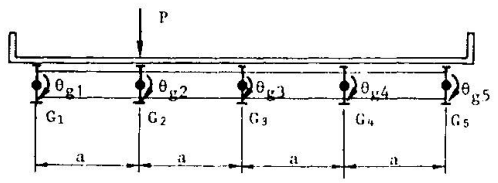

Fig.5 Cross-beam rotation θ_{gi}

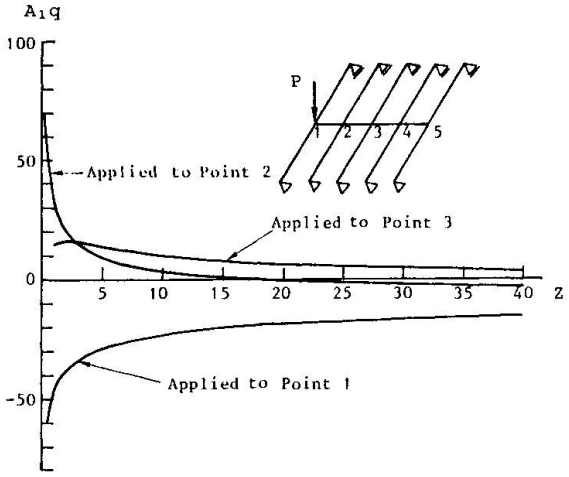

Fig.6 Relationship between $\mathbf{A}_1\mathbf{q}$ and z

increase of the local stresses of σ_{my} and σ_{by}.

2.3 Structural Parameters for Cross-Beam Rotation

In a plate girder bridge with five main girders as shown in Fig.5, the rotation θ_{gi} of the cross beam at the main girder G_i is given by[3]:

$$\theta_{gi} = \mathbf{A}_i\mathbf{v}/(56a) \tag{3}$$

where $\mathbf{v}=(v_1,v_2,v_3,v_4,v_5)^T$, v_i=vertical displacement of the girder G_i at the cross-beam connection, T=symbol representing transpose, and $\mathbf{A}_i$=row vector consisting of constants which correspond to θ_{gi}. When a concentrated load P is applied to the girder G_j, the vertical displacement v_i of the girder G_i is provided with

$$v_i = Pq_{ij}l^3/(48E_s r_i I_g) \tag{4}$$

where q_{ij}=load-distribution-coefficient from the girder G_j to G_i, l=span length of main girders, E_s=Young's modulus of steel, $r_i=I_{gi}/I_g$, I_{gi}=moment-of-inertia of the main girder G_i, and I_g=moment-of-inertia of any girder arbitrarily selected among the five main girders. The load-distribution-coefficient q_{ij} is expressed by a function of r_i and Z defined by

$$Z = (I_Q/I_g)\{l/(2a)\}^3 \tag{5}$$

where I_Q=moment-of-inertia of a cross beam. Substitution of Eq.(4) into Eq.(3) provides

$$\theta_{gi} = \{P/(2688E_s)\}\{l^3/(aI_g)\}\mathbf{A}_i\mathbf{q} \tag{6}$$

where $\mathbf{q}=(q_{1j}/r_1,q_{2j}/r_2,q_{3j}/r_3,q_{4j}/r_4,q_{5j}/r_5)^T$.

Figure 6 shows the relationship between $\mathbf{A}_1\mathbf{q}$ which corresponds to

the cross-beam rotation θ_{gl}, and Z. The calculation of $\mathbf{A_1 q}$ is carried out for all r_i=1. Except for the case of a concentrated load P applied to the girder G_3 above which a center divider exists on the roadway, $\mathbf{A_1 q}$ is approximately inversely-proportional to Z for Z≤10. Accordingly, when Z≤10, the term $\{l^3/(aI_g)\}\mathbf{A_1 q}$ in Eq.(6) is proportional to $\{l^3/(aI_g)\}/Z$, and then considering Eq.(5), $\{l^3/(aI_g)\}/Z$ is changed into $8a^2/I_Q$. On the other hand, when Z>10, only the term $l^3/(aI_g)$ is variable in Eq.(6), since $\mathbf{A_1 q}$ takes almost constant values for Z>10.

From the above, the following structural parameters are chosen for the cross-beam rotation θ_{gi}:

$$I_Q/a^2 \text{ for } Z\leq 10 \quad (7)$$
$$aI_g/l^3 \text{ for } Z>10 \quad (8)$$

The bridges with smaller values for these structural parameters suffer more chances of cracking, since the decrease of the parameters increases θ_g, which leads to the increase of the local stresses of σ_{my} and σ_{by}.

2.4 Relationship between Structural Parameters and Cracking

The relationship between I_Q/a^2 and initiation of Types 1 and 4 cracks is investigated for 158 plate girder bridges on a route of the Hanshin Expressway[4]. The structural parameter D_c/a is found to be almost invariable on this route.

Figure 7 shows the relationship between I_Q/a^2 and the number of bridges in which Type 1 cracks were detected. As shown in Ref.[4], the influence of θ_g on the local stress σ_{my} which causes Type 1 cracks is very small in the bridge with I_Q/a^2=3.1 cm^2. In Fig.7, however, Type 1 cracks occur in the bridges for I_Q/a^2>3.0 cm^2. This indicates that Type 1 cracks can be initiated by the

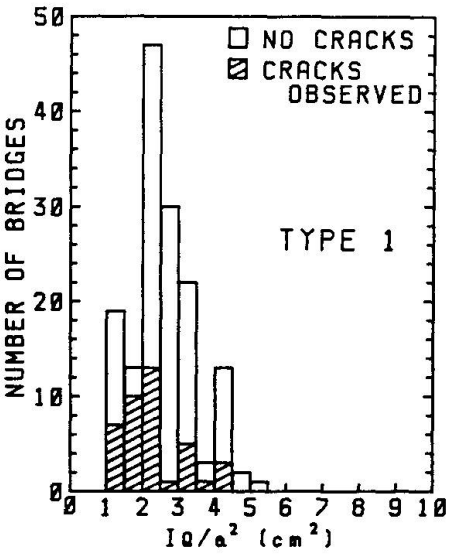

Fig.7 Relationship between I_Q/a^2 and the number of bridges in which Type 1 cracks were observed

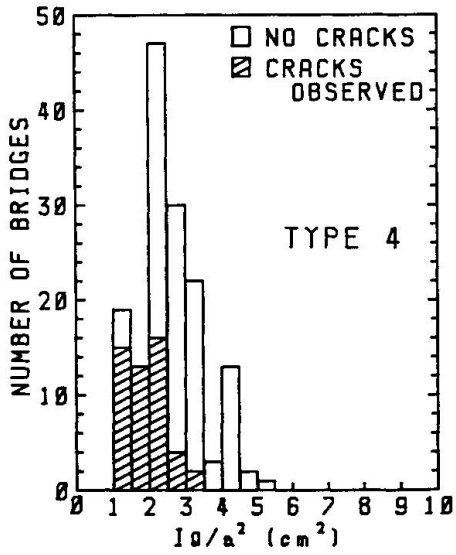

Fig.8 Relationship between I_Q/a^2 and the number of bridges in which Type 4 cracks were observed

concrete-slab rotation only.

Figure 8 shows the relationship between I_Q/a^2 and the number of bridges in which Type 4 cracks were observed. With the increase in I_Q/a^2, the number of bridges suffering from cracking gradually decreases, since the influence of θ_g on the local stress σ_{by} which causes Type 4 cracks becomes small. No cracks occur in the bridges for $I_Q/a^2>3.5$ cm^2.

3. FATIGUE TESTS OF CROSS-BEAM CONNECTIONS

3.1 Fatigue Test Specimens

As can be seen from Eq.(1), the local stresses σ_{my} and σ_{by} are provided with the sum of stress components due to the rotations of concrete slab and of cross beam. This implies that effects of concrete-slab rotation and of cross-beam rotation on the local stresses can be divided. Then in order to clarify the influence of the concrete-slab rotation on the cracking at cross-beam connections, fatigue tests are carried out on the specimens as shown in Fig.9. The specimens consist of cross-beam connections and of

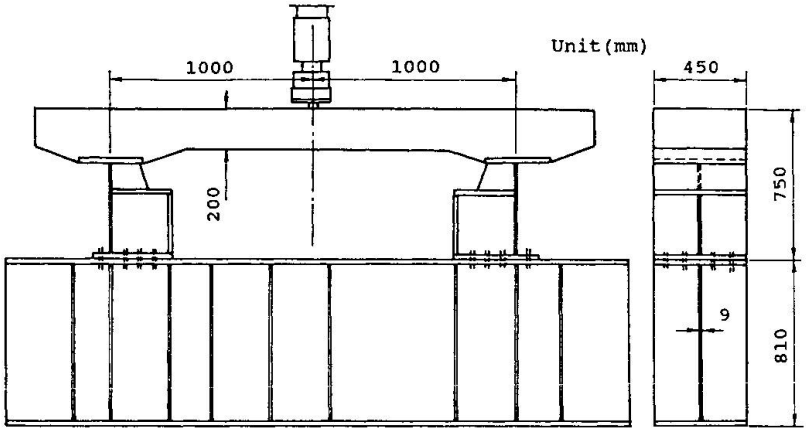

Series A

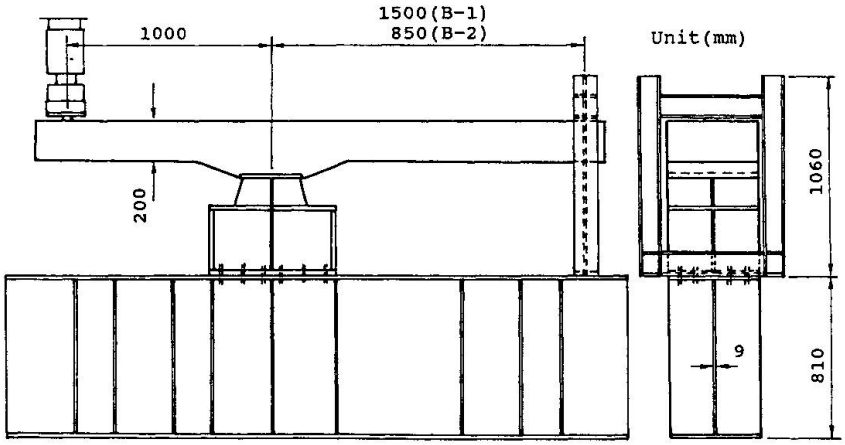

Series B

Fig.9 Fatigue test specimens

a concrete slab in a stripped form. The series A corresponds to the cross-beam connections of exterior main girders. The series B does for interior main girders. In the series B, negative moment is created in the concrete slab above the cross-beam connection.

3.2 Connection Details between Girder Flange and Concrete Slab

In order to examine the effects of connection details between girder flange and concrete slab on the cracking, the number of stud shear connectors and their arrangement are changed at each cross-beam connection, as shown in Fig.10. In the right side of Specimen A-2 and in Specimen B-2, a slab anchor is used.

3.3 Results of Fatigue Tests

The following observations are drawn from the fatigue tests:

-The similar cracks as shown in Fig.1 occur at all the cross-beam connections, not depending on the connection details between girder flange and concrete slab.
-In the series A corresponding to the cross-beam connections of exterior main girders, there exists no order in initiation of Types 1 and 4 cracks, while in the series B corresponding to the

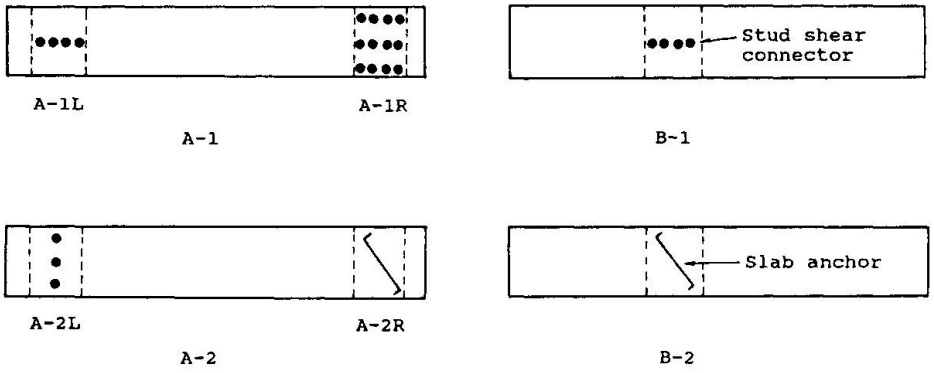

Fig.10 Connection details between girder flange and concrete slab

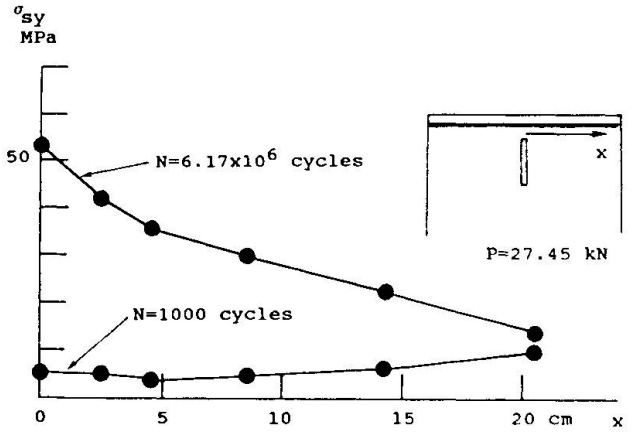

Fig.11 Distribution of web surface stress σ_{sy} along the flange-to-web fillet weld(Specimen B-1)

cross-beam connections of interior main girders, Type 4 crack follows Type 1 crack.

The distribution along the flange-to-web fillet welds of the stress σ_{sy} on the surface of the web plate is shown in Fig.11 for Specimen B-1. In the figure, at N=1000 cycles σ_{sy} is very small and Type 1 crack does not occur, while at N=6.17×10^6 cycles σ_{sy} becomes large and Type 1 crack is initiated and grows. Therefore in the series B the propagation of Type 1 crack makes the local stress σ_{by} increase, and then results in Type 4 crack initiation.

3.4 Characteristics of Occurrence of Local Stresses

In order to make clear the occurrence of the local stresses σ_{my} and σ_{by}, a finite element analysis is carried out for a model as shown in Fig.12. It consists of a girder flange, girder web and connection plate, and a half of them is divided into finite elements from symmetry. The bottom edges of the girder web and connection plate are fixed. The forces which are determined by the measurements of displacement of the concrete slab and by the measurements of strain of the stud shear connectors are applied to the girder flange of the F.E.M. model, as shown in Fig.13. The vertical forces on the girder flange are produced by the pull-out action of stud shear connectors and by the contact action between concrete slab and girder flange. The horizontal forces on the girder flange are created by the shear resistance of stud shear connectors.

Comparison of F.E.M. values with the measured ones is shown in Fig.14 for σ_{my} and σ_{by}. As for σ_{my}, F.E.M. values are close to the measured ones. As for σ_{by}, the distribution of F.E.M. values shows the same tendency as that of the measured ones, though the former shifts slightly from the latter.

The local stresses σ_{my} and σ_{by} can be correlated with the forces Q and S. Here Q is, as shown in Fig.13, the total of the vertical forces on the girder flange, while S is the total of the horizontal forces on the girder flange. The stress components of σ_{my} and σ_{by} against Q and S are listed in Table 1 for the series A. The stress values in the table are obtained at the points of the strain gauges nearest to the crack initiation in the fatigue tests. Connection A-0, which is just a model for the F.E.M. analysis, corresponds to the cross-beam connections in which neither stud shear connectors nor slab anchors are used between concrete slab and girder flange. In this model, the concentrated load of 49.0 kN is applied vertically to the edge of the girder flange just above the connection plate.

The following are pointed out from Table 1:

-The local stress σ_{my} is mostly produced by the vertical force Q, while the local stress σ_{by} is produced by both Q and S.
-The stress values of Connection A-0 are much smaller than those of any other connection model.

In order to reduce the local stresses and thus to prevent cracking, it is recommended that neither stud shear connectors nor slab

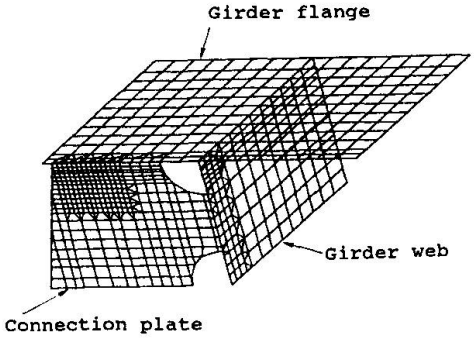

Fig.12 Mesh division

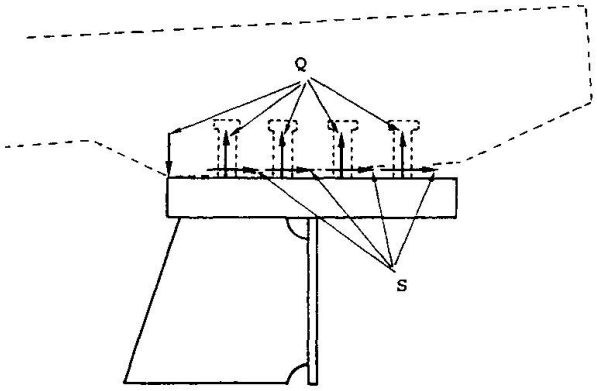

Fig.13 Forces acting on F.E.M. model

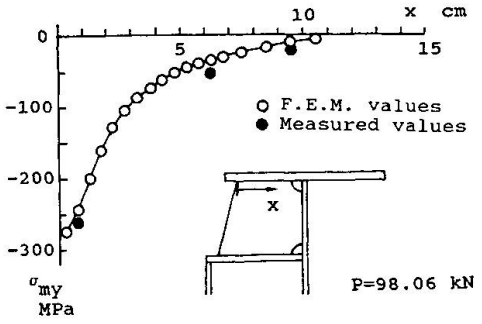

(a) σ_{my} at connection plate

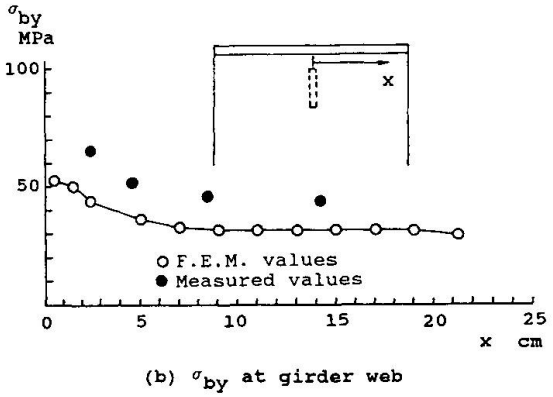

(b) σ_{by} at girder web

Fig.14 Comparison of F.E.M. values with measurement values(Connection A-1L)

Table 1 Comparison of stress components against Q and S

Connection	Q (kN)	S (kN)	σ_{my} (MPa)	σ_{mQ} (MPa)	σ_{mS} (MPa)	σ_{by} (MPa)	σ_{bQ} (MPa)	σ_{bS} (MPa)
A-1L	48.88	41.45	-237.9	-240.8	2.9	43.2	8.6	34.6
A-1R	49.17	56.43	-292.3	-296.2	3.9	96.3	49.2	47.1
A-2L	56.03	66.08	-275.4	-279.8	4.4	77.1	21.1	55.9
A-2R	42.02	44.32	-295.9	-298.9	2.9	26.5	-11.9	38.5
A-0	49.03	0.0	-184.0	-184.0	0.0	-9.7	-9.7	0.0

Note: $\sigma_{my} = \sigma_{mQ} + \sigma_{mS}$
$\sigma_{by} = \sigma_{bQ} + \sigma_{bS}$
σ_{mQ} = membrane stress component produced by Q
σ_{mS} = membrane stress component produced by S
σ_{bQ} = plate-bending stress component produced by Q
σ_{bS} = plate-bending stress component produced by S

anchors be placed above the connections of cross beams to main girders.

4. CONCLUSIONS

(1)The structural parameters governing the fatigue cracking at the connections of cross beams to main girders in plate girder highway bridges were specified as follows according to the rotations of

concrete slab and of cross beam:

a) For the concrete-slab rotation, D_c/a.
b) For the cross-beam rotation, I_Q/a^2 when $Z \leq 10$, and aI_g/l^3 when $Z > 10$. Here $Z=(I_Q/I_g)\{l/(2a)\}^3$.

The bridges with smaller values of the above structural parameters become more susceptible to cracking. Type 1 cracks at the connection plates can be initiated by the concrete-slab rotation only.

(2) From the fatigue tests to investigate the influence of the concrete-slab rotation on the cracking, it was revealed that cracks are initiated at the cross-beam connections with stud shear connectors regardless of the number of them and their arrangement, and that they are also initiated at the cross-beam connections with slab anchors.

(3) To reduce the local stresses and thus to prevent cracking, it was recommended from a F.E.M. analysis that neither stud shear connectors nor slab anchors be placed above the connections of cross beams to main girders.

ACKNOWLEDGMENT

The authors would like to thank Mr. H. Inoue, graduate student of Osaka University, and Mr. Y. Yamada, Takadakiko Co., Ltd. for their help in carrying out the fatigue tests. The first author would also like to acknowledge the Kajima Foundation, Japan, who offered him the traveling expenses for his presentation in EPFL, Switzerland.

REFERENCES

1. OKURA I., HIRANO H. and YUBISUI M., Stress Measurement at Cross Beam Connections of Plate Girder Bridges, Technol. Repts. Osaka Univ., Vol.37, No.1883, 1987, pp.151-160.

2. OKURA I. and FUKUMOTO Y., Fatigue of Cross Beam Connections in Steel Bridges, IABSE, 13th Congress, Helsinki, 1988, pp.741-746.

3. OKURA I., YUBISUI M., HIRANO H. and FUKUMOTO Y., Local Stresses at Cross Beam Connections of Plate Girder Bridges, Proc. of JSCE Struc. Eng./Earthq. Eng., Vol.5, No.1, 1988, pp.89s-97s.

4. OKURA I., TAKIGAWA H. and FUKUMOTO Y., Structural Parameters Governing Fatigue Cracking at Cross-Beam Connections in Plate Girder Highway Bridges, Technol. Repts. Osaka Univ., Vol.39, No.1980, 1989, pp.289-296.

Assessment of the Remaining Fatigue Life of Defective Welded Joints

Evaluation de la durée de vie restante de joints soudés défectueux

Abschätzung der Restlebensdauer schadhafter Schweissverbindungen

O.D. DIJKSTRA
Civil Engineer
TNO-IBBC
Delft, The Netherlands

Onno Dijkstra, born 1945, received his civil engineering degree at the Delft University of Technology. He has been involved in fatigue and fracture mechanics since 1974. Onno Dijkstra is now in the Steel Department of TNO-IBBC and is responsible for fatigue and fracture mechanics research.

H.H. SNIJDER
Civil Engineer
Netherlands Railways
Utrecht, The Netherlands

Bert Snijder, born 1959, obtained his civil engineering degree at the Delft University of Technology. For five years, he was involved in steel structures research at TNO-IBBC. Topics of interest include stability and fatigue. Bert Snijder is now in a design office and is responsible for the design of steel buildings and bridges.

H.J.M. VAN RONGEN
Senior Scientist
TNO Metals Research Inst.
Apeldoorn, The Netherlands

Bob van Rongen, born 1933, received his physics degree at the University of Leiden. He has been involved in fracture mechanics since 1972. Bob van Rongen is now in the welding and materials department and is responsible for the use and dissemination of fracture analysis methods.

SUMMARY
This paper deals with the determination of the remaining fatigue life of defective welded steel structures. Highlighted are defect schematization and recategorization, crack-growth laws and their constants, stress-intensity-factor solutions for welded joints and a fatigue crack-growth calculation procedure. The information given can be used for two dimensional and three dimensional welded geometries.

RÉSUMÉ
Cet article traite de la détermination de la durée de vie restante de structures soudées en acier contenant des défauts. L'accent est mis plus particulièrement sur la schématisation et la classification des défauts, sur les lois de propagation des fissures et leurs constantes, sur les valeurs du facteur d'intensité de contraintes pour des joints soudés, et sur la procédure de calcul de la propagation des fissures de fatigue. L'information présentée ici peut être utilisée pour des géométries d'éléments soudés bidimensionnels et tridimensionnels.

ZUSAMMENFASSUNG
Dieser Bericht befasst sich mit der Bestimmung der Restlebensdauer geschweisster Stahltragwerke, die Schäden aufweisen. Beleuchtet werden die systematische Darstellung und Klassierung von Schäden, Rissfortschrittsgesetze und deren Konstanten, Spannungsintensitätsfaktoren für Schweissverbindungen sowie ein Verfahren zur Berechnung des Ermüdungsrisswachstums. Alle Angaben sind sowohl für geschweisste Verbindungen zweidimensionaler als auch für solche dreidimensionaler Geometrie gültig.

1. INTRODUCTION

Steel structures may contain defects in the (welded) connections. These defects can be discovered directly after fabrication by non destructive testing or during service by inspection. Repair of these defects is often costly and time consuming. The costs may be extremely high when an existing structure has to be taken out of service or when the use of a new structure is delayed. Furthermore, a repair of a structure has to be carried out in an unfavourable situation with regard to the accessibility and restraint. Therefore, these repairs are often not beneficial to the integrity of the structure.
The above mentioned reasons make that a "fitness for purpose" assessment of a defective joint may be useful and may lead to the conclusion that the safety of the structure is not reduced by the presence of the defect discovered. In a statically loaded structure an assessment of the risk of instable (brittle) fracture initiated from the defect discovered is sufficient. However, for a fatigue loaded structure a small non critical defect may grow to a larger defect with a critical size due to the service load. Therefore, crack growth estimation is essential for a fitness for purpose assessment of fatigue loaded structures. The crack growth estimation may show that a repair can be postponed to a more suitable time or even show that the defect will not become critical during the service life (This may be due to the fact that the defect is in or growing into a low stressed area).
This paper deals with the fatigue crack growth part of the fitness for purpose assessment. A brief summary of a guideline drawn up in the Netherlands [1] is given. The various parts of a fatigue assessment will be highlighted, such as: defect schematization and recategorization (see section 2), crack growth laws and their constants (see section 3), stress intensity factors (see section 4) and a calculation procedure (see section 5).
The paper ends with conclusions and recommendations for further research (section 6).
Sections 2,3,4 and 5 are mainly based on a study carried out by TNO (Netherlands Organisation for Applied Scientific Research) within the framework of a NIL (Nederlands Instituut voor Lastechniek) and CS (Centrum Staal) research project [1, 2, 3 and 4].

2. DEFECT SCHEMATIZATION

2.1. Idealization of defects

The size and the location of the defect is normally determined by non destructive testing. The actual measured dimensions can be irregular and not suited for a crack growth calculation procedure. In general a fatigue crack will tend to grow to an idealized shape. Therefore an idealization of the measured dimensions is allowed.
Three types of planar flaws can be considered:

- Through flaws	idealization:	rectangle	width 2a
- Surface flaws	:	semi-ellipse	depth a, width 2c
- Embedded flaws	:	ellipse	minor axis a and major axis c

Their dimensions (a and c) are determined from the height and the length of their containment rectangles (see table 1). The plane in which the idealized flaw is located is perpendicular to the stress that is used for the calculation of the fatigue crack extension. The actual flaw should be projected to that plane and then be idealized. This idealization procedure is in accordance with other guidelines [5 and 6].

type of flaw	actual flaw	idealization
through flaw	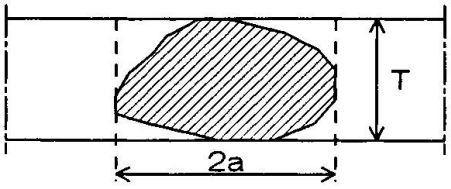	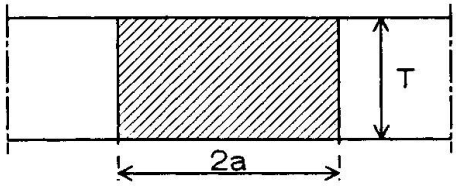
surface breaking flaw	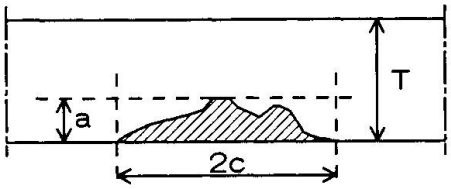	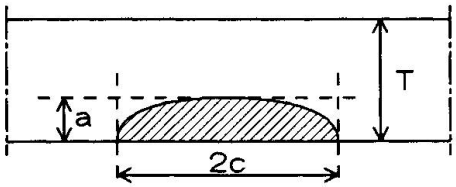
embedded flaw	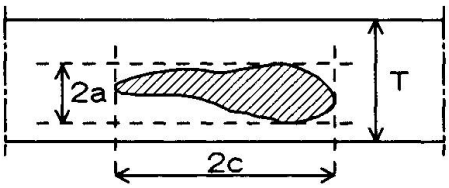	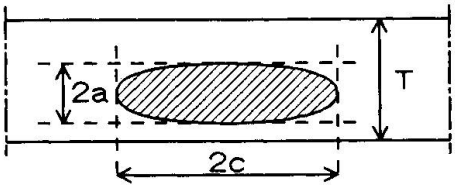

Table 1 Idealization of flaws

2.2 Interaction of defects

During the fatigue crack growth, interaction of two ore more defects can occur. This is often the case at weld toes, where multiple crack initiation followed by coalescence and crack growth at low aspect ratios occurs. Interaction between a defect and a free surface is also possible.
Existing interaction criteria [5 and 6] are developed for the assessment of instable (brittle) fracture and are not suitable for fatigue crack growth (see [20]). Therefore a new set of interaction criteria is proposed [4].
In general, interaction is considered if the distance of two flaws, in relation to the dimensions of these flaws, is smaller than a given value or zero. When this criterion is met the two flaws have to be considered as one single flaw with the idealization rules given in 2.1. Table 2 gives the new fatigue interaction criteria for through flaws, surface flaws and embedded flaws. Mutual interaction and interaction with a free surface is considered.
When interaction occurs during the fatigue crack growth, the calculation is resumed after recategorization, starting with the new idealized crack dimensions.

3. CRACK GROWTH MODELS AND CONSTANTS.

3.1. Crack growth models.

Fatigue crack growth models for welded structures, based on linear elastic fracture mechanics have been described recently by several authors [7, 8, 9, 10, 11, 12 and 14]. In general, the crack growth model gives the relation between the crack growth rate (da/dN) and the fatigue loading parameter (stress intensity factor range (ΔK)). This relation, called the Paris-Erdogan relation is as follows (see region II in figure 1) :

interacting flaws and surfaces	criteria	recategorized flaw
two through flaws 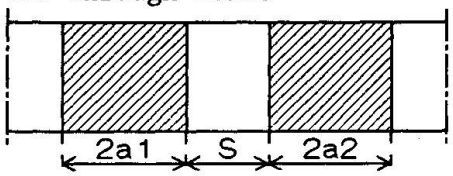	$a_1 < a_2$ and $S < 2a_1$	one single through flaw 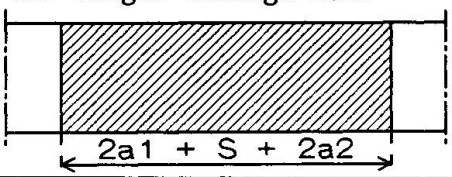
through flaw and surface flaw 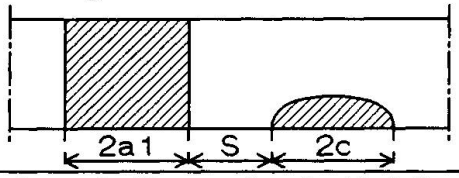	$S < 2a_1$ and $S < 2c$	one single through flaw 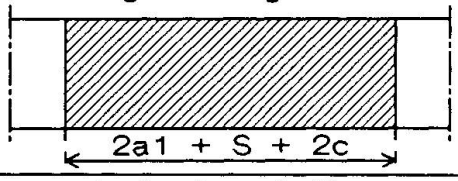
through flaw and embedded flaw 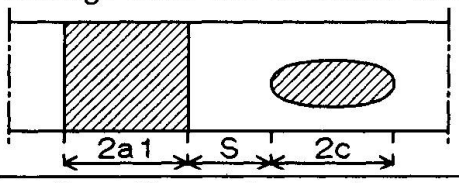	$S < 2a_1$ and $S < 2c$	one single through flaw 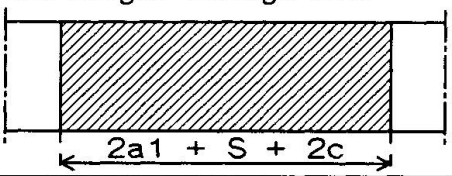
surface flaw and opposite surface 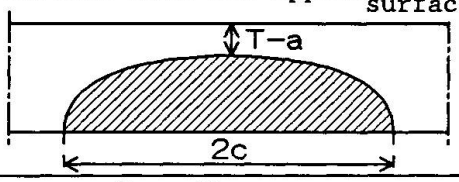	T-a = 0	one single through flaw 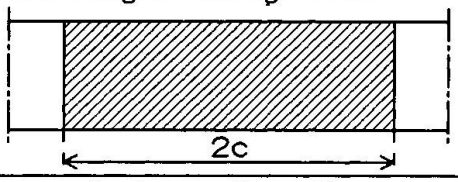
two surface flaws 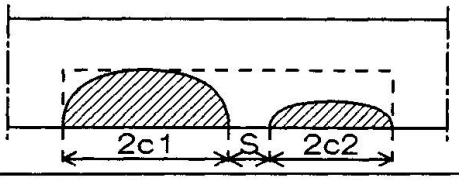	S = 0	one single surface flaw 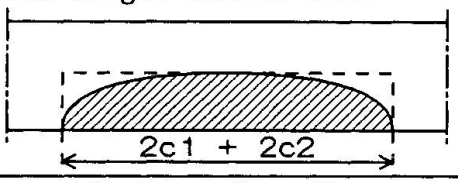
surface flaw and embedded flaw 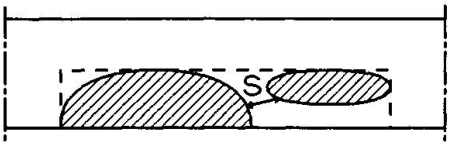	S = 0	one single surface flaw 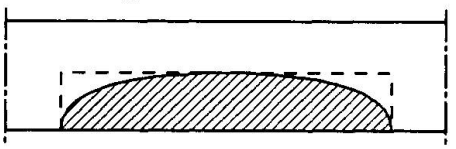
embedded flaw and free surface 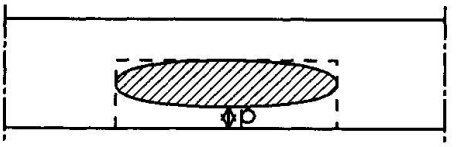	p = 0	one single surface flaw 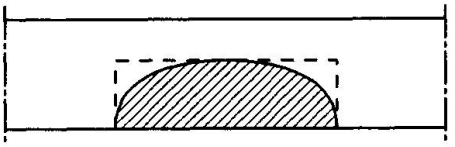
two embedded flaws 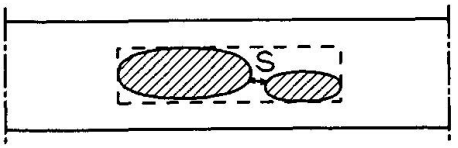	S = 0	one single embedded flaw 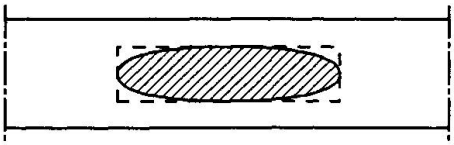

Table 2 Interaction of coplanar flaws during fatigue crack growth.

$$da/dN = C\ (\Delta K)^m \qquad (1)$$

where C and m are crack propagation constants.

In the near threshold range (region I) the influence of the threshold value of ΔK (ΔK_{th}) can also be incorporated in the relation:

$$da/dN = C\ (\Delta K^m - \Delta K_{th}^m) \qquad (2)$$

In the upswing of the crack growth curve (region III) the influence of the critical value of K (K_c), combined with the load ratio R ($=F_{min}/F_{max}$) can be taken into account.

$$da/dN = \frac{C\ (\Delta K)^m}{(1-R)K_c - \Delta K} \qquad (3)$$

Fig 1 gives a general view of the da/dN-ΔK curve and the validity of the three crack growth relations mentioned above.

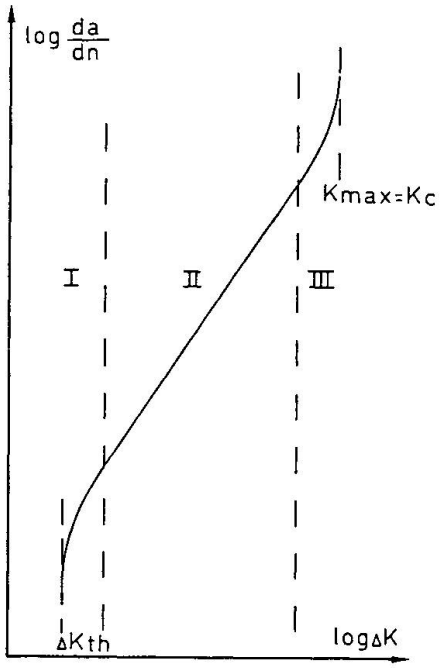

Fig. 1 Crack growth rate curve.

3.2. Crack propagation constants

The crack growth constants C and m, and ΔK_{th} have to be determined for the relevant material and conditions (environment, frequency, etc). Figure 2 shows an experimental crack growth curve of an Fe E 355-KT material used in an ECSC-SMOZ project [12]
When no specific data are available the following values can be used for ferritic steels with a proof stress below 600 N/mm2 operating in air or other non aggressive environments at temperatures up to 100 °C:

$$m = 3$$
$$C = 3\ 10^{-13} \text{ (units N and mm)} \qquad (4)$$

For marine environment and normal wave frequency ($\approx$ 0.1 Hz) C becomes:

$$C = 2.3\ 10^{-12} \text{ (units N and mm)} \qquad (5)$$

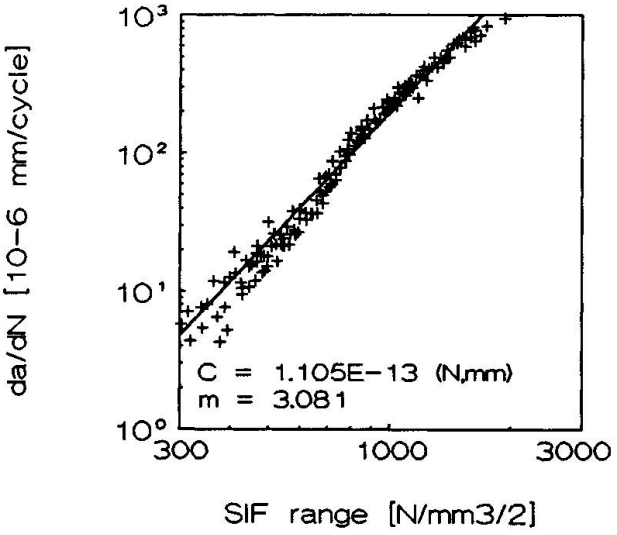

Fig. 2 Experimental da/dN-ΔK curve.

The values of (4) and (5) are a safe upperbound of the crack growth data.
For as-welded structures the following threshold value of ΔK should be used:

$$\Delta K_{th} = 63\ N/mm^{3/2} \qquad (6)$$

4. STRESS INTENSITY FACTORS

4.1. Governing stresses.

The stress intensity factor (SIF,K) range is the difference between the maximum SIF and the minimum SIF during a load cycle. The SIF is a measure for the magnitude of the stresses near the crack tip; eqn. (7).

$$K = Y \sigma \sqrt{(\pi a)} \qquad (7)$$

where: σ = remotely applied stress
Y = correction factor depending on geometry and loading conditions
a = crack depth

The stress variations for a fatigue crack growth calculation have to be determined from the complete load history during the (remaining part of the) service life or from the expected load history to the next inspection.
The stresses in a welded detail can be separated in (see figure 3):

a) Membrane stresses (σ_m), being the average nominal stress across the section thickness due to the applied load on the section.
b) Bending stress (σ_b), being the bending part of the nominal stress across the section thickness due to the applied load on the section.
c) Residual stress (σ_r) across the section thickness. These stresses are self-equilibrating. σ_r is often due to the welding or fabrication process of the detail.
d) Peak stress (σ_p) due to local discontinuities (such as: weld toes, etc.).

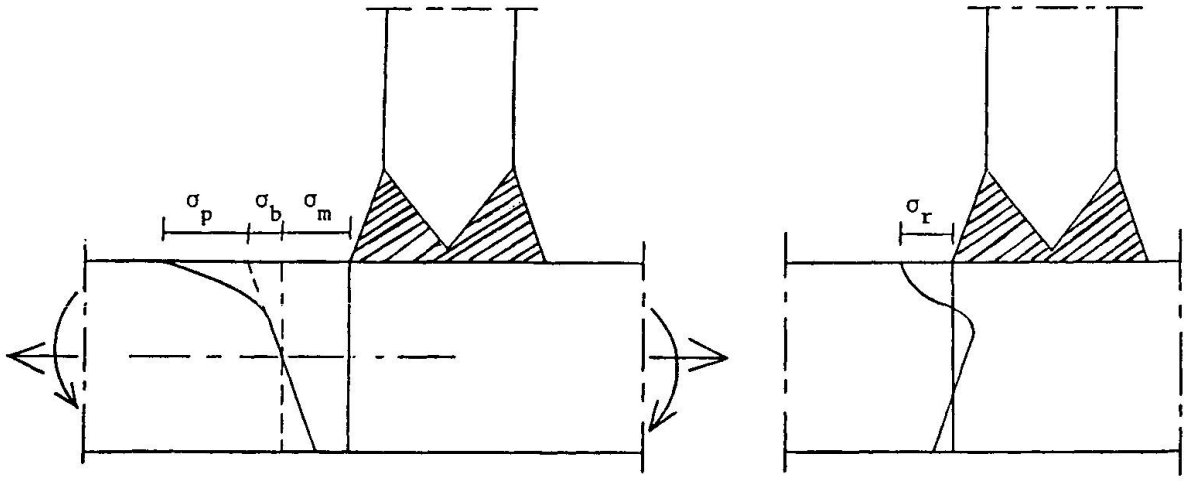

Fig. 3 Stresses in a welded detail.

The governing fatigue stresses for an as-welded structure are the elastic stress ranges of σ_m and σ_b at the crack location for the uncracked geometry. The effect of the global geometry should be incorporated in the stress analysis, while the effect of the local geometry (weld shape, etc.; causing σ_p) should be excluded. This effect of the local geometry will be incorporated in the determination of the stress intensity factor by the stress intensity concentration factor (M_k).
For as welded structures the mean stress level has no influence on the fatigue crack growth. The residual stress level at the weld toe in as welded structures generally approaches the tensile yield stress. This implies that the stress range is always fluctuating from tensile yield stress downwards and the complete stress range is effective for crack growth.
For stress-relieved structures loaded with a fatigue load with a negative R ($=\sigma_{min}/\sigma_{max}$)ratio, the complete stress range may not be effective. However due to settlements or assembling stresses the actual stress level may differ from the calculated one. Therefore it is recommended for steel structures not to use the possible beneficial effect due to stress relieving. For special structures

where the value of the mean stress is known (e.g. a complete stress relieved structure) the beneficial effect of a low mean stress level may be used.
In case of a random load sequence a counting procedure (such as rainflow counting) may be used to determine the governing stress ranges.
The stress range perpendicular to the crack surface (mode I stress range) is the governing stress range in complex stress situations (e.g. biaxial stresses).

4.2. SIF in 2-D geometries

The SIF of a constant depth edge crack in a welded 2D geometry (see fig. 4) is generally given as follows:

$$K = [M_{k,m}\, M_m\, \sigma_m + M_{k,b}\, M_b\, \sigma_b]\, \sqrt{(\pi a)} \qquad (8)$$

where: M_k - stress intensity concentration factor for the influence of the weld geometry
M - stress intensity correction factor for the strip without the weld geometry
m and b as index means for membrane stress and for bending stress respectively.

M is a function of the relative crack depth (a/T). Formulas can be found in literature [1, 9 and 13].
M_k is a function of a/T , the weld dimensions (see fig. 4) and the weld type. Assuming no interaction between the influence of the relative weld width (L/T), the weld angle (θ) and the relative weld toe radius (ρ/T) the following formula for M_k can be written.

$$M_k = f_L(a/T, L/T).f_\theta(a/T, \theta).f_\rho(a/T, \rho/T) \qquad (9)$$

where: f_L - a correction factor for the influence of the relative weld width (L/T) for a specific weld type with a certain weld angle and weld toe radius.
f_θ - a correction factor for the influence of the weld angle (θ).
f_ρ - a correction factor for the influence of the relative weld toe radius (ρ/T).

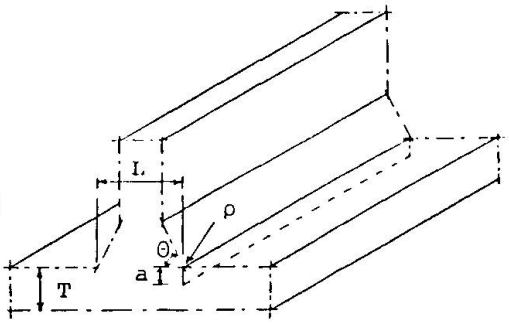

Fig. 4 Constant depth crack.

A powerful tool to determine SIFs and M_k values of weld geometries is the finite element method (FEM) [9 , 14 and 18].
Smith and Hurworth [15] and Maddox et al. [16] have determined M_k values with a FEM technique for butt welds and T-and X-joint geometries (see fig. 5). For butt welds and X-joints a set of formulas for M_k values was derived by Maddox et al. [16]. These formulas are valid for weld toe angle $\theta = 45°$ and weld toe radius $\rho = 0$. The formulas are functions of the relative crack depth (a/T) and relative weld width (L/T).

$$M_k = f_L(a/T, L/T) \qquad (10)$$

The functions f_L and the range of applicability can be found in [5, 14 and 16]

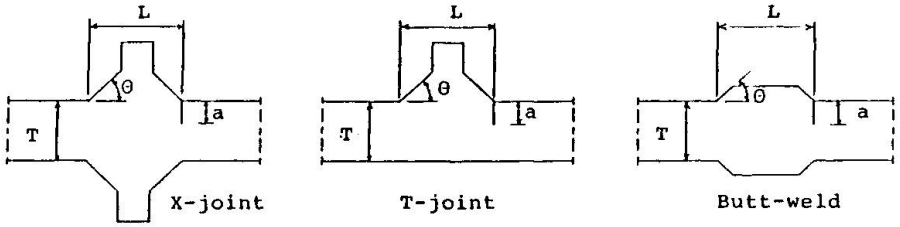

Fig. 5 Geometries studied by Smith and Hurworth [15] and Maddox et al. [16].

Dijkstra et al. [14] determined M_k values for T-joint geometries (see fig 6). A formula (eqn. 11) was developed for geometries with $\theta = 70°$ and $\rho = 0$.

$$M_k = A + \frac{B}{a/T-C} \qquad (11)$$

The values of A, B, and C are given in table 3.
The influence of the relative weld toe radius was also expressed in a formula (eqn 12).

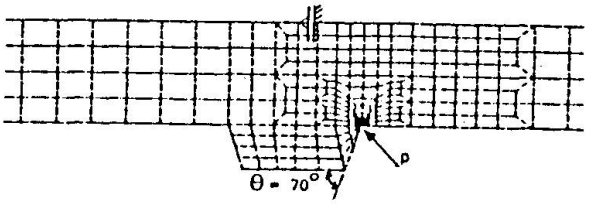

Fig 6. Finite element mesh of T-joint.

$$f_\rho = 1 - A_\rho . e^{-B_\rho . a/T} \quad \text{for } a/T \le 0.1 \qquad (12) \quad \text{and} \quad f_\rho = 1 \quad \text{for } a/T > 0.1 \qquad (13)$$

$$\text{where: } A_\rho = A_{\rho 1} + A_{\rho 2}/(\rho/T - A_{\rho 3}) \qquad (14) \quad \text{and} \quad B_\rho = B_{\rho 1} + B_{\rho 2}.(\rho/T)^2 \qquad (15)$$

See table 4 for the coefficients $A_{\rho 1}$ to $B_{\rho 2}$ (applicability $.00714 \le (\rho/T) \le .125$).

So the M_k value for a T-joint with $\theta = 70°$ and a relative weld toe radius $0.00714 \le (\rho/T) \le 0.125$ can be determined as follows:

$$M_k = [A + B/(a/T-C)].f_\rho \qquad (16)$$

where: A, B, and C are the values given in table 3.
f_ρ is the function of eqn. (12 to 15)

Based on the information given by Smith and Hurworth [15] Dijkstra et al. [14] developed a formula for f_θ with $\theta = 45°$ as reference value:

$$f_\theta = (10.a/T)^{-\frac{1}{2}\log A_\theta} \quad \text{for } 0.001 \le a/T \le 0.1 \qquad (17)$$

$$\text{where: } A_\theta = 13.096\ 10^{-3} + 28.119\ 10^{-3}\theta - 139.45\ 10^{-6}\theta^2 \qquad (18)$$

$$f_\theta = 1 \quad \text{for } a/T > 0.1 \qquad (19)$$

The range of application of eqns. (17 to 19) is: $25° \le \theta \le 65°$.

With the information given in this section one can determine the SIF of a welded T- or X-joint taking the influence of L/T, ρ/T and θ into account for a 2-D geometry.

region	load case	A	B	C
I	b	1.1362	0.015011	-0.0034398
$0 \le a/T < 0.025$	m	1.0291	0.012040	-0.0034689
II	b	0.88539	0.031426	-0.015361
$0.025 \le a/T < 0.1$	m	0.93832	0.016203	-0.0065430
III	b	0.95471	0.019388	0.0047441
$0.1 \le a/T < 0.4$	m	0.96858	0.011363	0.0044927

Table 3 Curve fitting coefficients for Mks at weld toes in T-joints with $\theta = 70°$ and $\rho = 0$.

loading	$A_{\rho 1}$	$A_{\rho 2}$	$A_{\rho 3}$	$B_{\rho 1}$	$B_{\rho 2}$
bending	0.70754	-0.020160	-0.024502	75.323	-1541.7
membrane	0.71032	-0.024015	-0.028061	105.29	-1993.8

Table 4 Curve fitting coefficients for f_ρ.

4.3 SIF in 3-D geometries.

The SIF of a semi-elliptical crack at a weld toe in a 3D geometry can be expressed in the crack depth (a) direction and in the crack width (c) direction (see fig. 7) as follows:

$$K_a = [M_{k,m,a}\, M_{m,a}\, \sigma_m + M_{k,b,a}\, M_{b,a}\, \sigma_b]\sqrt{(\pi a)}/\Phi \qquad (20a)$$

$$K_c = [M_{k,m,c}\, M_{m,c}\, \sigma_m + M_{k,b,c}\, M_{b,c}\, \sigma_b]\sqrt{(\pi a)}/\Phi \qquad (20b)$$

where: a and c as index means for crack depth and for crack width direction respectively.
Φ = elliptical integral of the second kind,
approximation $\Phi = [1 + 1.464\ (a/c)^{1.65}]^{0.5}$
for other symbols see equation (8)

The correction factors for the flat plate ($M_{m,a}$, $M_{b,a}$, $M_{m,c}$ and $M_{b,c}$) presented by Newman and Raju [17] can be used.

The 3-D SIF can also be determined with FEM. Van Straalen et al. [18] determined SIFs for a T-plate with a weld discontinuity. The geometry and the finite element model are given in fig. 8 and 9. SIFs were calculated for four crack geometries. The most important results are given in table 5. More results are given in [18 and 14]. For comparison the M_k values for a similar 2D geometry have also been tabulated. The 2D M_k values are higher than the 3D M_k values. This can be explained by the stiffening effect of the stub in the uncracked part of the plate in the 3D geometry. The ratio (ω) of $M_{k,3D}$ and $M_{k,2D}$ is also given in table 5. This ratio can be seen as a reduction factor for the application of 2D M_k values in a 3D geometry. Due to the limited amount of data no general expression of this reduction factor can be given.

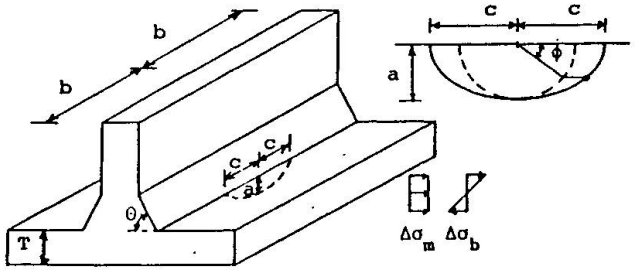

Fig 7 Semi-elliptical crack at the weld toe.

Comparison of the calculated SIF with experimental crack growth data showed a lower crack growth rate than predicted with the theoretical SIF for the geometry of fig 8 and 9 [12].

loadcase	direction	crack depth a [mm]	crack width c [mm]	M_k 3D	M_k 2D	ratio $\frac{M_{k,3D}}{M_{k,2D}}$ ω
membrane	depth a	6.49	10.14	0.964	1.041	0.926
		8.95	15.80	0.930	1.020	0.912
		11.85	25.90	0.920	1.008	0.913
		16.00	40.70	0.926	1.000	0.927
membrane	width c	6.49	10.14	1.260	1.498	0.841
		8.95	15.80	1.234	1.498	0.824
		11.85	25.90	1.166	1.498	0.778
		16.00	40.70	1.225	1.498	0.818
bending	depth a	6.49	10.14	0.986	1.078	0.915
		8.95	15.80	0.926	1.043	0.888
		11.85	25.90	0.899	1.021	0.872
		16.00	40.70	0.895	1.000	0.895
bending	width c	6.49	10.14	1.353	1.650	0.820
		8.95	15.80	1.325	1.650	0.803
		11.85	25.90	1.286	1.650	0.779
		16.00	40.70	1.324	1.650	0.802

Table 5 SIF and M_k for geometry D-2-2

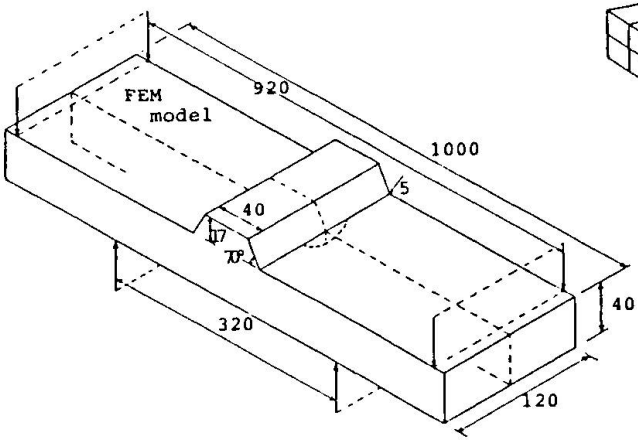

Fig 8. Dimensions of 3-D specimen

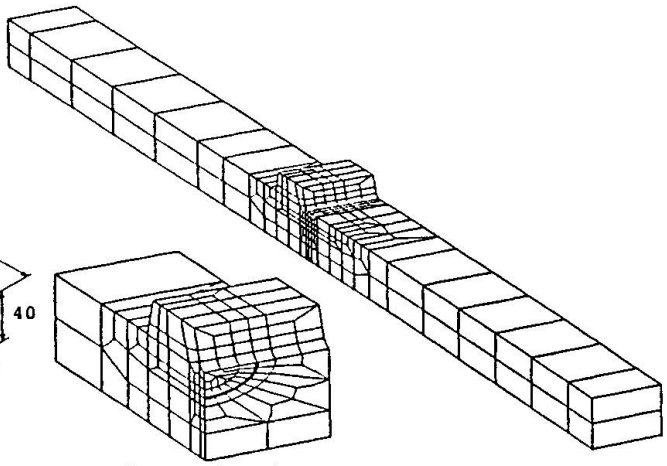

Fig 9. Mesh of 3-D specimen.

5 CALCULATION PROCEDURE.

The lifetime can be calculated by integrating the crack growth law from the initial defect size (a_i) to the final (allowable) defect size (a_f). The integration can be done either analytically or numerically. Due to the complex relation between ΔK and a the analytical integration of the crack growth law is an impractical procedure. Therefore a numerical (step by step) calculation procedure carried out by a computer is recommended.
TNO-IBBC has developed the program FAFRAM (FAtigue FRActure Mechanics) [19]. As the governing parameter for the calculation a crack extension (Δa) relative to the existing crack depth (a) was chosen. In order to get acceptable accuracy relatively small values should be taken for Δa (Crack extensions Δa of 5% of the present crack size give in general acceptable results). The numerical procedure will be illustrated for the semi-elliptical crack of figure 7. Assuming only bending stresses ($\Delta\sigma$) the expressions for ΔK_a and ΔK_c can be simplified to:

$$\Delta K_a = f_a \cdot \Delta\sigma \sqrt{\pi a} \qquad (21a)$$

$$\Delta K_c = f_c \cdot \Delta\sigma \sqrt{\pi a} \qquad (21b)$$

$$\text{where: } f_a = \frac{M_{k,b,a} \cdot M_{b,a}}{\Phi} \qquad (22a)$$

$$f_c = \frac{M_{k,b,c} \cdot M_{b,c}}{\Phi} \qquad (22b)$$

The procedure is as follows (see table 6 as a way of presenting the results):

1. With the actual crack depth (a_i) and half crack width (c_i) and the other geometrical parameters the values for f_a and f_c can be calculated.
2. Using the stress range ($\Delta\sigma$) the SIFs for crack depth (ΔK_a) and crack width (ΔK_c) can be calculated with equation (21).
3. Assuming a crack extension Δa the corresponding number of cycles can be calculated with the Paris relation.

$$\frac{\Delta a}{\Delta N} = C\,(\Delta K_a)^m \qquad \text{or:} \qquad \Delta N = \frac{\Delta a}{C\,(\Delta K_a)^m} \qquad (23)$$

4. The crack extension in the width direction can also be calculated with the Paris relation.

$$\frac{\Delta c}{\Delta N} = C\,(\Delta K_c)^m \qquad \text{or:} \qquad \Delta c = \Delta N\, C\,(\Delta K_c)^m = \Delta a\,\left(\frac{\Delta K_c}{\Delta K_a}\right)^m \qquad (24)$$

5. The number of cycles has to be increased with ΔN.
$$N_{i+1} = N_i + \Delta N \quad (25)$$

6. The crack dimensions have to be increased with the crack extensions:
$$a_{i+1} = a_i + \Delta a \quad \text{and:} \quad c_{i+1} = c_i + \Delta c \quad (26)$$

7. With the new crack dimensions (a_{i+1}, c_{i+1}) the next step can be calculated, starting with point 1 above.
8. The calculation has to be continued until the allowable crack depth (a_f) or until the required number of cycles (N_{req}).
9. The calculated number of cycles or crack size has to be assessed at its acceptability.

For 2D geometries the calculation has to be carried out in the a-direction only.

crack dimensions		a-direction			c-direction			number of cycles		
depth a [mm]	width c [mm]	f_a [-]	ΔK_a [N/mm$^{1.5}$]	Δa [mm]	f_c [-]	ΔK_c [N/mm$^{1.5}$]	Δc [mm]	N_i [-]	ΔN [-]	N_{i+1} [-]
0.25	0.25	2.177	196.12	0.025	2.901	270.19	0.065	0	33141	33141
0.28	0.32	2.242	217.60	0.028	2.929	285.14	0.062	33141	26692	59834
a_i	c_i	f_{a_i}	ΔK_{a_i}	Δa	f_{c_i}	ΔK_{c_i}	Δc	N_i	ΔN	$N_i+\Delta N$
$a_i + \Delta a$	$c_i + \Delta c$									

Table 6. Calculation of crack growth

More results of crack growth calculations can be found in earlier papers and reports [8, 9, 12, 14 and 20]. The effect of several parameters are demonstrated in these publications.

6 CONCLUDING REMARKS AND RECOMMENDATIONS

- With the information in the paper and the references given to open literature a fatigue crack growth calculation of a defective welded joint can be carried out.
- The recategorization rules for interacting fatigue cracks given in this paper are less conservative than existing rules (Existing rules are developed for instable (brittle) fracture).
- The Paris-Erdogan relation can be applied in most cases as the crack growth law.
- Stress intensity factors for 2-D weld geometries are given.
- The influence of the weld on the stress intensity factor (SIF) is smaller for a 3-D geometry (semi-elliptical crack) than for a 2-D geometry (constant depth crack). However the information of 3-D SIF is limited. Therefore it is recommended to generate more information for 3-D cracks.
- Experimental crack growth data for 3-D geometries is needed to validate the crack growth model for a 3-D situation.
- A fatigue crack growth calculation procedure suitable for a computer program is given.

REFERENCES

1. DIJKSTRA, O.D., SNIJDER, H.H. and RONGEN, H.J.M. van., Fitness for purpose assessment of fatigue loaded welded joints in steel structures. IBBC-TNO report BI-87-110/63.4.5700 March 1989.

2. SNIJDER, H.H. and DIJKSTRA, O.D., Stress intensity factors for cracks in welded structures and containment systems. IBBC-TNO report BI-88-128/63.4.5700, August 1988.
3. DIJKSTRA, O.D. and SNIJDER, H.H., Fatigue crack growth models and their constants. IBBC-TNO report BI-88-027/63.4.5700, February 1989.
4. RONGEN, H.J.M. van., Categorization and interaction of fatigue cracks. MI-TNO report 89M/02316/ROH, February 1989.
5. IIW recommendation on "The Application of an Engineering Critical Assessment in Design, Fabrication on Inspection to assess the Fitness for Purpose of Welded Products", Part 4, Fatigue, IIW document V-878-88/X-1167-88/XIII-1283-88/XV-665-88.
6. British Standards Institution "Guidance on some methods for the derivation of Acceptance levels for defects in fusion welded joints", PD6493; 1980, London.
7. BELL, R., VOSIKOVSKY, O., BURNS, D.J., MOHAUPT, U.H., A Fracture Mechanics Model for Life Prediction of Welded Plate Joints. Steel in Marine Structures, edited by C. Noordhoek and J. de Back, Elsevier, pp 901-910, 1987.
8. DELFT, D.R.V. van, DIJKSTRA, O.D., and SNIJDER, H.H.,The Calculation of Fatigue Crack Growth in Welded Tubular Joints Using Fracture Mechanics. 18th Offshore Technology Conference, OTC 5352, Houston, 1985.
9. DIJKSTRA, O.D., SNIJDER, H.H., OVERBEEKE, J.L., WILDSCHUT,H., Prediction of Fatigue Crack Growth for Welded Joints Using Stress Intensity Factors Determined by FEM Calculations. Steel in Marine Structures, edited by C.Noordhoek and J. de Back, Elsevier, pp 885-899, 1987.
10. THORPE, T.W., A Simple Model of Fatigue Crack Growth in Welded Joints. Department of Energy, Offshore Technology Report, OTH 86 225, Her Majesty's Stationery Office, 1986, London.
11. VOSIKOVSKY, O., BELL, R., BURNS, D.J., MOHAUPT, U.H., Fracture Mechanics Assessment of Fatigue Life of Welded Plate T-Joints Including Thickness Effect. Behaviour of Offshore Structures, Elsevier, Amsterdam, 1985.
12. DIJKSTRA, O.D., SNIJDER, H.H., OVERBEEKE, J.L., WILDSCHUT, H. and SCHOLTE, H.G. Fatigue behaviour of welded joints in offshore structures. ECSC convention 7210-KG/602(F7.5/84) Delft, December 1988.
13. ROOKE, D.P. and CARTWRIGHT, D.J., Compendium of Stress Intensity Factors.London, Her Majesty's Stationary Office, 1976.
14. DIJKSTRA, O.D., SNIJDER, H.H. and STRAALEN IJ.J., Fatigue crack growth calculations using stress intensity factors for weld toe geometries. OMAE conference, The Hague, March 1989.
15. SMITH, I.J. and HURWORTH, S.J., The effect of geometry changes upon the predicted fatigue strength of welded joints. The Welding Institute Report 7819.01/84/394.3, Cambridge, 1984.
16. MADDOX, S.J., LECHOCKI, J.P., ANDREWS, R.M., Fatigue analysis for the revision of PD 6493: 1980'The Welding Institute Report 3873/1/86, Cambridge, 1986.
17. NEWMAN, J.C., and RAJU, I.S., Stress intensity factor equations for cracks in three-dimensional finite bodies subjected to tension and bending loads. NASA TM 85793, Langley Research Center, Virginia, 1984.
18. STRAALEN, IJ.J. van, DIJKSTRA, O.D. and SNIJDER,H.H., Finite element calculations to obtain stress intensity factors of semi-elliptical surface cracks in a finite width plate with stub and without stub - Calculations with DIANA for specimen D-2-2 of the SMOZ fracture mechanics programme, Report no. BI-88-015/63.8.0310 and BI-88-133/63.5.5860-310, TNO-IBBC, Rijswijk, The Netherlands,1988.
19. SNIJDER, H.H. and DIJKSTRA, O.D., FAFRAM - Computer program for the evaluation of FAtigue behaviour of structures using FRActure Mechanics. TNO-IBBC report BI-85-102, Rijswijk, 1985.
20. SNIJDER, H.H., DELFT, D.R.V. van, DIJKSTRA, O.D., and NOORDHOEK, C., Fatigue crack growth modelling for multiple initiated cracks at weld toes in tubular joints. BOSS conference June 1988, Trondheim.

An Alternative to Miner's Rule for Cumulative Damage Calculations?

Une alternative à la loi de Miner pour calculer le cumul du dommage?

Eine Alternative zur Miner'schen Regel für die Berechnung der Schadens-Akkumulation?

Tim GURNEY
Chief Research Engineer
The Welding Institute
Cambridge, England

Tim Gurney, born 1929, read Mechanical Sciences at Cambridge University where subsequently, he also obtained his PhD. Following four years with a firm of Consulting Engineers, he joined The Welding Institute, where he has worked primarily on fatigue of welded structures.

Stephen MADDOX
Principal Fatigue Consultant
The Welding Institute
Cambridge, England

Apart from three years' industrial consultancy at Southampton University, Stephen Maddox has been with The Welding Institute since graduating in Civil Engineering in 1966. His research field is fatigue of welded structures, including design recommendations and the application of fracture mechanics, for which he received his PhD.

SUMMARY

Based upon an analysis of the available variable amplitude fatigue test results for welded joints, it is shown that, in some circumstances, Miner's rule may be unsafe and that the Area rule may be a better alternative. This applied particularly for short block length loading and wide band loading. However, further work is required to confirm these findings.

RÉSUMÉ

Sur la base d'une analyse des résultats d'essais de fatigue à amplitude variable sur des joints soudés, on peut montrer que, dans certains cas, la loi de Miner n'est pas du côté de la sécurité, et que la «règle des surfaces» serait une meilleure alternative. Ceci s'applique en particulier quand la contrainte maximum se produit fréquemment et pour des chargements à bande étendue. Cependant, des études supplémentaires doivent être faites pour confirmer ces conclusions.

ZUSAMMENFASSUNG

Basierend auf einer Analyse der erhältlichen Versuchsresultate zur Ermüdung von Schweissverbindungen unter variabler Amplitude wird gezeigt, dass unter gewissen Umständen die Miner-Regel auf der unsicheren Seite liegt und deshalb die Anwendung der «Oberflächen-Regel» angebracht erscheint. Dies trifft besonders auf «short block length-» und «wide band loading»-Spektren zu. Um diese Beobachtungen zu bestätigen, sind jedoch weitere Forschungsarbeiten unabdingbar.

1. INTRODUCTION

In service, the great majority of structures which are liable to suffer fatigue failure are subjected to variable amplitude loading. For historical reasons, however, and particularly on account of the capabilities of fatigue testing machines, most of the experimental data, certainly for welded joints, has been obtained under constant amplitude loading. The assessment of the fatigue life of structures therefore requires the use of some sort of cumulative damage rule and Miner's [1] linear damage rule is the one most commonly used.

As far as is known, the first time that this rule appeared in a Standard for the design of welded joints was in 1962 when it was introduced into BS 153, Steel Girder Bridges. At that time such an action was probably quite unjustified; it was really a simple 'act of faith'. After all, Miner had originally proposed his rule for defining the life to crack initiation of unnotched specimens of aluminium alloy. There were no sound reasons for assuming that it would be equally applicable to the life to rupture of severely notched members in steel, where it was known that the great majority of the life consisted of crack propagation. It was only much later that it was shown by Maddox [2] that Miner's rule could be derived by fracture mechanics for any specimen/joint involving crack propagation to failure. Since then, however, Miner's rule, or a simplified rule based on Miner's rule, has appeared in several National Standards.

The obvious problem is, "Is it right?" In order to try to answer that question an extensive literature survey has recently been carried out to gather together and analyse all the available test results for welded steel specimens subjected to variable amplitude loading, either of the programmed or random variety, in air. This included recalculating the values of $\Sigma\frac{n}{N}$ for every test specimen so as to ensure that all the results were defined in the same manner; unbroken specimens were ignored.

It was found that numerous test series gave mean values, and particularly lower limit values, of $\Sigma\frac{n}{N}$ which were less than 1.0. This has sometimes been taken as proof that Miner's rule is unsafe. However, that is not necessarily true, since one could reasonably expect the scatter in variable amplitude test results to mirror that found in constant amplitude results. In other words, if a specimen would have given a low life under constant amplitude loading, it seems reasonable to assume that it would also be expected to give a low life under variable amplitude loading. Furthermore, to a first approximation, it also seems reasonable to assume that the amount of scatter would be the same with the two different types of loading.

Although no detailed analysis has been made of the scatter in constant amplitude results, inspection of a number selected at random suggests that in a single S-N curve the overall scatter can be represented by a factor of between 2 and 3 on life. For comparison Haibach [3] proposed that his 'standard curve' should have corresponding factors of 3 at 10^5 and 4 at 10^6 cycles.

For a factor of 2.0 the corresponding expected range of values of $\Sigma\frac{n}{N}$ becomes about 0.7 - 1.4, while for a factor of 3.0 it is about 0.6 - 1.8. Thus any values of $\Sigma\frac{n}{N}$ greater than about 0.6 - 0.7 can reasonably be regarded as normal, provided that in a test series there are also some corresponding 'high' values. Thus, for Miner's rule to be proved safe one should expect a series of variable amplitude fatigue tests to give a mean value of $\Sigma\frac{n}{N}$ approximately equal to 1.0 (or more) but with individual results down to about 0.6. In fact it was found that many test series gave values which were considerably lower, thereby suggesting that Miner's rule certainly is not safe under all conditions.

Fig. 1 shows the same data expressed in terms of the 1292 individual test results. The values extend from 0.16 to 9.12 but it should be noted that three test series for which the mean values of $\Sigma\frac{n}{N}$ were in the range 12.3 - 15.7 have been ignored. These were so out of line with the other results that it was assumed that some error must have occurred in reporting the results. Results

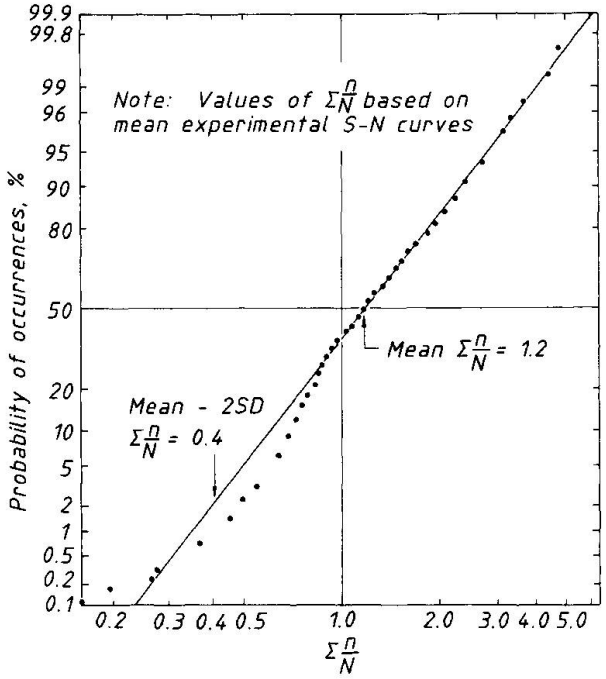

Fig.1 Summary of published values of $\Sigma\frac{n}{N}$

obtained using spectra in which all cycles pulsated downwards from a constant maximum stress have also been omitted. As before, the results are based upon the corresponding mean experimental S-N curve extrapolated linearly downwards.

Although the individual values of $\Sigma\frac{n}{N}$ varied widely, the mean and mean minus 2 standard deviations (SD) values were approximately 1.2 and 0.4 respectively. It is therefore tempting to argue that Miner's rule, with $\Sigma\frac{n}{N}$ = 1.0, is a satisfactory design approach, since the low value of 0.4 is counterbalanced by the fact that design is normally based upon the mean minus 2 SD design curve and not the mean curve. In the British design rules the difference in life between the two curves, represented by the ratio $\frac{\text{mean - 2 SD life}}{\text{mean life}}$ at any given stress, is as follows:

Class	D	E	F	F2	G
Ratio of lives	0.381	0.315	0.366	0.350	0.437

Thus, in all cases except Class G, the reduction in life between the two curves is more than 0.4 so that, basing the calculation on the mean minus 2 SD curve would be safe for more than 97.7% of situations.

This is, however, a fallacious approach. The reduction in life between the mean and mean - 2 SD design curve only takes account of the scatter found in constant amplitude tests, caused by such variables as differences in local joint geometry. It does not allow for any extra variability in life, if such exists, due to variable (rather than constant) amplitude loading. It is therefore necessary to consider the influence of the type of loading separately and not to assume that it is necessarily covered by using the mean - 2 SD design curve.

2. INFLUENCE OF TYPE OF LOADING ON FATIGUE LIFE

The following information about the influence of the type of loading on the value of $\Sigma\frac{n}{N}$ is based heavily on the results of work at The Welding Institute [4,5] over the last six or seven years. All the work involved longitudinal non-load-carrying fillet welds, either on the edge or surface of the stressed plate, because of the known tendency of such joints to give very little scatter; it was therefore hoped that it would be easier to define any trends which might emerge. It is convenient to consider the results more or less in chronological order.

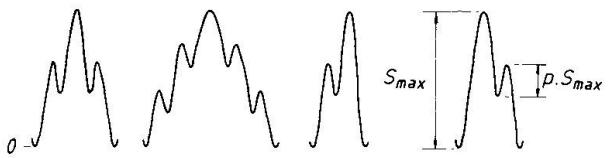

Fig.2 Typical loading in initial tests

The initial tests [4] were carried out with very simple stress histories, consisting essentially of constant amplitude loading with one or more excursions applied on each stress cycle (Fig. 2). With this type of loading there are few real problems

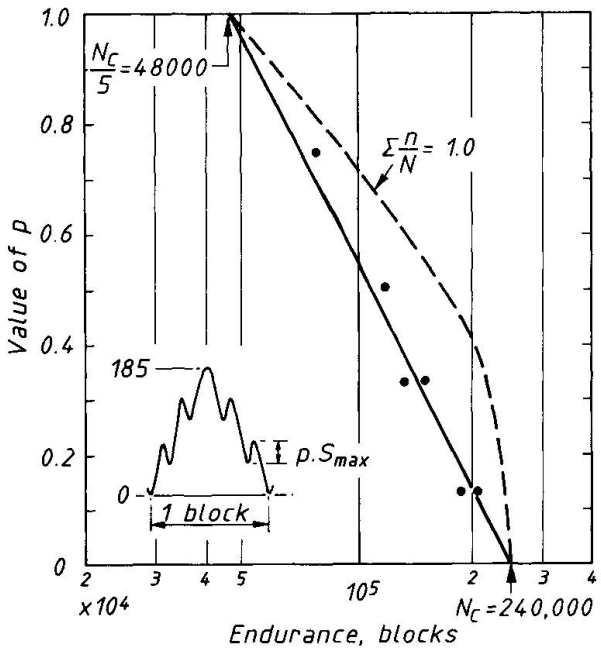

Fig.3 Typical results obtained using simple stress sequences

with stress counting, although in all cases the reservoir method was used. On the other hand there is certainly a potential stress interaction problem and the expectation was that the tensile peak of the main constant amplitude cycle would tend to introduce compressive residual stresses at the crack tip and thereby make the smaller cycles less damaging. As a result of this stress interaction it was anticipated that the life would always be greater than that predicted by Miner's rule - in other words it was expected that $\Sigma\frac{n}{N}$ would be greater than 1.0. In fact the opposite was found to be true.

A typical set of results is shown in Fig. 3. They relate to specimens tested under a main constant amplitude cycle of 185 N/mm² at R = 0 with four subsidiary cycles of magnitude p. In this context p represents the ratio between the stress range of the excursions and of the main cycle. Thus, using this nomenclature, p can clearly vary from 0 to 1.0 and at the two extremes (p = 0 or p = 1.0) the loading degenerates to constant amplitude. At p = 0 the four subsidiary cycles disappear, so that the life under the complex load cycle merely becomes N_c, the constant amplitude life under the peak stress range. At p = 1.0 all the cycles (one main and four subsidiary) have the same magnitude, so that the life in 'blocks' (where a block is defined as consisting of the main constant amplitude cycle and all its associated subsid- iary cycles) becomes $N_c/5$. It will be seen from Fig. 3 that there is an excellent linear relationship between p and Ln (N_B), where N_B is the life measured in 'blocks', joining these two end points. The relationship between p and N_B is therefore

$$N_B = N_c\ (1 + v)^{-p}$$

where v is the number of subsidiary cycles per block (4 in Fig. 3).

For comparison, the lives required to give $\Sigma\frac{n}{N}$ = 1.0 are also indicated. As noted above, it is clear that the actual values of $\Sigma\frac{n}{N}$ were consistently less than 1.0, except at the two limits (p = 0 and p = 1.0).

The same general form of behaviour was found to occur with each of the loading blocks shown in Fig. 2. It was also found with as-welded specimens subjected to an alternating, rather than pulsating tension, main cycle and with stress relieved specimens under a pulsating tension cycle. Anomalies were found, however, with stress relieved specimens subjected to an alternating main cycle, particularly when the subsidiary cycles were at a different mean stress so that they were either fully tensile or fully compressive. This problem of the influence of mean stress in stress relieved specimens remains to be fully resolved.

If one assumes (even if there is no obvious reason for it) that the behaviour indicated in Fig. 3 will also occur when there are subsidiary cycles of several different magnitudes associated with each main cycle, instead of only one, it is easy to deduce that the expected life (in blocks) can be written as

$$N_B = N_c\ e^{-Area}$$

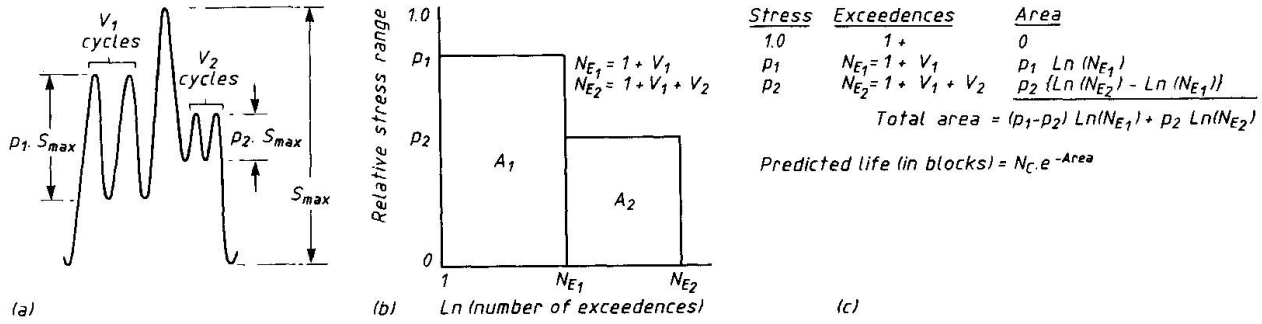

Fig.4 Example of life calculation using the area rule

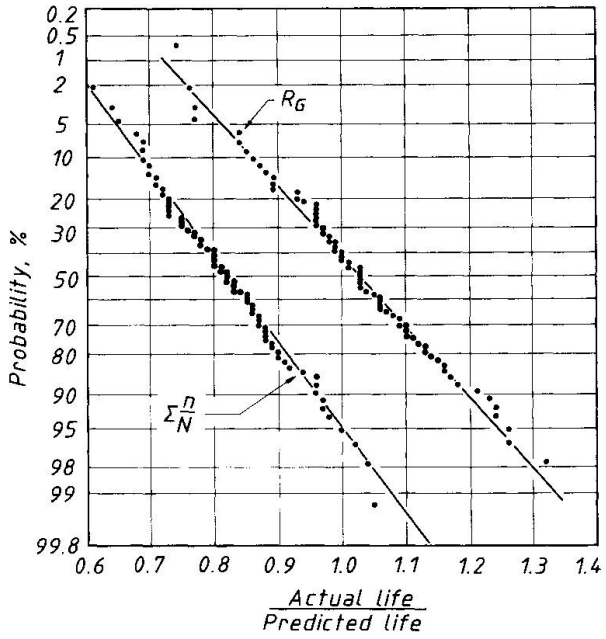

Fig.5 Comparison of Miner's rule and area rule for short blocks

where 'Area' is the area under the p v. Ln N_E exceedence diagram for the loading spectrum, N_{E_i} being the number of exceedences of stress p_i per block. A simple example is shown in Fig. 4. Like Miner's rule, the 'area rule' at least has the merit of simplicity. The problem is, 'Is it any better?' In order to make the comparison it is convenient to express experimental results in terms of the ratio R_G (= actual life/life predicted by the area rule). This is directly comparable to the value $\Sigma \frac{n}{N}$ for Miner's rule.

A summary of all the results obtained for very simple loading of the type shown in Fig. 2, but ignoring the results for stress relieved specimens under alternating loading (where special considerations apply) is shown in Fig. 5. Clearly for those types of loading the area rule is superior to Miner's rule.

The next step was therefore to compare the two under more complex load spectra and the initial tests [5] involved Rayleigh distributions of stress ranges of various block lengths (and hence various clipping ratios). In all cases the individual cycles forming a block were applied in random order at R = 0 and the block was then repeated, in the same order, until failure occurred.

The results, in terms of $\Sigma \frac{n}{N}$, are shown in Fig. 6(a). They show two interesting features:

1. a clear tendency for $\Sigma \frac{n}{N}$ to increase with increasing block length
2. an equally clear tendency for $\Sigma \frac{n}{N}$ to decrease as the stress magnitude is decreased.

In other words, at least for this particular type of spectrum, the trends suggest that Miner's rule would become unsafe at short block lengths, with the critical block length increasing as the applied stresses decrease.

In contrast, the results expressed in terms of the area rule were all safe (Fig. 6(b)), although their trend suggested that it might well become unsafe at very long block lengths (approx. 10^6 cycles). On the other hand, the great accuracy of the prediction for the very simple type of loading obviously did not carry through to these particular tests, since R_G obviously rose to a peak at a block

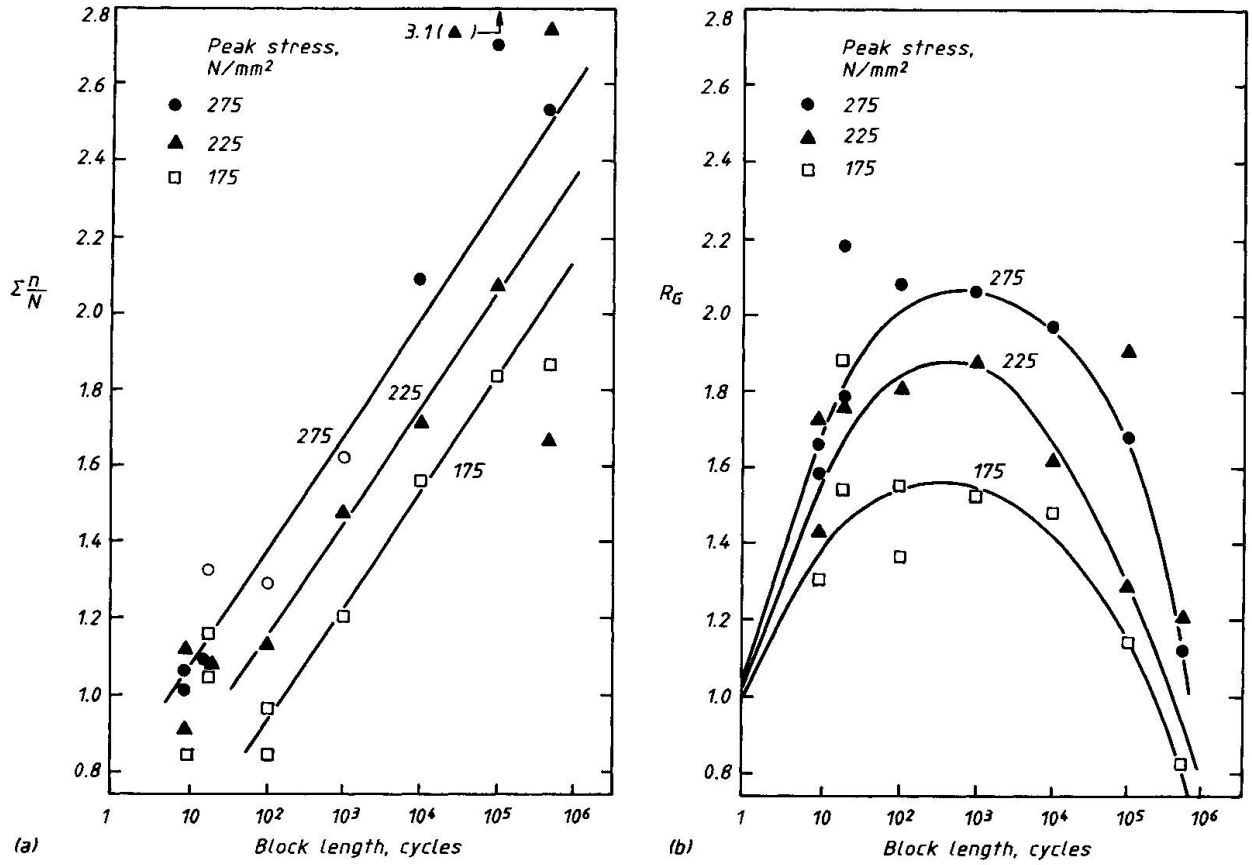

Fig.6 Influence of block length on (a) $\Sigma\frac{n}{N}$ and (b) R_G for Rayleigh spectra

length of about 10^3 cycles before reducing again; equally, like the value of $\Sigma\frac{n}{N}$, R_G was obviously also a function of the stress magnitude.

In passing, it is worth noting that these results show, quite conclusively, that there is little benefit to be gained by working in terms of 'equivalent stress' (cube root mean cube stress range) or any variety of rms stress. As can be seen from Fig. 7 the use of these parameters does not normalise the results to a single curve. Not only do results at different stress ranges with the same spectrum plot on different curves, but so do the results for different spectra (in this case Rayleigh and Laplace).

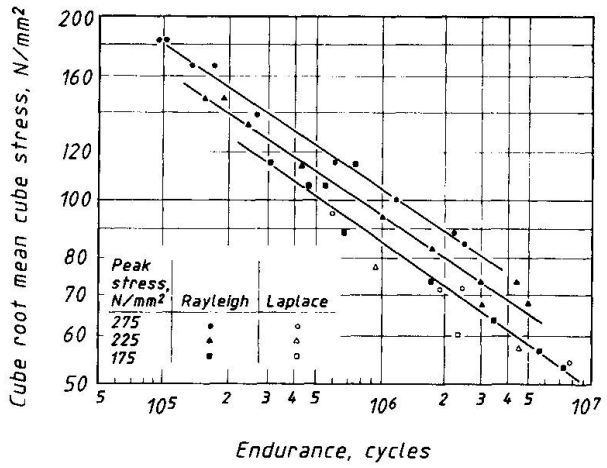

Fig.7 Results for Rayleigh and Laplace spectra

As stated previously, one interpretation of the results in Fig. 6 is that $\Sigma\frac{n}{N}$ tends to increase as block length increases, but an equally good interpretation, since clipping ratio is related to block length, is that $\Sigma\frac{n}{N}$ tends to increase as clipping ratio increases. Since they are related it is impossible, for any particular shape of spectrum, to determine which is the more relevant variable. However, by varying spectrum shape as well, it was possible to carry out tests with the same block lengths but different clipping ratios and also with the same clipping ratios but different block lengths. The spectra were based upon the 2 parameter Weibull

distribution and the results again showed that both $\Sigma\frac{n}{N}$ and R_G tended to decrease as the stress level decreased; at 275 N/mm² the values were typically 19% higher than at 175 N/mm². It was therefore possible to increase the database by applying that correction and assuming that all specimens were tested at 275 N/mm².

Analysis of the results after applying that correction showed that the value of $\Sigma\frac{n}{N}$ was almost completely insensitive to clipping ratio but, as with the Rayleigh spectra (Fig. 6(a)) there was again a fairly general tendency for $\Sigma\frac{n}{N}$ to increase with increasing block length, although there were some 'outlying' results. Similarly, the influence of block length on the value of R_G appeared to be very like that shown in Fig. 6(b).

Since these results appear to show that R_G gives safe predictions of life at short block lengths but that they become unsafe at long block lengths, all the available test data from the literature were re-analysed in order to derive the values of R_G at failure. The results are summarised in Fig. 8, but it does not include those for very short block lengths, which were summarised in Fig. 5. For relatively short block lengths (up to 10^5 cycles) the results were nearly all 'safe', even with N_c derived from the mean S-N curves. If the mean - 2 SD design curves had been used, only 2 results would have been 'unsafe'. However, it is clear that, for long block lengths ($\geq 2 \times 10^5$ cycles), R_G certainly does tend to become unsafe.

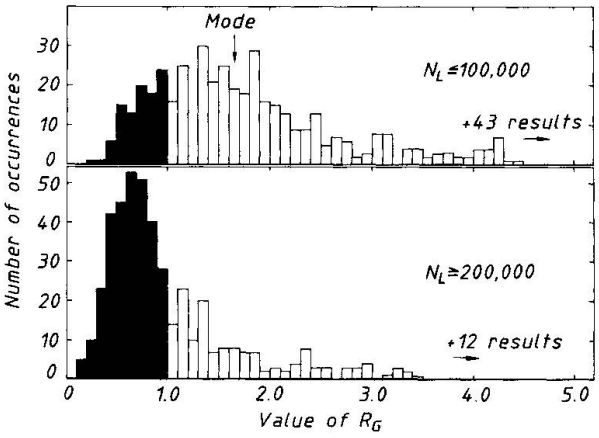

Fig.8 Summary of values of R_G

Up to this point all the results considered, except a few of the tests with very simple stress cycles (Fig. 2), involved all the cycles being applied at R = 0. The next stage therefore involved some exploratory tests to study the influence of stress ratio and mean stress. They were based upon 2 stress spectra, each with a block length of 128 cycles. The particular variants which were employed were:

a) All cycles at R = 0, random order

b) All cycles at R = -1, same order

c) All cycles with the same S_{max}, again in the same order (cf stalactites)

d) With the peak cycle at R = 0 or R = -1 but with the stress ratios of the other cycles varied within the overall range of the peak cycle (i.e. wide band loading). Again the order of the cycles was the same as before.

e) With the cycles arranged in decreasing-increasing order, as in a typical block programme test. These tests involved all cycles being at the same stress ratio (R = 0 and R = -1).

Apart from (e), all variants had the same stress ranges applied in the same order so that, in terms of stress range, their rainflow (or reservoir) counts were identical.

The average values of $\Sigma\frac{n}{N}$ which were obtained are summarised in Table 1. It is obvious that there was a tendency for $\Sigma\frac{n}{N}$ to be lower under alternating than under pulsating tension loading, although the difference was small under wide band loading. Surprisingly, extremely few other tests seem to have been carried out at R = - 1 except under programmed block loading. A comparison of those results with similar ones obtained at R = 0 is shown in Fig. 9. In that case also, there was a reduction in $\Sigma\frac{n}{N}$ at R = - 1, typically of about 28%. While there is obviously a need for more information this evidence does suggest that

Type of loading	Peak stress at R = 0	R = -1
All cycles at same stress ratio, in random order	1.32	0.75
'Stalactitic' spectrum	0.55	
Decreasing-increasing block programme	1.59	0.88
Wide band (variable R)	0.80	0.75

Table 1 Values of $\Sigma\frac{n}{N}$ using different types of loading

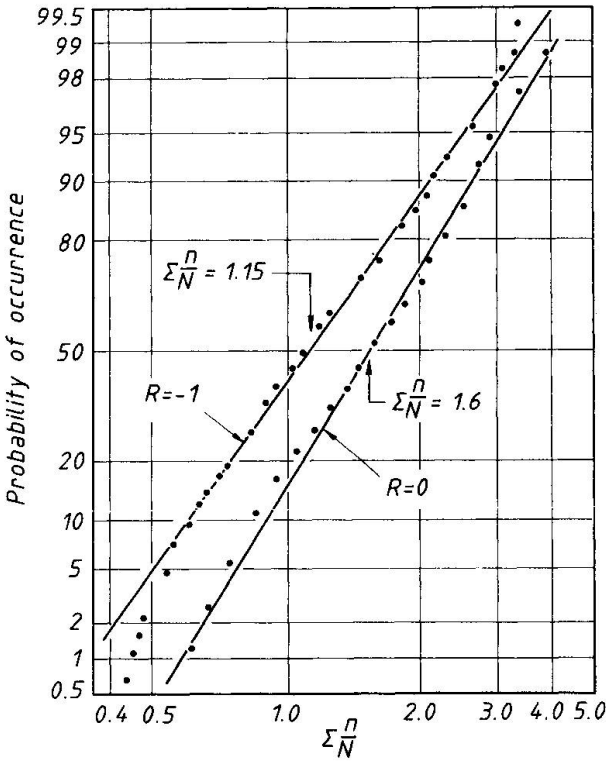

Fig.9 Effect of R on values of $\Sigma\frac{n}{N}$ for block programme tests

lower values of $\Sigma\frac{n}{N}$ are to be expected under alternating loading.

Similarly the tests in which all the cycles had the same maximum stress (what one might call a stalactitic spectrum) also gave a much lower value of $\Sigma\frac{n}{N}$, with a typical value of $\Sigma\frac{n}{N}$ = 0.55. That is very similar to the value obtained by Maddox in similar tests using the BS 5400 Axle loading spectrum. These were, incidentally, the results which were omitted omitted from Fig. 1. The original idea behind testing with this type of spectrum was that it would be an easy way to simulate the presence of high tensile residual stresses, which would be expected to be present in a large structure, in a small specimen. If correct, the results are obviously a little worrying, but it remains to be proved whether or not this method of simulation is too severe.

Turning now to the effect of wide band loading, the results were analysed using the S-N curves corresponding to the stress ratio of the peak stress ange, regardless of the fact that most of the smaller cycles were at different stress ratios. On this basis the values of $\Sigma\frac{n}{N}$ were very similar for the two stress ratios and ranged from approximately 0.5 - 1.0 with a mean value of about 0.76.

In the context of whether or not one should use Miner's rule to design structures subjected to such loading, this result is also a little worrying, particularly bearing in mind the numbers of specimens for which the predicted lives were safe or unsafe (see Table 2). On the other hand, the Area rule did appear to give either safe or acceptable predictions with these particular spectra. It must be remembered, however, that all these tests were carried out using spectra with relatively short block lengths (128 cycles); it has yet to be proved whether or not the results are block length dependent under wide band loading.

Finally, the opportunity was taken to obtain comparative results for the same spectra but with the individual cycles arranged in decreasing-increasing order, so as to simulate a typical block programme test. In this way it was hoped to obtain some evidence as to the likely accuracy of other block programme tests, since such results make up a very large proportion of the variable amplitude

Type of loading	No. of tests	Miner's rule		Area rule	
		>1.0	≥1.0	<1.0	≥1.0
Peak stress at R = 0					
All cycles at R = 0	4	–	4	–	4
All cycles with peak stress = S_{max}	4	4	–	1	3
Ordered block loading	7	–	7	–	7
Wide band loading	24	23	1	–	24
Peak stress at R = -1					
All cycles at R = -1	4	4	–	–	4
Ordered block loading	5	4	1	–	5
Wide band loading	29	28	1	10	19

Table 2 Summary of numbers of safe and unsafe predictions using Miner's rule and the 'area' rule

database and, as far as is known, no other directly comparable tests have been reported previously.

As can be seen from the summary of the results set out above, there was a substantial difference between the 'block programme' results and the 'random order' results at both stress ratios; typically the value of $\Sigma\frac{n}{N}$ obtained under block programme loading was 20% higher at both stress ratios. Clearly this must cast some doubt on the validity of all the earlier block programme results and it is obvious that further check tests are required for other types of spectra.

3. SUMMARY OF THE CURRENT POSITION AND FUTURE WORK REQUIREMENTS

As was shown at the beginning of this review, the available experimental evidence indicates that Miner's rule, based on the mean - 2 S.D. design S-N curves, should be a satisfactory design method in most situations. Nevertheless, there are clearly some where it may be unsafe.

The most obvious of these is when the loading involves short block lengths - in other words when the peak stress in the spectrum occurs fairly frequently. A typical example might be an overhead travelling crane working on a production process. Similarly, certain types of earth-moving plant, where the machine essentially goes through a continuous series of digging and unloading cycles, might also qualify. There are almost certainly many other examples. The evidence certainly seems to suggest that the 'area rule' would be an advance on Miner's rule for dealing with this particular type of loading.

The second major problem area seems to be the tendency for $\Sigma\frac{n}{N}$ to decrease as the applied stresses decrease. It is a trend which seems to be very evident under tensile loading when the individual stress ranges in the spectrum are applied in random order and when the peak stresses are fairly high. Much work is, however, still needed to confirm the extent to which the trend continues to lower stresses and also whether it also applies at other stress ratios and mean stresses.

If it is a general problem it would be worrying for two reasons. In the first place, almost the whole database of variable amplitude test results, which justify the continued use of Miner's rule, would be suspect. After all, nearly all the tests have, quite deliberately, been carried out at relatively high stresses in order to give shortish lives and hence reduce testing costs.

Secondly, many structures have been designed at much lower stresses, which implies that their lives might become much shorter than expected. Although it is easy to understand why tests have largely been restricted to high stresses and short lives, there is obviously a need to obtain data for more realistic stresses and longer lives.

Associated with this problem of decreasing $\Sigma\frac{n}{N}$ as stresses decrease is, of course, the question of what constitutes a 'short block length' at low applied stresses. Clearly, one would expect the critical block length to increase, but by how much will certainly need to be established.

In the light of the evidence pointing to a marked reduction in the value of $\Sigma\frac{n}{N}$ at R = -1 as compared to R = 0, and also under 'stalactitic' loading with a constant maximum tensile stress, there is also a need to investigate the influence of mean stress. In particular, it needs to be established whether stalactitic loading is a realistic simulation of the high tensile residual stresses which may occur in actual structures, and also whether the use of S-N curves related to stress range alone (i.e. ignoring mean stress) is a sensible basis for design under variable amplitude (as opposed to constant amplitude) loading.

The available evidence also suggests that there are likely to be problems under wide band loading, but it must be remembered that that evidence was obtained using short block lengths (128 cycles). It is at least possible that the problems will disappear with longer block lengths, but that is an area which also remains to be investigated.

REFERENCES

1. MINER M.A., Cumulative Damage in Fatigue. J.Appl.Mech., Vol. 12, No. 3, Sept. 1945, pp 159–164.

2. MADDOX S.J., A Fracture Mechanics Approach to Service Load Fatigue in Welded Structures. Weld.Res.Int., Vol. 4, No. 2, 1974, pp 1–30.

3. HAIBACH E., The Fatigue Strength of Welded Joints examined by Local Strain Measurement. LBF Report FB77, 1968.

4. CURNEY T.R., Fatigue Tests on Fillet Welded Joints to assess the Reliability of Miner's Cumulative Damage Rule. Proc.Roy.Soc., 1983, A386, pp 393–408.

5. GURNEY T.R., Some Variable Amplitude Fatigue Tests on Fillet Welded Joints. Conf. 'Fatigue of Welded Constructions', Brighton, April 1987.

Numerical Simulation of Fatigue Crack Growth

Simulation numérique de la propagation de fissures de fatigue

Numerische Simulation des Ermüdungsrisswachstums

Carlo A. CASTIGLIONI
Assist. Professor
Politecnico di Milano
Milan, Italy

Carlo A. Castiglioni, born 1956, is currently an Assistant Professor at the Structural Engineering Department, at Politecnico di Milano. After receiving his Laurea in Civil Engineering from Politecnico di Milano in 1980, he was part of the Visiting Faculty at Lehigh University, Bethlehem, PA, USA, in 1984. He is the Italian representative in ECCS Committee 6, «Fatigue» and his main research fields are high and low cycle fatigue of steel structures.

SUMMARY

This paper compares fatigue test data on full-scale structural-steel details under both constant and variable amplitude loading with results obtained through numerical simulation. Objectives include modelling fatigue crack growth in structural details commonly used in steel constructions, such as coverplates and web attachments. Random variability of parameters governing the fatigue crack propagation process is accommodated.

RÉSUMÉ

Cet article compare les résultats d'essais de fatigue sur des détails de structures en acier de dimension réelle sollicités sous charge d'amplitude constante et variable, avec les résultats obtenus à l'aide d'une simulation numérique. L'un des objectifs consiste en la modélisation de la propagation de fissures de fatigue dans des détails couramment utilisés en construction métallique, tels que des semelles de renfort et des liaisons à l'âme. La variation aléatoire des paramètres déterminants pour le comportement des fissures de fatigue est également prise en compte.

ZUSAMMENFASSUNG

Der vorliegende Beitrag vergleicht Resultate aus Ermüdungsversuchen an Bauteilen, die sowohl unter konstanter wie auch variabler Spannungsamplitude durchgeführt wurden, mit Resultaten aus entsprechenden numerischen Simulationen. Eines der angestrebten Ziele ist es, das Wachstum von Ermüdungsrissen, ausgehend von gebräuchlichen Stahlbau-Konstruktionsdetails, wie beispielsweise Lamellen oder auf Stege aufgeschweisste Laschen, modellieren zu können. Die Streuung der für den Rissverlauf massgebenden Parameter wird berücksichtigt.

1. INTRODUCTION

Although in reality fatigue cracking is generally caused by random variable amplitude loading, to date there are very few available results of long life ($N>10^7$ cycles), variable amplitude loading fatigue tests carried out on full scale structural elements [1]. This is due to the fact that full scale, random loading fatigue testing, in the long endurance range, requires long testing periods, with very high costs. While experimental research is absolutely necessary and fundamental, the time and money needed for this type of approach induces to take into consideration the possibility of studying numerical procedures that, calibrated on few test results, may be able to supply useful indications and improve our understanding of the problem under investigation. Though a series of numerical models of fatigue crack growth are already available in the literature [2-10], they deal with cases of ideal growth and are not aimed at the study of details typically adopted in steel constructions. Furthermore, for one way or another, none of the models to the author's knowledge, can be regarded as complitely satisfactory for the simulation of fatigue crack growth in structural steel details. In fact, the existing numerical models can be subdivided into three main groups:

1) deterministic models, like [2], that allow the simulation of the detail behavior during all phases of crack growth (fig. 1.1);
2) probabilistic approaches, capable of interpreting the low frequency random aspects of crack growth, by assuming the coefficients in the crack propagation law as random variables (fig. 1.2);
3) probabilistic approaches, capable of interpreting, during the intermediate, linear, phase of crack growth even the high frequency aleatory components, by means of the superposition of the Paris's Law with a random noise (fig. 1.3).

Fig. 1.1

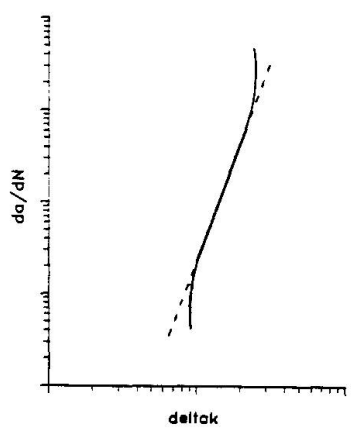

Fig. 1.2

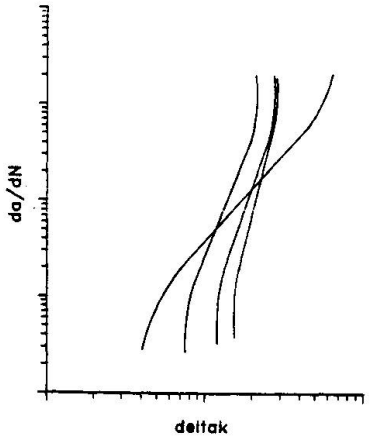

Fig. 1.3

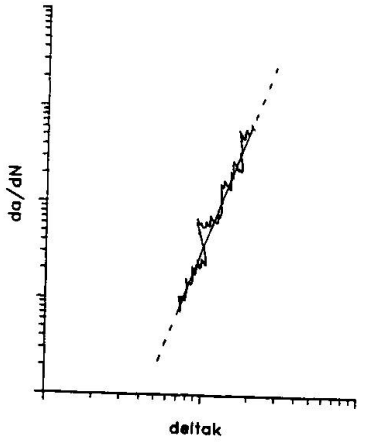

Fig. 1.4

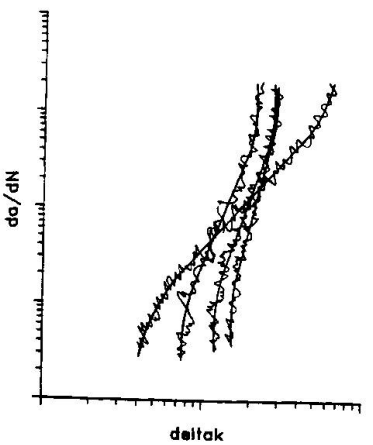

Recently, Castiglioni and Rossi [11] proposed a numerical model that encompasses the characteristics of all the three types discussed above (fig. 1.4), i.e. capable of simulating both types of random non-homogeneity (at high and low frequency), even in the two extreme phases of crack growth, i.e. in proximity of the threshold value ΔK_{th} and of the critical one ΔK_c of the stress intensity factor range.
In fact, a propagation law is assumed of the type:

$$da/dN = f(\Delta K)\, Z(a) \qquad (1)$$

in which Z(a) is a random function, as proposed in [9], and f(ΔK) is the deterministic function proposed by Newman [12]:

$$f(\Delta K) = C\,(1 - R)^m\, \Delta K^n\, (\Delta K - \Delta K_{th})^p\, [(1 - R)K_c - \Delta K]^{-q} \qquad (2)$$

where C, m, n, p and q are material dependent parameters, considered to be random variables. It is immediately recognized that (2) as a whole includes the most commonly used propagation laws, as Paris's (m=p=q=0), Forman's (m=p=q=1) and Walker's (p=q=0, $m=n[m_w-1]$).

The model presented in [11] takes into account:
1) various crack configurations and loading conditions (fig. 2)
2) retardation effects due to overloading according to Willenborg's model [13]
3) crack closure according to Newman's model [14]
4) stress concentrations due to geometric effects, and relative stress intensity factor's correction factors
5) stress corrosion

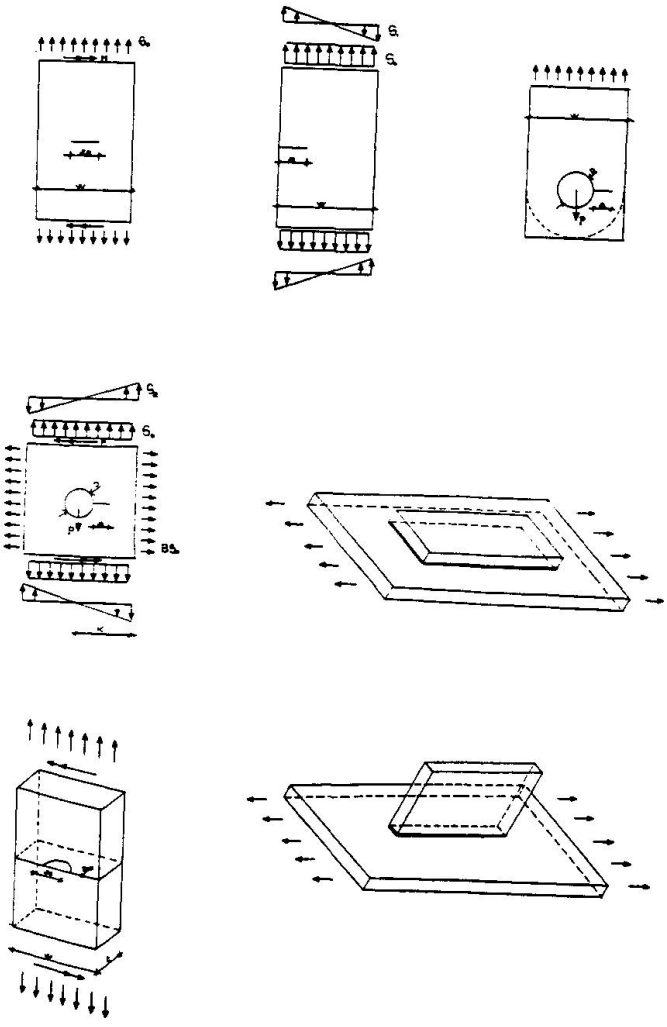

Fig. 2

In this paper, some results are presented obtained by means of model [11]. The behavior of typical structural steel details is simulated and the numerical results are compared with those of available experimental tests. In the case of fatigue under constant amplitude loading cycles, the results reported in the literature [15-17], relating to the weld toes at the ends of web attachments and of coverplates on beam flanges, are taken into consideration. Finally the influence of the loading history on the fatigue life of some structural details is investigated. To begin with, in order to determine the correspondence of the model with the physical reality, the case is considered of a plate with a through crack, for which the test results are widely presented in the literature. Attention is then focused on longitudinal web attachments and, in order to make a comparison, geometries similar to those adopted in the tests presented in [18] are considered.

2. ANALYSIS OF THE RESULTS

In order to correctly simulate fatigue tests on typical structural details, the model was previously calibrated [11] on the basis of available experimental results. In [11], at first the effect of the single parameters governing the model is investigated, with reference to the simple case of a plate with a through crack. It is concluded that the variability of the parameters of the propagation law (functions of the material), during crack growth, does not substantially influence the fatigue life of the structural detail. On the contrary, the superposition to the propagation law of a high frequency noise Z(a), defined by a stationary stochastic process with a log-normal statistics has an influence on the fatigue life that is comparable with that of the initial defect size.
In this paper, the simulation of some experimental tests on full scale beams is presented. Furthermore, the influence of the loading history is investigated, with reference to the case of a plate with a through crack.

2.1 Constant Amplitude Loading

The test results reported in [15-17], concerning coverplated beams and web attachments are taken into consideration.

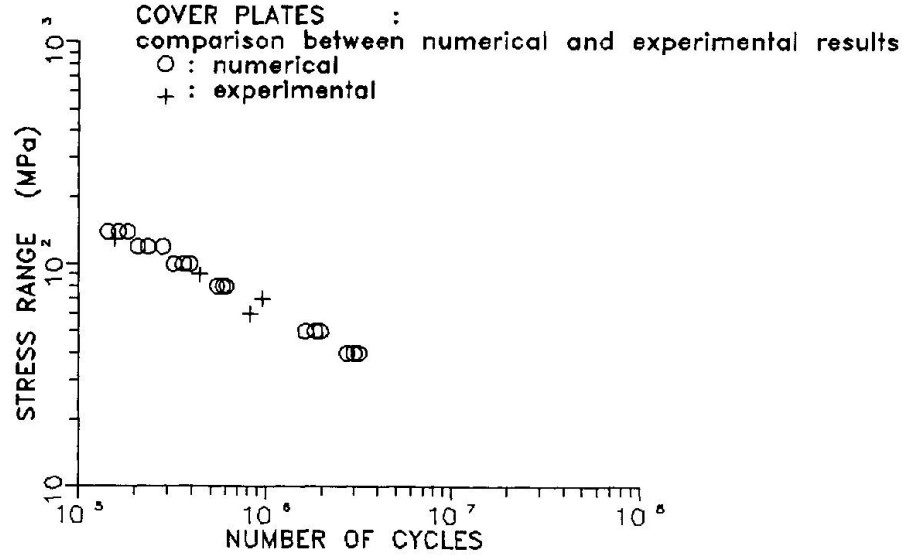

Fig. 3

Various numerical simulations were carried out at the same stress range level, considering different initial crack depths chosen from a sample having a normal distribution, 0.1 mm mean value and 40% standard deviation. The crack shape correction factor was computed, as a function of the crack size (a), with reference to the relationships between crack depth (a) and crack width (c) proposed, for both coverplates and web attachments by Fisher [19].
The parameters of the crack propagation law were calibrated on the test data presented in [18] for a plate with a central through crack, while the material parameters were obtained from [16,17].
Fig. 3 shows a comparison between numerical and experimental results in the case of coverplates on beam flanges.
It can be noticed that the numerical results interpret fairly well the trend of the experimental data, at all the stress range levels considered.
Fig. 4 shows the comparison between experimental test data and numerical simulation results in the case of web attachments. Also in this case it can be noticed that the numerical simulation interprets fairly well the trend of the experimental data.
Examining fig. 4 it can be noticed that the scattering in the numerical results is greater for the lower stress ranges than for the higher ones. This is also in agreement with the experimental evidence.
It is important to notice that, from both figs. 3 and 4, independently on the stress range level, it is evident a greater scattering in the experimental

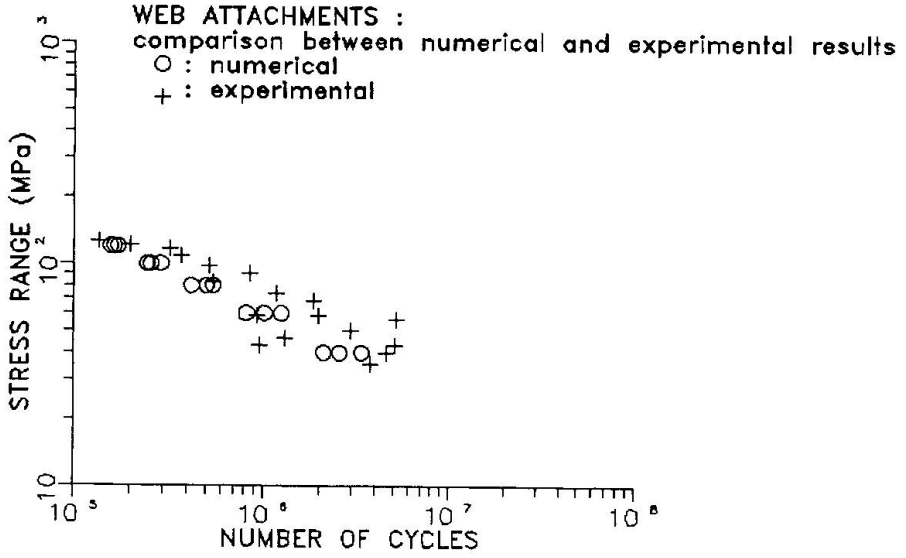

Fig. 4

data than in the numerical ones. This is probably due to two main reasons:
- the actual initial defect size is greater than that assumed in the numerical simulation. This fact might be easily corrected by generating a new sample of initial defects, with a larger mean value and standard deviation;
- the presence of residual stresses due to the welding process influences relevantly the fatigue life of actual welded components, as widely demonstrated and discussed in the literature [19,20]. Of course, the statistics of the residual stress distributions are characterized by large standard deviations from the mean value, depending on such factors as, for example, the plates' thickness and the welding process. In the numerical

model, at the present state, the presence of residual stresses in the joints is complitely disregarded, thus reducing the possible causes of randomness, and the scattering of the results.

From examining both figures 3 and 4, however, it can be concluded that the numerical model is capable of predicting the fatigue life of web attachments and coverplated beams under constant amplitude loading in fairly good agreement with the experimental results.

2.2 Variable Amplitude Loading

2.2.1 Influence of the Loading History

In order to verify the model's capacity to interpret the loading spectrum's influence on fatigue life, a plate similar to the one shown in fig. 5 is first examined.

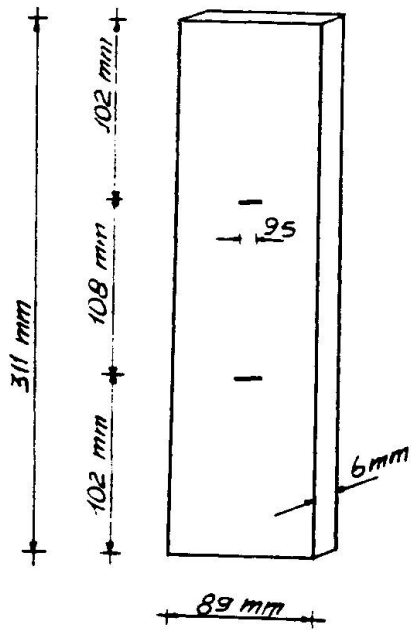

Fig. 5

A set of random loading histories, with a Rayleigh type distribution of the variable amplitude loading cycles are generated, with stress ranges S ranging from 5 MPa to 13.5 MPa.
The loading histories differ from one another either in the value of the stress ratio R between the minimum and maximum stress, or in the exceedence rate γ, i.e. the probability that the maximum cycle amplitude (S_{max}) exceeds a specific limit value (S_{lim}). Stress ratios R=0.5 and 0.7, and exceedance rates γ=0.1%, 1% and 5% were considered. Furthermore, for fixed R and γ values, three loading histories are randomly generated, each one different from the other only for the sequence of the stress ranges. Each loading history consists of a block of 5,000 cycles, repeatedly imposed on the simulated specimen until collapse situation is reached; in any case the simulation was interrupted after a maximum of 50,000 repetitions (equivalent to 250×10^6 cycles).
The results obtained are presented in fig. 6, where the simulated fatigue lives (N) are plotted against the root mean cube (equivalent) stress range,

$$S_{eq} = (\Sigma_i \alpha_i S_i^3)^{1/3} \qquad (3)$$

By examining fig. 6 it can be noticed how the model can interpret the effect of the stress ratio R, on the fatigue life. In fact, for each exceedance rate level, the numerical model predicted shorter endurances for those specimens subjected to stress histories associated with the higher R ratios (R=0.7).
The effect of the exceedance rate on fatigue life is also evident, in fact, for a fixed R ratio value, decreasing γ results in longer endurances.
By examining fig. 6 it can also be noticed that fatigue life is strongly influenced not only by the stress ratio R and the exceedance rate γ, but also by the loading sequence. In fact, for R=0.5 and γ=0.1%, certain cases did not reach critical conditions after 250×10^6 cycles, and are plotted in fig. 6 as run-outs.

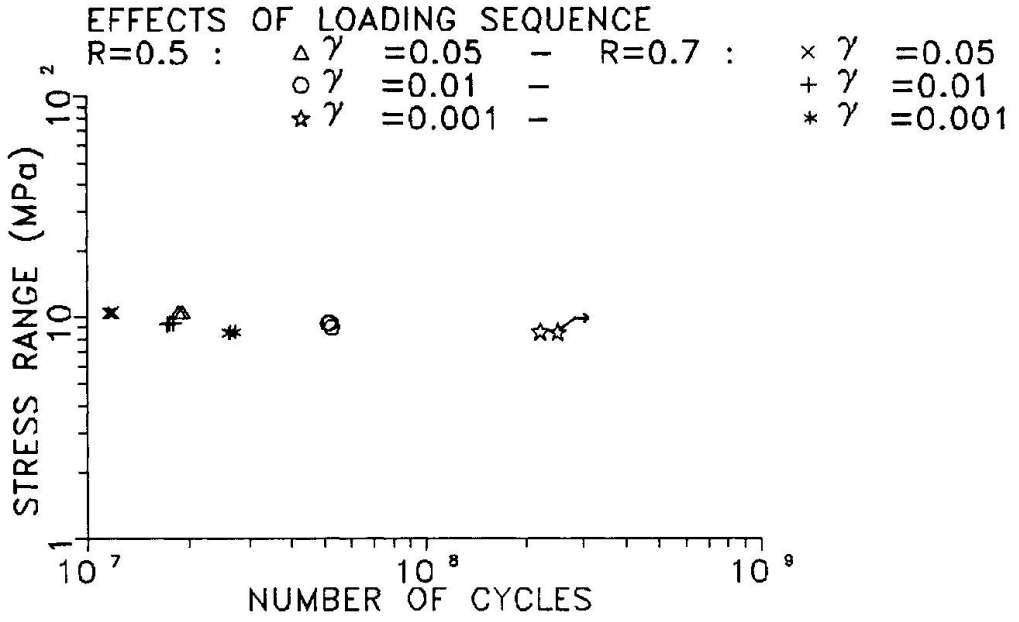

Fig. 6

It can be concluded that the numerical results are in good agreement with the physical reality, though it is not possible to make comparisons with the experimental results reported in [9], because these were obtained by varying in each case the stress range, both in order to compensate the effects due to the increase in crack size and to get as close as possible to the threshold value.

2.2.2 Simulation of Web Attachments

Finally, an attempt is made to simulate some of the experimental tests on web attachments under variable amplitude loading by Fisher, Mertz and Zhong, reported in [18].
The various numerical simulations were carried out considering different initial crack depths chosen from a sample having a normal distribution, 0.1 mm mean value and 40% standard deviation.
Loading histories are generated, similar to those adopted in the experimental tests [18], and consisting of a block of 5,000 cycles, repeatedly imposed on the joint. This loading history has a probability γ=0.1% that the maximum stress range exceeds the value S_{lim}= 31 MPa, assumed by the AASHTO Specifications [21] as the constant amplitude fatigue limit for this structural detail.
The comparison between the experimental data and the numerical simulation results is presented in fig. 7, where the number of cycles (N) is plotted against the root mean cube (Miner's) equivalent stress range (S_{eq}).

A reasonable agreement between numerical and experimental results can be noticed by examining fig. 7, confirming the remarkable versatility and acceptable reliability of the numerical model [11].

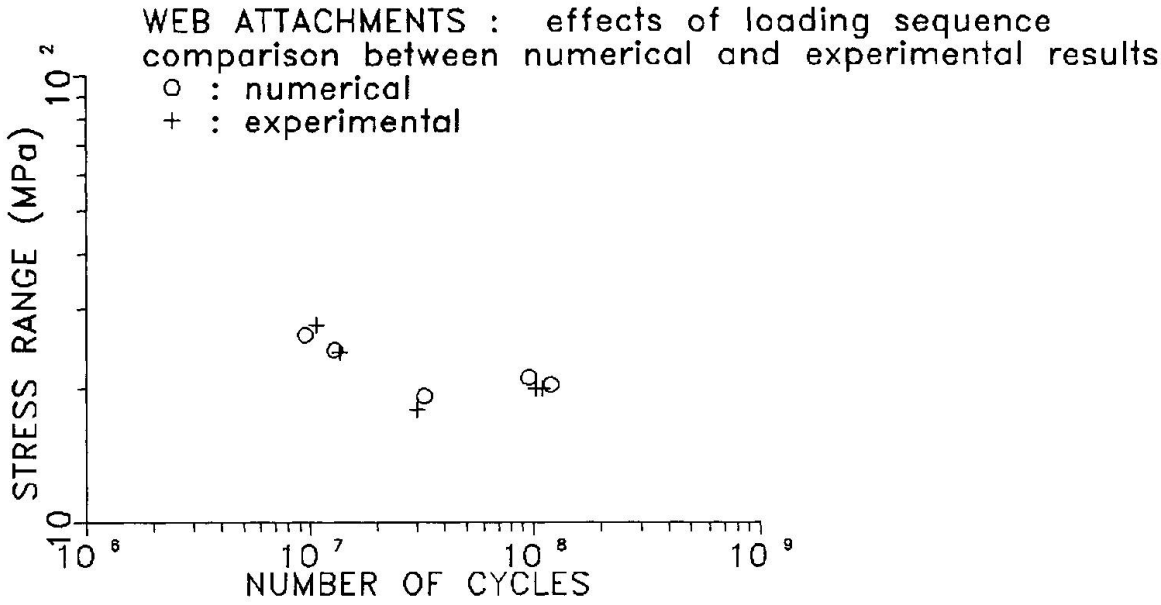

Fig. 7

3. CONCLUSIONS

Although the model presented in [11], in its present state, can be furtherly improved by implementing the possibility of considering for example the presence of residual stresses and/or other geometries and structutal details, it nevertheless seems to be a valid starting point for a reliable numerical simulation of fatigue crack growth in structural steel details (both welded and unwelded).

The good agreement between numerical and experimental results has been shown in this paper, by comparing experimental test data with numerical results.

Once the reliability of the model has been checked on the basis of available experimental test data, attention can be focused on its possible future applications.

Two main field can be immediately identified, one regarding its use for increasing the available data base in the long life region ($N>50x10^6$ cycles), the other aimed to the prediction of the fatigue life of a given component subjected to a known loading history.

In the first case, the model can be calibrated on a few test data either available or obtainable submitting the structural detail to constant amplitude loading, even at relatively high stress range levels. Once the model is calibrated, estimates of the fatigue life can be obtained by projection into the long endurance range. From this estimates trends can be identified rather quickly, avoiding the lengthy and expensive experimental long life fatigue tests. These will be in fact necessary only in a limited number, in order to double-check the numerical estimates obtained.

Adoption of the model for estimating the remaining fatigue life of a given component might be more difficult because it requires, in addition to the test data on which the model must be calibrated, also precise informations about the loading history experienced by the component during the service life, and an estimate of the future loading conditions. This last one is however a problem which is common to whatever procedure for estimating the remaining fatigue life of a structural detail, and does not represent an handicap of the presented numerical model.

4. AKNOWLEDGEMENTS

The numerical work was performed using the computer facilities at the Structural Engineering Department, Politecnico di Milano, Italy, and was funded by the Italian National Research Council, Structural Engineering Group (CNR-GIS).
The cooperation of Stefano Rossi, graduate student at the Structural Engineering Department of Politecnico di Milano, during the developement of the numerical model was deeply appreciated.
The author wishes to thank Prof. G. Ballio, of the Structural Engineering Department, Politecnico di Milano, Dr. Uwe Bremen, ICOM, Construction Metallique, Ecole Polytechnique Federale, Lausanne, CH, and Prof. P. Keating, Civil Engineering Department, Texas A&M University, Texas, USA, for helpful discussions.

5. REFERENCES

[1] Keating, P.B., Fisher, J.W. "Evaluation of fatigue tests and design criteria on welded details", NCHRP rept. 286, 1986.
[2] ESACRACK, User's Manual ESA PSS-03-209, European Space Agency, May, 1989.
[3] Arone, R., "Influence of random overloads on fatigue crack lifetime and reliability", Engineering Fracture Mechanics, Vol. 30, n.3, 1989.
[4] Langley, R.S., "Stochastic models of fatigue crack growth", Engineering Fracture Mechanics, Vol. 32, n.1, 1989.
[5] Ihara, C., Misawa, T., "A stochastic model for fatigue crack propagation with random propagation resistance", Engineering Fracture Mechanics, Vol. 31, n.1, 1988.
[6] Salivar, G.C., Yang, J.N., Schwartz, B.J., "A statistical model for the prediction of fatigue crack growth under a block type spectrum loading", Engineering Fracture Mechanics, Vol. 31, n.3, 1988.
[7] Alawi, H., "A probabilistic model for fatigue crack growth under random loading", Engineering Fracture Mechanics, Vol. 23, n.3, 1986.
[8] Ortiz, K., Kiremidjian, A.S., "Time series analysis of fatigue crack growth rate data", Engineering Fracture Mechanics, Vol. 24, n.4, 1986.
[9] Ortiz, K., Kiremidjian, A.S., "Stochastic modelling of fatigue crack growth", Engineering Fracture Mechanics, Vol. 29, n.3, 1988.
[10] Ortiz, K., "On stochastic modelling of fatigue crack growth", PhD. Thesis, Stanford University, 1985.
[11] Castiglioni, C.A., Rossi, S., "Un modello stocastico per la stima della vita a fatica di dettagli strutturali in acciaio", Technical Report 7/89, Structural Engineering Department, Politecnico di Milano, Italy.
[12] Newman, J.C.Jr., Raju, I.S., "Prediction of fatigue crack growth patterns and lives in three dimensional cracked bodies", VI International Conference on Fracture, New Delhi, India, 1984.
[13] Willenborg, J., Engle, R.M., Wood, H.A., "A crack growth retardation model using an effective stress concept", AFFDL-TM-71-1-FBR, 1971.
[14] Newman, J.C.Jr., "A crack opening stress equation for fatigue crack growth", International Journal of Fracture, Vol. 24, n.3, 1984.
[15] Shilling, C.G., Klippstein, K.H., Barsom, J.M., Blake, G.T., "Fatigue of welded steel bridge members under variable amplitude loading", NCHRP Rept. n.188, 1978.
[16] Fisher, J.W., Hirt, M.A., McNamee, B.M., "Effect of weldments on the fatigue strength of steel beams", NCHRP Rept. n.102, 1970.
[17] Fisher, J.W., Yen, B.T., Klingerman, D.J., McNamee, B.M., "Fatigue strength of steel beams with welded stiffeners and attachments", NCHRP Rept. n.147, 1974.

[18] Fisher, J.W., Mertz, D.R., Zhong, A., "Steel bridge members under variable amplitude long life loading", NCHRP Rept. n.267, 1983.
[19] Fisher, J.W., "Fatigue and Fracture in Steel Bridges. Case Studies", John Wiley & Sons, New York, 1984.
[20] Keating, P.B., "High Cycle Fatigue Behavior of Welded Details Under Variable Amplitude Loading", PhD. Thesis, Lehigh University, 1987.
[21] AASHTO, "Standard Specifications for Highway Bridges", 1983.

Fatigue Crack Growth in Complex Tubular Joints

Propagation de fissures de fatigue dans des joints tubulaires complexes

Ermüdungsrisswachstum in komplexen Verbindungen von Rohrprofilen

Björn SKALLERUD
Research Eng.
SINTEF
Trondheim, Norway

Björn Skallerud, born 1959, received his master of engineering and doctoral degrees at the Norwegian Inst. of Technology. He has been working with problems related to cyclic plasticity and low and high cycle fatigue.

Oddvar I. EIDE
Senior Research Eng.
SINTEF
Trondheim, Norway

Oddvar I. Eide, born 1951, obtained his master of engineering degree at the Norwegian Inst. of Technology. He is performing research in fatigue and fracture of welded structures, in this area he also holds a doctoral degree.

Stig BERGE
Professor
Norw. Inst. of Techn.
Trondheim, Norway

Stig Berge, born 1942, received his master of engineering and doctoral degrees at the Norwegian Inst. of Technology. He is a professor at the Division of Marine Structures, where he teaches and carries out research in the area of fatigue and fracture of offshore structures.

SUMMARY
Fatigue crack growth data from tests of stiffened tubular joints are reported. Fracture mechanics models for part through and through crack growth analysis are presented, and these results are compared with experimental data.

RÉSUMÉ
Des résultats de propagation de fissures de fatigue provenant d'essais sur des joints de tubes raidis sont présentés. D'autre part, des modèles de la mécanique de la rupture pour la propagation de fissures à travers l'épaisseur de la pièce sont également présentés, et ces résultats sont comparés avec les valeurs expérimentales.

ZUSAMMENFASSUNG
Berichtet wird über Resultate aus Versuchen an ausgesteiften Verbindungen röhrenförmiger Profile. Bruchmechanische Modelle zur Analyse des Wachstums durchgehender und nichtdurchgehender Risse werden vorgestellt. Die Resultate dieser Analysen werden mit denjenigen der Versuche verglichen.

1. INTRODUCTION

One common type of stiffened tubular joints is the connection between a brace and a comparatively much larger chord, like brace column or brace/pontoon connections of semi-submersible rigs. These connections are based on load transfer through internal stiffening of the brace into an array of stiffened deck and bulkhead details in the column or pontoon. Due to the complicated geometry, it is difficult to calculate the stress flow through structural details of this type, and in particular to assess realistic stress concentration factors for the various weld details. Service experience has proved these joints to be fatigue vulnerable. Similar type of joints may also be used in deep water jacket structures, in which fatigue damage may become very critical due to the general problems of detection and repair at great waterdepths.

With the development of fracture mechanics, methods have become available for calculation of the significance of defects, residual life of cracked structures etc., which are required in order to establish rational criteria for inspection, maintenance, and repair procedures. Furthermore, fracture mechanics has proved to be a useful tool in the analysis of fatigue test data, enabling conclusions to be drawn on the basis of physical models rather than statistical analysis of S-N data.

Within a recent research program, fatigue behaviour of simplified but realistic models of brace/column connections has been studied. The aims of the investigation were to provide S-N data for this type of structural details. Furthermore, to investigate crack growth behaviour in this type of joints in order to establish and verify fracture mechanics models for assessment of residual life and consequences of cracking if detected. S-N data obtained with the brace/column models are reported elsewhere [1]. The emphasis in the present paper is on fracture mechanics modelling and analysis of fatigue crack growth.

2. EXPERIMENTAL INVESTIGATION

2.1 Specimen and loading

The specimens were simplified but realistic models of brace/column connections with internal stiffening. The main dimensions are shown in Fig. 1. The models were constructed such that two connections could be tested simultaneously. The brace dimensions were 711 mm outer diameter and 12.5 mm plate thickness. Due to the comparatively much larger column dimensions for this type of joints, the column was modelled by plane plates. Two models were produced. In order to investigate the effects of external stiffeners on fatigue behaviour of the present type of joints, one of the models was tested with external gussets at the brace/column intersection, cf. Fig. 1.

The brace material was spiral welded tube made from structural steel to NVE-36. The spiral welds were ground flush prior to specimen fabrication. The plate material was a structural steel to St52-3. The yield strengths were in the range 360-400 MPa.

The models were produced by manual metal arc welding, using basic electrodes. All welds were made as fillet welds. Nominal weld throat was 40 per cent of the plate thickness. The weld details at the end of the internal stiffening in the brace (Position 3 in Fig. 1) were post weld treated by grinding. All other welds were in the as-welded condition.

Testing was performed in constant amplitude axial loading using a 2 MN dynamic actuator. The test rig arrangement is shown in Fig. 2. Nominal stress in the braces were measured by strain gauges attached 300 mm from the brace end and spaced 90 degrees around the brace circumference. No global bending of the braces was observed. Measured stresses were within the range 1.0-1.1 of the computed nominal stress in the brace, the stress enhancement being interpreted as effects of local cross sectional imperfections.

During testing, fatigue cracks developed at the brace/column welds (Pos. 1) and at the ends of external gusset (Pos. 2) and internal stiffener (Pos. 3). The welds were periodically checked for crack initiation by spraying white spirit on the surface during testing. Fatigue cracks were then clearly visible by the pumping of liquid in and out of the crack. When cracks were detected, through thickness crack growth was monitored by a high-frequency, alternating current potential drop system. Surface crack lengths were obtained by visual measurements, using white spirit. Fracture surface examinations showed that the use of white spirit also deposited beachmarks at the fracture surfaces. At the end of testing, crack growth data was checked against the surface markings, providing a direct calibration.

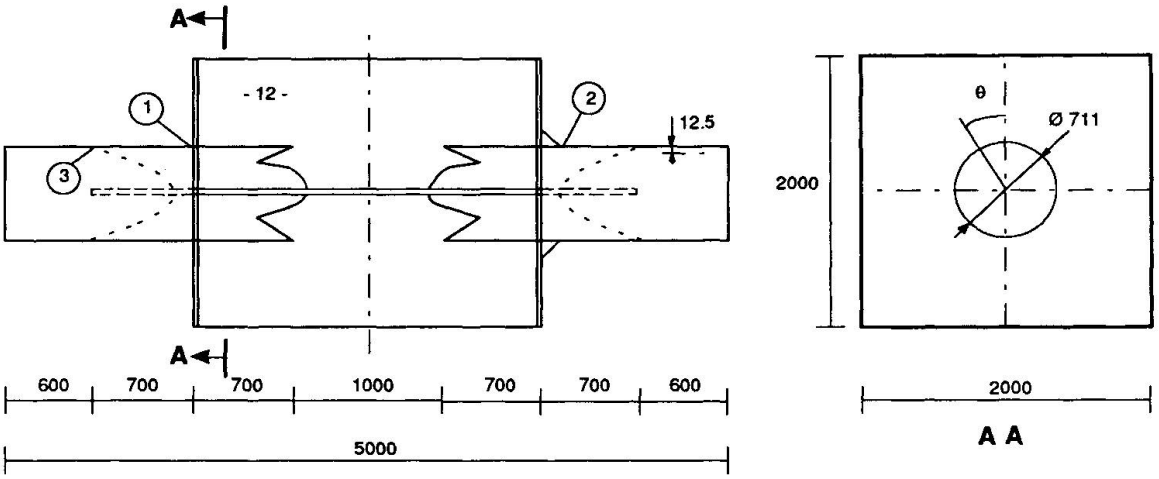

Figure 1 Specimen

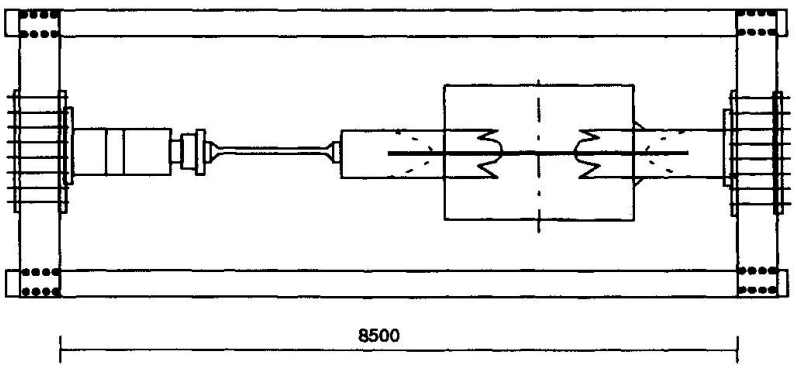

Figure 2 Test rig

2.2 Crack initiation and growth

Fracture surface examinations showed that multiple cracks developed along the welds during the first stage of crack growth, i.e. fatigue cracks were initiated at various sites along the weld toe before joining into one single crack (crack coalescence). Typically crack coalescence occurred at a crack depth of 3 mm.

Cracks at the brace column weld (Pos. 1) had a two stage development as shown in Fig. 3. In stage 1, a semi-elliptical surface crack generated from multiple crack initiation was growing in the through thickness direction of the brace wall. Typically 5-7 crack initiation sites were observed in the hot spot region. The surface crack length at the stage of through thickness crack penetration was typically 5-6 times the wall thickness. The through thickness crack was detected by leakage of white spirit.

Once the crack front had penetrated the wall thickness, the crack grew as a three-fronted crack in the brace and in the internal stiffening. Due to significant local bending at the brace/column weld, the growth rate in the brace wall at the external surface significantly exceeded the growth at the internal surface. Crack growth into the internal stiffening was significantly delayed by the root gap of the fillet weld, due to the re-initiation period.

At the end of testing, one of the brace/column weld cracks had reached a surface length of 285 mm. The crack length into the internal stiffening was only 40 mm. The number of cycles applied at this stage exceeded life to through thickness crack penetration by a factor 2.2 approximately. Thus, significant residual life remained after through thickness crack growth at the brace/column weld.

Cracks causing failure at the gusset welds (Pos. 2) went through the same stages of crack growth as observed with the brace/column welds, cf. Fig. 4. In stage 1, however, the occurrence of multiple crack initiation was limited by the length of the gusset end weld. Typically 2-3 cracks developed. Moreover, after crack coalescence, subsequent crack growth in the width direction was delayed by the absence of the notch effect of the weld. For these reasons, the surface crack length at the end of stage 1 was somewhat smaller than observed with the brace/-column welds, being typically 3-4 times the wall thickness.

In stage 2, the transition into a through-thickness crack in the brace occurred within a small number of cycles. For reasons outlined above, crack growth into the internal stiffening was significantly delayed.

At the end of testing, one of the gusset weld cracks had reached a surface crack length of 320 mm. The number of cycles applied at this stage exceeded life to through thickness crack penetration by a factor 1.6 approximately. With reference to similar data obtained with the brace/column welds (Pos. 1) this is a significant reduction in residual life. In average, the growth of through thickness cracks at Pos. 2 was twice as large as the growth observed at Pos. 1. The total effect of the gusset was to increase the life to through thickness penetration, and to reduce residual fatigue life in stage 2 almost correspondingly.

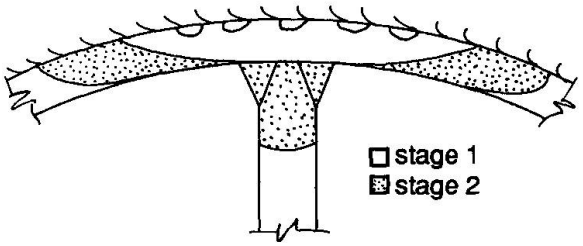

Figure 3 Stages of crack growth at brace/column welds

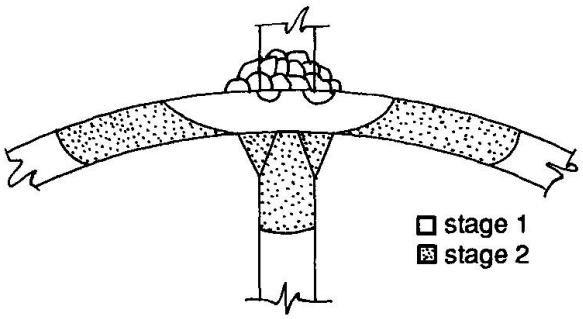

Figure 4 Stages of crack growth at external stiffener details

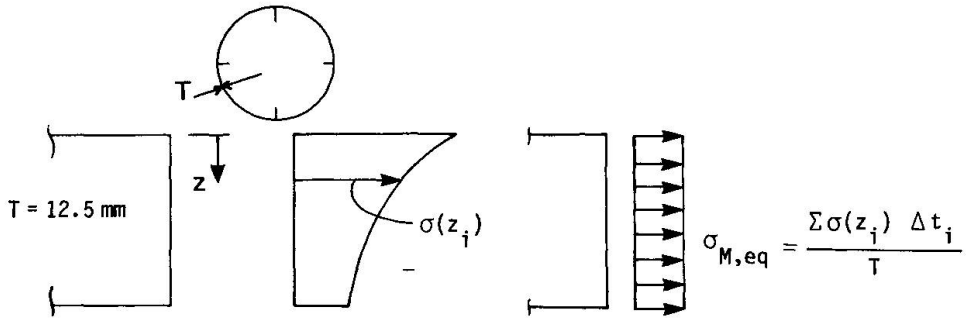

Figure 5

3. FRACTURE MECHANICS MODELS

Fatigue life of welded joints has been shown to consist mainly of crack growth from pre-existing crack-like defects in the weld toe region [2,3]. In the present study only the crack growth stage was considered, i.e. a possible crack initiation stage was neglected.

An in-house computer program, CALPRED [7], was used for the fracture mechanics calculations. Crack growth was assumed to follow the Paris-Erdogan type crack growth law

$$\frac{da}{dN} = C(\Delta K)^m \qquad (1)$$

Crack growth of surface cracks was calculated in two directions - through thickness at the deepest point and in the surface direction. A step-wise integration of crack growth with updating of the aspect ratio a/2c was applied. Numerical tests showed that the procedure had satisfactory accuracy.

The parameters C and m of Eqn. (1) were assumed to be equal at all positions along the crack front. Tests with simple specimens with semi-elliptical cracks, however, have shown that the crack growth rate tends to be lower at the free surface, most probably due to the larger plastic zone at this position [5]. This was taken into account by a reduction of the stress intensity factor K at the free surface by a factor $F_c = 0.91$, accounting for the plane stress condition at the surface.

The values of C and m were assumed as $C = 4.9 \cdot 10^{-12}$ [MPa $m^{1/2}$, m], $m = 3.1$. These values fall within the scatterband of crack growth data for various structural steels [6] and are recommended for fracture mechanics analysis of crack growth in welded steel structures [4].

In the analyses of the semi-elliptical cracks, i.e. stage I in Figs 3 and 4, the stress intensity factor determined by Newman and Raju [8] was applied.

$$K = (\sigma_M + H\sigma_B)\sqrt{(\frac{\pi a}{Q})} \cdot F^{N-R} \qquad (2)$$

The membrane and bendings stresses were obtained from shell analysis of the specimens [9]. Eqn. (2) does not account for the local stress concentration and corresponding nonlinear through thickness stress distribution at the weld toe. This was included in the following manner. In the deepest point of the crack, Eqn. (2) was used to account for the global stress concentration of the joint. The additional notch stress distribution due to the local stress concentration from the weld geometry was accounted for by the influence function method (point load model) proposed by Albrecht and Yamada [10] and developed further by Engesvik [11]. This leads to the resulting K in the deepest point.

$$K_{tot} = (\sigma_M + H\sigma_b)\sqrt{(\frac{\pi a}{Q})} \cdot F^{N-R} + \alpha_M \sigma_M \sqrt{(\pi a)} \cdot F^{A-Y} + \alpha_B \sigma_B \sqrt{(\pi a)} \cdot F^{A-Y} \qquad (3)$$

$$\alpha_M = SCF_{M,weld}^{-1}$$

$F^{A-Y} = F_S \cdot F_T \cdot F_W \cdot F_E \cdot F_G$, corrections for geometry of crack, specimen, stress distribution

In the surface width direction, the Newman-Raju solution was calculated using the stresses at the crack tip location, including the global stress variation from shell analysis, and the local stress concentration of the weld. The local stress distribution in the weld toe region was determined by plane FEM analyses with very small elements distributed through the thickness [9]. The parameters describing the weld geometry, i.e. throat angle θ and toe radius ρ, were obtained by measurements on the specimens.

For the analysis of through cracks, i.e. stage 2 in Figs 3 and 4, the solution for K for through cracks with a straight crack front was employed [12]. The loading was, however, separated in a nominal membrane stress which was constant around the circumference and a varying membrane stress distribution around the circumference due to reduction in stresses when the crack grew away from the stress concentration of the stiffener.

$$K_{tot} = \sigma_M \sqrt{(\pi a)} + \alpha_{eq} \sigma_M \sqrt{(\pi a)} \cdot F_{G,through} \qquad (4)$$

In the model the brace was assumed to be a plate of large width, hence the finite width correction F_W was negligible. The K-solution given in Eqn. (4) is limited to membrane stress. At the brace/column intersection, there were also shell bending and weld notch stresses, cf. Fig. 5. The distribution of these stresses was calculated around the circumference of the brace. An equivalent membrane stress, which at each location around the circumference would give the same cross sectional force as the total stress distribution, was calculated and applied in Eqn. (4), see Fig. 5.

4. FRACTURE MECHANICS ANALYSIS AND DISCUSSION

4.1 Analysis of growth of semi-elliptical cracks

One of the major problems in fracture mechanics analysis of fatigue cracks initiating at weld toes, is the assessment of the size and shape of initial cracks. It has been demonstrated that crack-like defects in the weld toe region is an inherent feature of welds produced by conventional welding processes. These defects are non-metallic slag intrusions along the fusion line, formed when the metal is melted or pasty during welding. The size and shape of the defects have been found to be quite random, with typical depths in the range 0.05-0.4 mm [2,3].

In Fig. 6 are shown experimental crack shape data for brace/column weld cracks (Pos. 1) with fracture mechanics predictions assuming an initial crack $a_0/2c_0$ = 0.4/0.8. Similar data obtained for the gusset cracks (Pos. 2) are shown in Fig. 7.

In the analysis, growth of a single crack was modelled, i.e. the multiple crack initiation and crack coalesence effects were not taken into account. These effects were particularly pronounced at the brace/column weld (Fig. 6). For long cracks, the computational model and the test data appear to be converging towards an aspect ratio a/2c in the range 0.2-0.3. In the initial stages of crack growth, however, there is a significant discrepancy.

The data from Pos. 2 (Fig. 7) were less affected by multiple initiation, and there is an overall agreement between analysis and experiments. However, the scatter in experimental data makes conclusions uncertain.

In Figs 8 og 9 are shown crack growth data and analysis for through thickness crack growth at the two positions of the model. With assumptions of an initial crack size within what has been reported for manual welds [2, 3], there is an overall agreement between tests and analysis. It is noted that at Pos. 1, the predictions tend to underestimate crack growth, i.e. good fit is obtained if a relatively large initial defect size to assumed. The reason for this is most probably the effects of crack coalescence, Fig. 6.

In similar analyses, using a forcing function for a/2c in order to simulate crack coalescence, very good correlation between tests and analysis has been reported [11, 13]. However, in order to apply a forcing function, the experimental data for a/2c need to be known a priory, making the method less of a predictive nature. Also shown in Fig. 8 is the effect of omitting the variation in stress around the circumference of the weld (dotted line), i.e. performing the analysis on the basis of the stress at Pos. 1.

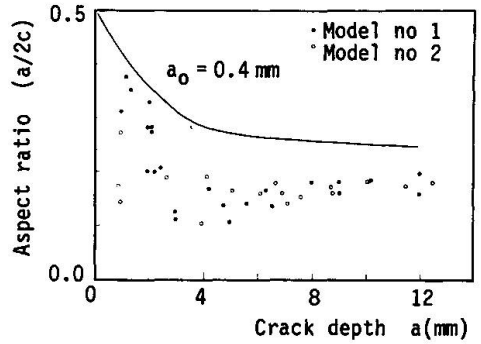

Figure 6 Crack shape data for part-through cracks at brace/column weld (Position ①, cf. Fig.1)

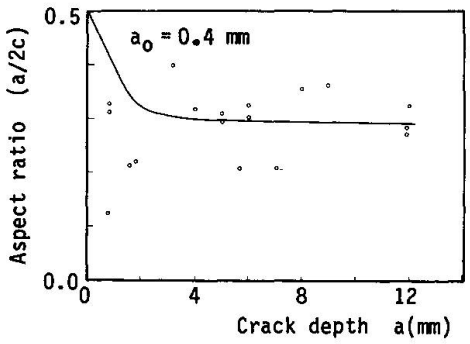

Figure 7 Crack shape data for part-through cracks at external stiffener welds (Position ②, cf. Fig.1)

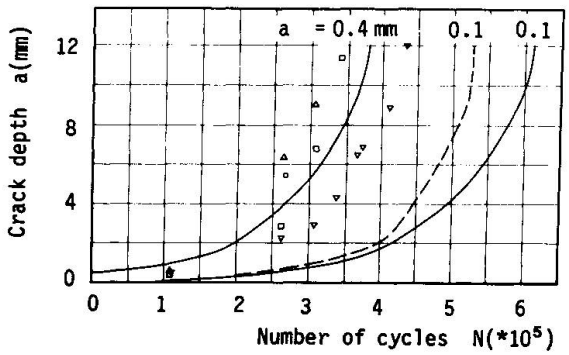

Figure 8 Crack growth data for part-through cracks, position ①, model no. 2

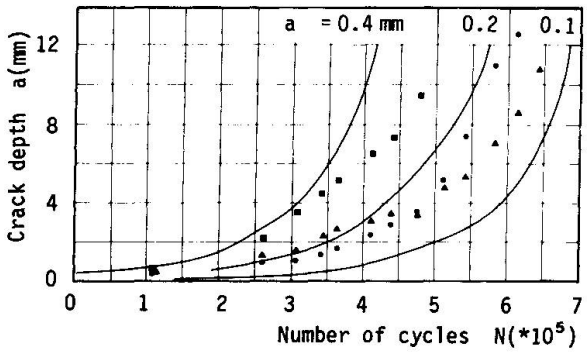

Figure 9 Crack growth data for part-through cracks, position ②, cf. Fig.1

4.2 Analysis of through thickness cracks

In Fig. 10 the development of through cracks at the brace/column weld is shown. The transition from a semi-elliptical crack to a through crack was modelled by simply taking a straight crack front with a width equal to the surface width of the semi-elliptical crack at the stage of through thickness penetration. As seen from Fig. 3 the crack front is far from being straight due to the significant bending and notch stresses.

Two values for the initial through thickness crack size were employed. The top curve in Fig. 10 was obtained with the measured mean value of the width of the three cracks. The lower curve was obtained with the width of the computed crack, i.e. a computational model covering both stages of crack growth. This value was smaller than the measured ones due to an overestimated a/2c - ratio in the calculation of semi-elliptical crack growth (Fig. 6). The figure shows that for cracks larger than ~ 150 mm, the computed crack growth rate is too high compared to the test results. This may be explained by the stress redistribution from the brace wall and into the stiffener. Since the computed results are based on the stresses in the original uncracked geometry, the redistribution is not accounted for.

In Fig. 11 the crack growth results of through thickness cracks at end of the gusset (Pos. 2) are shown. In this case the initial crack width obtained from the width of the semi-elliptical crack at through thickness corresponded closely with the test results. The gusset weld and internal stiffener had only a local influence on the crack growth at this position. For the through thickness crack stage, the membrane stress in the chord wall was dominating, and the uncertainty in modelling Eqn. 4 was much less than in the case of the brace/column weld. Still, there is a significant difference between the computed and the measured crack developments, underlining the assumption that load shedding effects are important.

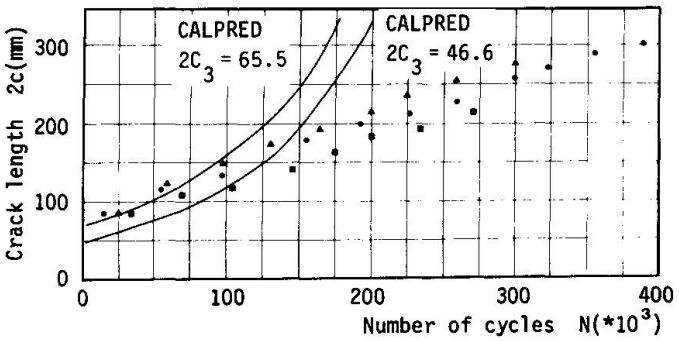

Figure 10 Crack growth data for through-thickness cracks, position ① , cf. Fig.1

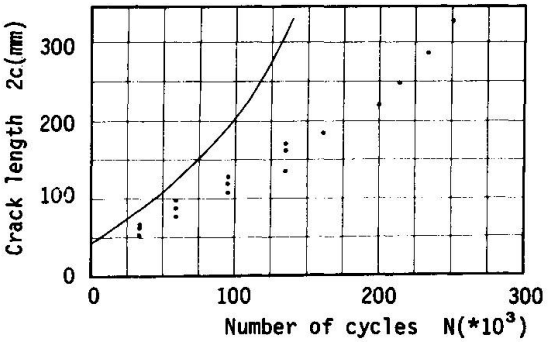

Figure 11 Crack growth data for through thickness cracks, position ② , cf. Fig.1

5. CONCLUSIONS

Fatigue crack growth in simplified but realistic models of brace/column connections typical of semi-submersible rigs was studied. A fracture mechanics model was established in order to predict the observed crack growth behaviour. The following observations were made,

- Significant multiple crack initiation occurred at hot spot regions of the brace/column welds. Crack coalescence occurred at a typical crack depth of 3 mm, introducing a significant change in the crack shape development.
- For surface cracks, a two-parameter fracture mechanics model calculating crack shape development was established. Without taking crack coalescence into account, the model gave results in reasonable agreement with test data.
- At external gusset welds, multiple crack initiation was less pronounced. In this case, good agreement between predicted and experimental data was obtained for through thickness crack growth.

- After through thickness penetration, a significant residual fatigue life remained before catastrophic crack growth took place. For the brace/column weld, the total life was as much as 2.2 times the through thickness life. For the external gusset, the same factor was 1.6. Total life for both details was approximately the same.
- The predicted growth of through thickness cracks tended to underestimate residual life, probably due to load shedding effects which were not accounted for.

6. REFERENCES

1. EIDE, O.I. and BERGE, S.: Fatigue Capacity and Crack Growth in Stiffened Tubular Joints. SINTEF Report STF71 A89011, 1989. Also OMAE 1990.

2. SIGNES, E.G. et al.: Factors Affecting Fatigue Strength of Welded High Strength Steels. British Welding Journal, March 1967.

3. WATKINSON, F. et al.: The Fatigue Strength of Welded Joints in High Strength Steels and Methods for its Improvement. Proceeding Conference on Fatigue of Welded Structures, Brighton 1970.

4. DnV Classification Note 30.2: Fatigue Strength Analysis for Mobile Offshore Units, 1984.

5. RAJU, I.S. and NEWMAN, J.C.: An Empirical Stress Intensity Factor Equation for the Surface Crack. Eng. Fract. Mech., Vol. 15, pp. 185-192, 1981.

6. ECSC Conference on Steel in Marine Structures, Institut de Recherches de la Siderurgie Francaise, Paris, 1981.

7. SKALLERUD, B.: CALPRED, Computer Aided Life Predictions. SINTEF Report STF71 A89055, 1989.

8. NEWMAN, J.C. and RAJU, I.S.: Stress Intensity Factor Equations for Cracks in Three-Dimensional Finite Bodies Subjected to Tension and Bending Loads. Chpt. 9 in Computational Methods in the Mechanics of Fracture, Ed. S.N. Atluri, Elsevier Science Publ. B.V., 1986.

9. BRODTKORB, B.B.: Stress Analysis of a Tubular Joint with Internal Stiffening. SINTEF Report STF71 A89006, 1989.

10. ALBRECHT, P., YAMADA, K.: Rapid Calculation of Stress Intensity Factors. Jour. Struct. Div., ASCE, Vol. 103, pp. 377-389, 1977.

11 ENGESVIK, K.: Analysis of Uncertainties in the Fatigue Capacity of Welded Joints. Dr.ing. Thesis, The Norwegian Institute of Technology, Division of Marine Structures, 1982.

12. TADA, H., PARIS, P.C., IRWIN, G.R.: The Stress Analysis of Cracks, Handbook. Del Research Corp., 1985.

13. EIDE, O.I. and BERGE, S.: Fracture Mechanics Analysis of Welded Girders in Fatigue. Int. Conf. Fatigue of Welded Constructions, Brighton, 1987.

Remaining Fatigue Life of a Spherical Joint

Durée de vie restante d'un joint sphérique

Restlebensdauer sphärischer Knoten

Zdenek KNESL
Dr.
Inst. of Physical Metallurgy
Brno, Czechoslovakia

Zdenek Knesl, born 1940, received his degree in theoretical physics at the University of J.E. Purkyne in Brno. For ten years, he studied dislocation theory, and is currently applying numerical methods to fracture mechanics and fatigue-crack propagation.

Pavel MAREK
Assoc. Prof.
Sportovni stavby
Prague, Czechoslovakia

Pavel Marek, born 1932, received his civil engineering degree and PhD at the Czech Technical University in Prague. For 25 years, he did research and taught in structural steel at Czech and foreign Universities. At present, he is visiting professor at San Jose State University California.

Pavel POLCAR
Dr.
Inst. of Physical Metallurgy
Brno, Czechoslovakia

Pavel Polcar, born 1950, received his degree in mathematics at the University of J.E. Purkyne in Brno. For seven years he was involved in mathematical modelling of processes in rotary cement kilns. For the last eight years, he has taken part in various programming projects in continuum mechanics.

Milos VLK
Assoc. Prof.
Technical University
Brno, Czechoslovakia

Milos Vlk, born 1937, received his mechanical engineering degree and PhD at the Technical University in Brno. For 23 years, he has been engaged in problems of fatigue and brittle fracture and their applications to industrial practice. At present, he is a university teacher.

SUMMARY
The investigation of the remaining fatigue life of a spherical joint is based on the evaluation of a conical fatigue crack growing from the sphere to tube weld. An attempt is made to optimize the geometrical parameters of the joint in order to improve remaining fatigue life.

RÉSUMÉ
Le problème de la durée de vie restante d'un joint sphérique est basé sur l'évaluation d'une fissure de fatigue cônique se propageant depuis ce joint dans la soudure du tube. Une tentative d'optimisation des paramètres géométriques du joint a été faite dans le but d'en améliorer la durée de vie restante.

ZUSAMMENFASSUNG
Anhand der Beurteilung eines konischen Ermüdungsrisses, der von einer Kugel-Rohr-Schweissverbindung ausgeht, wird die Restlebensdauer eines sphärischen Knotens untersucht. Es wird versucht, die geometrische Form zu optimieren und dadurch die Ermüdungsfestigkeit solcher Verbindungen zu erhöhen.

1. INTRODUCTION

The Limit States Method, introduced in Czechoslovak Specifications for Structural Steel Design in 1969, was applied in case of dimensioning and reliability assessment of a 340 m high guyed latticed tubular steel TV mast located near Plzeň. Special attention was paid to the investigation of the actual behaviour of welded joints (especially of the details like tubes welded to spherical nodes) exposed to fatigue. The information on response history, results of experimental investigation and on the final set up of the TV mast are discussed in [1].

The experimental study on fatigue strength of spherical joint was followed by a pilot study on crack propagation. The definition of the applied model based on the linear fracture mechanics and FEM is summarized in [2].

The steps following the pilot studies on the actual fatigue strength of spheric joints, mentioned above, were focused on the residual fatigue life and optimization of the geometrical proportion of spheric joint. The results are subject of this paper.

2. RESIDUAL FATIGUE LIFE OF THE CRACKED SPHERICAL JOINT

2.1 The formulation of the problem

In order fo formulate the problem, the experimental facts are summarized first:

During testing, the equivalent loading was represented by a force with amplitude of 350 kN and mean value of 250 kN. The crack was detected after 129 000 loading cycles and final fracture of the brittle type occured after approximately 150 000 loading cycles. On the basis of the fractographic study of the fractured surface of the failured spherical joint, the direction and the form of the fatigue crack were determined.

The sectional view of the spherical joint is given in Fig. 1. In accordance with the experimental set up, the boundary conditions for fatigue life calculations are modelled as follows (Fig.2): The external load is simulated by a constant stress σ acting on the tube in Z direction, the displacements in R direction equal to zero for the edge A and displacements in R direction equal to zero for the edge B of the sphere. The crack propagation direction is given by the angle α and crack grows along the surface of the cone created by rotation of the straight line p around the Z axes. The crack length a is measured along the straight line p (Fig.2).

On the basis of the above assumptions, the problem can be solved as an axialsymmetric one and for description of the stress state in the vicinity of the crack tip the plane strain approximation can be used.

In the following paragraphs the results are presented for the remaining fatigue life of the cracked spherical joint with the preexisting crack of the length a_0. The computation is based on

$$\frac{da}{dN} = C.(\Delta K_I)^m \qquad (1)$$

where ΔK_I is a range of the stress intensity factor.

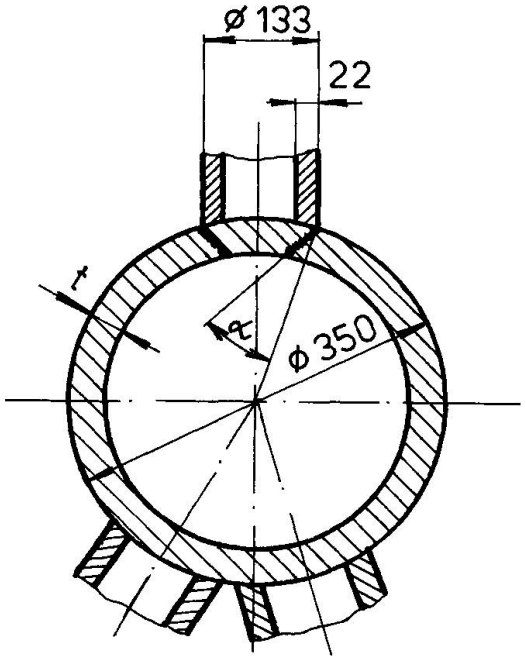

Fig.1 Sectional view of the spherical joint with conical crack

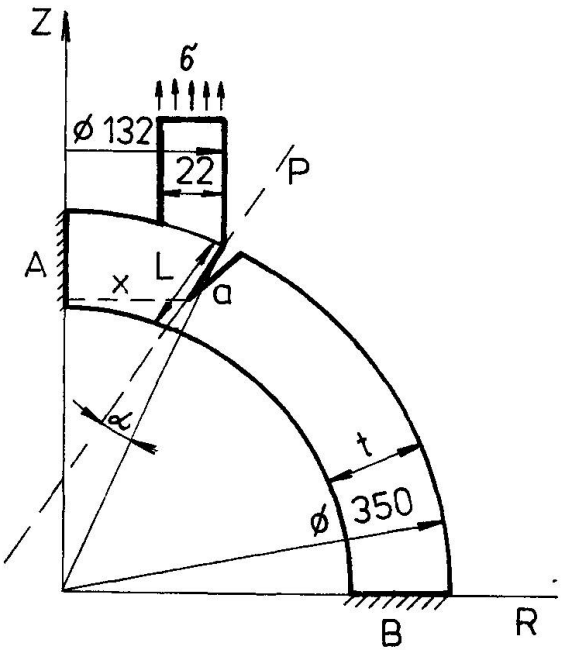

Fig.2 Numerical model used for FEM calculations

To this aim, the K_I calibration curve is calculated. Computations were performed by means of finite element method as implemented in PROKOP code [3].

2.2 K - calibration calculation

K - calibration curve, i.e. the dependence of the stress intensity factor K on the crack length a, was for our problem obtained by calculation of a strain energy release rate G(a)

$$G(a) = \delta U(a) / \delta a \ , \qquad (2)$$

where δa is a crack length increment causing a release of strain energy of amount δU. The stress intensity factors K_I (opening mode I) and K_{II} (shearing mode II) are directly related to the value of δU by equation (for plane strain)

$$G = (1 - \nu).(K_I^2 + K_{II}^2) \ / \ 2\mu \ , \qquad (3)$$

where ν, μ are Poisson´s ratio and shear modulus respectively.

K_I, K_{II} is calculated from (3) by means of procedure suggested in [3].

For δU calculation the method is used based on finite element design sensitivity analysis as implemented in PROKOP code [5].

The crack growth is modelled by means of a double noding technique [5]. The loading and boundary conditions correspond to those

formulated in 2.1.

The calculated K_I calibration curve can be approximated by the formula (for $0,15 \leq a/L \leq 0,8$)

$$K_I = \sigma . \sqrt{\pi a} . \left[8,178 \left(\frac{a}{L}\right)^{1/2} - 14,80\left(\frac{a}{L}\right)^{3/2} + 11,13.\left(\frac{a}{L}\right)^{5/2}\right] , \quad (4)$$

where σ is applied external stress acting on the tube (see Fig.2), $L = 34,61$ mm, $t = 30$ mm, $\alpha = 27^0$.

For the corresponding K_{II} value it holds (for $0,1 \leq a/L \leq 0,8$)

$$K_{II} \leq 0,06\ K_I \quad (5)$$

and so K_{II} values have practically no influence on the fatigue crack propagation rate and on the remaining fatigue life as well.

2.3 Results

The remaining fatigue life N_f was then calculated by integration of Paris´ law (1) between initial crack size a_0 and a chosen size a_f (for $m = 2,37$, $C = 5,70.10^{-11}$, da/dN [m/c], ΔK [MPa.$m^{1/2}$]) - see [2].

3. INFLUENCE OF THE SPHERICAL JOINT GEOMETRY

3.1 A fracture mechanics approach to the optimum design of structures [6]

In conventional strength calculations for loaded structures, usually the requirement is made, that a calculated stress should not exceed a critical value (e.g. design stress). If the main task of optimization is to improve conventional safety of the structure, the objective function is created from this point of view.

Evidently, in the case of structures weakened by cracks, the above conventional approach is no longer applicable and results of fracture mechanics should be taken into account.

The aim of the present chapter is to use the fracture mechanics as a tool for shape optimization of the spherical joint with respect to fatigue failure and remaining fatigue life.

3.2 Formulation of the optimization problem

The basic idea of fracture mechanics optimization is to decrease the probability of fracture by changes of geometry of structures under consideration.

The aim of our procedure is to increase the remaining fatigue life $N_f\ (a_0, a_f)$ of the spherical joint.

The value of N_f depends on geometry of structure Γ, material properties M, history of the response of the structure to external loading F and boundary conditions B. For the given boundary conditions B, history of response F and material properties M the crack trajectory and, remaining fatigue life N_f as well, depends on the geometry of the structure only

$$N_f = N_f . [A (\Gamma)] , \qquad (6)$$

where $A(\Gamma)$ describes the crack trajectory.

The optimization procedure can be formulated as

$$N_{max} = \max_{g_i} N_f [A (\Gamma)] , \qquad (7)$$

where set of parameters g_i (describing the geometry Γ) creates design variables

$$g_i \in \Gamma . \qquad (8)$$

Constraints for g_i follow from construction requirements and moreover have to prevent other types of construction collapse. In order to solve the problem, it is required with regard to each structure :

(1) To determine the initial crack propagation direction it may be supposed, that the location of the crack initiation is known.

(2) For the given initial crack to find numerically its trajectory $A(\Gamma)$ (i.e. crack propagation tracking).

(3) For the given crack trajectory $A(\Gamma)$ to calculate the values of the stress intensity factors (i.e. corresponding K - calibration curves) and remaining fatigue life N_f $[A(\Gamma)]$.

It is evident, that the formulated optimization problem is too complicated and cannot be completely solved. But, following the basic ideas of the procedure, some very useful conclusions for the design of structures can be obtained.

With respect to this fact, we have limited our considerations on the study of the influence of the sphere thickness t (see Fig.2) on the residual fatigue life N_f of the spherical joint. Supposing that the crack is initiated at the joining weld between tube and sphere, the dependence

$$N_f = N_f (t) \qquad (9)$$

can be calculated for particular orientation of crack - see next paragraph.

3.3 The orientation of the pre-existing crack

For the determination of the pre-existing crack orientation the energy criterion is used. Accordingly, the crack will propagate in direction $\alpha = \alpha_m$ identical to the direction of the minimum of the strain energy density w :

$$w (\alpha_m) = w_{min} (\alpha) . \qquad (10)$$

Strain energy density w is determined on the basis of finite element calculations and the eq. (10) is solved numerically. The computations were done for $a_o = 1,7$ mm.

As a result, the dependence $\alpha_m = \alpha_m(t)$ is given in Fig.3.

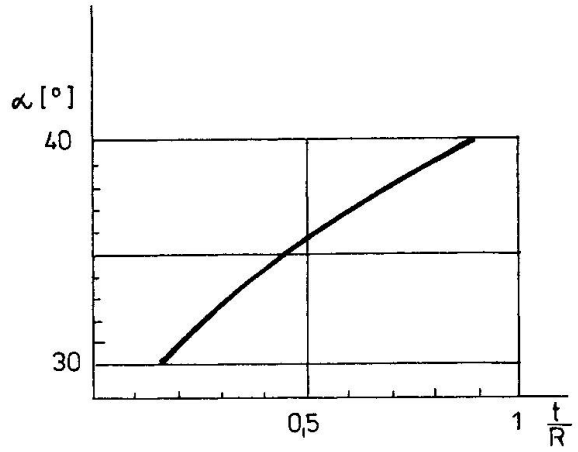

Fig.3 Dependence of crack propagation direction on sphere thickness t (R = radius of the sphere)

3.4 The determination of the fatigue crack trajectory

Generally, the fatigue crack initiated at the weld will propagate under mixed mode I and II conditions. In consequence of it, the crack trajectory have to be calculated first.

An essential ingredient of a crack propagation tracking is a criterion to predict the direction of crack propagation. Numerous past investigators have studied the problem, but there are still some disagreements among the various theoretical approaches (see e.g. [7]). In presented considerations, the strain energy density criterion as suggested by Sih - S criterion (e.g. [8]) is used. Following this criterion, the crack propagation direction depends on the ratio K_{II}/K_I and if $K_{II} \to 0$ the crack propagates directly along the straigt line.

For crack lengths in the interval $a_0 < a < 10$ mm, the ratio $K_{II}/K_I \leq 0{,}05$. So, as the first approximation let be supposed, that the crack trajectory is not influenced by mode II loading and crack propagates along the surface of the cone as in Chapter 2. Geometry of the cone is given by the value of $\alpha_m(t)$.

This approximation holds good for relatively short crack length ($a \leq 10$ mm). For crack length $a > 10$ mm and especially for ratio $t/R \to 1$ (full sphere) and for more exact calculations the real crack path should be taken into account.

In the following paragraph it is supposed for all calculated cases, that the crack trajectory creates a cone. The changes of the sphere thickness t influence the angle α_m only.

3.5 K - calibration curves for spherical joint with different sphere thickness

Based on the same procedure as in 2.2 the K_I calibration curves were calculated for various values of the sphere thickness t. Results hold in the crack length interval 1,7 mm to 25 mm.

3.6 Remaining fatigue life calculations

The remaining fatigue life N_f (a) is calculated by integration of Paris equation (1). As the ratio K_{II}/K_I changes slightly, K_I values can be taken as the parameter controlling the crack propagation rate. The value K_{II} has influence on the crack trajectory only [9].

3.7 Results

Using the same procedure and material characteristics as in the Chapter 2., the remaining fatigue life for various values of the sphere thickness (t = 30, 60, 90, 120, 150 mm) were calculated. To illustrate the influence of t on the remaining fatigue life of the spherical joint, the results for two limiting cases (t=30mm and t=150 mm) and initial crack length 2 mm and 15 mm are presented in the Fig. 4.

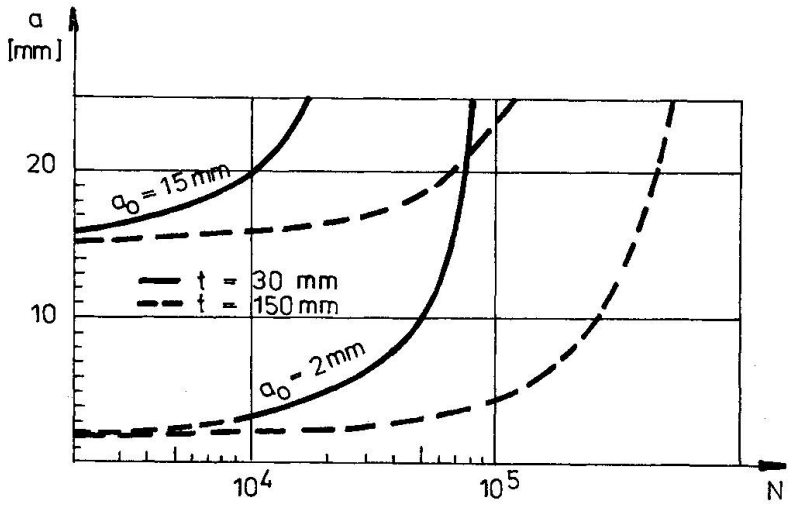

Fig.4 Remaining fatigue life of the spherical joint for two limiting thickesses t (a_o = initial crack length, N = number of cycles)

4. CONCLUSIONS

Linear elastic fracture mechanics and finite element method allow the evaluation of the remaining fatigue life of the spherical joint. With the aim to optimize the geometry of the joint, the influence of the sphere thickness on the fatigue life was studied. From this point of view, the full sphere of the joint gives the best results.

REFERENCES

1. MAREK P. - POVAŽAN J. - ŘEHOŘ P. - SCHRÁNIL J. - VLK M. - VOJTÍŠEK J., Investigation of Spherical Welded Joint of a Tubular Structure. In: Welding of Tubular Structures, Proceedings of 2nd Int.Conference IIW held in Boston, USA July 1984. Pergamon Press.

2. KNÉSL Z. - POLCAR P. - MAREK P. - VLK M., Analysis of Life of a Spherical Node by the Linear Fracture Mechanics Approach (in Czech). Zváranie 36, No 12, December 1987.

3. HOLUŠA L. et al., PROKOP-85. Research Report ÚFM ČSAV and OVC VUT (in Czech). Brno 1985.

4. KNÉSL Z., Determination of the Stress Intensity Factor for Mixed Mode by means of the Driving Force. Strojírenství 38, 1988, 163-166 (in Czech).

5. KNÉSL Z. - VRBKA J., The K Calculations by means of the Sensitivity Analysis. In: IV. Conference on Numerical Methods in Mechanics, Boboty 1989, p. 279-282 (in Czech).

6. KNÉSL Z. - VRBKA J., A fracture mechanics approach to the optimum design of structures. In: XI. Internationaler Kongress über Anwendungen der Mathematik in den Ingenieurwissenschaften, Weimar 1987, Berichte I, p.36-38.

7. WANG M.H., A modified S theory, Engng. Fract. Mech., 22,1985, 579.

8. SIH G.C., Strain-energy-density factor applied to mixed mode crack problems, Int. J. Fracture, 10, 1974, 305.

9. KNÉSL Z. - KUNZ L., A fatigue crack growth under mixed mode conditions. In: I. Conference on Mechanics, Praha 1987, (eds. J.Němec, R. Skrúcaný), vol. 4, p.127.

Fatigue Resistance of Orthotropic Steel Decks

Résistance à la fatigue des dalles orthotropes en acier

Dauerfestigkeit orthotroper Stahl-Fahrbahnplatten

André BIGNONNET
Engineer ENSM
IRSID
St. Germain-en-Laye, France

Bernard JACOB
Civil Engineer, IPC
LCPC
Paris, France

Jean CARRACILLI
Engineer
LCPC
Paris, France

Michel LAFRANCE
GTS TFK
Dunkerque, France

SUMMARY
The present study is a part of a large European research program dealing with the fatigue behaviour of stiffener to deck-plate welded connections. A numerical model has been developed to evaluate the durability of fatigue loaded structures. Theoretical analyses have employed fracture mechanics to describe the growth of fatigue cracks. A model has been fitted with experimental results from tests of large welded specimens which were representative of a true structure. Application of the model to existing bridges leads to prediction of fatigue damage which is in agreement with problems observed in service.

RÉSUMÉ
Cette étude réalisée dans le cadre d'un programme communautaire CECA traite du comportement en fatigue de la liaison soudée tôle de platelage-auget. Un modèle numérique de prédiction de la durabilité des structures a été développé. Il s'agit d'une analyse théorique basée sur l'approche par la mécanique de la rupture de propagation des fissures de fatigue. Le modèle a été ajusté à l'aide du travail expérimental effectué sur des éprouvettes soudées soumises à des situations de contrainte rencontrées sur les structures réelles. L'application du modèle aux cas de ponts existants a conduit à des prédictions d'endommagement par fatigue cohérentes avec des désordres observés en réalité.

ZUSAMMENFASSUNG
Diese im Rahmen eines EGKS-Programmes durchgeführte Untersuchung behandelt das Ermüdungsverhalten von geschweissten Verbindungen zwischen Belagsblech und Versteifungselement. Ein numerisches Modell für die Voraussage der Dauerfestigkeit der Strukturen wurde entwickelt. Es handelt sich um eine theoretisch-bruchmechanische Analyse der Rissausbreitung. Das Modell wurde anhand von Resultaten aus experimentellen Untersuchungen geeicht. Letztere erfolgten an geschweissten Proben, die Beanspruchungen unterworfen wurden, wie sie für wirkliche Strukturen repräsentativ sind. Die Anwendung des Modells auf existierende Brücken führte zu Vorhersagen der Beschädigung, die den tatsächlich beim Betrieb beobachteten Schäden entsprechen.

1. INTRODUCTION

The fatigue strength is an important safety criterion for the steel structures such as the orthotropic decks. For that reason the European Coal and Steel Community (ECSC) has supported a wide research program for 12 years. The last phase (1986-89) was devoted to the study of the behaviour of the most sensitive details, such as the connection between the longitudinal stiffener and the plate presented in this paper. An experimental work was conducted by the IRSID in order to establish the S-N curves adapted to the actual performant welding conditions and to provide measured lifetimes under controlled loading cases. The LCPC developed a physical model of crack propagation calculation, based on the fracture mechanics theory and implemented it to the tested specimens and to some existing bridges on which measurements were done. By this way the model calibration and validation was possible and then the results concerning the bridges were compared with those by the classical S-N approach with a Miner's summation.

2. EXPERIMENTAL WORK

2.1 Type of Connection

The work undertaken dealt with the stiffener to deck plate connection. The experimental program included two aspects :

- the optimization of the welding procedure,
- the influence of an accosting gap, 0 or 2 mm, between the stiffener and the deck plate during the welding.

The specimens whose geometry is given on figure 1 are sliced from 5.50 m long assemblies. The material used is a structural steel E 36-4 (standard NFA 501-87), TMCP steel 6 mm thick for the stiffener and normalized steel 12 mm thick for the deck plate.

2.2 Welding Operation

The stiffeners have been welded in one run in horizontal position, 2F, using a submerged arc welding automatic machine, without pre-heating nor post-heating. Filler metal and flux are of the type SAF-AS35/AS462. The influence of the edge preparation has been checked, chamfered edge at 60° or 45° and without chamfer.

The welding energy has been ajusted to minimize the lack of penetration.

From these sets of welding tests, presented in more details in reference [1] it has been shown that without edge preparation, no chamfer, a satisfactory penetration (lack of penetration $\simeq$ 1 mm) is obtained for a welding energy of 20 kJ/cm, figure 2, and this even with an accosting gap of 2 mm.

2.3 Static Tests

Tests have been performed with 3 points bending as indicated in figure 1.

For a good knowledge of the strees distribution, static tests have been done on an instrumented specimen, figure 3a. It is noted that in the median axis of the specimen the loading is biaxial with $\sigma_2/\sigma_1 = 1/3$ (σ_1 is in the direction of the bending stresses).

The nominal stresses definition to be used in the fatigue S-N diagrams are derived from these tests :

- extrapolation of the stress in the deck plate to the weld-toe, figure 3b, definition generally used when the cracks propagate through the deck plate from the weld-toe,
- extrapolation of the stress in the stiffener to the weld root, figure 3c, definition generally used when cracks propagate through the weld from the root of the weld.

2.4 Fatigue Tests

Fatigue tests have been performed in alternate bending : R=-1 ($R = S_{min}/S_{max}$).

The results are expressed in terms of the nominal stress range in the deck plate as defined above, $R = S_{max} - S_{min}$, versus the number of cycles to failure.

Two different criteria have been used in the presentation :

N_1= crack detection by extensometry, a ≃ 0.3 mm (see reference [1]).

N_4= end of test (large displacement of the actuator).

The welding procedure used leads to a lack of penetration lower than 1 mm and a throat of about 6 mm. With these conditions for R = -1, the cracks initiate systematically in the deck plate at the weld toe.

The results given in figure 4 show that for the welding conditions used there is no difference in fatigue behaviours between a stiffener welded with a gap of accosting of 2 mm and a stiffener welded without gap. The whole results with R = -1 lead to a Wöhler curve, figure 4, such as ΔS (MPa) = 26477 $N^{-1/3}$, standard deviation = 24 MPa.

On figure 5, these results are compared with those from Liège University [2] and from CRIF [3], for comparable R ratio (between -0.57 and -1) in terms of nominal stress range in the stiffener at the weld root. The primarily difference with IRSID results is that experiments of Liège University [2] and CRIF [3] show a crack initiation at the weld root, and the failure occurs in the weld. As shown in table 1, the specimen used at CRIF [3] welded by manual arc welding involve an important lack of penetration.

It is clear from figure 5 that the fatigue strength significantly increases when using submerged arc welding, this technique allows larger penetration and larger throat of the weld. Nevertheless, it is shown that cracks initiate at the weld of the root for a lack of penetration larger than 2 mm. Conversely if the welding operation is properly optimized the lack of penetration can be limited at about 1 mm and for alternate or repeated tensile bending in the deck plate the crack initiate at the weld toe, and the fatigue strength is improved. This is interesting for the purpose of inspection and structure safety. If the lack of penetration remains of the order of 1 mm, the risk of fatigue cracking is reported at the weld toe which is more accessible to control.

References	Lack of penetration (mm)	Throat (mm)
this work	1 to 1.5	5.5 to 6.5
[2]	2 to 2.5	5 to 6
[3]	3 to 4.5	3.5 to 4.5

Table 1 : Geometric welds characteristics, presented here and references

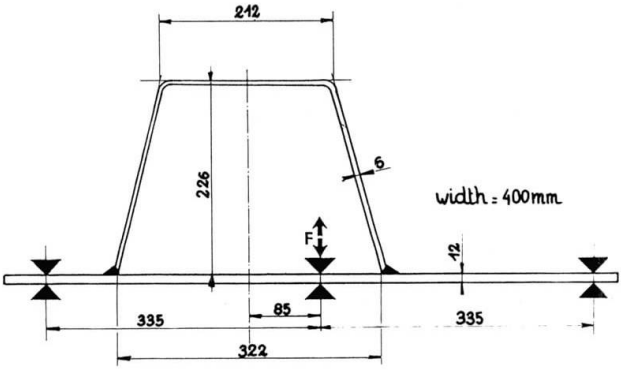

Fig.1 : Geometry of the specimen

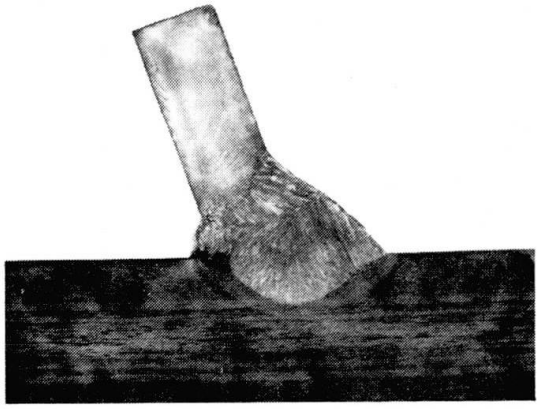

Fig.2 : Macrography of the weld

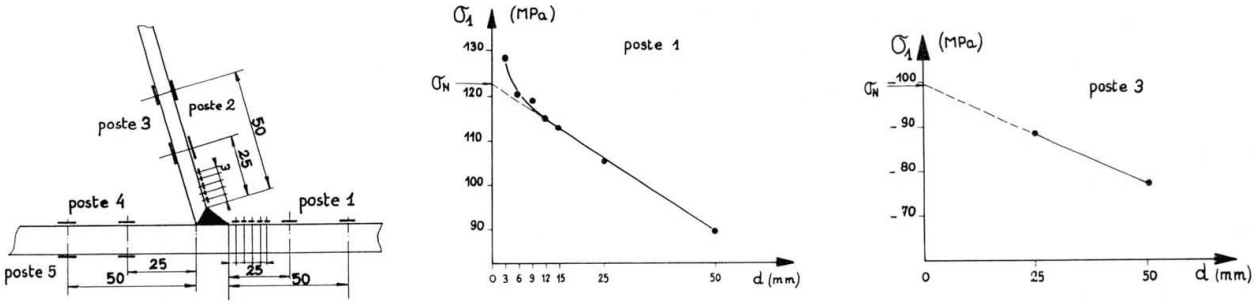

Fig.3 : Gauge instrumented specimen a), and nominal stress definition in the deck plate b) and in the stiffener c).

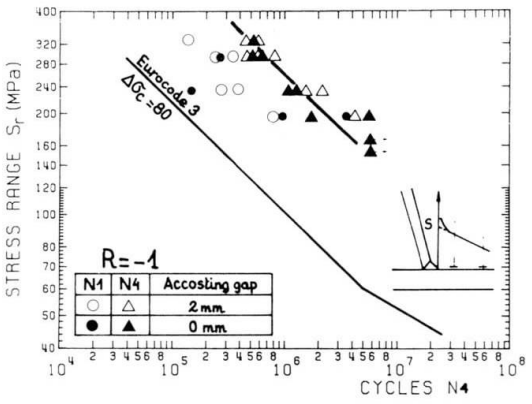

Fig.4 : Wöhler curve at R=-1 for two accosting gaps, on the basis of the stress range in the deck plate.

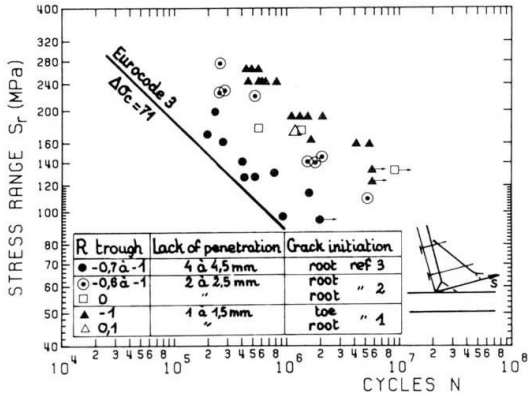

Fig.5 : Comparison of fatigue results with litterature data, on the basis of of the stress range in the stiffener.

3. FRACTURE MECHANICS ANALYSIS

3.1 Model of Damage

The classical fatigue S-N calculation with a Miner's summation, generally used by the engineers, remains the basis of most of the codes. But the strong assumptions about the linear damage accumulation, which does not take into account the stress variation time history, make this approach very poor and far from the real crack propagation phenomena.

The fracture mechanics applies the principles of the continuum mechanics to describe the crack propagation. The stress distribution is analysed in detail around the crack end. Here, only the mode I - crack opening - is considered, and the propagation time is computed. The time of crack initiation is not taken into account because it is assumed that the local surface defects already provide small cracks. This initial state is summarized by a conventionnal crack length a_0.

3.2 Propagation Law

The crack propagation is governed by the stress intensity factor K, which characterizes the local geometry of the structure and the effect of a stress variation on the crack growth rate. Between the many models proposed, we have chosen the Paris law with a threshold, one of the simplest but realistic models. The crack growth rate is given by :

$$\frac{da}{dN} = C(\Delta K - \Delta K_S)^m \qquad (1)$$

where da is the elementary increase of the crack length under dN stress variation cycles, C and m are two constant parameters which characterize the material ; ΔK_S is a threshold of non propagation. The increase of the stress intensity range under a stress variation $\Delta\sigma$ may be written :

$$\Delta K = K_M - K_m = \sqrt{\Pi a}\ \Delta\sigma\ f(a) \qquad (2)$$

where f(a) is a magnification factor representing the local geometry.

Finally, the lifetime is obtained by integration of (1) :

$$N = N_0 + \frac{1}{C}\int_{a_0}^{a_r} \Delta K^{-m}\, da \quad , \text{ where } a_r = e/2 \text{ is the failure criteria} \qquad (3)$$

e beeing the plate thickness.

3.3 Calculation of the Stress Intensity Factor

If the stress diagram $\sigma(x)$ in the non-cracked section is expressed as a polynom of x :

$$\sigma(x) = A_0 + A_1 x + A_2 x^2 + A_3 x^3 + A_4 x^4 \qquad (4)$$

then the stress intensity factor of equation (2) may be written as :

$$K = \sqrt{\Pi a}\ \left[A_0 F_0 + \frac{2a}{\Pi} A_1 F_1 + \frac{a^2}{2} A_2 F_2 + \frac{4a^3}{3\Pi} A_3 F_3 + \frac{3a^4}{8} A_4 F_4\right] \qquad (5)$$

where the F_i are the magnification factors, functions of a, the present crack length. They are calculated using a superposition principle and the successive

application of simple stress diagrams, and for a finite set of values of a. A finite element method is used in this determination. As an example, F_0 and F_1 are plotted as functions of a in the figure 6.

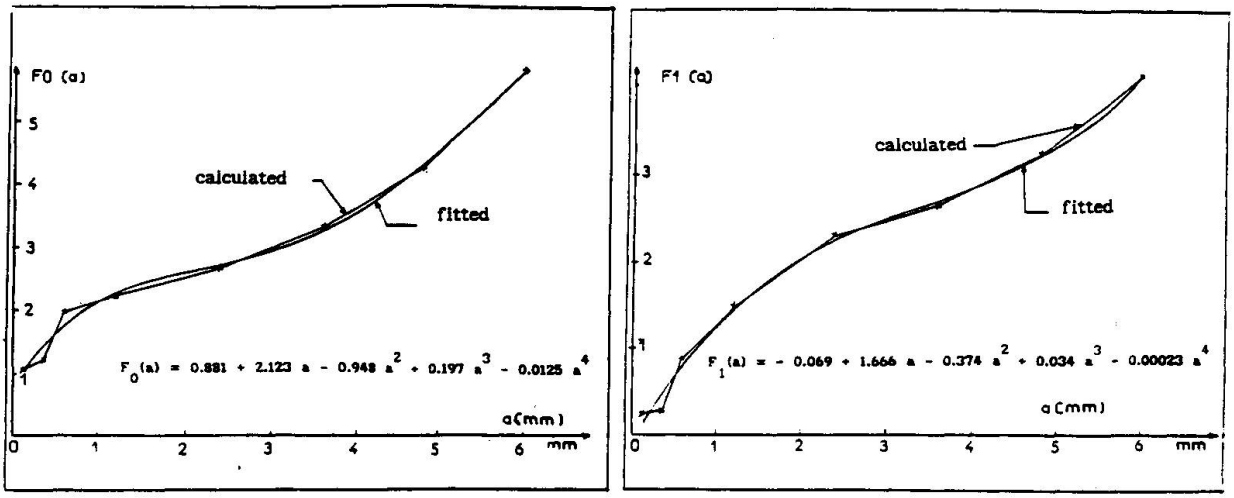

Fig. 6 Magnification factors F_0 and F_1

4. APPLICATION TO EXISTING BRIDGES

The part considered is the longitudinal welded connection between the stiffener and the plate of the orthotropic decks. It is one of the most sensitive element to fatigue damage. Several cracks have already been found in some existing bridges, especially for thin plates of 10 mm [4].

4.1 Crack Propagation Calculation

The crack is located in the plate, in a plane which is perpendicular to its surface and which contains the weld. The magnification factors are calculated as explained in the § 3-3.

The stress time history, measured by strain gauges on the bridges under a real traffic or computed by the LCPC's program CASTOR [5] by using the influence surface and a traffic record made by piezo-electric cables [6], is summarized in an histogram for a reference period T (generally T = 1 week). If N_i and N_c are the number of stress cycles with an amplitude σ_i and the total number of cycles by time unit, equations (1), (2) and (5) give :

$$da = \sum_{i=1}^{N_c} f(a,\sigma_i) N_i \, dt \quad , \text{ or } \quad da_{n+1} = \varepsilon\, a_n = \sum_{i=1}^{N_c} f(a_n,\sigma_i) N_i \, dt_{n+1} \tag{6}$$

after discretization, and with $a_r/a_0 = (1+\varepsilon)^j$; j corresponds to the total number of time steps when the failure occurs ($a = a_r$). The total lifetime is :

$$D = a_0 \sum_{k=1}^{J} \frac{\varepsilon\,(1+\varepsilon)^k}{\sum_{i=1}^{N_c} f(a_0(1+\varepsilon)^k,\sigma_i) N_i} \tag{7}$$

A computer program PROPAG [1] was written in order to compute this lifetime and to provide the crack evolution.

4.2 Model Calibration

The crack propagation calculation was first applied to the test specimens presented in the § 2, in order to calibrate some parameters and to check its results. A finite elements calculation made on the structure with the real loading and boundary conditions provided the stress diagram in the section of the plate :

$$\sigma(z) = 157.21 - 55.82\ z + 8.93\ z^2 - 0.866\ z^3 + 0.029\ z^4 \qquad (8)$$

The crack length increases were recorded during the tests for two stress amplitudes (200 and 300 MPa), and the coefficients C and m of (1) have been fitted to the results. They were found close to those proposed in the litterature and finally adopted : $C = 8.10^{-12}$, and $m = 2.85$, for ΔK in MPa $\sqrt{m}$ and da/dn in m/cycles.

In the tests we used the ratio $R = \sigma_{min}/\sigma_{max} = -1$. Because it was shown by other tests that the lifetime is highly dependent on this ratio and that only the tensile stresses allow to increase the crack, the stress amplitude taken into account here was $\sigma/2$.

The results of the calculation are compared with the experimental ones for several nominal stress from $\Delta\sigma = 200$ MPa to $\Delta\sigma = 340$ MPa, each time with 5 initial crack lengths between 0.05 mm and 0.4 mm (table 2). It is easy to conclude that an appropriate initial crack length under these welding conditions is 0.1 mm.

$R = \frac{\sigma_M}{\sigma_m}$	$\Delta\sigma$ (MPa)	Number of cycles at failure (IRSID tests)	Fracture mechanics model	
			a_0 (mm)	N. of cycles at failure
-1	200	2031000 729000 3443000 m= 2068000	0.05 0.10 0.15 0.20 0.40	3166000 1608000 1052000 777900 399900
-1	240	1076000 1274000 1767000 m= 1372000	0.05 0.10 0.15 0.20 0.40	1884000 957000 626000 463000 238000
-1	300	315000 548000 m = 431500	0.05 0.10 0.15 0.20 0.40	998000 507000 332000 245000 125900
-1	340	350000	0.05 0.10 0.15 0.20 0.40	698000 355000 232000 172000 88100

Table 2 : Comparison of the tested and computed lifetimes

4.3 Lifetimes of Existing Bridges

We present here the application of our model to the connection between the plate and the longitudinal stiffener for three cases of orthotropic deck bridges. Two of these bridges are temporary structures with a thin plate of 10 mm and a 6 mm thick stiffener (Montlhery and Choisy). The third one is the large box-girder bridge of Caronte, with a main span of 130 m and a total length of 300 m. The plate thickness is 12 mm.

In the cases of Caronte and Montlhery, the stress variations were measured under the traffic loads during previous phases of a ECSC's contract [7], by strain gauges sticked close and perpendicular to the weld. The nominal stress is obtained by a linear extrapolation, from two other points. In the case of Choisy, the stress variations are calculated by the program CASTOR, using the measured influence surface and the recorded traffic loads. The calculation is done with two traffics : the real one (RN 305) and the traffic of the RN 23 which is heavier and denser, in order to predict the consequences of an increase of the loads and traffic density.
The stress diagrams are for Montlhery and Choisy :

$$\sigma(z) = 7.533 - 2.706\ z + 0.481\ z^2 - 0.0788\ z^3 + 0.0055\ z^4 \qquad (9)$$

and for Caronte : $\sigma(z) = 6.024 - 3.287\ z + 1.075\ z^2 - 0.19\ z^3 + 0.0123\ z^4$ (9')

Due to the high residual stresses, all the stress variations under traffic loads are assumed to be in the tensile domain and hence are taken into account. The threshold of non-propagation ΔK_s has been chosen in accordance with the fatigue limit of the ECSC's S-N curves [8]. An initial crack length of 0.3 mm has been adopted corresponding to the welding conditions of these structures.

In all cases, the lifetime calculations were made by our fracture mechanics model and by the classical S-N curves and Miner's summation. The results are presented and compared in the table 3. The relevant S-N class for our element is 50 at least for the thin plates ; for Caronte the class 63 or 71 can be used. The figure 7 shows the crack evolution in the time in all cases ; a conservative choice of ΔK_s, which corresponds to the class 50, was made. This non-linear evolution is clearly different as the S-N approach. The lifetimes obtained by our model are slightly longer than those by S-N calculation, but, above all, the sensitivity to the S-N class is much lower, which seems to be more realistic.

CLASS	MONTLHERY		CARONTE		CHOISY Traffic RN 306		CHOISY Traffic RN 23	
(ECSC)	S-N	F.M.	S-N	F.M.	S-N	F.M.	S-N	F.M.
36	6	30	37	188	26	107	6	24
40	8	31	57	218	37	112	8	26
45	14	34	99	269	60	121	13	28
50	21	38	172	371	92	132	21	30
56	33	44	315	∞	138	147	31	34
63	55	55	600	∞	224	176	51	42
71	103	78	1393	∞	401	234	94	59

Table 3 : Computed lifetimes (in years) of existing bridges and comparison with S-N approach.

5. CONCLUSIONS

Two important points can be pointed out :

1/ From the manufacturing point of view it is clear that with a properly optimized automatic welding, improved fatigue resistance can be easily obtained. Therefore, taking into account the modern production tools, widely used in the european industry, it appears that the actual regulations are somewhat too conservative.

2/ From the point of view of the reliability of the structures we have shown that the physical approach of the fatigue for steel bridges can be made with a simple model which gives realistic fatigue lives, and with a lower scattering than with the classical S-N approach. The numerical program developped together with finite elements codes available, allows to make this type of calculation on a micro computer.

This study and parallel works done within the framework of the ECSC program show that the evaluation of the reliability of our bridges and the competitiveness of the steel structures still improve.

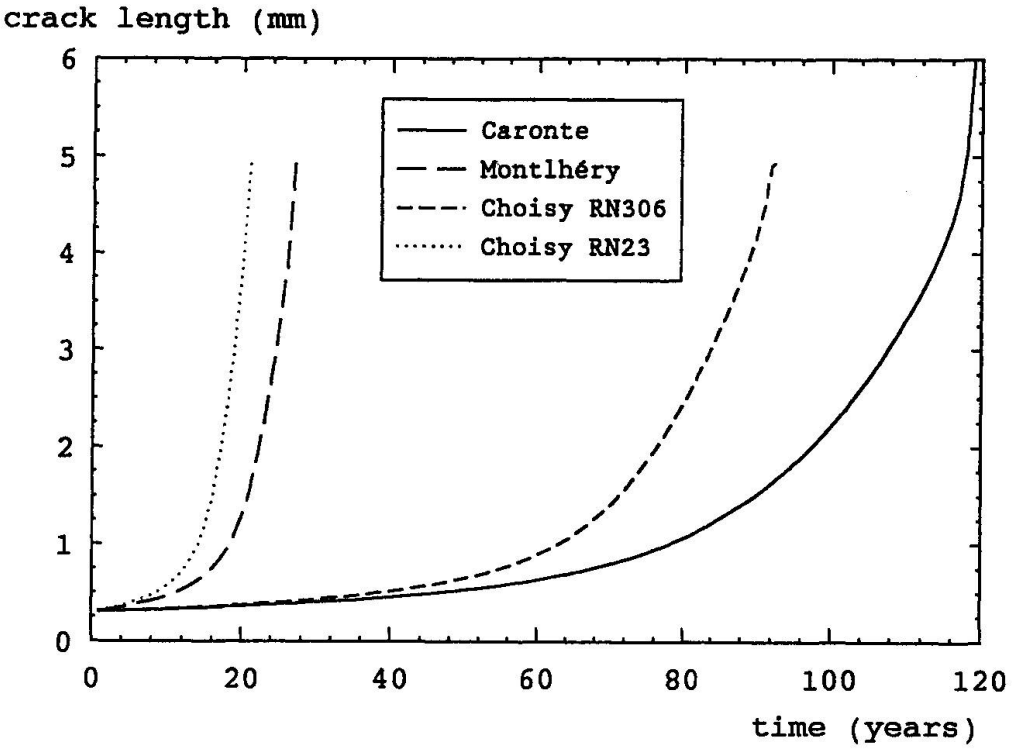

Fig. 7 : CRACK GROWTH

REFERENCES

1. BIGNONNET A., CARRACILLI J., JACOB B., Comportement en fatigue des ponts métalliques. Application aux dalles orthotropes en acier. Rapport final convention CECA, 7210 KD 217, Août 1989.

2. BRULS A., POLEUR E., Résistance à la fatigue des dalles en acier des ponts-routes. Rapport final convention CECA, KD 201, Avril 1989.

3. THONNARD, JANSS, Comportement en fatigue des dalles orthotropes avec raidisseurs trapézoïdaux. Rapport CRIF, MT 161, Août 1985.

4. MEHUE P., Fissures de fatigue dans les viaducs métalliques démontables, 13e congrès AIPC, Helsinki, juin 1988.

5. EYMARD R., JACOB B., Le programme CASTOR pour le Calcul des Actions et Sollicitations du Trafic dans les Ouvrages Routiers. Bull. liaison des LPC, n° 164, novembre-décembre 1989.

6. JACOB B., Connaissance du trafic routier et des sollicitations induites dans les ouvrages. Annales de l'ITBTP, n° 478, novembre 1989.

7. JACOB B., CARRACILLI J., Mesure et interprétation des charges dynamiques dans les ponts - Etude de la fatigue. Rapport final convention CECA, 7210 KD 311, juillet 1983.

8. Convention Européenne de la Construction Métallique, Recommandations pour la vérification en fatigue des structures en acier. Construction Métallique, n° 1 - 1987.

Fatigue Behaviour of Field-Welded Rib Joints in Orthotropic Steel Bridge Decks

Comportement à la fatigue des connexions de raidisseurs soudés dans des dalles orthotropes de ponts en acier

Ermüdungsverhalten in situ geschweisster Rippen orthotroper Stahlfahrbahnplatten

Henk KOLSTEIN
Research Engineer
Delft Univ. of Technology
Delft, The Netherlands

Henk Kolstein, born 1952, joined the Delft University of Technology in 1971. He is involved in research in steel structures at the Stevin Laboratories, investigating static and fatigue behaviour of bolted and welded joints. Since 1978, he has been participating in ECSC research within the domain of bridge loading and fatigue of orthotropic steel decks.

Jacobus DE BACK
Professor
Delft Univ. of Technology
Delft, The Netherlands

Jacobus de Back, born 1924, joined the Delft University of Technology in 1951. He was nominated as Professor of steel structures in 1972. Since 1957, he has been involved in research in steel structures. He is a member of several technical and standardization committees in The Netherlands and international committees of ECSC, ECCS, IIW and CIDECT.

SUMMARY
This paper describes the results of several research programs related to fatigue behaviour of field-welded rib joints in othotropic steel bridge decks. Constant as well as variable amplitude tests were carried out on several connections. Eurocode 3 fatigue design lines are considered. Fatigue cracks growing from welded details in an existing bridge and subsequent activities are reported. Finally, a fatigue design method which uses standard design curves and influence lines related to the static design load is introduced.

RÉSUMÉ
Cet article présente les résultats de plusieurs programmes de recherche relatifs au comportement à la fatigue des connexions de raidisseurs soudés dans des dalles orthotropes de ponts en acier. Des essais de fatigue sous amplitudes constante et variable ont été effectués sur différents types de connexions. Les courbes de fatigue de l'Eurocode 3 ont été considérées. Des fissures de fatigue apparues dans des détails soudés de ponts existants sont présentées, ainsi que les actions entreprises pour y remédier. Finalement, une méthode de calcul utilisant les courbes de Wöhler standardisées et les lignes d'influence relatives au modèle de charge statique est introduite.

ZUSAMMENFASSUNG
Dieser Artikel stellt die Resultate verschiedener Forschungsprogramme vor, die das Ermüdungsverhalten auf der Baustelle geschweisster Rippen orthotroper Fahrbahnplatten von Stahlbrücken betreffen. Verschiedene Arten solcher Verbindungen wurden sowohl unter konstanter als auch variabler Amplitude getestet. Dabei wurden die im Eurocode 3 enthaltenen Ermüdungsfestigkeitskurven berücksichtigt. Über Ermüdungsrisse, die in bestehenden Brücken von geschweissten Konstruktionsdetails ausgehen, wird ebenso berichtet, wie über die in solchen Fällen zur Auswahl stehenden Instandstellungsmassnahmen. Schliesslich wird eine Methode für die Ermüdungsbemessung vorgestellt, basierend auf normierten Wöhlerkurven und Einflusslinien in Verbindung mit den statischen Bemessungslasten.

1. INTRODUCTION

In most large orthotropic steel bridge decks, field splices are necessary because transportation of the complete bridge from the shop to the site is seldom possible. In general, both longitudinal and transverse field splices have to be made. In the longitudinal splices, only the deck plate has to be connected. This is mostly done by butt welding and as the weld is accessible both from above and from below, a good quality of the weld can be achieved. The same applies to the transverse butt splice weld in the deckplate. At the transverse splice the longitudinal ribs have to be connected as well.
With closed ribs, mostly used in modern bridges, the most appropriate way of splicing is by welding but as the welds can only be made from the outside in an unfavourable overhead position, the quality of those welds will be dubious. Depending on the location of the splice in the deck, the load on the splice can have a fluctuating part due to the traffic load, dominating the static loading, so conditions for fatigue damage are present.
As the splice in the ribs frequently occurs in a bridge deck, an investigation of the fatigue behaviour of field splices is worth while. Besides cracks were discovered in several field welded splices in a rib of a bridge which was 15 years in duty.

2. FATIGUE TESTS ON FULL SCALE TEST SPECIMENS

In this paper, the results of the fatigue tests are plotted in a S-N-diagram on a log-log scale. The regression mean-line minus twice the standard deviation is used to make comparisons with the fatigue design curves, defined by the Eurocode 3.

2.1. Constant amplitude tests

2.1.1. Dutch research

In 1974 [1], a research programme was set up to investigate the design of field splices in orthotropic steel bridge decks with respect to economy and fatigue strength. Laboratory tests were conducted at IBBC-TNO and at the Stevin Laboratory. The specimens for the bending tests were single trapezoidal rib specimens 2/325/6, steelgrade Fe 510. Three types of field splices were selected, as shown in figure 1.

- Type A : Butt splice with back-up strips (4 mm root gap)
- Type B : Lap splice with fillet welds
- Type C : Butt splice with a thick joint plate.

The conclusion (fig.1) can be drawn that the fatigue behavior of type C is the best (EC 125) and of type B is the worst (EC 56), with type A in between (EC 80). Nevertheless, with respect to type C, it must be noted that apparently this type is very sensitive to the quality of the workmanship, for the first series of specimens made with less care gave very bad results. That is one of the reasons why type A is often used.

As all tests were carried out at high stress range levels ($\geq$ 120 MPa), where the shape of the S-N curve amounts 3, no information is available at the lower stress regions and on the fatigue limit. This stress range region is very important, for measurements carried in ECSC research [2,3] showed for this type of connection a maximum stress range of $\pm$ 80 MPa.

In 1986 [4], an ECSC research program started at the Stevin Laboratory in which among other things, constant amplitude tests were carried out on the type A

detail at stress ranges beyond 2.10^6-3.10^7 cycles. Besides, the effect of the root-gap of the weld has been examined by varying the gap between the stiffener and the splice in 0, 2 and 4 mm. Furthermore tests were executed with an improved form of the weld (V-groove). The fatigue results are gathered in figure 2.

For the specimens with a root gap of 4 mm it appears that, the specimens tested at stress ranges > 120 MPa fall within the spread band of the previous tests [1]. At 105 MPa the fatigue strength is far more than one would expect. The fatigue cracks appeared over 9 million cycles instead of about 3 million cycles. The specimen tested at a stress range level of 90 MPa did not fail after almost 30 million cycles.
Comparing the results it appears furthermore, that a weld with a root gap of 0 or 2 mm can result in a fatigue strength far below the strength of the weld with a root gap of 4mm (a factor 12 - 18).
Changing the weld geometry by using a V-groove did not give the expected improvement.

2.1.2. Comparison with foreign research

In 1988 an Japanese IIW document [5] was published which contained, analogous to the Dutch researches [1,4], fatigue results on trapezoidal ribs. Also in this research, a great influence of the largeness of the root gap on the fatigue strength was found. Summing up these two test programmes, it can be concluded that Class 71 according the Eurocode 3 can be recommended for field splices type A, with a root gap ≥ 3 mm (fig.3a). If the root gap < 3 mm the classification decreases to a Eurocode Class 36 (fig.3b). Naturally it is better to avoid the last situation, but it is known that some of the existing bridges contain the type A detail with very small root gaps.

Simultaneous to the Dutch ECSC research [4] the Italian partners in this joint ECSC research investigated the fatigue behaviour of field splices in ribs of orthotropic decks [6]. They studied a triangular shape of the trough instead of a trapezoïdal one. Following details were tested (fig.4a):
- Butt splice using a V-groove with a root gap of 6 mm and a backing strip.
- Butt splice using a X-groove with a root gap of 4 mm, without backing strip.

From the results as given in figure 4a it can be concluded, that the V-groove specimens conducted better than the X-groove type. In both cases the behaviour is better than the Dutch [1,2] and Japanese [3] researches. However it must be noticed that all the welding of the Italian research have been checked by means of visual and magnetic controls. The butt welding, moreover, have been 100% X-rayed and repaired if necessary.

A triangular shape was also studied in the United Kingdom [7] in 1982. The following details were tested (fig.4b):
- Butt splice with backing strip and a root gap of 12 mm.
- Three series of butt splices with a sealing plate of 19 mm. The welding procedure as well as the influence of stress relieving was studied.

From the results as given in figure 4b it can be concluded that the fatigue strength of these testspecimens is comparable with those of the Italian research. Besides, the behaviour of the welded connections with a sealing plate of 19 mm is better than the one with a backing strip (Type E).

Gathering the Italian and UK-tests together, it can be noticed that perhaps for the triangular shapes containing a weld with backing strip and a root gap of 6 - 12 mm, a Eurocode Class 112 can be considered (fig.4c).

2.2. Variable amplitude tests

In above mentioned Dutch ECSC programme [4], also some variable tests were carried out. Special attention was performed to long life (low stress) fatigue results and testing the Miner summation by comparing variable and constant amplitude tests.

2.2.1. Load-spectra for the variable amplitude test.

Axleload-spectra and stress-spectra measured in the ECSC-research [2,3] together with the computer assessment programme of the University of Liege, were used. For the computer simulation , the traffic flow of the Rheden Bridge and a theoretical influence line were used to simulate a test-load spectra for the field splice in a longitudinal rib. Analysis of the simulated spectra showed, that the low stress ranges cause only 7% of the total damage of the spectra. These stress range classes amounts however 84 % of the total number of cycles (fig.5a). So leaving out these classes, resulted in a 'reduced spectrum' saving a lot of testing time without attacking the potential fatigue damage of the spectrum (fig.5b).
Besides the above mentioned simulated test-load spectrum, for one of the specimens a measured stress-spectrum was used. This spectrum (fig.6) was measured on the the Forth Bridge in the United Kingdom [2,3]. Considering the constant amplitude tests the stress range level of the actual measured and simulated were raised to a higher level for the variable amplitude tests.

2.2.2. Analysis of the spectra using Miner

To compare the variable amplitude test results with the constant amplitude ones, the applied stress-spectra were analyzed in two different ways.

a. An equivalent stress range $\Delta\sigma_e$ was calculated in a way that n-cycles of that stress range have the same fatigue damaging potential as n-cycles of the stress-spectrum, using a third power relationship;

$$\Delta\sigma_e = \left(\frac{1}{n_i} \Sigma n_i \Delta\sigma_i^3\right)^{1/3} \text{ MPa.}$$

b. The University of Liege proposed [3] the following equivalent stress $\Delta\sigma_m$ and belonging number of cycles n_m;

$$\Delta\sigma_m = \frac{\Sigma n_i \Delta\sigma_i^3}{\Sigma n_i \Delta\sigma_i^4} \text{ MPa} \quad \text{and} \quad n_m = \frac{\Sigma n_i \Delta\sigma_i^3}{\Delta\sigma_m^3}.$$

In these formulae : $\Delta\sigma_i$ = individual stress range

n_i = individual number of cycles belonging to $\Delta\sigma_i$

$\Delta\sigma_m$ = equivalent stress range

n_m = number of cycles belonging to $\Delta\sigma_m$.

In this paper both methods are be used (fig. 5 and 6).

The fatigue results of the variable amplitude tests are presented in figure 7. It appears, that there is a very good agreement between the constant amplitude tests and the variable amplitude tests using the Miner calculation. Furthermore no cracks were found in the specimen with a maximum stress range of the spectrum of 132 MPa after testing for 48 million cycles. Comparing the results of the tests applying the "measured-stress-spectrum" and the "simulated stress-spectrum", the difference seems to be very small.

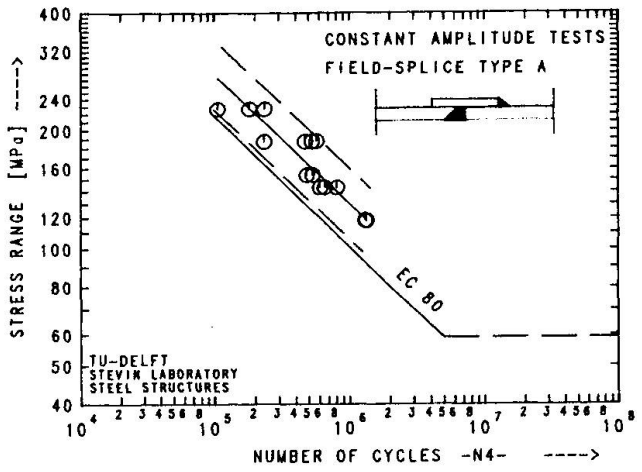

-1a-

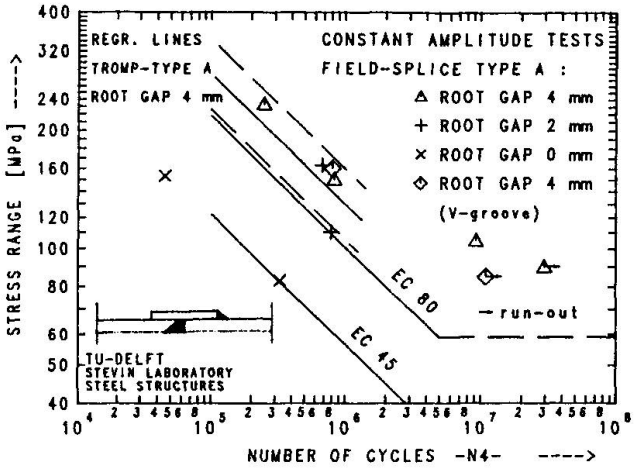

Test results Kolstein [Ref.4.]
Figure 2.

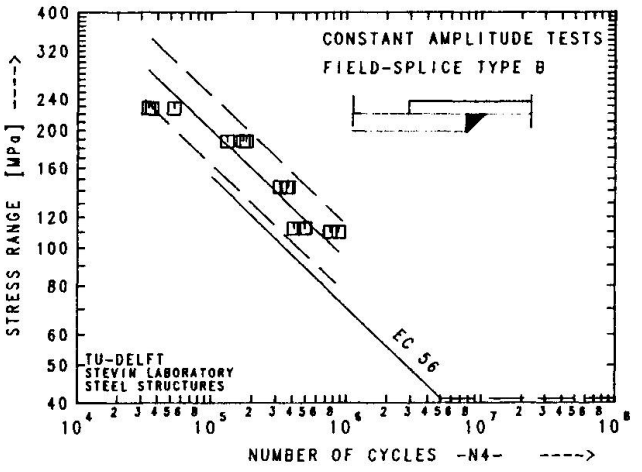

-1b-

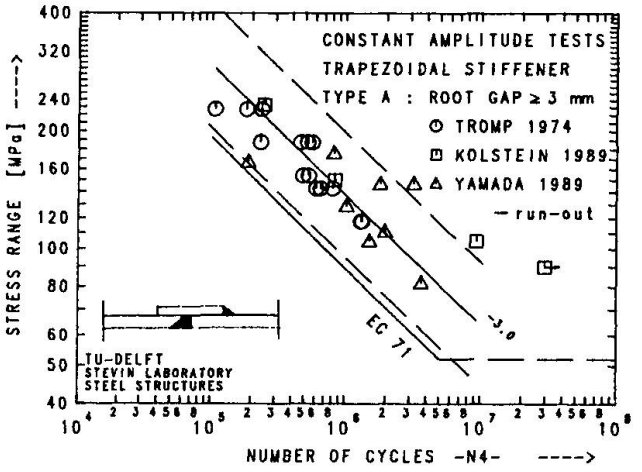

-3a-

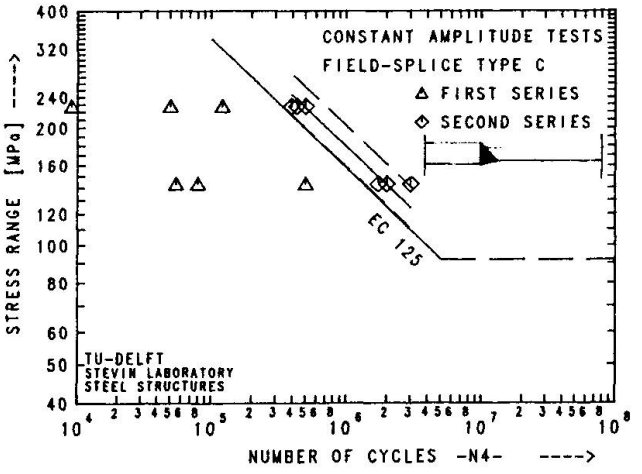

-1c-
Test results by Tromp [Ref.1].
Test results by Kolstein [Ref.4].
Figure 1.

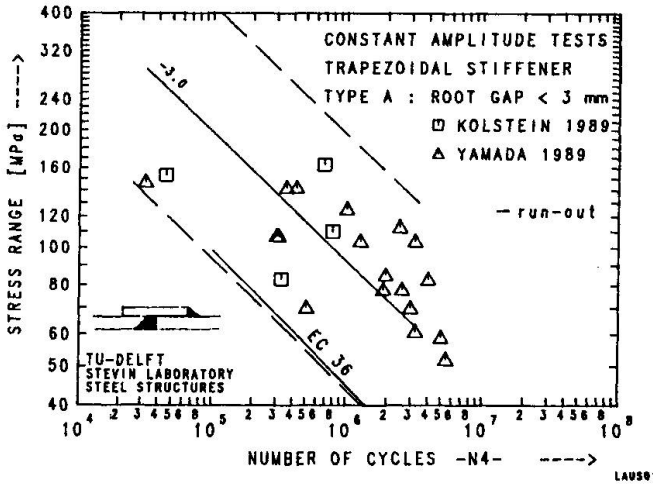

-3b-
Comparison test results; Tromp, Kolstein and Yamada [1,4,5].
Figure 3.

3. FATIGUE CRACKS IN AN EXISTING BRIDGE

During the course of routine maintenance work on the Muiden Bridge in 1985, in one of the 68 longitudinal ribs, cracks were found in several field-welded splices. For some of these connections about 70% of the total cross-section was cracked. The rib splice detail is similar to the type-A detail with a root gap of 2 mm. Due to the fact this bridge was used for only 15 years and the specific detail had been used in a lot of other bridges a research was urgently needed.

Calculations and measurements were executed to find reasons for this cracks and the remaining fatigue life of the bridge [8]. The fatigue calculations are made by using at first a derived load spectrum and in the second place a measured stress-spectrum for this detail.

3.1 Traffic loading during 15 years

Since the opening of the Muiden Bridge in 1970, traffic measurements had been carried out. These measurements concerned the counting of the vehicles. Three categories of vehicles are considered:
- B1: Light-weight vehicles (a passenger car, a delivery van, a motor-cycle),
- B2: Rigid commercial vehicles (a bus, a rigid truck without trailer),
- B3: Articulated commercial vehicles (a rigid truck and trailer, a trailer truck).

In the period 1970 - 1985 a total of $1,07.10^7$ vehicles was counted.

Using measurements from ECSC research [2,3], the following distribution of categories B2 and B3 over the fast and slow lane could be derived:

TYPE	TOTAL: $1,07.10^7$	FAST LANE	SLOW LANE
B2	4,2% → $4,5.10^6$	18% → $0,8.10^6$	82% → $3,7.10^6$
B3	2,9% → $3,1.10^6$	23% → $0,4.10^6$	87% → $2,7.10^6$

The number of axle loads ≥ 10 kN (N10) in the Slow Lane amounts 3,5 times the number of trucks B2 and B3, which results in N10 = $2,2.10^7$.

3.2. stress-spectrum of the field splice in a longitudinal rib

Relating the measured axle load spectra and stress-spectra of the Forth Bridge (fig.6) it appeared, that the number of stress range cycles ≥ 10 MPa (NR) is equal to 0,42.N10. That means for the Muiden Bridge a number NR = $0.928*10^7$. Assuming as a first approach that 10 kN wheel load results in a stress range of 15 MPa for the considered field splice, a stress-spectrum based on an load spectrum for the period 1970 - 1985 was determined. For the first fatigue calculation the measured axle load spectrum from the Rheden Bridge was used (SPECTRUM-I). A second fatigue calculation was made using directly the measured stress-spectrum of the Forth Bridge. In this case the number NR is the same as with the first calculation (SPECTRUM-II).
In figure 8 both stress-spectra and the Eurocode S-N curve EC 80 are plotted.

3.3. Calculated fatigue lives

Using Miner the following life-times could be calculated:
- SPECTRUM-I : Load spectrum Rheden Bridge and 10 kN → 15 MPa : 13,3 years,
- SPECTRUM-II: stress-spectrum Forth Bridge : 55,5 years.

The longer fatigue life of the second calculation is perhaps too optimistic because the measured axle loads in the United Kingdom are lower than in the

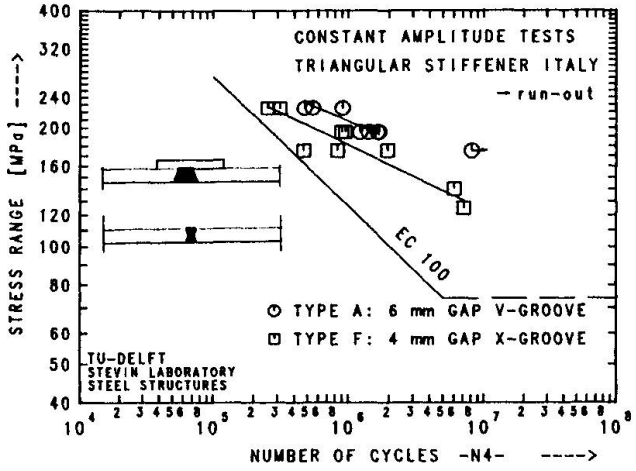

-4a-

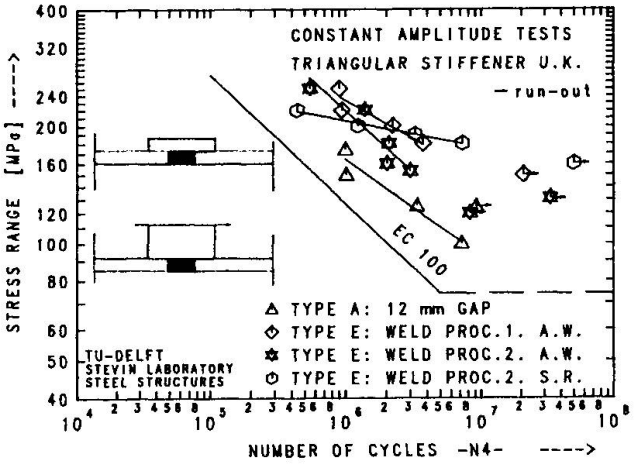

-4b-

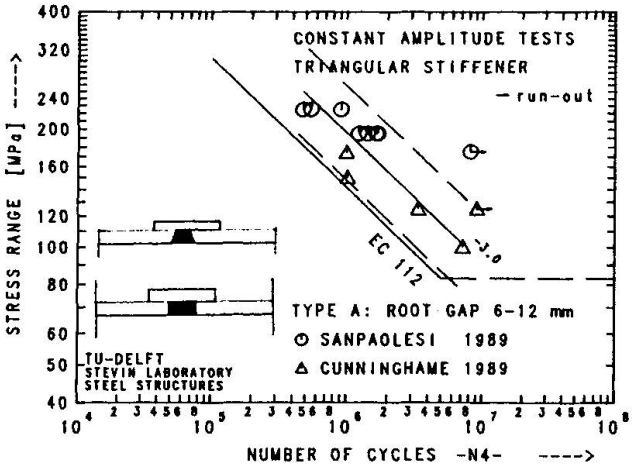

-4c-

Test results Sanpaolesi [Ref.6] and Cunninghame [Ref.7].
Figure 4.

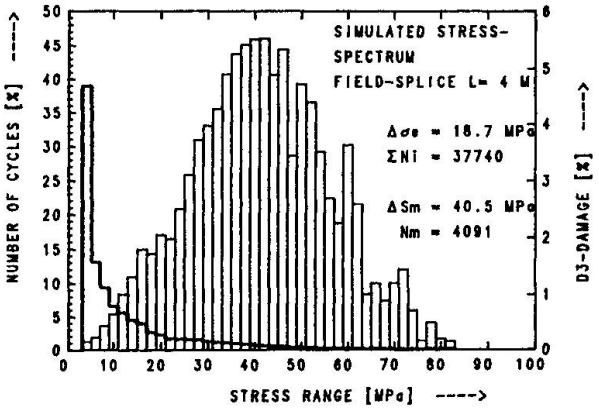

-5a-

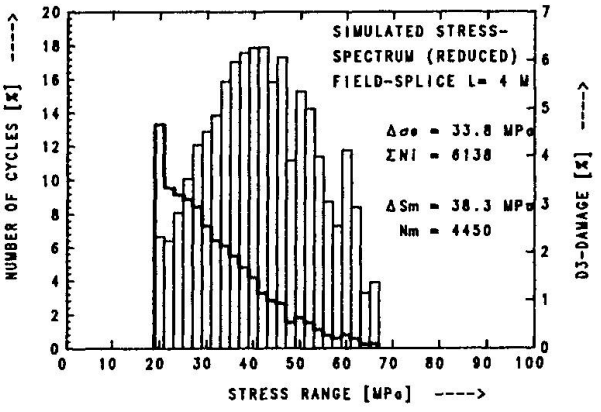

-5b-

Simulated stress spectra [Ref.2,3].
Figure 5.

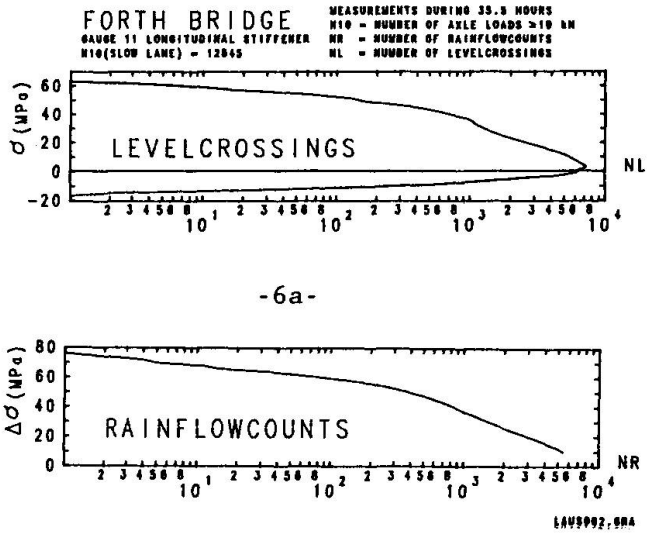

-6a-

-6b-

Netherlands (fig.9). At this stage of the research it was clear that the cracks and fatigue calculation agree, which was a very unlucky situation.
To check the assumed relation load-stress, strain measurements on the Muiden Bridge were carried out.

3.4. Strain measurements

Strain gauges were fixed on several longitudinal ribs to check if the damaged rib was the most heavily loaded one. Three types of measurements were carried out:

- Measurements without interrupting the the real traffic,
- Static measurements with a calibrated truck,
- Dynamic measurements with a calibrated truck.

The analyzed stresses by counting levelcrossings are given in figure 10. It can be seen that the measured stresses on the Muiden Bridge are little lower than those measured on the Forth Bridge and the damaged rib (gauge 2) had to sustain the highest stresses.

The results of the measurements with the calibrated truck are summarized as follows:

static	front wheel	10 kN → 11,8 MPa
	rear wheel	10 kN → 10,0 MPa
dynamic	front wheel	10 kN → 7,9 MPa
	rear wheel	10 kN → 7,5 MPa

It is clear that the assumption of 10 kN wheel load resulting in a stress of 15 MPa is not realistic for this detail.

3.5 Second series of fatigue calculations

Using the load spectrum of the Rheden Bridge a second series of fatigue calculations was made. The results are summarized below:

- SPECTRUM III : 10 kN → 12 MPa : 28,6 years
- SPECTRUM IV : 10 kN → 10 MPa : 66,0 years
- SPECTRUM V : 10 kN → 8 MPa : 145,6 years

It can be concluded, that the calculated fatigue life for the field splice in the longitudinal rib of the Muiden Bridge is much longer than 15 years. Knowing that the calculations were made in the most unfavorable situation, all wheel loads in the same track, the number of years must be higher.

3.6 Quality of the welds

Examination of cracks showed, that the quality of the welds was very bad. It was concluded that the very bad execution of the welds was the main reason for the observed cracks in this detail. However it must be remembered that the root gap of the detail in this bridge was 2 mm and with the knowledge of the later executed laboratory tests [4,5], it is clear that the EC 80 is too high and more cracks are not excluded in the future.

4. FATIGUE DESIGN USING STANDARD FATIGUE DESIGN CURVES [9,10]

When the static design stresses $\Delta\sigma st$ are known, there is a possibility to have a relationship to the actual stress ranges due to real traffic. The actual stress ranges can be expressed in a proportion of the stress range $\Delta\sigma st$. This opens the way to investigate the fatigue problem for existing bridges but also

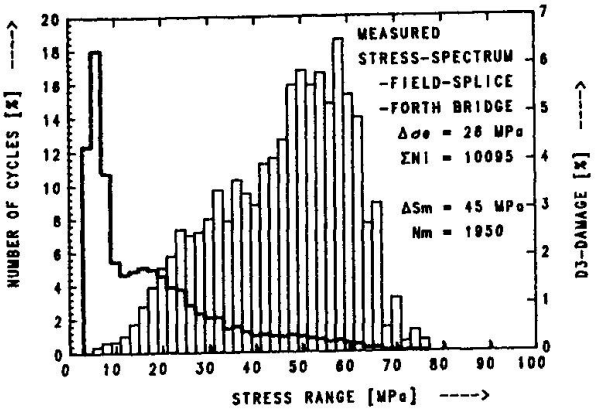

-6c-

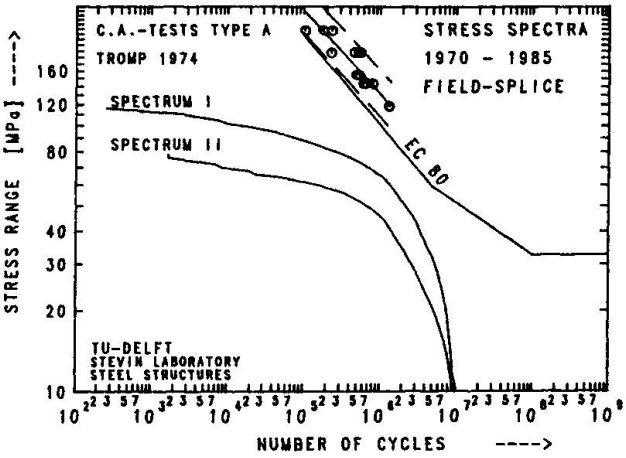

Stress spectra Muiden [Ref.8].
Figure 8.

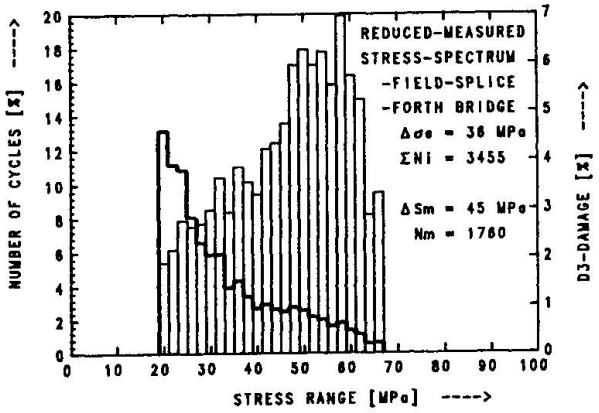

-6b-
Measured stress spectra [Ref.2,3]
Figure 6.

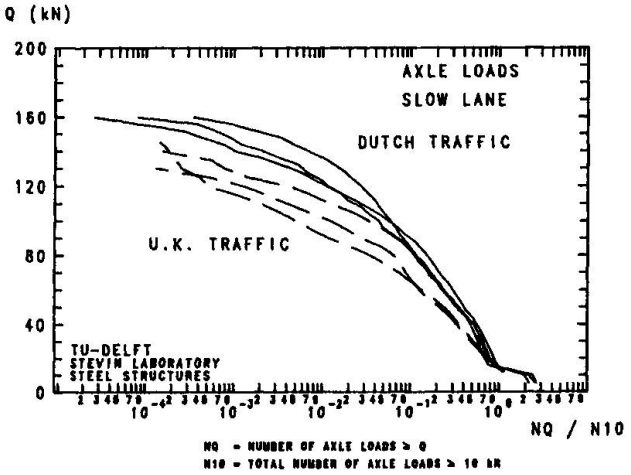

Axle load spectra [Ref.2,3].
Figure 9.

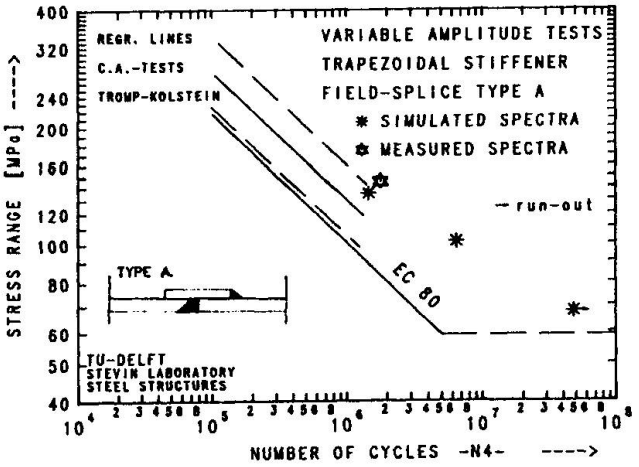

Test results Kolstein [Ref.4].
Figure 7.

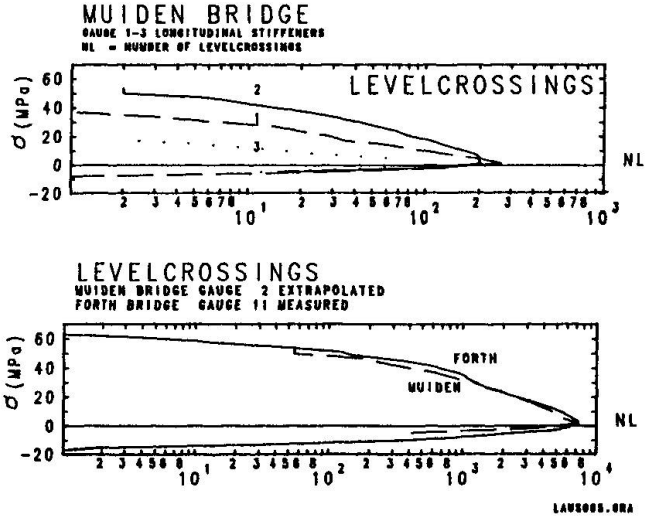

Measured stresses Muiden [Ref.8].
Figure 10.

for the design of new bridges [9]. Knowing the composition of a traffic, stress-time histories can be calculated by running that traffic over static influence lines.
Instead of the impact factor a so called fatigue-coefficient is used to represent the dynamic influence. It has been shown from measurements that the application of the usual impact factor led to results which are too pessimistic while the impact factor covers maximum values of the dynamic effect. In reality there is a scatter of stresses which have to be considered. A fatigue-coefficient being an average of the impact factor seems to be more realistic.
Using the rainflow counting method the stress-time histories are transformed into a number of stress cycles. After that the evaluated stress ranges of the different vehicles are expressed in a ratio to the the stress range $\Delta\sigma st$.
Doing this for several spans spectra of stress ranges can be composed for each span. To evaluate the fatigue life the cumulative damage hypothesis of Palgrem-Miner is applied, using the fatigue strength curves of the Eurocode.
Knowing the spectra with stress ranges expressed in a ratio to $\Delta\sigma st$, the fatigue life can be calculated for bridges of several spans and a chosen value $\Delta\sigma st$.
Figure provides the course of the procedure using an arbitrary S-N curve.
While all fatigue strength curves are similar, having the same slope and the kneepoint at the same number of cycles $N = 5.10^6$, a simplification in the calculations can be achieved by transforming the stress range $\Delta\sigma st$ into a dimensionless value, dividing $\Delta\sigma st$ by the value $\Delta\sigma$-2.10^6 of the considered S-N curve.
Now factors, k_1, applicable for all S-N curves can be evaluated to define the limiting stress range $\Delta\sigma st$ for an assumed life and the standard traffic.

$$\Delta\sigma_{st(lim)} = \frac{\Delta\sigma \; 2.10^6}{k_1 . \gamma}$$

Figure 11 shows the derivation and gives a set of factors k_1 for an assumed fatigue life of 50 years, respectively 100 years, for the mentioned standard traffic.

It can be concluded for a field splice in a longitudinal rib the static design stress range $\Delta\sigma_{st(lim)}$ with a cross-beam span of 4 meter and a weld class EC 80 must be $\leq$ 100 MPa. Considering the transverse distribution of the wheels and belonging influence line (fig.12) a fatigue reduction factor k_2 can be calculated by the following formula ;

$$k_2 = (\alpha_1 . \beta_1^m + \ldots\ldots + \alpha_i . \beta_i^m)^{1/m}, \text{ in which:}$$

α = transverse distribution factor of the wheel load
β = influence line factor for a specific point
m = slope of the S-N curve.

Now: $$\Delta\sigma_{st(lim)} = \frac{\Delta\sigma \; 2.10^6}{k_1 . k_2 . \gamma} .$$

For above mentioned situation $\Delta\sigma_{st(lim)}$ must be $\leq$ 140 MPa.

5. NEED FOR FURTHER WORK

It can be concluded, that the remaining fatigue life of the field- welded splices in longitudinal ribs in existing bridges will be very actual the following years. Therefore it is necessary to develop economic repairing techniques for these welded connections. Based on the available results on these detail, a better design can be realized for new bridges. However it is required to be very accurate concerning the quality of the welds.

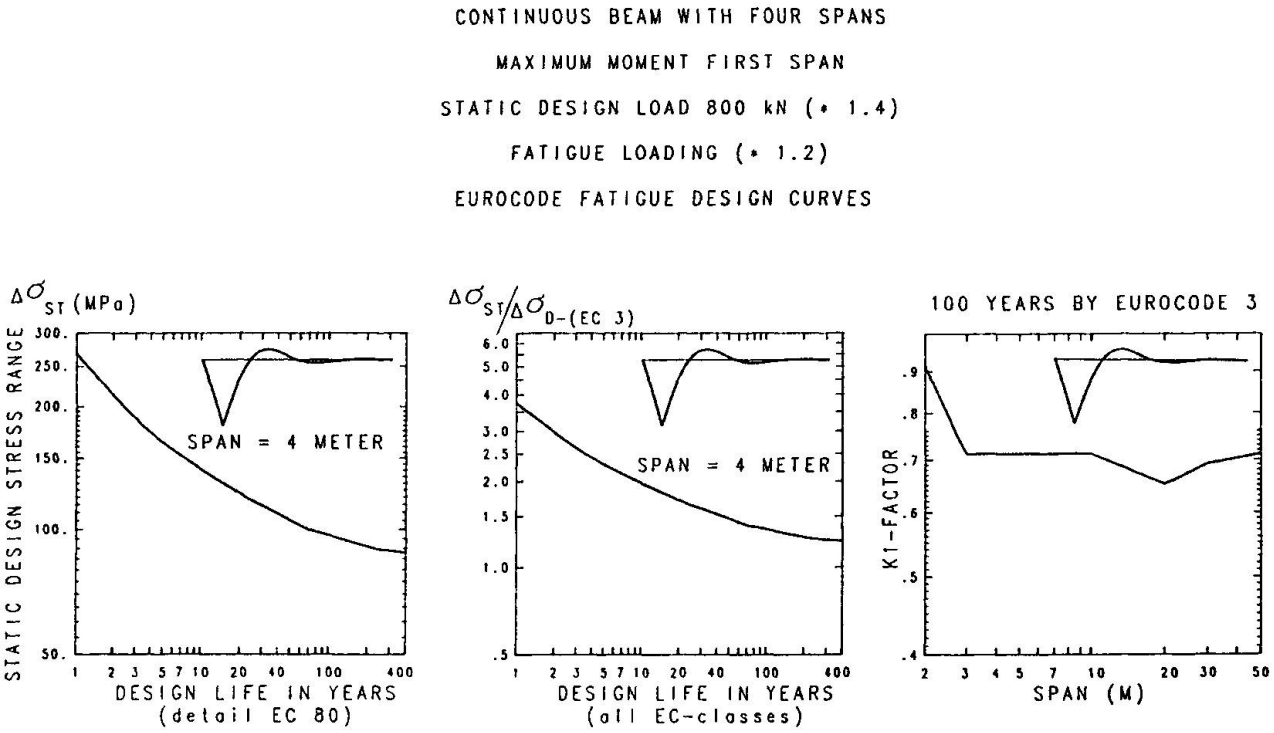

Fatigue design curves [Ref.9,10].
Figure 11.

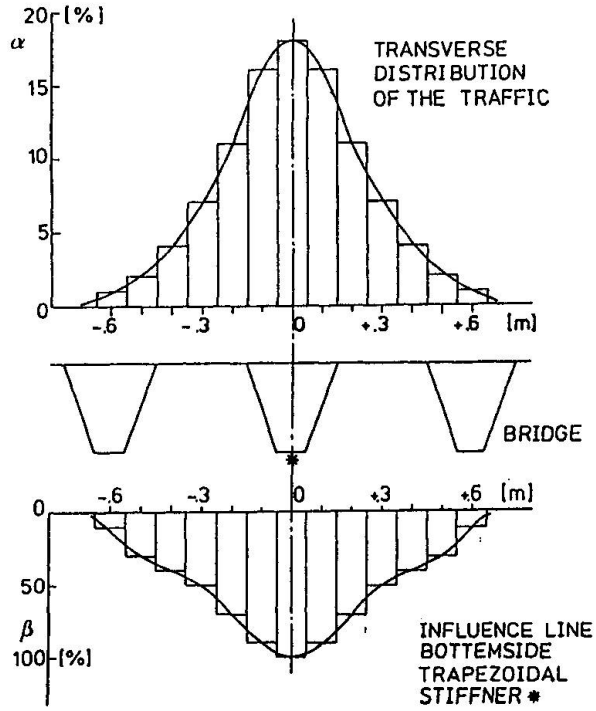

Transverse load distribution and influence line [Ref.10].
Figure 12.

6. ACKNOWLEDGMENTS

The authors wish to thank the colleagues in the European Working Group for their competent and stimulating discussions about the programmes and the results.
Some of the work described was carried out for the bridge department of the Dutch Governmental Organization 'Rijkswaterstaat'. Partial the published work was possible due to the financial aid of the Commission of the European Communities.
Moreover the authors wish to thank 'Rijkswaterstaat' and the Commission of the European Communities for their permission to publish this paper.

7. LITERATURE

1. TROMP W.A.J., Fatigue of field splices in ribs of orthotropic steel bridge decks. Stevinreport 6-74-15, Stevin Laboratory - Steelstructures Delft University of Technology, The Netherlands, 1974.

2. DE BACK J. BRULS A. CARRACILLI J. HOFFMANN E. SANPAOLESI L. TILLY J.P. ZASCHEL J.M., Measurements and Interpretation of dynamic Loads on Bridges, Synthesis Report - Phase 1, Commission of the European Communities, EUR 7754, 1982.

3. HAIBACH E. DE BACK J. BRULS A. CARRACILLI J. JACOB B. KOLSTEIN M.H. PAGE J. PFEIFER M.R. SANPAOLESI L. TILLY J.P. ZACHEL J.M. HOFFMAN E., Measurements and Interpretation of dynamic Loads on Bridges, Synthesis Report - Phase 2, Commission of the European Communities, EUR 9759, 1986.

4. KOLSTEIN M.H. DE BACK J., Fatigue strength of orthotropic steel decks; Part 1: Field-welded rib joints. ECSC Contract no. 7210-KD/609-F4.4/86. Stevinreport 25.6.89.30/A2, Stevin Laboratory - Steelstructures Delft University of Technology, The Netherlands, 1989.

5. YAMADA K. e.a., Fatigue Strength of Field-Welded Rib Joints of Orthotropic Steel Decks. IIW Doc. XIII-1282-88, Department of Civil Engineering, Nagoya University, Chikusaku, Nagoya 464, Japan, 1988.

6. SANPAOLESI L., Misure ed Interpretazioni dei Carichi dinamici sui Ponti Fase 3. Convenzione n° 7210-KD/411-F4.4/86. Instuto di Scienza della Costruzioni, Universita di Pisa, Italia, 1989.

7. CUNNINGHAME J.R., Fatigue performance of joints between longitudinal stiffeners. TRRL Laboratory Report 1066, Transport and Road Research Laboratory - Bridges Division, Crowthorne, United Kingdom, 1982.

8. KOLSTEIN M.H., Stuikverbindingen in trogvormige langsverstijvingen in een orthotrope rijvloer van een stalen verkeersbrug. Stevinreport 6-85-5, Stevin Laboratory - Steelstructures, Delft University of Technology, The Netherlands, 1986.

9. VAN MAARSCHALKERWAART H.M.C.M., Evaluation of existing structures. Proceedings of Fatigue aspects in structural design, Delft, The netherlands, 1989.

10. KOLSTEIN M.H., Presentatiewijze voor het op vermoeiing bereken van stalen verkeersbruggen. Stevinreport 6-85-17, Stevin Laboratory - Steelstructures, Delft University of Thechnology, The Netherlands, 1985.

Fatigue Tests of Stiffener to Cross Beam Connections

Essais de fatigue de liaisons entre raidisseur et entretoise

Versuche zur Ermüdung des Anschlusses einer Steife an einen Querträger

Hans-Peter LEHRKE
Dr.-Ing.
Frauenhofer-Inst. für Betriebsfestigkeit
Darmstadt, Fed. Rep. of Germany

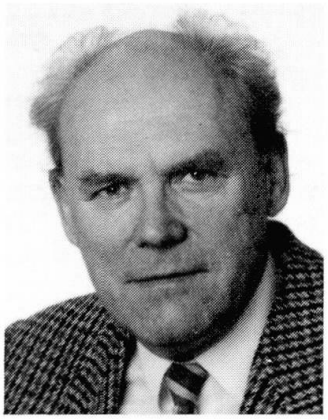

H.-P. Lehrke, born 1936, received his civil engineering and doctoral degrees at the Technical University, Braunschweig. After employment as an assistant at the Technical University, he was involved in mechanical and mathematical engineering problems at Krupp-Forschungsinstitut, Essen. Since 1973 he has been senior research engineer at LBF (Frauenhofer-Institut für Betriebsfestigkeit). Main research topics are fatigue, stress analysis, and dynamics of structures.

SUMMARY

Traffic loads produce high stress concentrations leading to fatigue cracking at the edges of cut-outs in webs of cross beams. High local stresses can be reduced by improved shaping of cut-outs. Fatigue tests were performed using two types of specimens; one with a commonly used shape of cut-out and the other with a new shape. The results showed a considerable increase of fatigue life for the new shape. However residual stresses of unknown distribution and high intensities were observed in all specimens and these may have influenced the increase in fatigue strength.

RÉSUMÉ

Les charges du trafic produisent des concentrations de contraintes élevées aux bord des découpes dans les âmes des entretoises pouvant conduire à un dommage en fatigue. Ces pointes de contraintes peuvent être réduites par des géométries de découpes plus favorables. Des essais de fatigue ont été réalisés sur des entretoises comprenant l'ancienne et la nouvelle géométrie. Bien que les résultats montrent un accroissement considérable de la durée de vie pour la nouvelle découpe, ceux-ci demandent encore à être confirmés du fait de la présence dans les éprouvettes de contraintes résiduelles inconnues et élevées qui peuvent avoir influencé cette amélioration.

ZUSAMMENFASSUNG

Verkehrslasten rufen an den Rändern der Ausnehmungen in den Stegblechen von Brückenquerträgern hohe Spannungsspitzen und möglicherweise Ermüdungsschäden hervor. Diese Kerbspannungen können durch eine günstigere Ausnehmungsform reduziert werden. Ausgeführt wurden Ermüdungsfestigkeitsversuche an Querträgern mit einer derzeit gebräuchlichen und einer neuen Ausnehmungsform. Die bisher erzielten Ergebnisse ergaben eine deutliche Lebensdauersteigerung für die neue Form, können aber nicht als abgesichert gelten, weil unbekannte Eigenspannungen hoher Intensität in sämtlichen Versuchsträgern beobachtet wurden.

1. INTRODUCTION

During the last years institutes from six European countries have performed a joint research program on steel bridges supported by the EC with the following main topics

- measurement and description of traffic loads
- operational stresses in steel bridge components and
- fatigue of orthotropic steel bridge decks.

The longitudinal stiffener to cross beam connection is one design detail of orthotropic decks susceptible to fatigue failure.

In orthotropic steel decks the traffic loads are transferred from the deckplate via the longitudinal stiffeners to the cross beams and from there to the main structure of the bridge. Depending on the number of traffic lanes, one cross beam may gather the loads of several wheels and axles belonging to more than one vehicle. Cross beams have the dimensions of beams. They are stressed by bending moments, shear forces and torsional moments. Besides the globally distributed beam stresses, additional stress fields are distributed more locally e.g. due to the load introduction and due to local stress concentrations.

Orthotropic decks in modern design contain cut-outs in the web of the cross beams to let the longitudinal stiffeners pass through. The cut-outs interrupt the stress fields and evoke stress concentration at their free edges. Besides the highly stressed edges, the welds connecting the stiffeners to the webs of the cross beams must also be regarded to be potentially critical to fatigue failure.

Approaching the real stress state in a bridge, two main load cases may be defined stressing the longitudinal stiffener to cross beam connection at the two critical points just mentioned:

- the load introduction into the cross beam which is passing the welds connecting the stiffeners to the web and
- the load transfer in the cross beam from the points of load introduction to the main structure of the bridge.

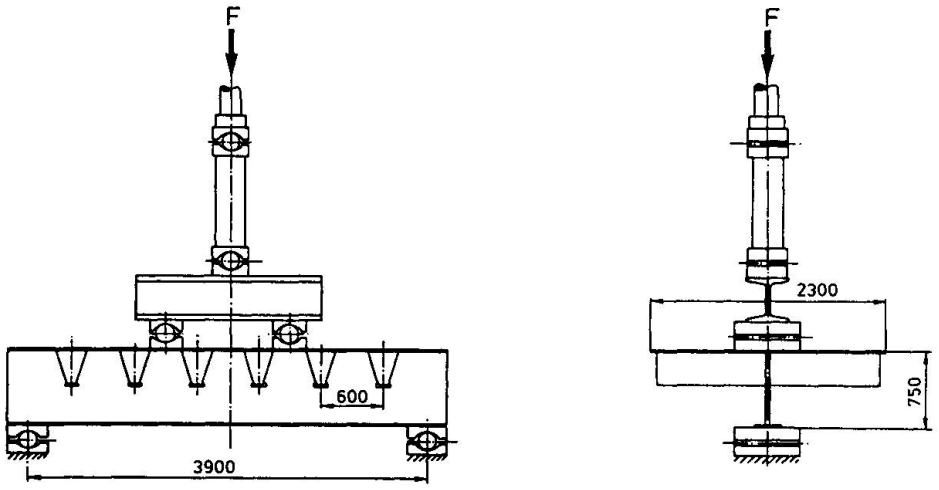

Fig. 1 Testing performed

Each load case may produce fatigue at both critical points. While the firstly mentioned load case is investigated by other groups in the joint research project, the objective of this paper is limited to the second load case. Thus, the function of cross beams to carry the loads of several wheels introduced at different points, as in large bridges with several traffic lanes, is emphasized.

2. STRESS ANALYSIS

A simply supported cross beam loaded by a shear force and a bending moment may be used as a model to simulate the load case of interest.

As a first approach to calculate the stress distribution in the critical regions, the web was modelled by two-dimensional in-plane finite elements, and the deck plate together with the stiffeners by in-plane beam elements of equivalent stiffness.

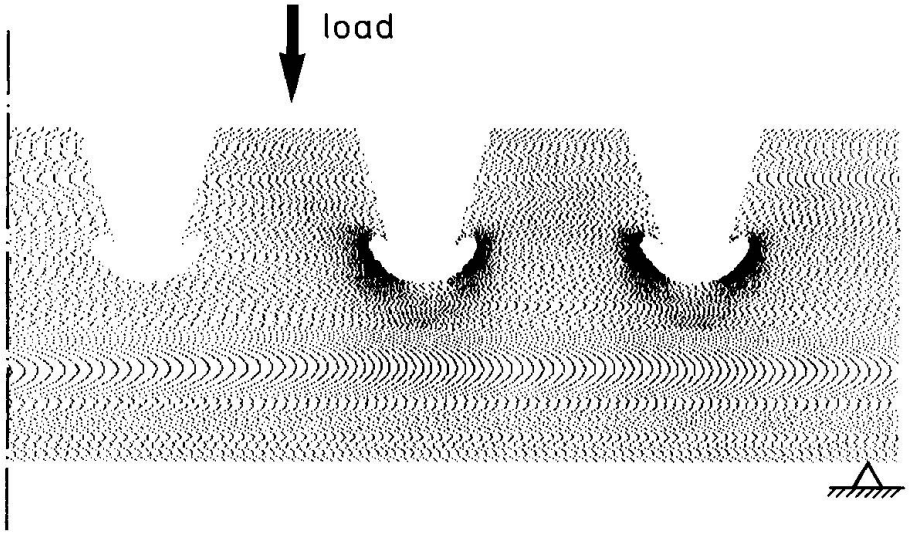

Fig. 2 Global stress distribution in one half of the web loaded as in Fig. 1

Fig. 2 gives an impression of the global stress distribution in the web of one half of the symmetrically loaded cross beam. High stress concentrations occur at the edges of the cut-outs but only in the beam segment loaded by a shear force. The level of high spot stresses depends on the shear force and nearly not on the bending moment. These high stresses at the edges of the cut-outs can be explained by bending the so-called teeth of the web located between each two cut-outs. The bending is produced by a shear force acting between each tooth and the deck plate because the deck plate is the upper flange of the cross beams.

Fig. 3 shows the distribution of the bending stresses in the narrowest section of one tooth between two cut-outs calculated by finite elements and verified by strain measurements. When comparing the highest spot stress with the nominal bending stress at the edge of the cut-outs, the stress concentration factor can be estimated. It yields $K_t \approx 2.8$ in this example.

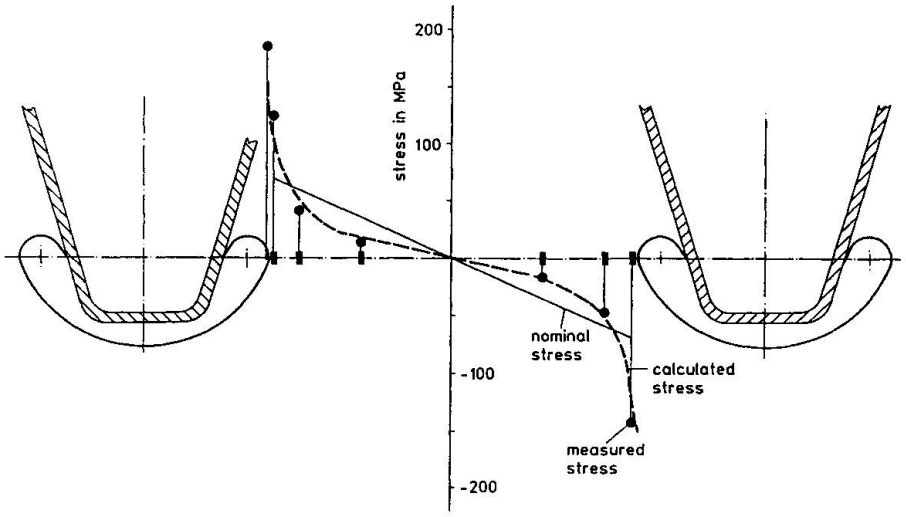

Fig. 3 Stress distribution in the narrowest section between two cut-outs

Generally, the stress level at the edges of the cut-outs exceeds the stresses in all other parts of the web by a factor larger than 5. Therefore, one design objective must be to have a better exploitation of material i.e. to reduce the stress concentration. Basically, this can be achieved by an extension of the distance between the stiffeners. This, however, requires a change of the whole orthotropic deck design. Therefore, the only reliable solution seems to be to change the cut-outs' shape. But this may influence fatigue at the second critical point where the welds connecting the stiffeners to the web meet the cut-outs.

After investigating cross beams of railway bridges, Haibach and Plasil proposed a new shape of cut-outs [1]. They found it superior with respect to fatigue to the commonly used shape when performing fatigue tests on cross beams simulating the particular load case of a railway bridge with one rail. But they did not quantify the gain with respect to strength and fatigue life. This question and the question whether the new shape can also be recommended for large highway bridges under the load case just defined are of interest.

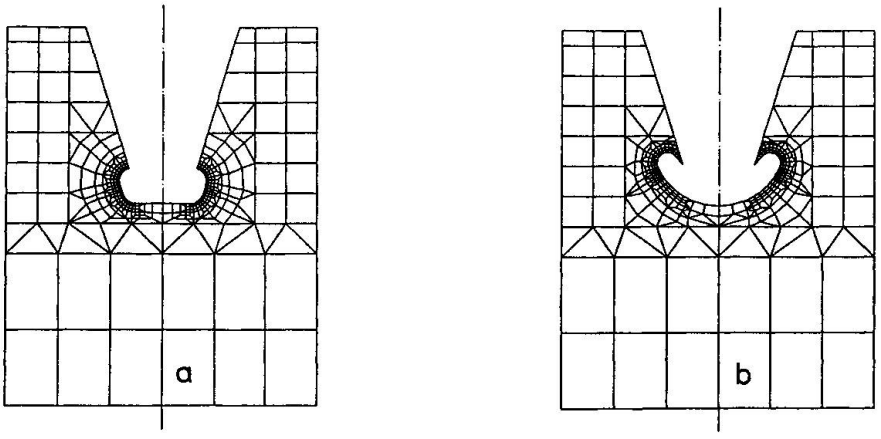

Fig. 4 Cut-outs of the commonly used (a) and of the new (b) shape modelled by finite elements

Fig. 4 shows the commonly used and the new shape of cut-outs modelled by finite elements. The stress distributions along the edges of both types of cut-outs differ significantly (Fig. 5) when the cross beam is loaded as shown in Fig. 1. But the levels of the maximum stresses are nearly the same. Only the volume of highly stressed material and the highly stressed surface at the edges of the cut-outs, respectively, are considerably larger for the commonly used shape. Besides this small advantage of the new shape at one of the critical points, the stresses are reduced at the second point where the welds meet the cut-outs. This result was verified by measurements because the accuracy of the used finite element model is questionable in the vicinity of the welds.

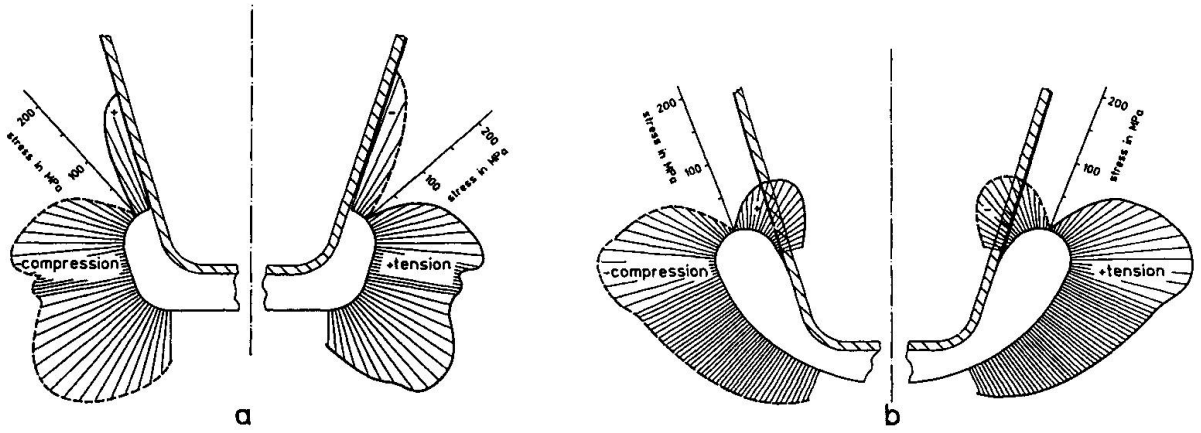

Fig. 5 Stress distribution along the edges of the cut-outs of the commonly used (a) and the new (b) shape

3. TEST DESCRIPTION

Three test specimens of nearly original size were fabricated as orthotropic decks of real bridges, each consisting of a cross beam, six stiffeners, and a deck plate made of structural steel St.53 (Fig. 1). The dimensions of all three specimens were identical except that one had cut-outs of the commonly used shape and the other two the proposedly improved shape. When a specimen is loaded as shown in Fig. 1, four of the six cut-outs are stressed nearly at the same level. This is due to the equal shear force at four of the cut-outs. Therefore, from each fatigue test up to four results could be expected, provided that cracks are detected early and repaired. Three fatigue tests were performed, one with constant amplitude loads applied to a specimen with cut-outs of the new shape and two using identical variable amplitude load sequences applied to the other two specimens with differently shaped cut-outs.

At the beginning of each test, the strains were measured at symmetrically located points on each specimen to guarantee the symmetry of loading. In particular, the torsional moment in the specimens was observed and reduced by changing the points of load introduction until its contribution to the maximum stresses was less than 5 %. Thus, reproducible test results could be expected.

The traffic induces mainly fluctuating compressive loads on the cross beams of bridges. The test rig with the simply supported cross beam allows to simulate this loading.

3.1 Constant amplitude test

The load range of the constant amplitude test was determined taking into account the test results of Haibach and Plasil [1] at

$\Delta P = 485$ kN
with an upper load of $P_u = 500$ kN
and a lower load of $P_l = 15$ kN.

This load results in a stress range of $\Delta \sigma = 480$ Mpa

at the edges of the cut-outs with
an upper stress of $\sigma_u = 495$ Mpa
and a lower stress of $\sigma_l = 15$ Mpa.

The results of the constant amplitude test are given in Fig. 6.

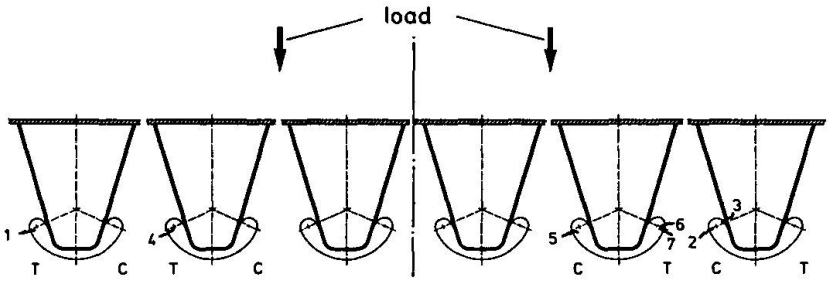

T: region with tension stresses
C: region with compression stresses

crack no. 1 after 205 000 cycles
crack no. 2 after 339 000 cycles
crack no. 3 after 339 000 cycles (no crack growth observed)
crack no. 4 after 344 000 cycles
crack no. 5 after 350 000 cycles
crack no. 6 after 350 000 cycles
crack no. 7 after 350 000 cycles

Fig. 6 Results of the constant amplitude test on one of the specimens with cut-outs of the new shape

3.2 Variable amplitude tests

Time histories of traffic loads acting on bridge components may be found by measurements or may be derived by a computer program developed as a part of the joint research project [2]. The program requires input data to describe the traffic on the bridge and the load transfer in the bridge from the wheel contact points to the points of interest. Fig. 9 shows a frequency distribution of range pair cycles counted from a load time history of a cross beam, which was calculated by the program due to 10000 vehicles passing the bridge on one lane.

From this range pair frequency distribution a first load sequence to be applied to the tests was developed by randomly deriving compressive load cycles. Although the initially calculated load time history contains small traction forces besides high compressive forces due to the applied influence line of load transfer, the load sequence used only compressive load cycles to maintain the simple test rig of Fig. 1.

As a result of damage calculation by Miner's Rule and in order to achieve acceptable test times an omission level was chosen that reduced the applied frequency distribution of Fig. 7 to 3084 from originally 15243 cycles which produce 98.5 % of the calculated damage. The load level was fixed to

the maximum load	P_{max}	=	500 kN
the minimum load	P_{min}	=	15 kN and
the maximum load range	ΔP_{max}	=	485 kN

which means the same nominal loads as in the constant amplitude test.

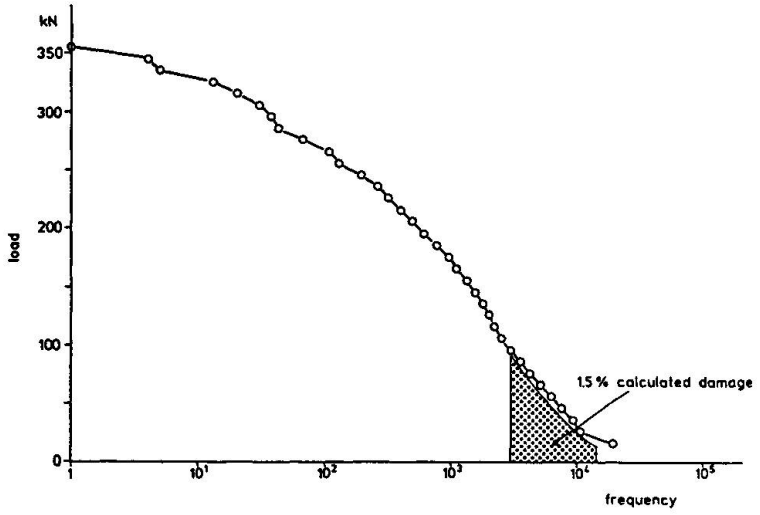

Fig. 7 Frequency distribution of the load sequence used in the variable amplitude tests

The results of both variable amplitude tests with the specimens of both cut-out types are given in Fig. 8 and 9.

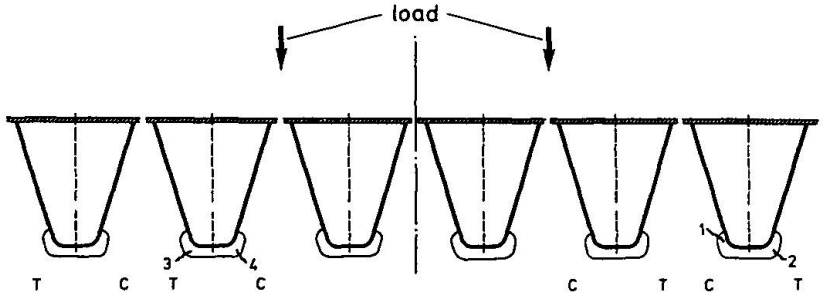

crack no. 1 after 2 844 200 cycles
crack no. 2 after 3 409 900 cycles
crack no. 3 after 4 541 000 cycles
crack no. 4 after 5 780 300 cycles
end of test after 5 926 600 cycles

Fig. 8 Results of the variable amplitude test on the specimen with the commonly used shape of cut-outs

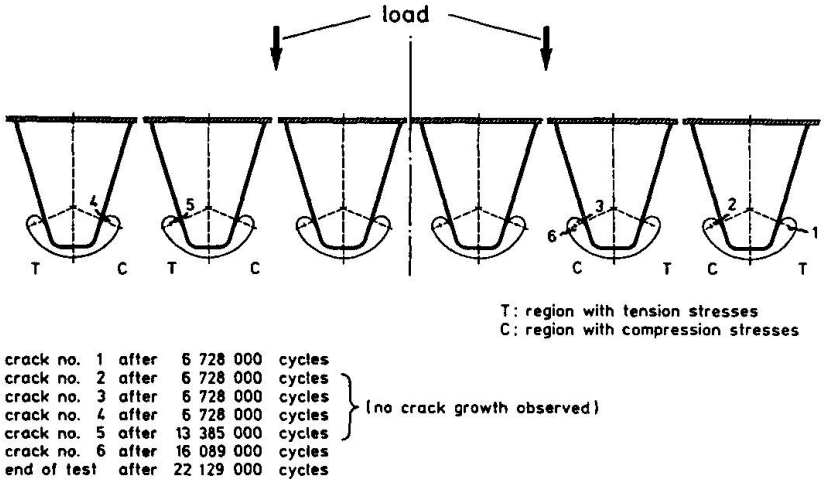

Fig. 9 Results of the variable amplitude test on one of the specimens with cut-outs of the new shape

4. DISCUSSION OF TEST RESULTS

Cracks were observed at both critical points of the stiffener to cross beam connection. Cracks at the ends of the welds occured only in the specimens with the new shape of cut-outs, although this shape was developed to reduce the stresses in this region. In fact, the stresses due to the external loads are really low, as proved by measurements. Therefore and since the cracks did not grow after their detection, residual stresses must have contributed to crack initiation.The new shape of the cut-outs seems to favour residual stresses to appear locally at the ends of the welds because the heat-flux into the web is during the welding restricted by the small area of material.

In contrast, the cracks initiated at the free edges of the cut-outs grew and would have destroyed the specimens if they had not been repaired. These cracks occurred at the cut-outs of the new shape after a 3 - 5 times higher number of load cycles than at the commonly used shape during the identical variable amplitude tests This is a considerable improvement of fatigue life.

However, cracks occurred at edges stressed in compression under external loads while other edges stressed in tension at the same level remained crack-free. The cracks under tension grew faster than those under compression. Moreover, the cracks in the compression regions remained open when the load was removed. These observations can only be explained by residual stresses globally distributed in all three specimens.

Residual stress fields are known to exist in large welded structures. Thus it is not clear, whether the observed increase of fatigue life can be attributed to the new shape of the cut-outs or is at least partially due to a more favourable residual stress distribution. These doubts are supported by the results of stress analysis which show no significant differences between the maximum stresses at both types of cut-outs (Fig. 5).

All test results are summarized in Fig. 10, those of the variable amplitude test on the specimen with cut-outs of the new shape in two representations one using nominal loads and really endured load cycles and the second using equivalent loads and equivalent load cycles as defined in Fig. 10. This was done to compare all results from the specimens with the new shape of cut-outs and to estimate their S-N-curve.

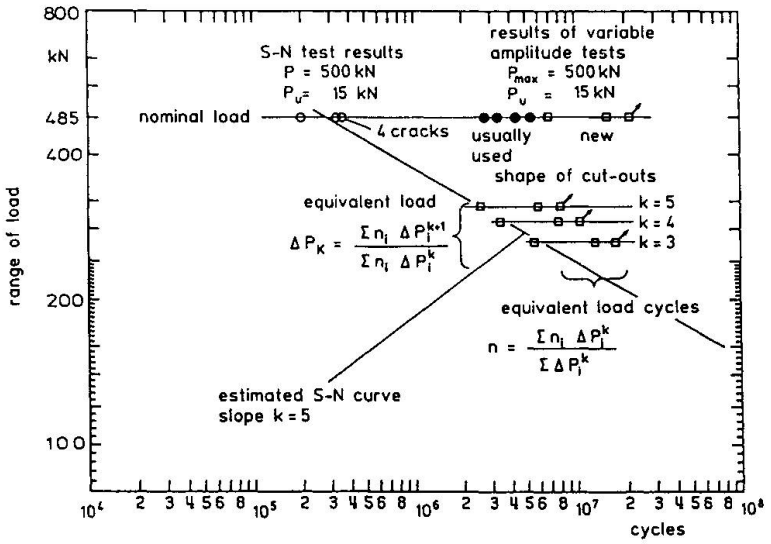

Fig. 10 All results of three tests

5 CONCLUSIONS

As a consequence of the above-mentioned shortcomings a recommendation for the new shape is not yet possible, though it showed an improved fatigue behaviour in the test performed. The following measures during design and fabrication can improve the fatigue strength at both mentioned critical points of the stiffener to cross beam connection

- a reduction of the stress concentration at the edges of the cut-outs by increasing the notch radius
- a reduction of the residual stresses at the ends of the welds between the stiffeners and the web by a shape which improves the heat-flux during welding
- the control of residual stresses introduced into the structure during fabrication to avoid unfavourable residual stresses.

REFERENCES

1. HAIBACH E., PLASIL I., Untersuchungen zur Betriebsfestigkeit von Stahlleichtfahrbahnen mit Trapezhohlsteifen im Eisenbahnbrückenbau. Der Stahlbau 9, 1983.

2. BRULS A., Mesures et Interpretation des Charges Dynamiques les Ponts. Rapport Final de la Premier Phase de la Research. Liège, 1979.

Leere Seite
Blank page
Page vide

Assessment of Fatigue Life of Orthotropic Steel Decks

Evaluation de la durée de vie des dalles orthotropes en acier

Berechnung der Lebensdauer orthotroper Platten aus Stahl

Aloïs BRULS
Lecturer
University of Liège
Liège, Belgium

Aloïs Bruls, born 1941, received his civil engineering degree from the University of Liège in 1965. He is currently a research engineer with the laboratory of the Department of Bridge and Structural Engineering at the University of Liège and a consultant with the company Delta G.C. in Liège.

SUMMARY

Using traffic measurements, a finite band computer program calculates stress range histograms at the joints where cracks occur. Further, as the fatigue strength has been obtained by tests, the fatigue life is calculated. Finally general information is given that allows an orthotropic steel deck design to account for traffic flow.

RÉSUMÉ

En considérant des mesures du trafic, un programme d'ordinateur utilisant les bandes finies calcule les histogrammes des amplitudes de contraintes aux points d'apparition des fissures. Par ailleurs, comme la résistance à la fatigue a été obtenue sur la base d'essais, la durée de vie est calculée. Finalement, des informations générales sont données pour la conception des dalles orthotropes en acier en fonction du volume de trafic.

ZUSAMMENFASSUNG

Mit Hilfe eines Finite-Elemente-Programmes werden unter Berücksichtigung von Verkehrsmessungen für Punkte, von denen Risse ausgehen, Histogramme der Spannungsamplituden berechnet. Da die Ermüdungsfestigkeit aus Versuchen bekannt ist, kann die Lebensdauer berechnet werden. Es folgen einige allgemeine Angaben zum Entwurf orthotroper Stahlfahrbahnplatten in Abhängigkeit des Verkehrsvolumens.

1. INTRODUCTION

The main parts of the connection stiffener-deck are the deck plate, the stiffener and the weld between them.
Usually the deck plate is minimum 10 or 12 mm thick and the surfacing thickness is, following the case +/- 10 mm or +/- 60 mm.

The stiffener studied have a closed trapezoïdal shape (Fig. 1). Stiffener dimensions are about 300 mm wide, 250 mm high and 6 mm thick. They are placed 300 mm apart. Because of the closed sections of stiffeners, welding is realized on only one side of the stiffener web. The aim of this work is to know the fatigue life of this weld. Therefore, we use wheel load measurements of traffics, a finite band computer program and fatigue tests. This paper summarizes a work realized in Belgium with the help of the European Community [1].

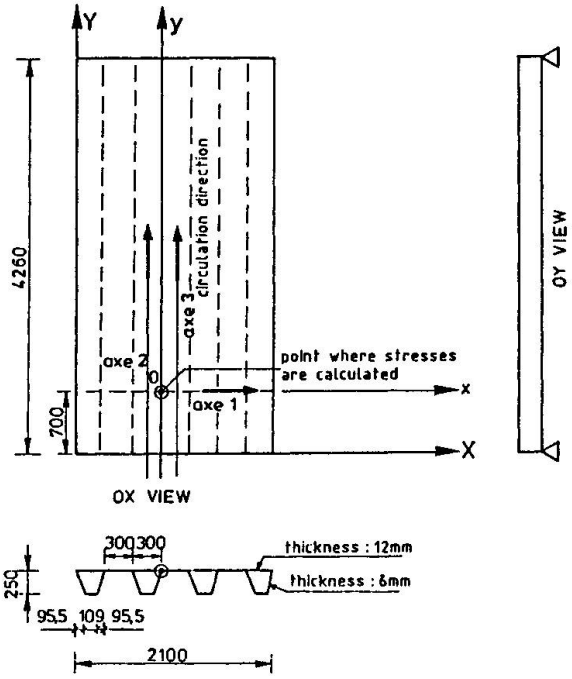

Fig.1 : Structure used for the calculation

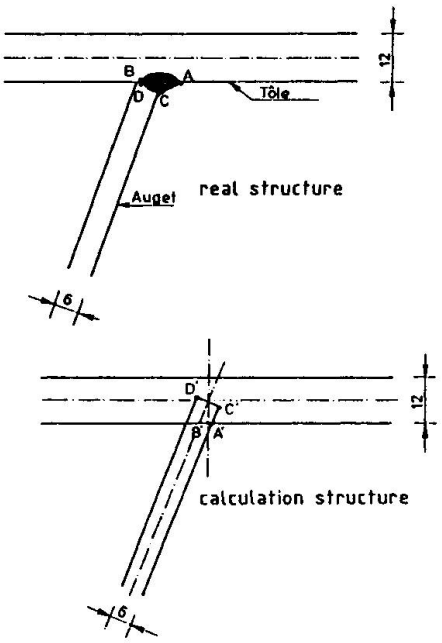

Fig. 2 : Detail

2. STRESS DETERMINATION

2.1 Traffic measurments

During previous works [2][3], the stresses near the weld are measured under traffic loads and under vehicles of calibrated load. These measurements are influenced by the distribution of wheel load, in intensity, in transverse position, and by temperature. The temperature influences the behaviour of the surfacing and its collaboration with the steel plate. On the other side, it is not possible to measure a stress at crack initiation point.
As simultaneously with the stress measurements, the axle loads of the vehicles are recorded, load histograms may be established for three types of wheels : normal wheel, extra large wheel, twin-wheels.

In this paper we consider only the traffic recorded in Rheden in 1978, because it is very well known and very aggressive [4].

2.2. Calculation

In view to have a general approach of the behaviour of the weld connection under wheel load, it is necessary to develop a stress calculation method. Stresses have been calculated by a finite band program. The frame used for the calculation has the geometry of orthotropic decks met in Belgium bridges (Fig. 1). The points where stresses are calculated are located in the neighbourhood of the weld (Fig. 2). Points A', B' : in the deck plate ; points C', D' : in the weld.

Axial and bending stresses are calculated in the cross-section in which they are the highest (section 0 - axis 1 - Fig. 1).
With the finite band program it is possible to study influences of the following parameters :

- dimensions of wheel contact area depending of the type of wheel (Fig. 3) and the surfacing :
  - deck without surfacing :load does not diffuse ;
  - deck with a 60 mm surfacing thickness : load diffuses through the tickness with an angle of 45° ; no composite effect is considered.

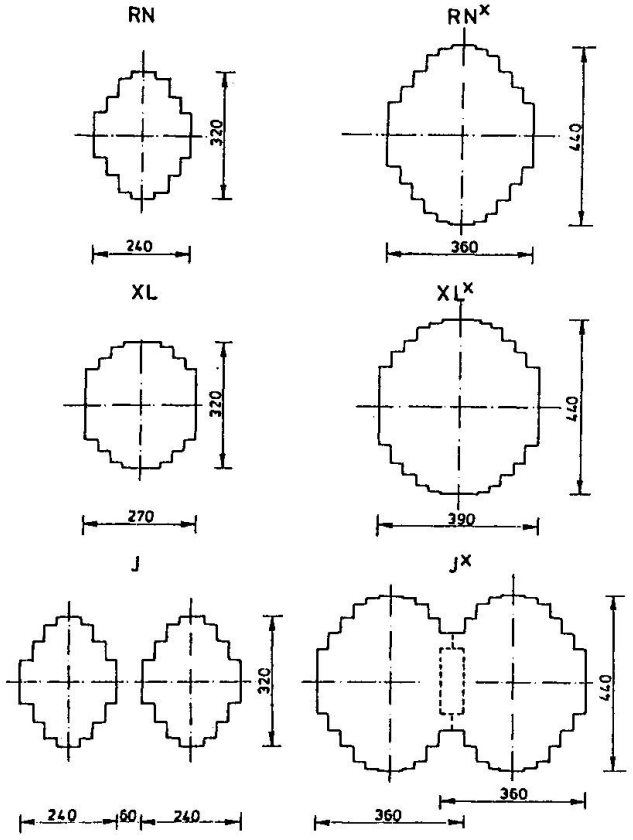

Fig 3 Wheel contact area

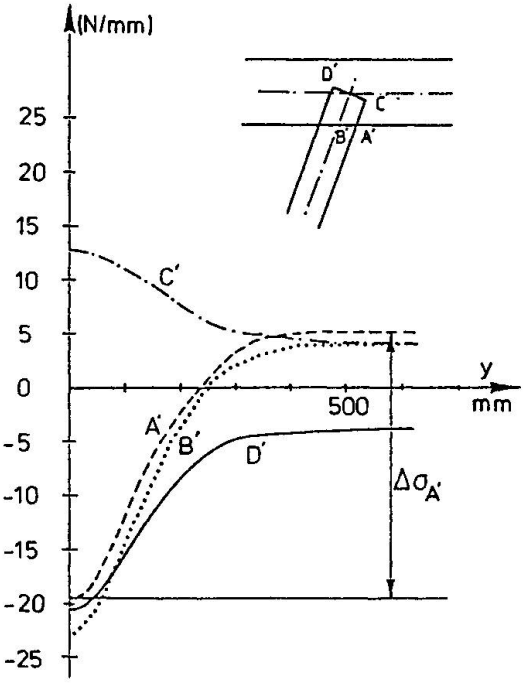

Fig. 4 σ influence line in 0 for a 10kN circulating on axis 2

- wheel longitudinal location : longitudinal influence lines are drawn in Fig. 4. It appears that at points A' and B' (deck plate) stress values change sign at a certain distance from 0 section. Thus stress amplitude at point A' and B' is higher than the maximum stress obtained when the wheel is on axis 1 ;
- wheel transverse location : results are presented in forms of transverse infuence lines (Fig. 5 and 6).

2.3. Stress histograms.

The calculation of the stress spectra is made by means of the simulation program [5][6]. For each axle of the traffic the program chooses at random a transverse position on the deck plate to which corresponds a value of the transverse influence line (Fig. 5 and 6). This value, multiplied by the load of the axle, gives the stress induced.

The data introduced in the simulation program are :

1. Traffic : the vehicle axles of the Rheden traffic have been divided in four groups according to their wheel type [4].
2. Transverse distribution : the axle transverse distribution is obtained from measurements [2][3].
3. Transverse influence lines : calculated following the above mentioned computer program.

The histogram obtained at point D' and given in the table 1 is used for fatigue tests under variable amplitude and for the fatigue life calculation.

Stresses σ_i (N/mm²)	Number	Stress-ranges $\Delta\sigma_i$ (N/mm²)	Number
70 - 80	13	10 - 20	6767
60 - 70	19	20 - 30	4163
50 - 60	61	30 - 40	2489
40 - 50	222	40 - 50	1690
30 - 40	635	50 - 60	1090
20 - 30	1175	60 - 70	872
10 - 20	2751	70 - 80	601
0 - 10	5176	80 - 90	441
0	12627	90 - 100	314
-10 / -0		100 - 110	253
-20 / -10	6629	110 - 120	142
-30 / -20	4348	120 - 130	134
-40 / -30	2348	130 - 140	81
-50 / -40	1668	140 - 150	48
-60 / -50	1068	150 - 160	17
-70 / -60	570	160 - 170	21
-80 / -70	365	170 - 180	11
-90 / -80	189	180 - 190	7
-100 / -90	83	190 - 200	5
-110 / -100	36	200 - 210	2
-120 / -110	9	210 - 220	2
-130 / -120	7		
-140 / -130	2		
TOTAL	40000	-	19150

Table 1

Stress and stress-range histograms at point D' (variable amplitude tests)

Fig 5 : σ_A Influence lines for a wheel (axis1 ; y=0)
transverse repartition

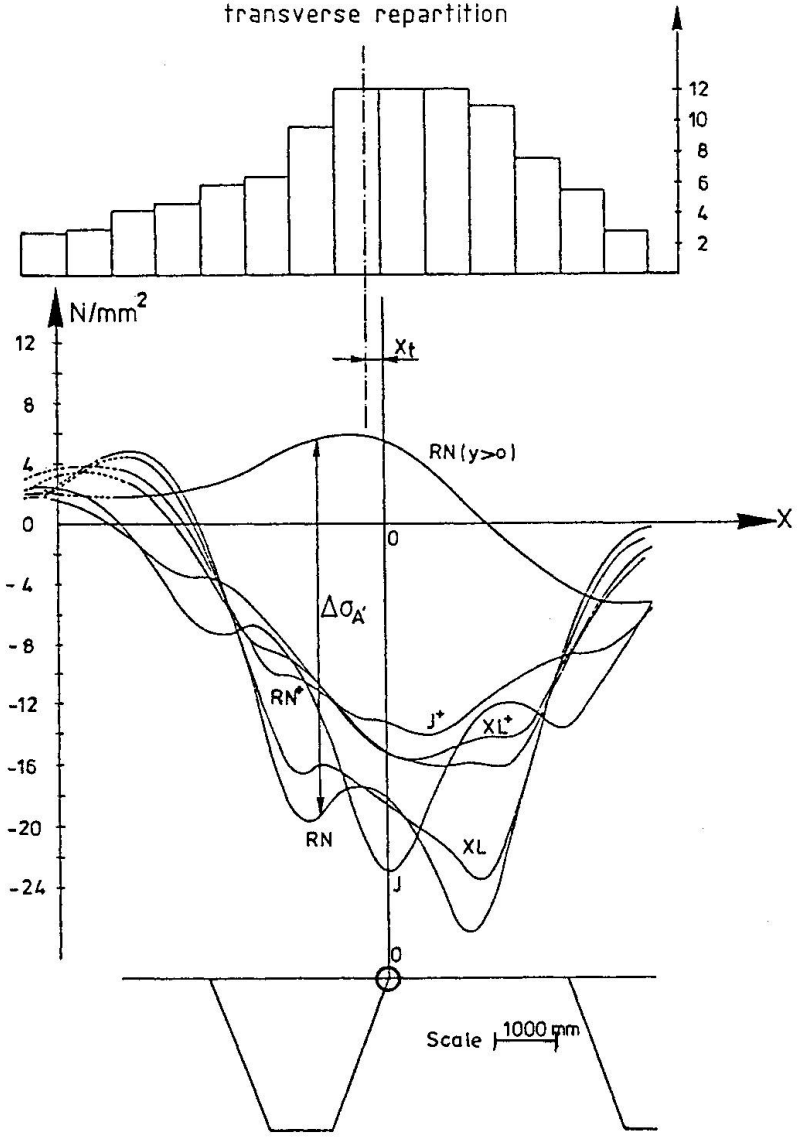

Fig 6 : σ_D Influence lines for a wheel (axis1 ; y=0)
transverse repartition

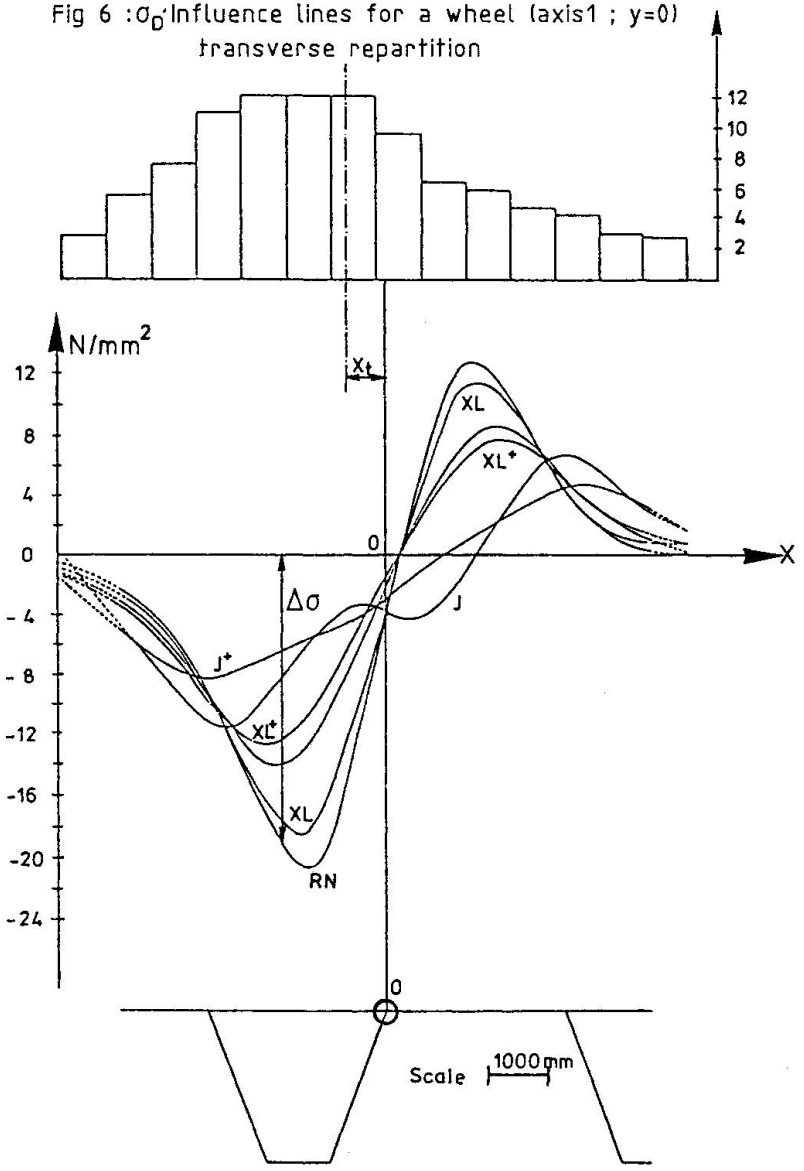

3. FATIGUE STRENGTH

3.1 Test specimens

The loading mode and the geometrical characteristics of the specimens are given in figure 7.
The material used is of the type E 36-4.
General welding procedure characteristics are :

- no edge stiffener preparation ;
- horizontal position ;
- one run ;
- no preheating ;
- no postheating ;
- automatic welding (submerged arc).

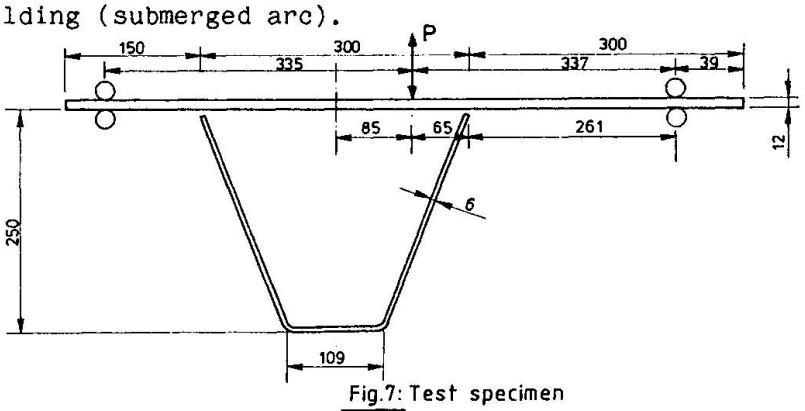

Fig.7: Test specimen

Welding procedure has evolved : firstly the procedure was manual (CRIF [7]), now it is automatic submerged arc welding and it is still evolving to obtain a smaller lack of penetration.

The geometrical characteristics of the welds tested are given in table 2.

Specimen	Lack of penetration	Fillet weld
CRIF [7]	3,0 to 4,5 mm	3,5 to 4,5 mm
Ulg [1]	1,5 to 2,5 mm	4,7 to 6 mm
IRSID [8]	+/- 1 mm	5,5 to 6,5 mm

Table 2

The tests realized under constant amplitude determine the S-N curve. Some tests realized under variable amplitude gives information about the possibilities of a damage calculation applicating the Miner Rule.

3.2. Test result

3.2.1. Presentation

Depending on the stress distribution in the deck plate and in the trough, as well as the weld quality (penetration, throat, underents, ...,) fatigue cracking may occur either :

a) from the weld toe on the deck plate, point A Fig. 2, and develops in the decks plate that corresponds to $\Delta\sigma_d$;

b) from the weld root in the stiffener, point D Fig. 2, and develops in the throat of the weld ; that corresponds to $\Delta\sigma_s$.

From these tests are derived the nominal stresses definition to be used in the fatigue S-N diagrams, by extrapolating the measured stresses.
The results obtained earlier by CRIF [7] and recently by ULg [1] and IRSID [8] are presented on Fig. 8 and Fig.9.

3.2.2. Failure in the deck plate $\Delta\sigma_d$.

Tests under constant amplitude determine the fatigue strength of the deck plate at the weld toe. Results are plotted on Fig. 8.

Main conclusions are :

- There is no significative differences between specimen with 2 mm gap between the top of the stiffener web and the deck plate and specimen with no gap provided the lack of penetration is less the 2 mm.
  The mean Wöhler curve is determined with $R_S = 1$ in the weld root for the specimen tested at IRSID :

$$\Delta\sigma_d = 26777\ N^{1/3} \quad (m = 3 \text{ imposed})$$

  and the characteristic value for 97,5 % is

$$\Delta\sigma_{dc} = 163\ N/mm^2 \text{ for } N_c = 2.10^6 \text{ cycles.}$$

- The two tests conducted at IRSID show a lower fatigue resistance at R = 0,1 than R = -1. Nevertheless, two similar tests performed at Liège do not indicate such a detrimental effect.
  In only two U.Lg. specimens did failure occur in the deck plate that corresponding to $R_S = 0$ (only tensile at point A).

The loading histogram used for tests under variable amplitude is the stress spectra calculated (table 1). This histogram simulates traffic effects. Loads are applied at random on the test specimen, taking in account the sign of the stresses. The results of tests are plotted in Fig. 8 by their equivalent values $\Delta\sigma_e$, n_e calculated from the histogram with an SN curve with a slope of -1/3, corresponds to the centre of gravity of the damage distribution [9][10] :

$$\Delta\sigma_e = \frac{\sum_{\Delta\sigma_i}^{\infty} n_i . \Delta\sigma_i^4}{\sum_{\Delta\sigma_i = 0}^{\infty} n_i . \Delta\sigma_i^3} \qquad n_e = \frac{\sum_{\sigma_{i=0}}^{\infty} n_i . \Delta\sigma_i^3}{\Delta\sigma_e^3}$$

Results are similar to those obtained with constant amplitude loading.

3.3.3. Failure in the weld $\Delta\sigma_s$.

Tests results under constant amplitude are plotted on Fig. 9.
Main conclusions are :

- the fatigue strength increases significantly when using automatic welding, this technique allows larger penetration and throat thickness at the weld.
- the mean S-N curve is determined for automatic welding :

$$\Delta\sigma = 17258\ N^{1/3}$$

and the characteristic value for 97,5 % is

$\Delta\sigma_{sc}$ = 114 N/mm² for $N_c = 2.10^6$ cycles.

- The tests show the importance of R_s ratio. To obtained the failure in the weld it was necessary to have more tension than compression at the root of the weld (point D) :

$1 < R_s < 0$ in the Ulg specimens

R_s = 0,1 in the IRSID specimen.

The loading histogram used for tests under variable amplitude is the calculated stress spectra (table 1).
The loads are applied random, but to obtain failure in the weld (point D), it has been necessary to change the sign of the stress calculated, so that there is more tension than compression : R_s = -0,5 instead of - 2,0 at the root for the highest stress range.
The results are plotted in Fig. 9 by their equivalent values assessed as in Fig. 8.
Results are similar to those obtained with constant amplitude loading.

4. FATIGUE LIFE CALCULATION

We consider as characteristic stress range the values deduced from the fatigue tests. For $N_c = 10^6$ cycles :

$\Delta\sigma_{sc}$ = 114 N/mm² , if the crack occurs in the weld (point D) ;

$\Delta\sigma_{dc}$ = 163 N/mm² if the crack occurs in the plate (pointe A).

Following Eurocode 3, the SN curves have two slopes : m = 3 for $N < 5.10^6$ and m = 5 for $5.10^6 < N < 10^8$.
If the traffic composition measured in Rheden is considered [4], the allowed number of lorries during the life time may be calculated. The results are given on table 3.
Putting there data in perspective the traffic flows recorded on highways generally comprise between 1000 and 4000 lorries during a working day [2][3]. Such flows produce after 100 years between 20 and 80.10^6 lorries.
The examination of table 3 calls the following comments :

1. The fatigue life calculated in the deck ($\Delta\sigma_d$) is always a little longer than in the weld ($\Delta\sigma_s$) : the higher strength is partially offset by higher stress ranges produced in this point by the traffic loads ;

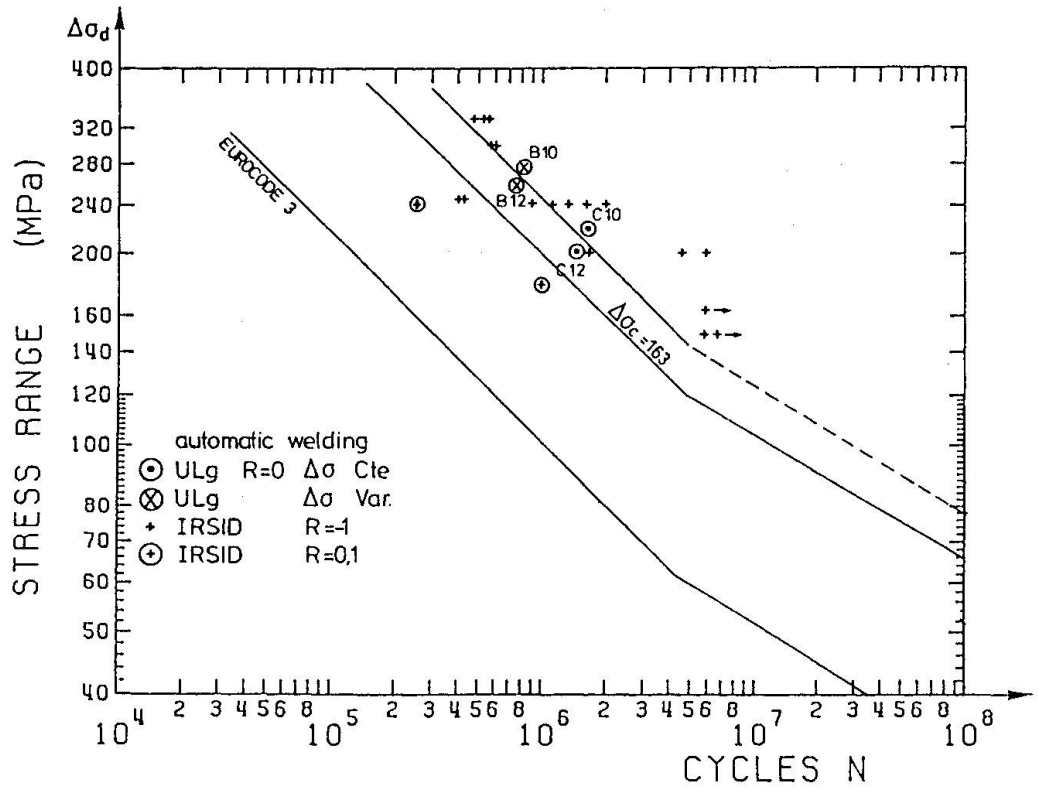

Fig.8: Crack initiation at the weld toe : $\Delta\sigma_d$

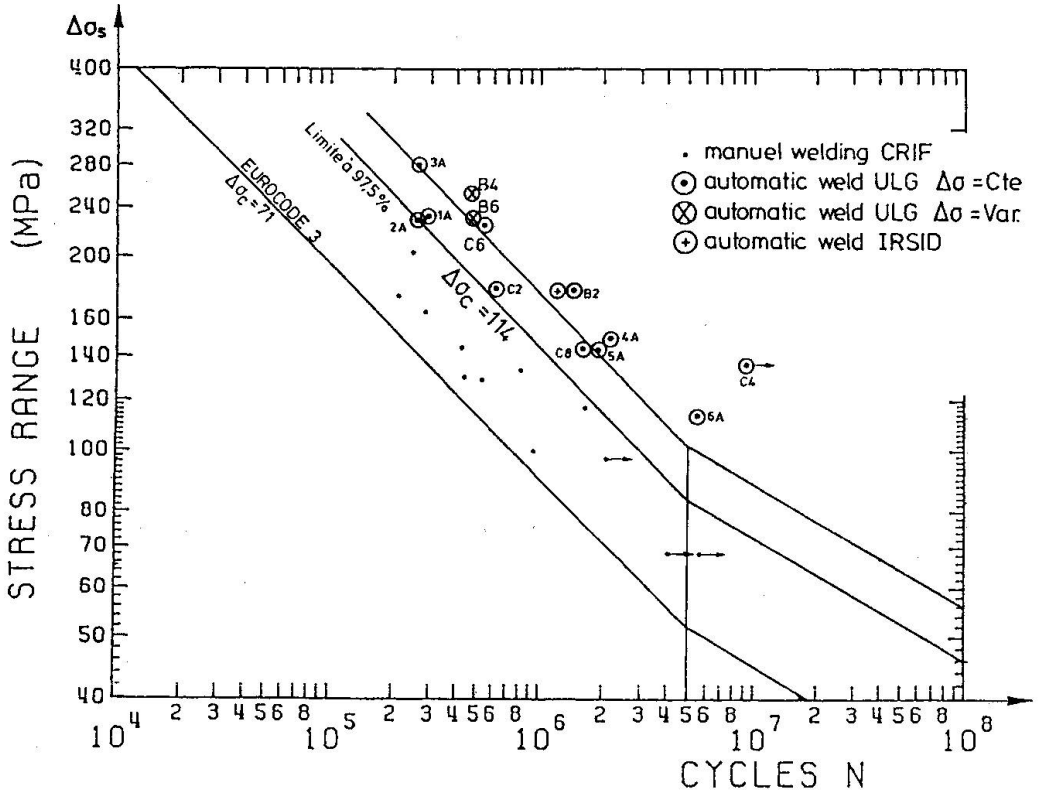

Fig.9: Crack initiation at the weld root: $\Delta\sigma_s$

Fatigue life

Connection Stiffener - Deck plate

Thickness (mm)			Number of lorries (10^6)	
Plate	Stiffener	surfacing	$\Delta\sigma_s$	$\Delta\sigma_d$
12	6	0	20	20
12	6	60	71	75
13	6	0	44	45
13	6	60	199	219
14	6	0	89	103
14	6	60	494	647
14	7	0	62	73
14	7	60	297	393

Table 3

2. A surfacing of 60 mm gives a fatigue life 3 to 5 times longer, than the unsurfaced deck ;

3. An increase in the plate thickness of 1 mm gives a fatigue life +/-2 times longer.

4. An increase in the thickness of the stiffener reduces the fatigue life a little.

5. The given fatigue lives are pessimistic, because the transverse position of the traffic flow considered in the calculation is the most unfavourable and in surfaced deks, now composite effect is considered.

We may conclude :

1° For the weld tested, the failure may not occur in the weld but in the plate, if the thickness of the plate is at least twice as thick as that of the stiffener ;

2° the required thickness of the deckplate depends on the expected number of lorries and the thickness of the surfacing.

5. CONCLUSIONS

The specimens used in the experiments were welded with automatic submerged arc welding in an industrial situation. It has been shown that full penetration, (lack of penetration lower than 1 mm.) can nearly be achieved without edge preparation.

In these conditions, there is no significant difference in fatigue behaviour for specimens with a 2 mm gap by welding or without gap.

For alternate bending, that is a little more severe than the loading in bridges, with a lack of penetration not greater than 1 mm, the cracks initiate at the weld toe in the deck plate.

Using a computer band program it is possible to calculate the fatigue life of the connection taking in account :

- thickness of the surfacing that increases the wheel contact area ;
- geometry of the orthotropic deck ;
- traffic defined by a number of lorries and by load histograms for each type of wheel.

To increase the fatigue life, the designer has the possibility to choose between increasing the thickness of the surfacing or that of the steel plate. Table 3 gives fatigue lives for common sizes of orthotropic plate (Fig. 1).

REFERENCES

[1] BRULS A., POLEUR E. Mesures et interprétation des charges dynamiques dans les ponts - 3e phase - Resistance à la fatigue des dalles orthotropes. Recherche CECA-1989.

[2] De BACK, BRULS, CARRACILLI, HOFFMAN, SANPAOLESI, TILLY, ZASCHEL. Mesures et interprétation des charges dynamiques dans les ponts. Rapport commun de synthèse - 1ère phase - Recherche CECA. Rapport EUR. 7754.1982.

[3] HAIBACH, BRULS, de BACK, CARRACILLI, JACOB, KOLSTEIN, PAGE, PFERFER, SANPAOLESI, TILLY, ZASCHEL. Measurements and interpretation of dynamics loads on bridges - Synthesis report of the 2nd phase - ECSC Research - Rapport EUR 9759. 1986.

[4] De BACK, KOLSTEIN, Measurements and interpretation of dynamics loads on briges. 2d phase. ECSC Research - Report 6.83-6. 1982.

[5] BAUS R. BRULS A. Etude du comportement des ponts en acier sous l'action du trafic routier. Rapport CRIF. MT 145 - 1981.

[6] BRULS A. Mesures et interprétation des charges dynamiques dans les ponts - 2ème phase. Recherche CECA. Rapport EUR 8864 - 198.

[7] THONNARD, JANSS. Comportement à la fatigue des dalles orthotropes avec raidisseurs trapezoidaux. Rapport CRIF MT161-1985.

[8] BIGNONNET, JACOB, Mesures et interprétation des charges dynamiques dans les ponts. 3ème phase. Recherche CECA. 1989.

[9] BRULS, POLEUR, Traffic loads on road bridges. Equivalent loads effects - Eurocode on actions - Part 12 - Traffic loads on raod bridges - Subgroup fatigue - Appendix 2 - 1989.

[10] BRULS, Calibration of a load model for fatigue caculation. AIPC - Workshop. Remaining Fatigue Life of Steel Structures. Lausanne 1990.

Leere Seite
Blank page
Page vide

Fatigue Behaviour of Orthotropic Steel Bridge Decks

Comportement à la fatigue des dalles orthotropes de ponts en acier

Ermüdungsverhalten orthotroper Platten in Stahlbrücken

Stefano CARAMELLI
Prof. of Struct. Eng.
University of Pisa
Pisa, Italy

Maurizio FROLI
Researcher of Struct. Eng.
University of Pisa
Pisa, Italy

Pietro CROCE
Dr. Eng.
University of Pisa
Pisa, Italy

Luca SANPAOLESI
Prof. of Struct. Eng.
University of Pisa
Pisa, Italy

SUMMARY
Recently, some orthotropic steel bridge decks have suffered fatigue cracks. For a better knowledge of this problem, the European Community promoted and financed collective research work in which seven laboratories in six European countries participated. The Italian contribution to this research, deals with the experimental determination, on full scale specimens, of the fatigue behaviour of two types of welded connections of longitudinal stiffeners.

RÉSUMÉ
Récemment, quelques dalles orthotropes de ponts en acier ont montré des fissures de fatigue. Afin d'améliorer la connaissance de ce problème, la Communauté Européenne a encouragé et financé un programme de recherche auquel ont participé sept laboratoires de six pays européens. La contribution italienne, avait pour but de déterminer, de façon expérimentale et sur des éprouvettes en vraie grandeur, la résistance à la fatigue de deux types d'assemblages soudés de raidisseurs longitudinaux.

ZUSAMMENFASSUNG
In letzter Zeit wurden in den orthotropen Platten einzelner Stahlbrücken Rissbildungen infolge Ermüdung beobachtet. Um die Ursachen dieses Problems zu ergründen, wurde unter dem Patronat der Europäischen Gemeinschaft ein Forschungsprogramm zusammengestellt, an dem sieben Laboratorien aus sechs verschiedenen europäischen Ländern beteiligt waren. Der italienische Beitrag behandelt die an Bauteilen durchgeführte experimentelle Bestimmung des Ermüdungsverhaltens zweier verschiedener Schweissverbindungen von Längsrippen.

1. INTRODUCTION

The fatigue cracks appeared on some orthotropic decks of steel bridges after nearly twenty years of service life [1] showed that steel orthotropic decks are sensitive to fatigue problems and that their fatigue strength may not be directly estimated by means of the S-N curves proposed by the European codes which concern simple details used in steel constructions instead of the complex shaped connections of the orthotropic decks.

Beside that, the codified S-N curves are based on experimental results of little size specimens generally free from residual stresses patterns due to the welding procedures and probably less affected than the real scale complex shaped connections by local in the welds. But, as noticed by FISHER [2] and confirmated recently by YAMADA, KENDO, AOKI and KIKUCHI [3], CUNNINGHAME [4], AGERSKOV, BJØRNABAK-HANSEN [5] and others, lack of penetration, residual stresses and dimensions of the connected pieces are the factors that mostly influence the fatigue resistance of the joints.

In order to aquire a deeper knowledge on the static and fatigue behaviour of steel orthotropic decks, the ECSC promoted and financed the collective research programme: "Fatigue strength of orthotropic decks of steel bridges", third phase of the general programme: "Measures and interpretations of dynamical loads on bridges".

The research programme, concluded in 1989, was carried out by seven laboratories of six European countries among those, for Italy, the Istituto di Scienza delle Costruzioni of the University of Pisa.

The Italian programme foresaw the theoretical and experimental determination of the nominal stresses in those points of a real scale orthotropic deck more sensitive to a fatigue cracking risk and the execution of constant amplitude fatigue tests of stiffener to stiffener connections performed both on real scale ribs samples (type B specimens) and on the orthotropic deck panel previously used for the static test (type A specimen) [6].

This paper illustrates that part of the research dealing with the fatigue experiences.

2. FATIGUE TESTS ON TYPE B SPECIMENS

2.1 Description of the specimens and test modalities

The Fe 510C steel specimens, 200 mm long, consist of triangular cross section ribs built by welding a cold formed 6 mm thick steel plate to a top plate 600 mm wide and 12 mm thick. At middle span of each specimen, a type I or type II joint was shop executed reproducing the same working modalities provided for field execution. In figure 1 both type I joint and type II joint are illustrated, while in figure 2 the welding geometries S1÷S4 are shown.

In type I joints, the ribs are interrupted at a distance of about 200 mm astride the connection. The two limbs of the top plate - one of which has the backing strip welded to it (S1 welding) - are placed in such a way to get a root gap of about 6 mm, and thus automatically welded. The missing rib element is then inserted and manually welded in overhead position (backing strip weld S3 (fig. 3)).

In type II joints, the top plate is interrupted for about 200 mm. The stiffener webs are butt welded, with complete penetration, using S4 welding (fig. 4) which is manually executed with coated electrodes. First, the internal part of the ribs is welded in ascending vertical position, then one proceeds to the grooving of the external part and to the restarting of the weld in overhead position. The joining is completed with the insertion of the missing top plate portion, the execution of the S1 flat position welding and the manual overhead remaining wel-

ding S2 between the top plate and the ribs.

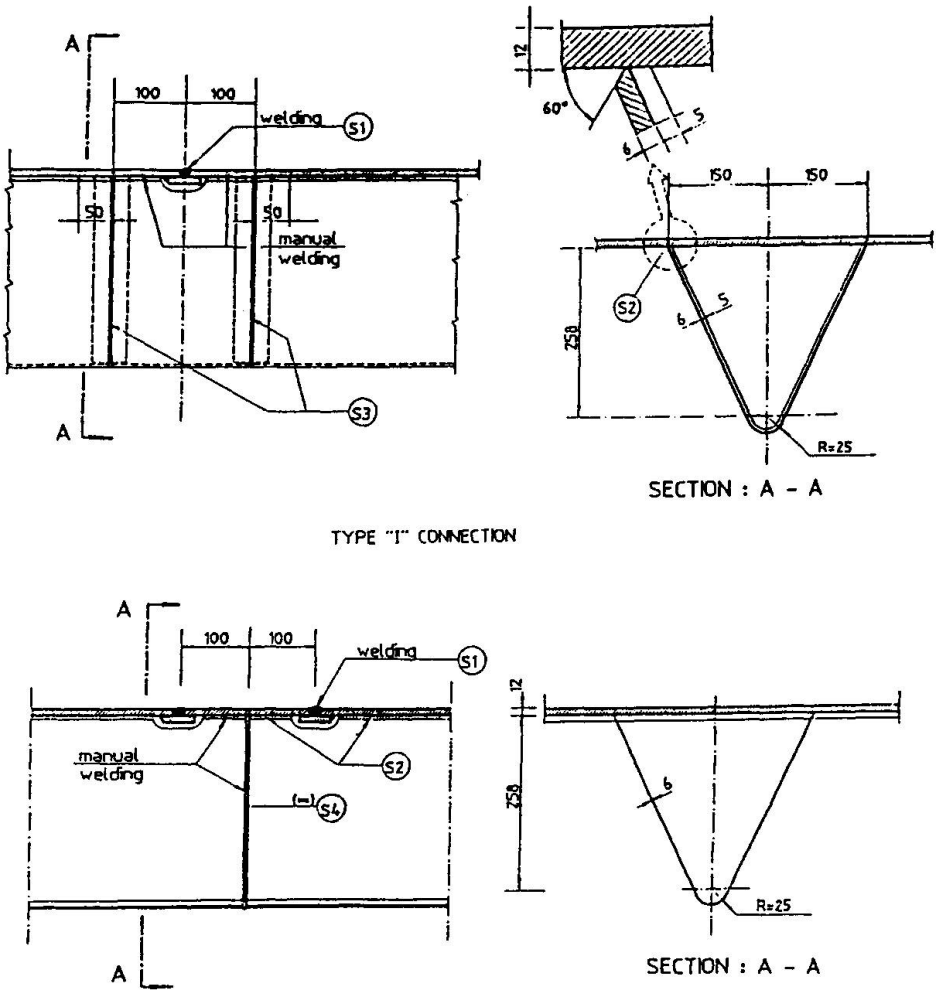

Fig. 1 Type I and type II stiffener to stiffener connections

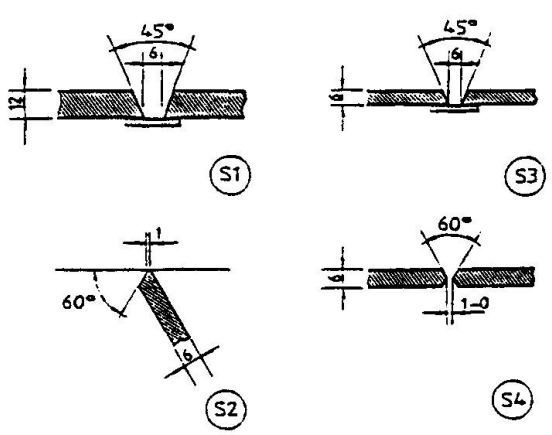

Fig. 2 Edge preparation

All the weldings have been checked by means of visual and magnetic controls. The butt weldings, moreover, have been 100 % X-raied and repaired where found (only one time) not acceptable according to the UNI 7278 Italian Standard.

The fatigue tests at constant stress amplitude, were carried out on nine type I joint specimens and on eight type II joint specimens.

The static test scheme is that of a simply supported beam, 2400 mm spanned, with the fatigue load applied at middle span by a pulsating hydraulic

jack acting with a frequency of 4 Hz.

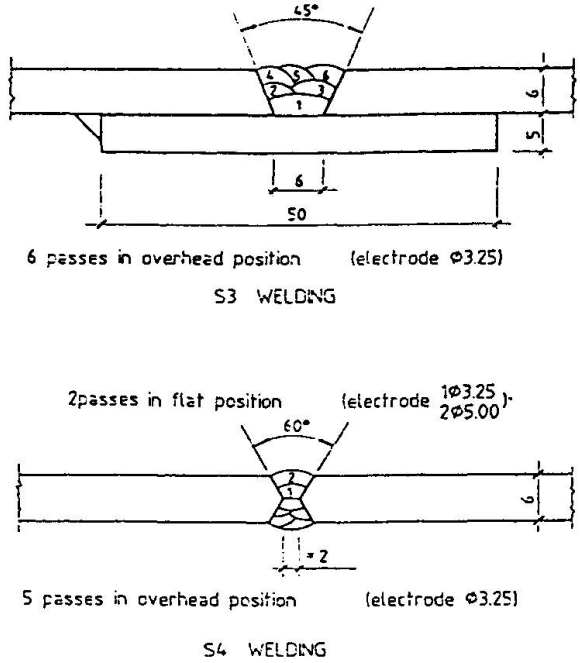

Fig. 3 S3 and S4 weldings

The load was applied on a rectangular neoprene strip 50 mm wide, 600 mm long and 10 mm thick, put between the moving jack and the top plate.

The stresses at the apex of the ribs were measured using electrical strain gauges, placed in a way that allowed the determination of the nominal stress amplitude excluding local peaks.

During the tests, the minimum nominal stress has been kept constantly at 1.5 KN/cm² for all the specimens.

Each test was interrupted at failure, recognized by the specimen's loss of stiffness (an increase of one centimeter of the maximum deflection under load), or when 8,000,000 cycles had been performed without any breaking.

2.2 Experimental results

The experimental results obtained on B specimens with type I joints and type II joints are respectively reported on the bilogarithmic S-N diagrams of figure 4 and 5 together with their mean life curves.

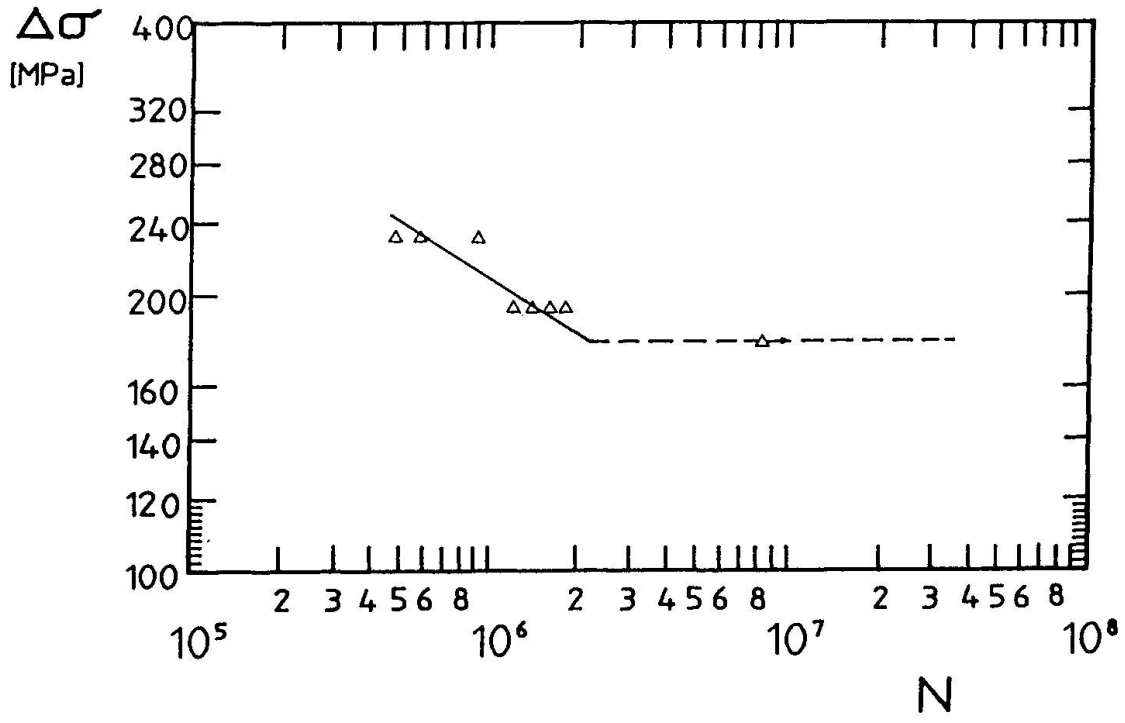

Fig. 4 Fatigue test results of type B specimens with type I joints

The two groups of results are then compared in the diagram of figure 6 from which the fatigue behaviour of type I joints appears to be better than that of

type II joints.

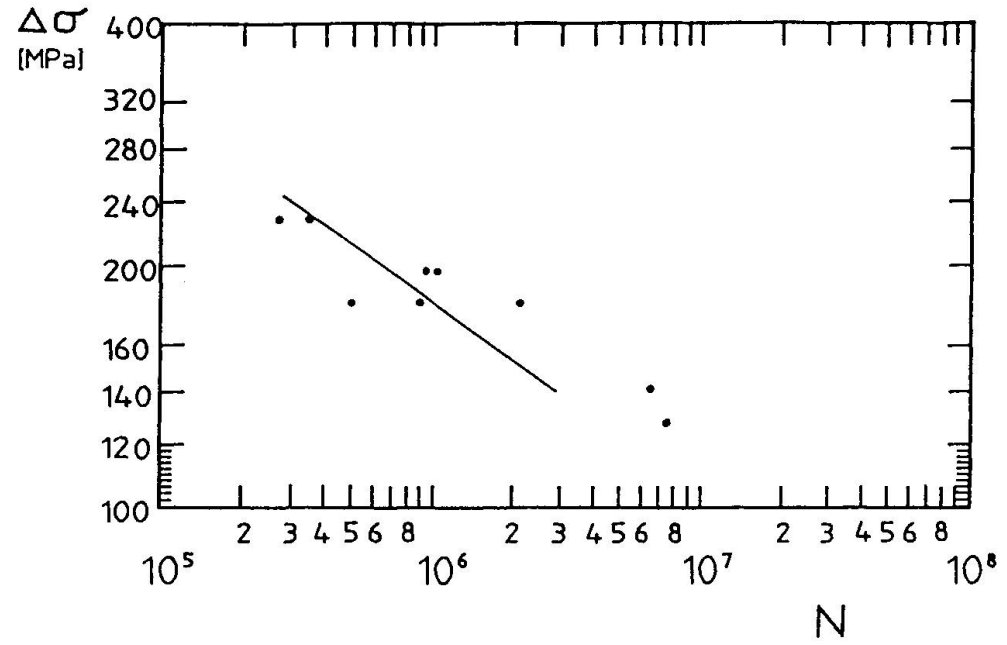

Fig. 5 Fatigue test results of type B specimens with type II joints

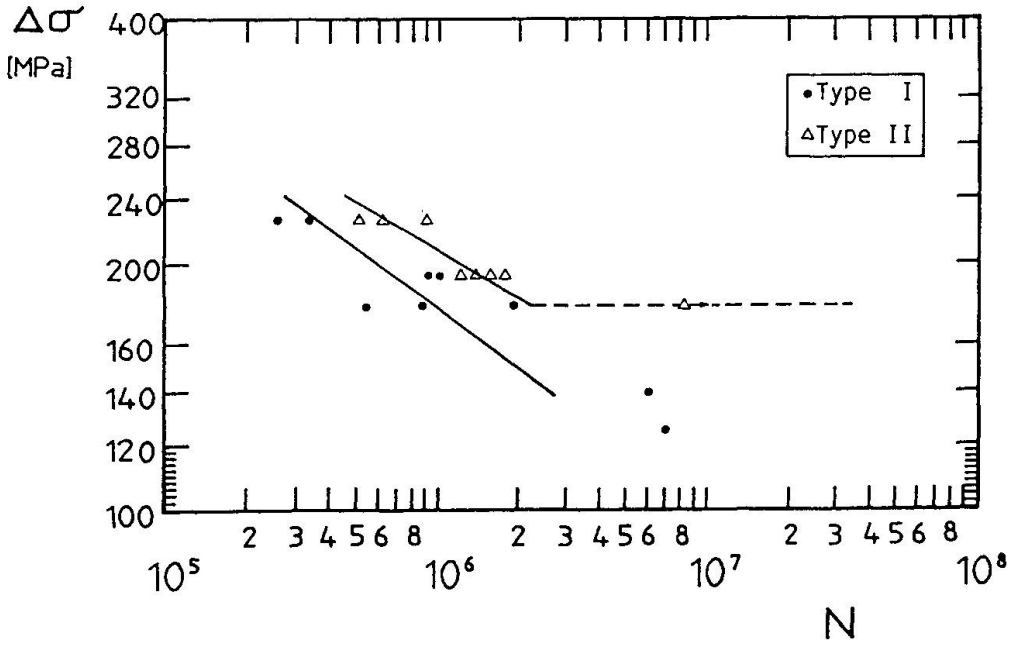

Fig. 6 Comparison between fatigue test results of type B specimens

3. COMPLEMENTARY TESTS

The previous result was rather unexpected because all the existing codes for fatigue design of steel structures classify backing strip welds in a lower position than complete penetration butt weldings (see for example [7]) and it is has also important consequences in the design practice because stiffener to stiffener connections with backing strip welds are more economic than the other welded connections.

In order to get a better understanding on the causes of the different behaviour of the two kinds of joints, it was decided to execute relaxation tests on type B specimens to control the residual stress levels and in the same time to perform a great number of fatigue tests on little size specimens provided with S3 and S4 weldings, for which residual stresses are negligible, to verify wether the different behaviour of the joints was to be attributed to the different types of weldings.

3.1 Residual stresses measurement in type B specimens

Residual stresses have been indirectly measured by means of mechanical relaxation tests executed on some type B specimens provided with type I and type II joints.

The test scheme is the same adopted for fatigue tests. During the test, some loading and unloading cycles have been performed until the steady cycle was reached. At each loading step the longitudinal strains at the lower apex of the stiffeners, close to the weld foot, have been measured.

Two typical load-strain curves related to type I joint and type II joint are reproduced in figure 7: it can be immediately noticed that residual stresses are almost absent in type I joints while one finds that they reach nearly 20 KN/cm² in type II joints.

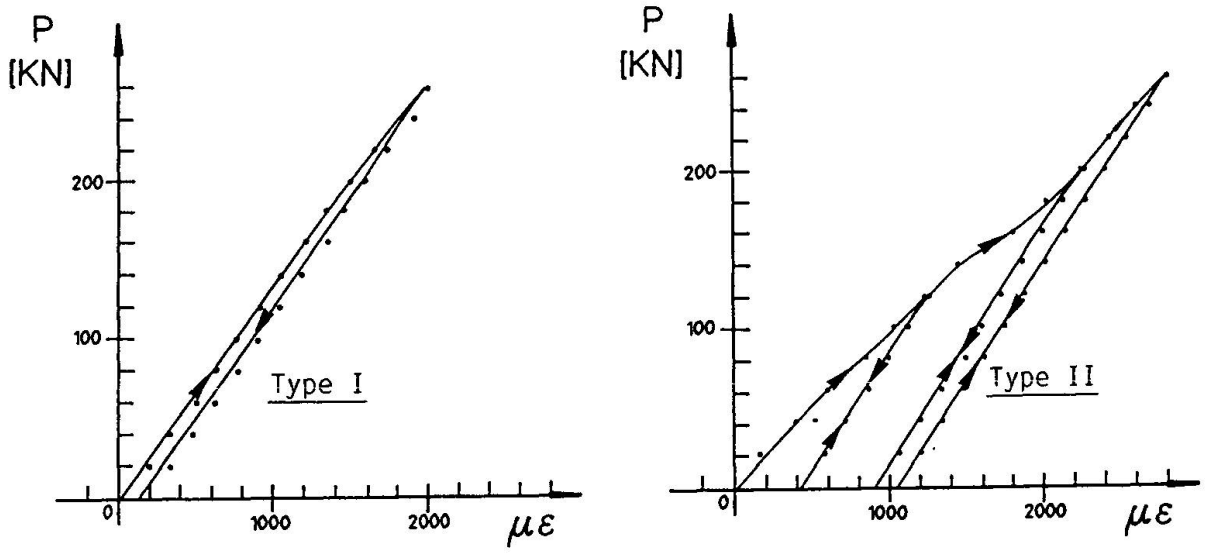

Fig. 7 Load-strain diagrams of the relaxation tests on type B specimens

3.2 Fatigue tests on welding specimens

The samples, 600 mm long, 35 mm wide and 6 mm thick, (figure 8) have been obtained by saw cutting two sheets 2000 X 300 X 6 mm of the same steel used for the stiffeners and welded together with the same modalities (operator position, number and sequence of passes, type of electrode) adopted for the S3 and S4 weldings used in type B specimens. Before cutting, the weldings have been submitted to the same checks executed for type B specimens without finding any defects.

In each specimen the surfaces of the cut have been ground to eliminate every stress concentration due to roughness and than fatigue tested under a tensile load pulsating sinusoidal with a frequency of 12 Hz, by means of a universal test machine Losenhausen UHP10. During the experience, the lowest tensile stress, kept constant for each specimen and equal to that of the type B speci-

mens, was 1.5 KN/cm².

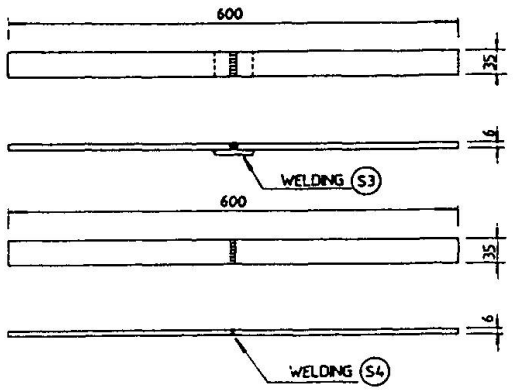

A number of 62 specimens have been tested: 31 with S3 weldings and 31 with S4 weldings.

The results are plotted on diagrams of figures 9 and 10, in which the mean S-N curves and the confidence band related with each group of results (fractile of 5% and of 95%), obtained following the ASTM E739-80, are reported too. It can be noticed that the two mean curves are practically coincident.

Fig. 8 Welding specimens

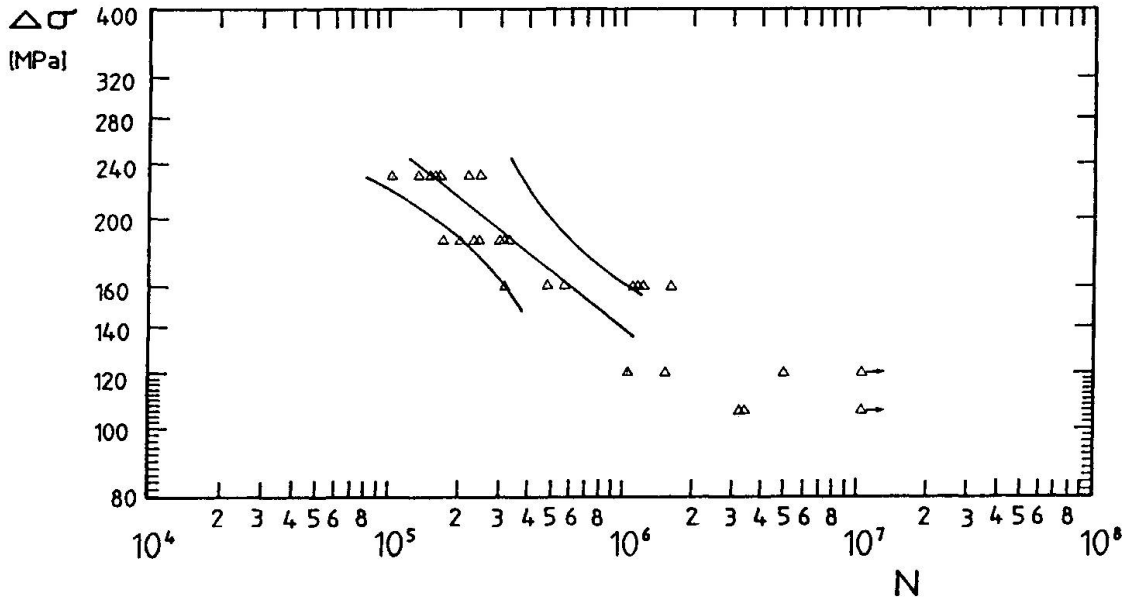

Fig. 9 Fatigue results on S3 welding specimens

4. FATIGUE TESTS ON TYPE A SPECIMENS

4.1 Description of the tests and test modalities.

In order to check the applicability of the fatigue results obtained on type B specimens to real deck joints, fatigue tests were carried out on two full scale orthotropic deck specimens provided with stiffener to stiffener type I joints which have been obtained by cutting crosswise along the central line the specimen used in the static test (type A specimen: see figure 11).

The test scheme is that of a plate with cantilever resting on two cross beams. The cantilever have been ballasted using two concrete blocks weighting totally 54 KN. The pulsating fatigue load, applied onto a 200X300 mm rectangular neoprene plate placed at middle span, induced a nominal stress delta at the lower apex of the central rib, close to the weld foot, equal to 22.5 KN/cm2 and a minimum stress of 1.5 KN/cm2, reference being the stress induced by the ballast and the self weight of the deck.

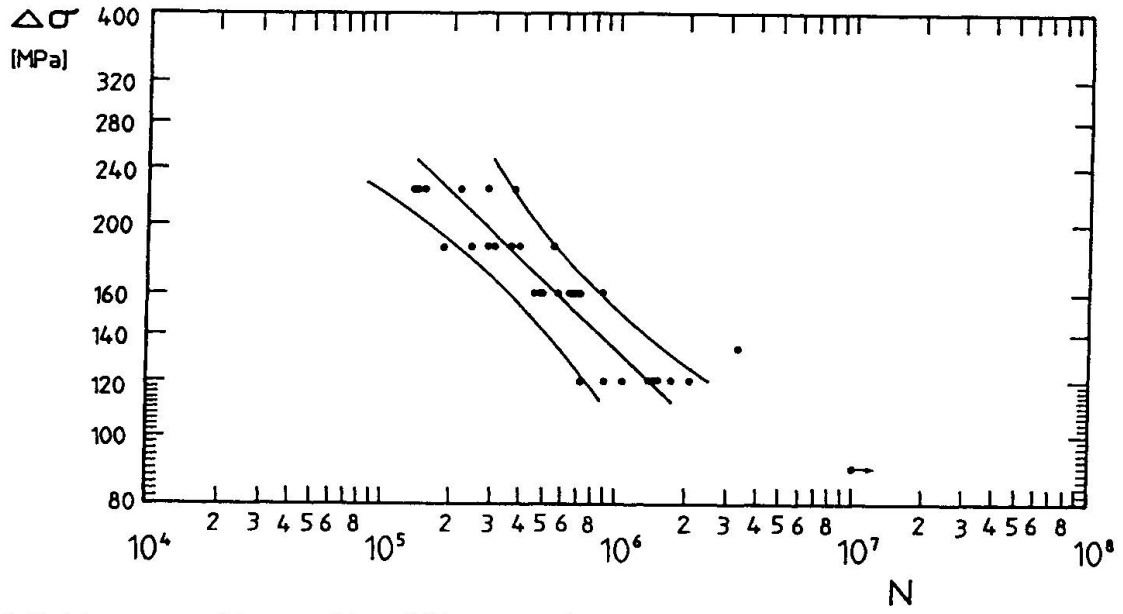

Fig. 10 Fatigue results on S4 welding specimens

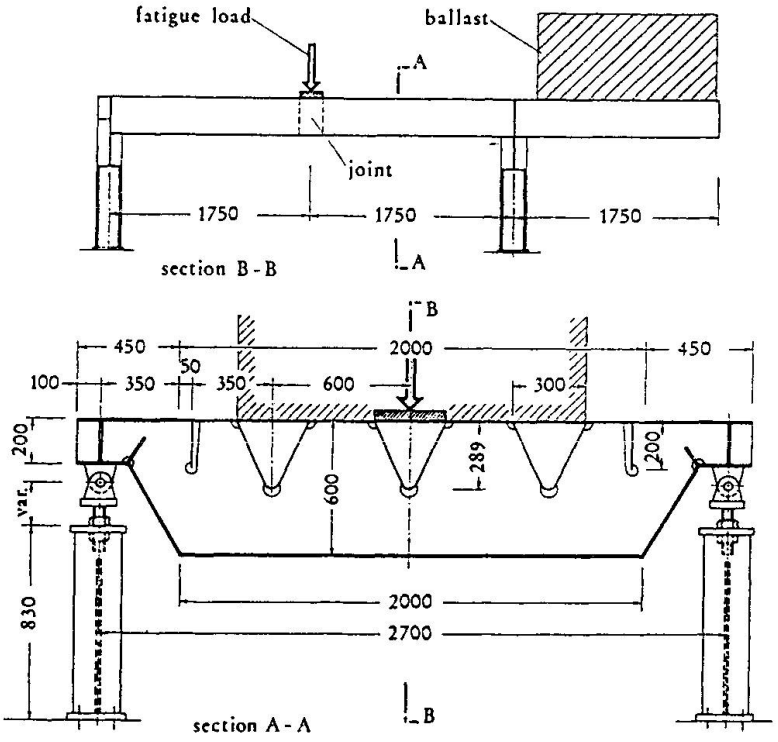

Fig. 11 Type A specimen

4.2 Experimental results

The first specimen failed after 240,000 cycles, the second one after 260,000 cycles. In both cases crack initiated in the weld at the apex of the rib and propagated in the weld too.

The comparison between the results obtained on the two types (A and B) of specimens reveals good accordance, within the normal dispersion limits. The lower fatigue strength revealed by type A specimens may be due to the residual stresses which in full scale orthotropic deck panels are to be expected higher than on simple ribs because of the greater stiffness of the deck.

5. CONCLUSIONS

The mean S-N curves of type B specimens and those regarding the welding specimens are compared in figure 12 where also the ECCS curves for backing strip weldings (class 71) and for full penetration weldings (class 80) are reported.

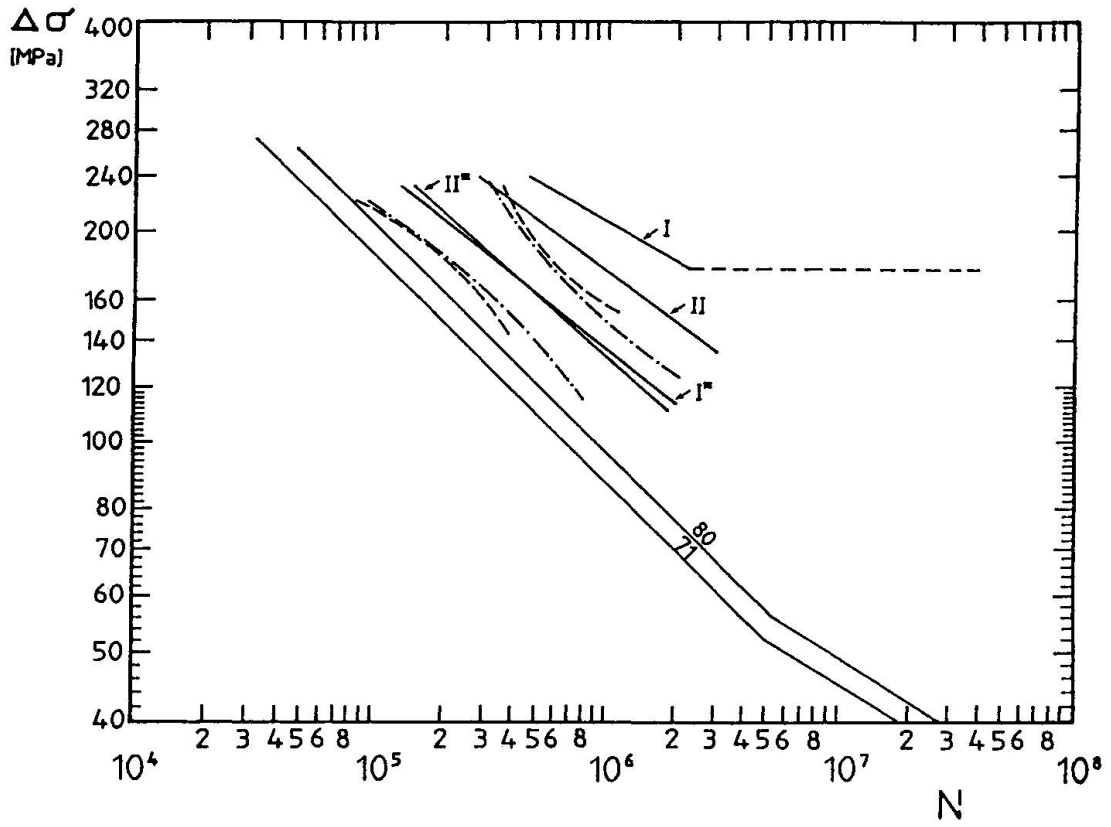

Fig. 12 Comparison between experimental results and ECCS curves

The S3 and S4 welding specimens have practically coincident fatigue strength and the 5% fractile curves of the two groups are situated both above ECCS curve 80. It can thus be concluded that the penalization of correctly designed and executed backing strip weldings, with respect to full penetration weldings, appears unjustified. On the contrary, type B specimens with type I joints have a higher fatigue life than that exhibited by type B specimens with type II joints (higher in both cases than that of the welding specimens because of the longer crack propagation life).

It follows then also that the fatigue life of the two types of joints does not dependent from the type of weldings (S3 or S4), if correctly executed and without defects, but depends from residual stresses.

Concluding, a distinction between joints, provided with backing strip weldings or full penetration weldings, based exclusively on the typology of the weldings and not taking into account the geometric features of the weldings themselves and the execution modalities of the connections is not justified. It is moreover not possible to assert "a priori" if it is safer or not to apply the present codified curves to complex details for which, at least for those most commonly used, it would be opportune to define specific S-N curves.

In our case, the authors mean that also backing strip weldings if correctly designed and executed, could be inserted in ECCS class 80.

Some aspects of the problem, such as more precise evaluation of residual stres-

ses, remain still not completely clarified and the authors intend to dedicate on them their future research work.

REFERENCES

1. WOLCHUK R., Lessons from weld cracks in orthotropic decks on three european bridges. ASCE Journ. Struct. Eng., 1990.

2. FISHER J.W., Fatigue and fracture in steel bridges. Wiley & Sons, New York, 1984.

3. YAMADA K., KONDO A., AOKI H., KIKUCHI Y., Fatigue strenght of field-welded rib joints of orthotropic steel decks. IIW Doc. XIII-1282-88, Department of Civil Engineering, Nagoya, 1988.

4. CUNNINGHAME J.R., Steel bridge decks: fatigue performance of joints between longitudinal stiffeners. TRRL Laboratory Report 1066, Crowthorne, 1982.

5. AGERSKOV H., BJØRNBACK-HANSEN J., Fatigue investigation on orthotropic steel bridge deck. IIW Doc. XIII-1195-86, Department of Structural Engineering, Lyngby, 1986.

6. CARAMELLI S., CROCE P., FROLI M., SANPAOLESI L., Misure ed interpretazioni dei carichi dinamici sui ponti. III fase. Resistenza a fatica delle piastre ortotrope da ponte in acciaio. Relazione tecnica finale della Ricerca CECA N.7210-KD/411, Istituto di Scienza delle Costruzioni, Pisa, 1989.

7. CECM Recommandations pour la vérification à la fatigue des structures en acier. Construction Métallique, 1987.

Fatigue Assessment of Orthotropic Steel Decks of Box Girder Bridges

Comportement à la fatigue des dalles orthotropes en acier de ponts en caisson

Einschätzung des Ermüdungsverhaltens orthotroper Stahlfahrbahnplatten von Hohlkasten-Brücken

Kentaro YAMADA
Professor
Nagoya University
Nagoya, Japan

Kentaro Yamada, born 1946, received his civil engineering degree at Nagoya University, and PhD at University of Maryland, MD, USA. Since then, he has been involved in fatigue tests of welded structures, application of fracture mechanics, and field measurement of service stresses of highway bridges.

SUMMARY

This report shows a case study on fatigue assessment of orthotropic steel decks of box girder bridges typically used for urban elevated highway systems in Japan. Cumulative fatigue damage for several welded joints on the bridge are computed using design wheel loads and truck models that represent service truck traffic.

RÉSUMÉ

Cet exposé présente une étude de cas sur le comportement à la fatigue des dalles orthotropes en acier de ponts en caisson typiques des autoroutes urbaines surélevées au Japon. Le cumul du dommage en fatigue pour plusieurs joints soudés du pont a été estimé à l'aide des charges de roue normalisées et des modèles de camion représentant le trafic usuel de poids lourds.

ZUSAMMENFASSUNG

Der vorliegende Bericht behandelt eine Fallstudie zur Einschätzung des Ermüdungsverhaltens orthotroper Stahlfahrbahnplatten von Hohlkasten-Brücken, wie sie in Japan für städtische Hochstrassen verwendet werden. Für Norm-Radlasten und Lastmodelle, die den Schwerverkehr darstellen, wird die Schadensakkumulation an verschiedenen geschweissten Verbindungen der Brücke berechnet.

1. INTRODUCTION

The orthotropic steel decks are susceptible to fatigue cracking when they are subjected to extremely heavy truck traffics [1, 2]. Actually, a few fatigue cracks have been observed in orthotropic steel decks, some of which are shown in Fig.1. It is due to the fact that the decks support directly the wheel loads that sometimes exceed the design ones. A load survey in Japan showed that there were trucks of about 378 kN (38 tons) and trailer trucks of about 666 kN (68 tons) [4], while the the design truck loads are based on 196 kN (20 tons, T-20 truck) and 421 kN (43 tons, TT-43 truck), respectively[5].

This report shows a case study on fatigue assessment of orthotropic steel decks of box girder bridges typically used for urban highway systems. Cumulative fatigue damages for several welded joints are computed for the design wheel loads and for a series of model trucks representing actual truck traffic observed in the Hanshin Expressway [4], one of the major elevated urban highway systems in Japan.

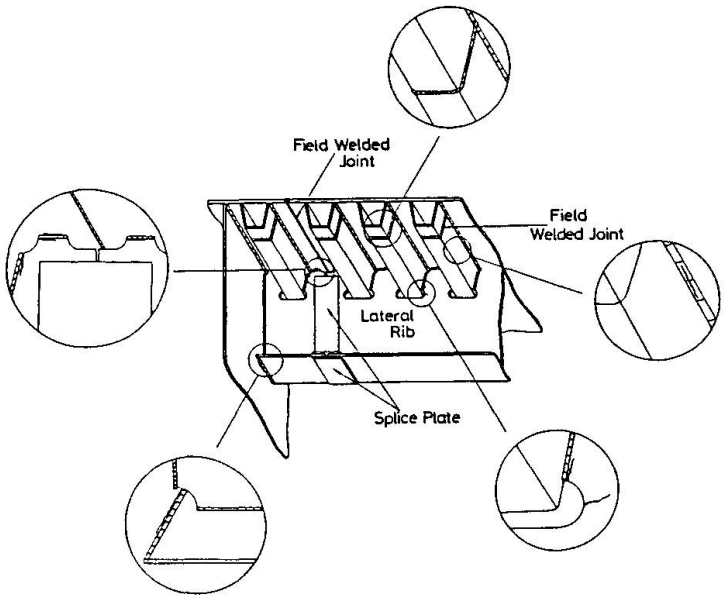

Fig.1 Example of fatigue cracks in orthotropic steel deck

2. FATIGUE ASSESSMENT OF ORTHOTROPIC STEEL DECKS

Fatigue assessment of orthotropic steel decks may be carried out by one of the following procedures.

(1) Assessment according to the design specifications

The current design specifications for the highway bridges [5] require fatigue assessment only for the orthotropic steel decks. The specifications give a few structural details and their fatigue allowable stress ranges corresponding to two million cycles. The stress ranges due to wheel loads should be less than these values [9]. The procedure is simple and feasible to most highway bridges. However, it seems insufficient when the decks are subjected to extremely heavy truck traffic with some overloadings.

(2) Assessment due to fatigue design load

An alternative way is to use an equivalent fatigue design loads, if any, which simulate the service loading condition. In order to compute the equivalent fatigue design loads, the weight and the frequency of the service loads are necessary. If the equivalent fatigue design loads are given as the fraction α of the static design loads, results for static design can be conveniently used for fatigue

assessment. The factor α is affected by the service load condition and the influence lines of the details of interest.

(3) Assessment using service loads

It seems more accurate when one can apply directly the service loads to the orthotropic steel decks and to count the resulted stress cycles. The stress cycles can be counted by the rainflow counting method and apply the Miner's cumulative damage rule. Because it needs accurate service loading prior to the computation and the computation is rather complex, it seems unrealistic to be used in design. However, the computed fatigue life seems reliable, when the reasonable S-N diagrams for the structural details are available.

(4) Assessment using measured service stresses

Recent development of so-called "Histogram Recorder" made it rather easy to measure service stresses in existing structures. Numerous measurements of service stresses in steel bridges were carried out throughout Japan [3]. The measured stress histograms can be used directly for fatigue assessment using the Miner's cumulative damage rule.

3. CASE STUDY ON FATIGUE ASSESSMENT OF ORTHOTROPIC STEEL DECKS

3.1 General Procedure

A part of a typical box girder bridge with orthotropic steel decks was selected and analyzed by grid theory. Design truck loads, T-20 and TT-43 trucks, and model truck loads that represent the service load condition are applied to the influence surfaces of the bending moments respectively to compute the resulting stress waves. The stress waves were then counted by the rainflow counting method and fatigue damages were computed by Miner's rule using appropriate design S-N curves.

3.2 Structural Analysis of Orthotropic Steel Decks

The model of the orthotropic steel decks was selected from "Typical Examples of Box Girder Bridge with Orthotropic Steel Decks," proposed by the Hanshin Expressway [6]. The bridge is consisted of two box girders of 72 m span carrying four-lane traffics, two lanes in each direction, as shown in Fig.2a. The grid analysis was carried out for a section of 12 m long with two cross beams and three lateral ribs of 3 m apart, as shown in Fig.2b. Influence surfaces were obtained for the structural details of interest.

The followings are the assumptions in the analysis.

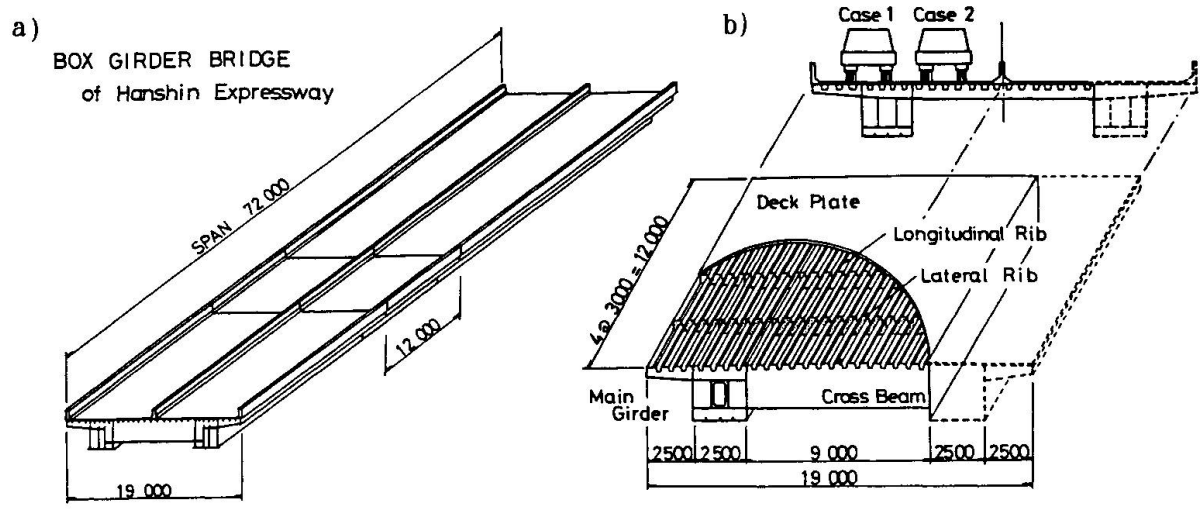

Fig.2 Analytical model of box girder bridge with orthotropic steel deck

(1) The orthotropic steel decks were assumed as a grid that consists of trapizoidal ribs, lateral ribs, cross beams and main girders.
(2) A box girder were divided into two I beams, each supporting the orthotropic steel decks at the upper end of the web.
(3) The effective widths of the decks were computed according to the Design Specification of the Highway Bridges [5].

3.3 Structural Details

Fatigue assessments were carried out for six welded joints, as shown in Fig.3. The arrows in Fig.3 indicate the stress direction. The design S-N curves were selected from the fatigue design recommendation for the welded structure proposed by the European Convention for the Constructional Steelwork (ECCS) [7]. The detail categories are numbered in the recommendation according to their fatigue strength at two million cycles. The structural details and their detail categories used in the computation were as follows.
(1) longitudinal fillet welds connecting trough ribs to deck; stress category 100.
(2) lower ends of fillet welds between trough ribs and web of the lateral rib subjected to stresses in the longitudinal direction; stress category 80.
(3) lower ends of fillet welds between trough ribs and lateral ribs with load carrying fillet welds; stress category 71 for toe crack and stress category 36 for root crack.
(4) upper end of the fillet welds between trough ribs and lateral ribs; stress categories 71 and 36.
(5) end of fillet welds between web of the lateral ribs and deck; stress category 71.
(6) full penetration groove welds between lateral ribs and web of main girder; stress category 71.

The fatigue assessments were carried out for the details in the structures that showed the maximum range of bending moment, when the design loads, T-20 and TT-43, moved on slow lane and passing lane. Stresses were computed by the beam theory.

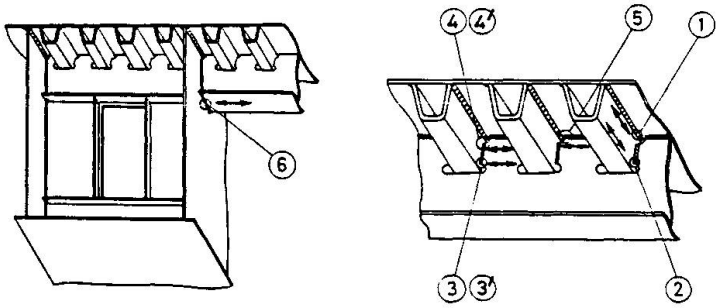

Fig.3 Welded joints for fatigue assessment

3.4 Computation of Stress Waves

The design truck loads and model truck loads were applied to the influence surfaces computed by the grid theory. The following assumptions were made in the analysis.
(1) The wheel loads were assumed as concentrated loads and the impact factor was not considered.
(2) The wheel loads passed on the same line, and the distribution in lateral direction was not considered.
(3) A single truck passes on the deck at a time.
(4) The truck passes either on the slow lane or the passing lane.
The stress ranges and the number of cycles were counted for those stress waves using rainflow counting method.

3.5 Design S-N Diagrams

The Miner's cumulative damage D can be expressed as follows:

$$D = \sum_{i=1}^{k} n_i/N_i \qquad (1)$$

where n_i is the number of cycles of stress ranges σ_{ri}, N_i is the design fatigue life of the detail at σ_{ri} obtained from design S-N diagram, and k is the number of stress ranges of variable amplitude.

The following three types of design S-N diagrams can be used, as shown in Fig.4 [7, 8].

I: A single S-N diagram of slope m = 3 is used. (Modified Miner's rule)
II: When stress ranges are below the constant amplitude fatigue limit of the detail at five million cycles, slopes of the S-N diagrams are changed into m = 5.
III: When stress ranges are below the cut-off limit at 100 million cycles, these stress ranges are neglected.

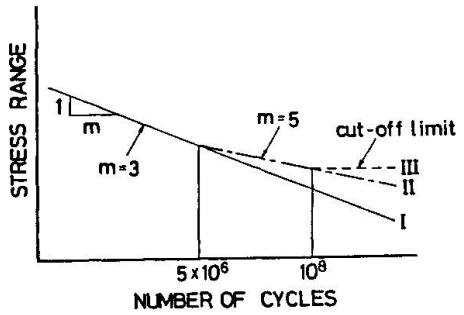

Fig.4 S-N diagram used for fatigue damage analysis

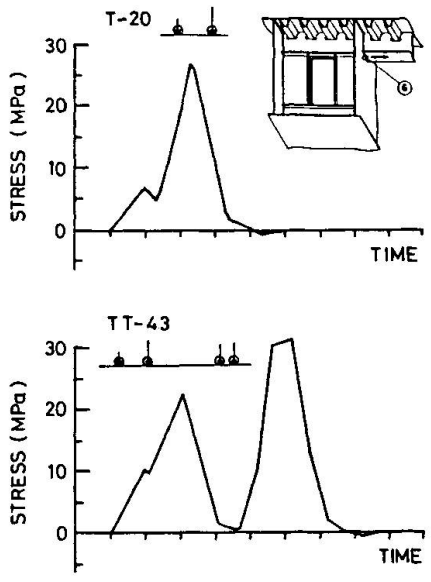

Fig.5 Stress wave due to model truck (lateral rib)

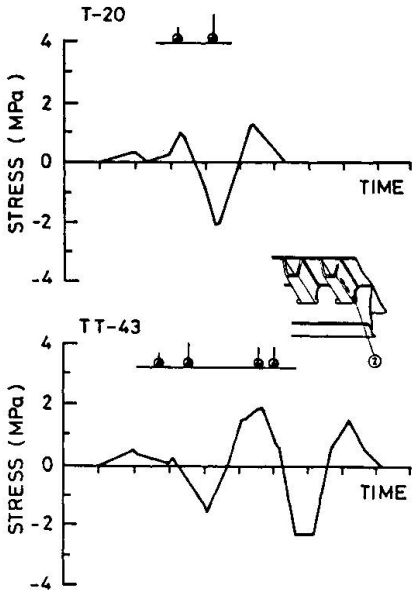

Fig.6 Stress wave due to model truck (longitudinal rib)

4. FATIGUE ASSESSMENTS FOR DESIGN TRUCKS

4.1 Stresses due to Design Truck, T-20 and TT-43

Computed stresses at the lateral ribs (detail No.6) due to T-20 and TT-43 trucks are shown in Fig.5. The T-20 truck has a wheel base of 4 m, which results in one large stress range per truck. On the contrary, the TT-43 truck gives two stress ranges per truck, because the distance between the front axle and the rear axle is about 7.8 m, and it is larger than the size of the influence surface of the details. The stresses at the longitudinal ribs (Detail No.2) are shown in Fig.6. The influence surface of this detail is small, and the fluctuating stresses appear for each passage of wheel.

4.2 Fatigue Damages

In order to compute fatigue damage due to the design trucks, design life and the number of design trucks passing on this bridge must be assumed. In this analysis

Table 1 Computed fatigue damage for design loads

Joint No.	Joint Classification (ECCS)	S-N Diagram	Fatigue Damage during 50 Years (4260/day/lane)		
			T-20		TT-43
			Case 1	Case 2	Case 2
①	100	I II III	no no 0.0	no no 0.0	no no 0.0
②	80	I II III	no no 0.0	3.0×10^{-3} no 0.0	6.6×10^{-3} no 0.0
③	71	I II III	no no 0.0	no no 0.0	no no 0.0
③'	36	I II III	no no 0.0	no no 0.0	1.2×10^{-3} no 0.0
④	71	I II III	no no 0.0	3.4×10^{-3} no 0.0	7.2×10^{-3} no 0.0
④'	36	I II III	no no 0.0	4.2×10^{-2} no 0.0	9.1×10^{-2} 2.1×10^{-3} 0.0
⑤	71	I II III	no no 0.0	6.0×10^{-3} no 0.0	1.3×10^{-2} no 0.0
⑥	71	I II III	no no 0.0	2.33 0.65 0.0	4.96 1.66 1.40

no : Fatigue Damage less than 10^{-3} is considered no Fatigue Cracking Condition.

it was assumed that the design life was 50 years and the number of daily design trucks was 4260. It corresponds to the trucks that constitute 14.2 percent of the 30,000 vehicles passing daily on one lane.

The computed fatigue damages in 50 years of life span for six structural details are summarized in Table 1. When the T-20 truck passes on the slow lane (case 1),

the computed fatigue damages are less than 0.001. Although various assumptions are made in the analysis, one can safely conclude that these details are not susceptible to fatigue, with the design trucks passing on the slow lane.

The following discussion forcus only on the case 2, where the design trucks pass on the passing lane. The computed fatigue damages due to the TT-43 truck are about 2 to 2.5 times that of the T-20 trucks. It is due to the fact that the computed stresses are about the same for both trucks, while the TT-43 truck gives the number of cycles about twice of that from T-20 truck.

The lateral ribs connected to the main girder webs showed rather large fatigue damage, especially when the modified Miner's rule (S-N diagram I) is used. This is maybe because a diaphragm is usually fabricated in the box girder, outside of which cross ribs are welded and thus provides a structural discontinuity point for the cross ribs.

5. FATIGUE ASSESSMENT FOR SERVICE LOADS

5.1 Model Trucks Simulating Service Loads

Weights of all passing vehicles were measured for 24 hours by the Hanshin Expressway Public Authority in 1982 [4]. As shown in Table 2, about 72,000 vehicles passed, and 14.2 percent of them were trucks. The maximum weight of the trucks were 236 kN (24.1 tons) for the trucks with two axles, 370 kN (37.8 tons) with three axles, and 670 kN (68.4 tons) for trailer trucks. About 38 percent of the two axle trucks and about 49 percent of the trailer trucks weighed more than the design T-20 truck (196 kN or 20 tons, two axles). About 5 percent of trailer trucks weight more than the design TT-43 truck (421 kN or 43 tons, four axles).

Table 2 Classification of vehicles passing on Hanshin Expressway

Traffic Classification			Daily Traffic	Percentage
Large Vehicle	2 axles		1,630	2.3 %
	Tandem axle	3 axles(1)	4,926	6.8 %
		3 axles(2)	2,019	2.8 %
		4 axles	152	0.2 %
	Trailer		1,565	2.2 %
	Total		10,292	14.2 %
Middle Vehicle			12,913	17.8 %
Car			49,189	67.9 %
Total			72,394	100.0 %

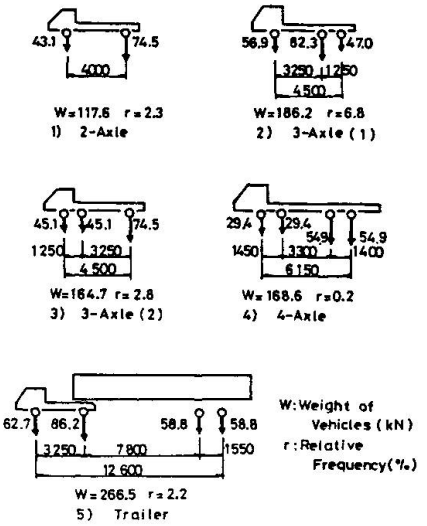

Fig.7 Model trucks representing service loading

The observed trucks were then re-grouped into five model trucks, as shown in Fig.7. They were; 1) two-axle truck; 2) three-axle truck with two rear axles; 3) three-axle truck with two front axles; 4) four-axle truck; and 5) trailer truck. The weights of the model trucks were computed using Eq.2.

$$W = \Sigma \ (f_i \ . \ W_1^m)^{1/m} \qquad (2)$$

where W_i is the measured truck weights and f_i is its relative frequencies. When m = 3 is used, W becomes so-called equivalent truck weights using modified Miner's rule. The wheel bases were also measured, and their mean values were computed, as shown in Fig.7. Each axle weight was also determined from the average axle weight ratio.

5.2 Computed Fatigue Damages and Equivalent Loads

The model trucks were applied to the passing lane, and fatigue damages for the six structural details were computed. It was assumed that the design life was 50 years and the average daily traffic was 30,000 vehicles in one lane. The results are summarized in Table 3. In general, for each structural detail, the three axle trucks with one front axle gives the most fatigue damages, owning to its relative frequency. The trailer trucks also gives large fatigue damages, because their weights are relatively large, and they usually gives more than two major stress ranges per truck.

Table 3 Computed fatigue damage due to model trucks measured by Hanshin Expressway Public Authority

Joint No.	S-N Diagram	Fatigue Damage during 50 years (30,000/day/lane)						Model Load (kN)
		2 axles (2.3%)	3 axles(1) (6.8%)	3 axles(2) (2.8%)	4 axles (0.2%)	Trailer (2.2%)	Total (14.2%)	
①	I	6.7×10^{-7}	4.3×10^{-6}	8.4×10^{-7}	2.2×10^{-7}	3.7×10^{-6}	9.7×10^{-6}	110
	II	2.2×10^{-11}	2.9×10^{-10}	2.5×10^{-11}	1.8×10^{-11}	3.2×10^{-10}	6.8×10^{-10}	
	III	0.0	0.0	0.0	0.0	0.0	0.0	
②	I	3.5×10^{-5}	2.3×10^{-4}	4.5×10^{-5}	1.2×10^{-5}	2.0×10^{-4}	5.2×10^{-4}	110
	II	1.7×10^{-8}	2.2×10^{-7}	1.9×10^{-8}	1.4×10^{-8}	2.5×10^{-7}	5.2×10^{-7}	
	III	0.0	0.0	0.0	0.0	0.0	0.0	
③	I	9.6×10^{-7}	1.1×10^{-5}	1.5×10^{-6}	2.1×10^{-7}	3.6×10^{-6}	1.7×10^{-5}	144
	II	5.0×10^{-11}	1.3×10^{-9}	9.8×10^{-11}	2.1×10^{-11}	3.0×10^{-10}	1.8×10^{-9}	
	III	0.0	0.0	0.0	0.0	0.0	0.0	
③'	I	1.2×10^{-5}	1.3×10^{-4}	1.9×10^{-5}	2.7×10^{-6}	4.5×10^{-5}	2.1×10^{-4}	143
	II	3.4×10^{-9}	9.0×10^{-8}	6.6×10^{-9}	1.4×10^{-9}	2.0×10^{-8}	1.2×10^{-7}	
	III	0.0	0.0	0.0	0.0	0.0	0.0	
④	I	7.6×10^{-5}	8.3×10^{-4}	1.2×10^{-4}	1.7×10^{-5}	2.9×10^{-4}	1.3×10^{-3}	142
	II	7.3×10^{-9}	1.9×10^{-6}	1.4×10^{-7}	3.0×10^{-8}	4.3×10^{-7}	2.6×10^{-6}	
	III	0.0	0.0	0.0	0.0	0.0	0.0	
④'	I	9.5×10^{-4}	1.0×10^{-2}	1.5×10^{-3}	2.1×10^{-4}	3.6×10^{-3}	1.6×10^{-2}	142
	II	4.9×10^{-6}	1.3×10^{-4}	9.6×10^{-6}	2.0×10^{-6}	2.9×10^{-5}	1.8×10^{-4}	
	III	0.0	0.0	0.0	0.0	0.0	0.0	
⑤	I	1.3×10^{-4}	1.5×10^{-3}	2.2×10^{-4}	2.2×10^{-7}	5.1×10^{-4}	2.4×10^{-3}	144
	II	1.9×10^{-7}	5.0×10^{-6}	3.7×10^{-7}	1.8×10^{-11}	1.1×10^{-6}	6.7×10^{-6}	
	III	0.0	0.0	0.0	0.0	0.0	0.0	
⑥	I	0.04	0.43	0.06	7.2×10^{-3}	0.14	0.64	127
	II	2.6×10^{-3}	0.06	4.5×10^{-3}	7.3×10^{-4}	0.01	0.08	
	III	0.0	0.0	0.0	0.0	0.0	0.0	

( ) : Relative Frequency

The structural detail No.6, which is the lateral ribs welded to the main girders, showed the largest fatigue damage. This was the same trend as in the case of design truck loads. However, the fatigue damage was 0.64 in 50 years, even when the modified Miner's rule is used. It implies that the detail is not susceptible

to fatigue crackings, when the loading pattern and the number of vehicles remain the same over the assumed design life of 50 years.

The model truck loads give smaller fatigue damages than the design T-20 or TT-43 truck loads. It implies that the weight of the design truck can be reduced by the factor α, when one wants to obtain the same fatigue damages as the model loads. The reduced design truck loads are computed and summarized as equivalent loads in Table 3. It is concluded that the equivalent loads are between 54 and 75 percent of the weight of the T-20 trucks.

5.3 Fatigue Damage due to Different Daily Trucks and Truck Ratio

Fatigue damages were also computed for different daily traffic and different truck ratio. The weights and the wheel bases as well as the relative frequencies of the model trucks were assumed unchanged during the design life of 50 years. The fatigue damages were computed for the structural detail No.6, and plotted in Fig.8. The fatigue damages were mainly caused by the large vehicles, and the damage does not exceed unity when the total vehicles are 10,000 and the trucks are 40 percent of them (i.e. 4,000 trucks per day). On the contrary, when the total

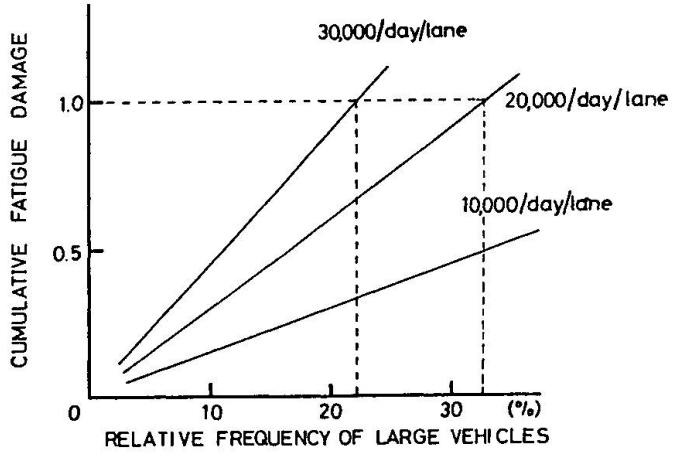

Fig.8 Effect of relative frequency of trucks on fatigue damage

vehicles is about 30,000, and the trucks are over 22 percent (i.e. 6,600 trucks per day), the damage exceeds unity. If the bridge carries 30,000 vehicles per day per lane and 44 percent of them are trucks, fatigue damage might exceed unity within 25 years at this detail.

6. SUMMARY OF FINDINGS

Fatigue damages were computed for the typical box girder bridge with the orthotropic steel decks using the design T-20 and TT-43 truck loads and the model truck loads. A part of the decks was analyzed and the stress waves were obtained by using grid thoery. The fatigue damages were computed for six welded details in the structure using the Miner's cumulative damage rule. The followings summarize the findings.

(1) The computed fatigue damages are normally larger when the trucks pass on the passing lane than on the slow lane.

(2) The lateral ribs welded to the webs of the main box girders showed the largest fatigue damage when the design trucks were applied.

(3) The model trucks, computed from the measured weights and the wheel bases by the Hanshin Expressway Public Authority, showed less fatigue damages than that due

to the design trucks. The fatigue damages were less than unity for all structural details with the current traffic condition, such as 30,00 vehicles per lane and 14.2 percent truck ratio.
(4) However, when the daily vehicles increase or when the number of trucks increase over the present condition, the computed fatigue damage may exceed the unity.
(5) The TT-43 truck gives about 2 to 2.5 times more fatigue damage than the T-20 truck, because the former gives two major stress ranges per truck for structural details of the orthotropic steel decks.
(6) When compared with the T-20 design trucks, the model trucks that represent the service condition of the Hanshin Expressway give fatigue damages between 0.16 and 0.40 depending on the structural details and the truck types. Therefore, the weight of the equivalent model trucks are about 54 to 75 percent that of the design T-20 truck.

ACKNOWLEDGEMENT

The author express his sincere appreciation to Dr. A. Kondo of Meijo University, Dr. H. Terada of the Yokogawa Bridges works, Mr. K. Hasegawa of Mitsubishi Heavy Industries, Mr. Ma Zhiliang of Nagoya University and Mr. H. Ishizaki of Hanshin Expressway Public Authority for their valuable discussion and suggestion throughout the study. A majority of this report was already published in Ref. 11 in Japanese and in Ref. 12 in English. The research was carried out under the Grant -in Aids for scientific research of Ministry of Education, Science and Culture.

REFERENCES

1. CUNINGHAM, J.K.: Strengthening fatigue prone details in a steel bridge deck, International Conference on Fatigue of Welded Constructions, Brighton, April 1987.
2. Subcommittee on Fatigue of Steel Orthotropic Deck; Fatigue of orthotropic steel bridge deck, Proc. of JSCE, No.410/I-12, 1989.10.
3. YAMADA, K. and MIKI, C.; Recent research on fatigue of bridge structure in Japan, Journal of Constructional Steel Research, Vol.13, 1989.
4. Hanshin Expressway Public Authority; Survey on service loads on the Hanshin Expressway, 1984.
5. Japan Road Association; Design specifications for highway bridges, 1980.
6. Hanshin Expressway Public Authority; Typical examples of box girder bridges with orthotropic steel decks, 1988.3.
7. European Convention for Constructional Steelwork; ECCS recommendations for fatigue design of Steel Structures, 1985.
8. British Standard Institution; Steel, concrete and composite bridges, Part 10, Code of Practice for Fatigue, 1980.
9. KUNIHIRO, T. and FUJIWARA, M.; Conventional design calculation of orthotropic steel decks using the orthotropic plate theory, Report of PWRI, No.137, 1969.
10. FUJIWARA, M. et al.; Survey on connection between lateral ribs and longitudinal ribs of orthotropic steel decks, Annual Convention of JSCE, No.43, 1988.
11. HASEGAWA, K. et al.; Fatigue assessment of orthotropic steel deck of box girder bridge, Journal of Structural Eng., JSCE, Vol.34A, 1989.3.
12. YAMADA, K. et al.; Fatigue assessment of orthotropic steel decks of box girder bridge, Pacific Structural Steel Conference, STEEL 2001, Gold Coast, 1989.